UNIVERSITÄT PADERBORN
Die Universität der Informationsgesellschaft

Fakultät für Naturwissenschaften - Department Chemie

Zinc complexes with N-donor ligands and their application as catalysts in the polymerisation of cyclic esters

Dem Department Chemie der Universität Paderborn zur Erlangung des akademischen Grades eines Doktors der Naturwissenschaften vorgelegte

Dissertation

von **M.Sc. Janna Börner**

Paderborn, 2009

Promotionskommission

Prof. Dr. Wolfgang Bremser (Vorsitzender)
Prof. Dr. Gerald Henkel (1. Gutachter)
Prof. Dr. Dirk Kuckling (2. Gutachter)
Prof. Dr. Heinz-Siegfried Kitzerow

Tag der Einreichung: 19. November 2009

Tag der mündlichen Prüfung: 18. Dezember 2009

Die experimentellen Untersuchungen zu dieser Arbeit wurden im Zeitraum von Januar 2007 bis Oktober 2009 unter der Anleitung von Prof. Dr. Gerald Henkel und Dr. Sonja Herres-Pawlis im Department Chemie der Universität Paderborn durchgeführt.

Zusammenfassung

Im Rahmen dieser Arbeit wurden katalytisch aktive Zinkkomplexe auf der Basis neutraler N-donor funktionalisierter Liganden synthetisiert und auf ihre Verwendung in der Massepolymerisation von Lactid untersucht.
Die meisten der bisher eingeführten Single-Site-Metallkatalysatoren für die Ringöffnungspolymerisation zyklischer Ester werden von anionischen Ligandensystemen stabilisiert, die neben der hohen katalytischen Aktivität auch eine hohe Sensibilität bedingen. Um anwendungsorientierte Katalysatorsysteme zu entwickeln, die eine hohe Aktivität aufweisen und gleichzeitig sehr robust sind, werden in dieser Arbeit neutrale Liganden verwendet. Als Ligandensysteme dienen hierbei Bisguanidine, Guanidin-Amin-Hybride, Imidazolin basierte Guanidine sowie aliphatische, aromatische und zyklische Amine. Für eine systematische Untersuchung eignen sich besonders die modular aufgebauten Guanidin- und Guanidin-Amin-Hybridliganden. Ihr flexibles Syntheseprotokoll gestattet die Variation einzelner Funktionalitäten und damit die Untersuchung ihres Einflusses auf die Komplexeigenschaften.
Durch die Umsetzung der Liganden mit verschiedenen Zinkverbindungen wurde eine Bibliothek aus Zinkkomplexen aufgebaut, deren Vielfalt (67 Komplexe aus 29 verschiedenen Liganden und 9 unterschiedlichen Zinksalzen) die systematische Bewertung der katalytischen Eigenschaften der einzelnen Komplexe sowie die Ermittlung entscheidender Einflussgrößen ermöglicht. Ausgehend von diesen Untersuchungen konnte gezeigt werden, dass sich alle verwendeten Ligandenklassen für die Synthese von aktiven Initiatorsystemen eignen. Der Einfluss der anionischen Komponente des Zinksalzes auf die molekulare Struktur und das Polymerisationsverhalten der Komplexe wurde ermittelt und für die Gruppe der Guanidin-Pyridin-Hybrid-Zinkkomplexe eine Struktur-Wirkungsbeziehung aufgestellt.
Die vielversprechendsten Katalysatorkomplexe sind Zinktriflatkomplexe mit Guanidin-Pyridin-Hybridliganden. Sie vereinen exzellente katalytische Aktivität mit hoher Robustheit gegenüber Luft, Feuchtigkeit sowie kleinen Monomerverunreinigungen und thermischer Belastbarkeit. Experimentelle und theoretische Studien zu ihrem Polymerisationsmechanismus erlaubten die Postulierung eines Koordinations-Insertions-Mechanismus, bei dem ein koordinierter Guanidinligand als Nukleophil agiert und die Ringöffnung unterstützt. Dies ermöglicht die Herstellung von Polylactiden mit hohen Molmassen ohne die Verwendung von Kokatalysatoren unter industriell attraktiven Bedingungen.
Die in dieser Arbeit beschriebene Erschließung von drei neutralen Ligandenklassen für die Herstelllung von Single-Site-Metallkatalysatoren für die Ringöffnungspolymerisation zyklischer Ester soll die Entwicklung von verbesserten Initiatoren ermöglichen und zu einem tieferen Verständnis des metallkatalysierten Polymerisationsprozesses beitragen.

Abstract

In this thesis catalytic active zinc complexes stabilised by neutral N-donor functionalised ligands were synthesised and investigated towards their application in the solvent-free polymerisation of lactide.
Most of the introduced single-site metal catalysts for the ring-opening polymerisation of cyclic esters contain anionic ligand systems. They provide high catalytic activity but also cause the high sensitivity of these catalysts. To develop application oriented catalyst systems combining high activity with high robustness, neutral ligand systems are used in this approach. They cover bisguanidines, guanidine-amine-hybrids, imidazoline based guanidines as well as aliphatic, aromatic and cyclic amines. For a systematic investigation, the modular assembled guanidine and guanidine-amine hybrid ligands are well suited. Their flexible synthesis protocol allows the easy variation of the individual moieties and thus permits the elucidation of influencing variables of the complex properties.
By reacting the ligands with various zinc components, a library of zinc complexes was generated. Its variety (67 complexes prepared of 29 varying ligands and 9 different zinc salts) allows the systematic evaluation of the catalytic properties of its single components as well as the elucidation of crucial influencing parameters. Based on this analysis it could be demonstrated that all utilised ligand classes are suitable for the synthesis of active initiator systems. The impact of the anionic component of the zinc salt on the molecular structure and on the polymerisation behaviour of the corresponding zinc complexes was determined and in the case of guanidine-pyridine hybrid ligands a structure-reactivity relationship was developed.
The most auspicious initiators were guanidine-pyridine zinc triflate complexes which combine excellent catalytic activity with high robustness towards air, moisture and small impurities in the monomer as well as thermal stability. They do not need co-catalysts like alkoxides or alcohols to give PLAs with high molecular masses under industrially attractive conditions via a coordination-insertion mechanism.
The herein described introduction of three neutral ligand classes into the field of single-site metal catalyst systems for the ring-opening polymerisation shall enable the development of improved initiators and contribute to a deeper understanding of the metal catalysed polymerisation process.

Danksagung

Ich möchte all jenen danken, die zum Gelingen dieser Doktorarbeit beigetragen haben. Mein besonderer Dank gilt

- Prof. Dr. Gerald Henkel, für die Möglichkeit in seinem Arbeitskreis meine Doktorarbeit anfertigen zu können und seine großartige Unterstützung.
- Dr. Sonja Herres-Pawlis, für die ausgezeichnete Betreuung meiner Doktorarbeit, die produktive Zusammenarbeit, ihre Unterstützung und für alles, was ich von ihr lernen durfte.
- Prof. Dr. Dirk Kuckling, für die Übernahme des Zweitgutachtens sowie ihm und seinem Arbeitskreis, insb. Artjom Döring, für die gute Zusammenarbeit in der Polymeranalytik und die hilfreichen Diskussionen.
- Dr. Ulrich Flörke, für die Durchführung der Einkristall-Röntgenstrukturanalysen, sein Engagement, mir die Grundlagen der Kristallographie näher zu bringen und für seine unermüdliche Geduld bei der Beantwortung meiner Fragen.
- Maria Busse (EA), Christiane Gloger (EA), Karin Stolte (NMR), Dr. Alexander Pawlis (Fluoreszenz), Dr. Heinz Weber (MS), Hans-Joachim Wolf (GPC) und Mariola Zukowski (MS, GPC) für die zahlreichen Messungen sowie Dr. Sonja Herres-Pawlis und Ines dos Santos Vieira für die DFT-Rechnungen.
- Dr. Matthew Jones, for special NMR measurements and exciting discussions.
- PD Dr. Hans Egold für seinen immer wertvollen Rat, nicht nur in NMR Fragen.
- der gesamten Arbeitsgruppe für die gute Arbeitsatmosphäre und Unterstützung. Wer Explosionen, Sintfluten und die SGU übersteht, schafft alles.
- dem gesamten Department Chemie, für die Unterstützung und gute Zusammenarbeit.
- Prof. Dr. Matthias Breuning, Prof. Dr. Carsten Strohmann und Prof. Dr. Matthias Tamm, sowie ihren Mitarbeitern Melanie Steiner, Viktoria Gessner, Priska Eckert und Thomas Glöge für die gute Zusammenarbeit im Rahmen der Kooperationen.

- der Stiftung der Deutschen Wirtschaft (sdw) für die finanzielle und ideelle Förderung meiner Arbeit im Rahmen eines Promotionsstipendiums.
- der Universität Paderborn und der Gesellschaft Deutscher Chemiker für die Finanzierung von Konferenzbesuchen.
- allen meinen Freunden, die für den notwendigen Ausgleich zur Arbeit gesorgt und mich immer wieder in die "normale" Welt zurückgeholt haben.
- meinem Freund Steffen, der für mich da war und mich immer unterstützt hat.
- meiner Familie, für die Unterstützung während meines gesamten Studiums und für den großartigen Rückhalt.

…und allen die in dieser Liste aus Versehen vergessen wurden. Danke!

Contents

List of abbreviations

aliph.	aliphatic
arom.	aromatic
bp	boiling point
br	broad signal (NMR)
cat.	catalyst
CI	chemical ionisation (MS)
d	doublet (NMR)
dd	double doublet (NMR)
δ	chemical shift (NMR)
δ	deformation vibration (IR)
DFT	density functional theory
EDX	energy dispersive X-ray spectroscopy
EI	electron impact ionisation (MS)
Et	ethyl
FDA	U.S. Food and Drug Administration
G/gua	guanidine
GPC	gel permeation chromatography
I	initiator
J	coupling constant (NMR)
m	multiplet (NMR)
m	medium (IR)
M	monomer to initiator ration
M	molecular weight
M/I	monomer to initiator ratio
Me	methyl
MeCN	acetonitrile
M_n	number-average molar mass
mp	melting point
M_v	viscosity-average molecular weight
M_w	weight-average molar mass

NHC	N-heterocyclic carbene
ν	valence or stretch vibration (IR)
OAc	acetate
OMes	mesylate, methane sulfonate
OTf	triflate, trifluoromethane sulfonate
PBS	polybutylene succinate
PBT	polybutyleneterephthalate
PCL	poly-ε-caprolactone
PE	polyethylene
PET	poly(ethylene terephthalate)
PGA	polyglycolide
PHA	polyhydroxyalkanoate
PLA	poly(lactic acid), polylactide
PMMA	poly(methyl methacrylate)
PP	polypropylene
P_r	probability of heterotactic enchainment
Pr	propyl
PS	polystyrene
PTT	polytrimethyleneterephthalate
PUR	polyurethane
PVC	polyvinylchloride
q	quartet (NMR)
R	alkyl moiety
ROP	ring-opening polymerisation
s	strong (IR)
sp	spacer
t	triplet (NMR)
THF	tetrahydrofurane
vs	very strong (IR)
vw	very weak (IR)
w	weak (IR)

List of compounds

Ligands

1 $DMEG_2e$
2 TMG_2e
3 btmgp
4 $MorphDMG_2e$
5 8MeBL
6 DMEGqu
7 TMGqu
8 DMPGqu
9 TEGqu
10 DPipGqu
11 DMorphGqu
12 MorphDMGqu
13 (R,R)-DMCHGqu
14 DMEGpy
15 TMGpy
16 DMPGpy
17 TEGpy
18 DPipGpy
19 DMorphGpy
20 MorphDMGpy
21 DMEGpico
22 TMGpico
23 DMEGimi
24 TMGimi
25 DMEGthio
26 TMGthio
27 $DMEG_4(baem)_2b$
28 $TMG_4(baem)_2b$
29 $DMEG_3tren$
30 TMG_3tren
31 TEG_3tren
32 qu
33 bipy
34 phen
35 TMEDA
36 TEEDA
37 (R,R)-TMCDA
38 (R,R)-TECDA
39 9-oxa

Complexes

1a $[Zn(DMEG_2e)Cl_2]$
1b $[Zn(DMEG_2e)(CH_3COO)_2]$
1c $[Zn(DMEG_2e)_2][CF_3SO_3]_2$
1d $[Zn(DMEG_2e)(C_6H_5COO)_2]$
2a $[Zn(TMG_2e)Cl_2]$
2b $[Zn(TMG_2e)(CH_3COO)_2]$
3a $[Zn(btmgp)Cl_2]$
3b $[Zn(btmgp)(CH_3COO)_2]$
5a $[Zn(8MeBL)Cl_2]$
5b $[Zn(8MeBL)(CH_3COO)_2]$
6a $[Zn(DMEGqu)Cl_2]$
6b $[Zn(DMEGqu)(CH_3COO)_2]$
6c $[Zn(DMEGqu)_2(CF_3SO_3)][CF_3SO_3]$
6d $[Zn_2(DMEGqu)(C_6H_5COO)_4]$
6e-1 $[Zn(DMEGqu)(CH_3SO_3)_2]$
6e-2 $[Zn(DMEGqu)_2(CH_3SO_3)][CH_3SO_3]$
6f $[Zn(DMEGqu)Br_2]$
6g $[Zn(DMEGqu)(C_5H_7O_2)_2]$
6h $[Zn(DMEGqu)_2(BF_4)][BF_4]$
6i $[Zn(DMEGqu)(\text{D,L-}C_3H_5O_3)_2)]$
7a $[Zn(TMGqu)Cl_2]$
7b $[Zn(TMGqu)(CH_3COO)_2]$
7c $[Zn(TMGqu)_2(CF_3SO_3)][CF_3SO_3]$
7d $[Zn(TMGqu)(C_6H_5COO)_2]$
7e $[Zn(TMGqu)_2(CH_3SO_3)][CH_3SO_3]$
7f $[Zn(TMGqu)Br_2]$
8a $[Zn(DMPGqu)Cl_2]$
8a/b $[Zn(DMPGqu)(CH_3COO)Cl]$
8b $[Zn(DMPGqu)(CH_3COO)_2]$
9a $[Zn(TEGqu)Cl_2]$
10b $[Zn(DPipGqu)(CH_3COO)_2]$
11a $[Zn(DMorphGqu)Cl_2]$
11b $[Zn(DMorphGqu)(CH_3COO)_2]$
11c $[Zn(DMorphGqu)_2][CF_3SO_3]_2$
12a $[Zn(MorphDMGqu)Cl_2]$
12b $[Zn(MorphDMGqu)(CH_3COO)_2]$
14a $[Zn(DMEGpy)Cl_2]$
14b $[Zn(DMEGpy)(CH_3COO)_2]$
14d $[Zn(DMEGpy)(C_6H_5COO)_2]$
15a $[Zn(TMGpy)Cl_2]$
15b $[Zn(TMGpy)(CH_3COO)_2]$
17a $[Zn(TEGpy)Cl_2]$
19a $[Zn(DMorphGpy)Cl_2]$
19b $[Zn(DMorphGpy)(CH_3COO)_2]$
20a $[Zn(MorphDMGpy)Cl_2]$
21a $[Zn(DMEGpico)_2Cl_2]$
22a $[Zn(TMGpico)_2Cl_2]$
22b $[(TMGpico)_2Zn_3(CH_3COO)_6]$
28a $[(TMG_4(beam)_2b)(ZnCl_2)_2]$
29a $[Zn(DMEG_3tren)Cl][Cl]$
30a $[Zn(TMG_3tren)Cl][Cl]$
32a $[Zn(qu)Cl_2]$
32c $[Zn(qu)_2(CF_3SO_3)_2]$
33a $[Zn(bipy)Cl_2]$
33b $[Zn_3(bipy)_2(CH_3COO)_6]$
33c $[Zn(bipy)_2(CF_3SO_3)_2]$
34a $[Zn(phen)Cl_2]$
34b $[Zn_2(phen)_2(CH_3COO)_4]$
34c $[Zn(phen)_2(CF_3SO_3)_2]$
35f $[Zn(TMEDA)Br_2]$
36f $[Zn(TEEDA)Br_2]$
37a $[Zn((R,R)\text{-}TMCDA)Cl_2]$
37f $[Zn((R,R)\text{-}TMCDA)Br_2]$
38a $[Zn((R,R)\text{-}TECDA)Cl_2]$
38f $[Zn((R,R)\text{-}TECDA)Br_2]$
39a $[Zn(9\text{-}oxa)Cl_2]$
39b $[Zn(9\text{-}oxa)(CH_3COO)_2]$

1 Introduction

1.1 Bioplastics

Polymers are ubiquitous in modern society; they can be easily produced, processed and handled and therefore provide a wide variety of applications. Conventional plastics like polyethylene (PE), polypropylene (PP), polyvinylchloride (PVC), polystyrene (PS), and poly(ethylene terephthalate) (PET) possess excellent properties such as lightness, durability, non-degradability and non-corrosivity to acids and alkalis. However, the high durability of these synthetic polymers has caused a crisis in solid waste management. This, together with the dwindling fossil resources, the increasing oil prices and the growing environmental awareness lead to modern approaches towards green and sustainable chemistry which focus on the substitution of petrochemical-based plastics with biorenewable and biodegradable materials.[1–6]

The term bioplastics (also called organic plastics, biobased plastic materials or artificial biopolymers[4]) has up to now no consistent definition. In general it includes polymers which are derived from renewable biomass sources and/or are biodegradable plastic materials.[1,2,7] It is important that bioplastics are not to be mistaken with biopolymers which are under the terms of IUPAC defined as macromolecules (including proteins, nucleic acids and polysaccharides) formed by living organisms.[2,8]

The class of bioplastics includes primarily four polymer types: polysaccharides, polyesters, polyurethanes and polyamides (for an overview see Table 1.1).[6] Beside their advantageous properties which are characteristic for plastics, bioplastics derived from annually renewable biomass sources provide a new source of income for the agricultural sector, as well as a higher

Table 1.1: Overview of currently most important groups and types of bioplastics

Type of polymer	Bioplastics (group)
Polysaccharides	Starch and cellulose polymers
Polyesters	Poly(lactic acid) (PLA), Polyglycolide (PGA), Poly-ε-caprolactone (PCL), Polytrimethyleneterephthalate (PTT), Polybutyleneterephthalate (PBT), Polybutylene succinate (PBS), Polyhydroxyalkanoates (PHAs)
Polyurethanes	Polyurethanes (PURs)
Polyamides	Nylon

independence of fossil resources like crude oil or gas and therefore fulfill the principles of sustainable chemistry. In addition, the biodegradability of plastic materials does not only help to solve the problems of solid waste management but also allows for contributions to environmental protection and new application fields, especially for packaging and for single-use disposal products.[1,2]

Biodegradation in general means according to a definition by IUPAC, the breakdown of a substance to its constituents, catalysed by enzymes or whole microorganisms.[8] This process is highly influenced not only by the primary chemical structure of these materials but also by their solid-state morphology and ordering phenomenons such as crystallinity and orientation.[1,2] To proof the biodegradability of certain polymer products the European Union established in 2000 the European norms EN 13432 / EN 14995, which regulate standard test methods for the investigation of degradability under laboratory and real-life conditions as well as the quality and ecotoxicity of the obtained compost. Products that pass the test are labeled with the logo for the certification of biodegradability of plastics (Fig. 1.1).[9–11]

Figure 1.1: DIN CERTO logo[9]

According to investigations by the nova-institute,[12] Europe is the most important market for bioplastics and their consumption ranges around 60,000 to 70,000 tons resulting in a market share of under 1 % in 2007. However, the growth rates are double-digit and the capacity of production of 265,000 tons does not cope with the demand. In the future, improvement of production techniques and material characteristics will allow for the economic production in industrial scale and therefore will lead to a massive reduction in price. Thus, it is assumed that the potential of bioplastic material is by far neither assessed nor utilised.

1.2 Polylactide

Polylactide or poly(lactic acid) (PLA) is an aliphatic polyester which can be produced by polymerisation of either lactic acid or lactide (IUPAC name: 3,6-dimethyl-1,4-dioxane-2,5-dione), the cyclic diester of lactic acid. PLAs have proven to be the most attractive and useful class of biodegradable polyesters among the numerous polyesters studied to date.[13]

Based on the 12 principles of green chemistry introduced by P. T. Anastas and J. C. Warner[14–16] PLA can be described as sustainable polymer in context of green chemistry. It can be made from inexpensive annually renewable resources and after its lifetime it can be recycled or it degrades through hydrolysis of the ester linkages by microorganisms and enzymes or simple acidic or alkaline catalysis into non-toxic, harmless natural products. Thus PLA is a low-impact greenhouse gas polymer because the CO_2 generated during the biodegradation is balanced by an equal amount taken from the atmosphere during the growth of plant feedstock.[16] The life cycle of PLA is depicted in Figure 1.2.

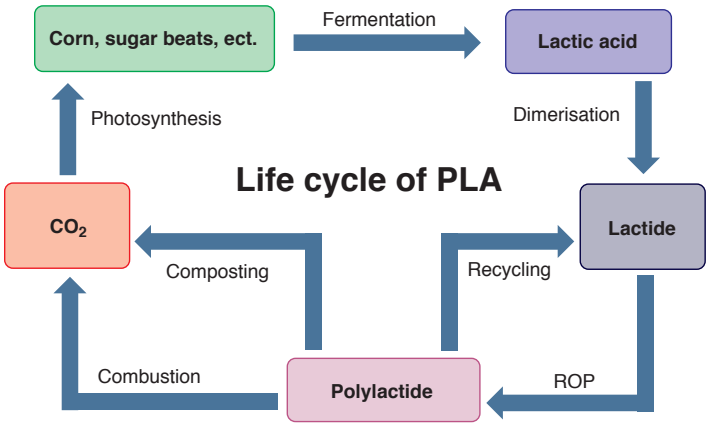

Figure 1.2: Life cycle of lactide polymers

Since lactic acid itself occurs in the metabolism of living organisms, PLA possesses a good biocompatibility which qualifies this polymer for pharmaceutical and medical applications (see below). Consequently, it is approved by the U.S. Food and Drug Administration (FDA) for biomedical applications. By using environmentally desirable solvent free reaction conditions the waste disposal of the production process can be further improved. Thus, the change of PLA from a specialty material to a large-volume commodity plastic is required in reference to green chemistry.[13,17–23] Today PLA is produced by more than ten chemical companies worldwide (e.g. marked under the trade names Natureworks^{TM}, Lacea^{TM} and Ingeo^{TM}) and has already left the niche of exotic polymers.[6,13]

Polylactide provides many advantageous properties such as biocompatibility, biodegradability both in vivo and in the environment, bacteriostatic and antifungal characteristics, high transparency, grease and oil resistance, high odour and flavour barrier, weather stability, dead-fold property, elastic recovery and good resilience and thermal bonding capabilities. PLA also benefits from its excellent mechanical properties like its thermoplastic processability which allows for the easily conversion into films, fibers, spun bond and melt blown products on existing processing equipment. Due to these favourable intrinsic properties PLA provides a versatile range of possible applications reaching from specialised medical and pharmaceutical products (drug delivery systems, sutures, surgical implants, devices for bone surgery like bone plates, screws, pins, etc.) to widespread use as coatings, fibers, films and packages including agricultural and civil engineering materials (mulch films, plant pots, root covers, fishing lines, string), geotextiles (sand bags, erosion protection, drainage), clothing and furnishings (casual wear, towels, mats), nonwovens as personal hygiene products (wipes, diapers, pad liners), packaging materials (wrapping, containers, coated paper, bags) and industrial uses (filters, drainage bags, tapes, ropes, carpets).[1,2]

The physical properties, hydrolysis and biodegradation behavior of PLA can be controlled not only by altering the averaged molecular weight and its distribution; in order to meet also the requirements of specific applications it is even possible to modify the properties of PLA by

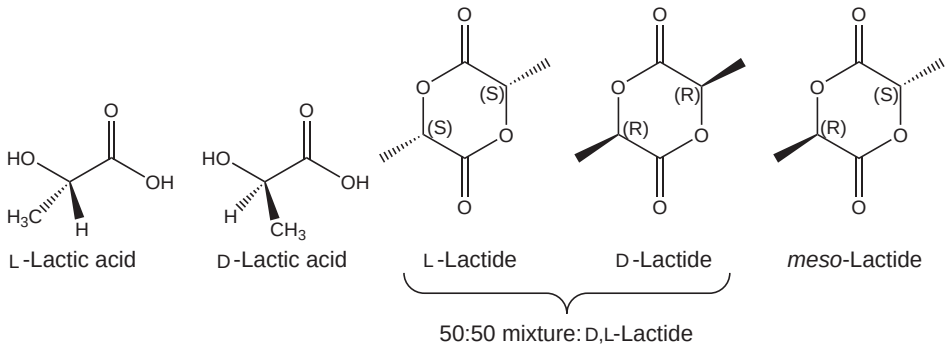

Figure 1.3: Stereoisomers of lactic acid and lactide

tailoring the macromolecular architecture and microstructure. As the monomers lactic acid and lactide themselves exist in different enantiomeric forms (Fig 1.3), the control of monomer stereochemistry by the enantiomer ratio in the feed and the stereoselection during the polymer chain growth provides a versatile family of homopolymers with particular different microstructures which have significant impact on the physical and mechanical properties of PLA. When pure D- or L-lactide is polymerised, optically pure poly(D-lactide) ($\{RRRR\}_n$) and poly(L-lactide) ($\{SSSS\}_n$) are obtained as isotactic polymers, respectively. The polymerisation of meso-lactide leads to the formation of syndiotactic PLA ($\{RSRS\}_n$). Poly(D,L-lactide) can be an atactic polymer with a random stereo sequence or a heterotactic enriched polymer containing the alternating units of D- and L-lactide ($\{RRSS\}_n$). Successive copolymerisation of D- and L-lactide generates stereoblock polymers.[5,20,24] For an overview of PLA microstructures see Fig. 1.4.

Optical pure isotactic PLA is a semi-cystalline, hard and rather brittle material and has an equilibrium crystalline melting point of 207°C, but due to impurities, slight racemisation and crystal defects the typical melting point ranges from 170 to 180°C.[13,19,25] A higher melting stereocomplex of a 1:1 mixture of L-PLA and D-PLA is also known (mp 230°C).[25,26] However, syndiotactic, heterotactic and atactic PLA are amorphous, transparent polymers with a softening point observed around 60°C.[13,27] The amorphous polymer is soluble in most common organic solvents such as ketones, tetrahydofurane, benzene, acetonitrile, dioxane and chlorinated solvents whereas the crystalline material is only soluble in chlorinated solvents or benzene at elevated temperatures.[13]

The further change of macromolecular architecture can be achieved by ring-opening polymerisation in the presence of multifunctional alcohols (e.g. pentaerythritol, sorbitol) or dendric macromolecules generating star-shaped and dendrimeric polymers, respectively.[1] Copolymerisation and blending are also proven tools for the modification of polymer properties. PLA with tailor-made properties is obtained by blending with other bio-based polymers like starch or polyhydroxyalkanoates or by copolymerisation of lactide with similar cyclic monomers like ε-caprolactone and glycolide to mention just a few.[6,16]

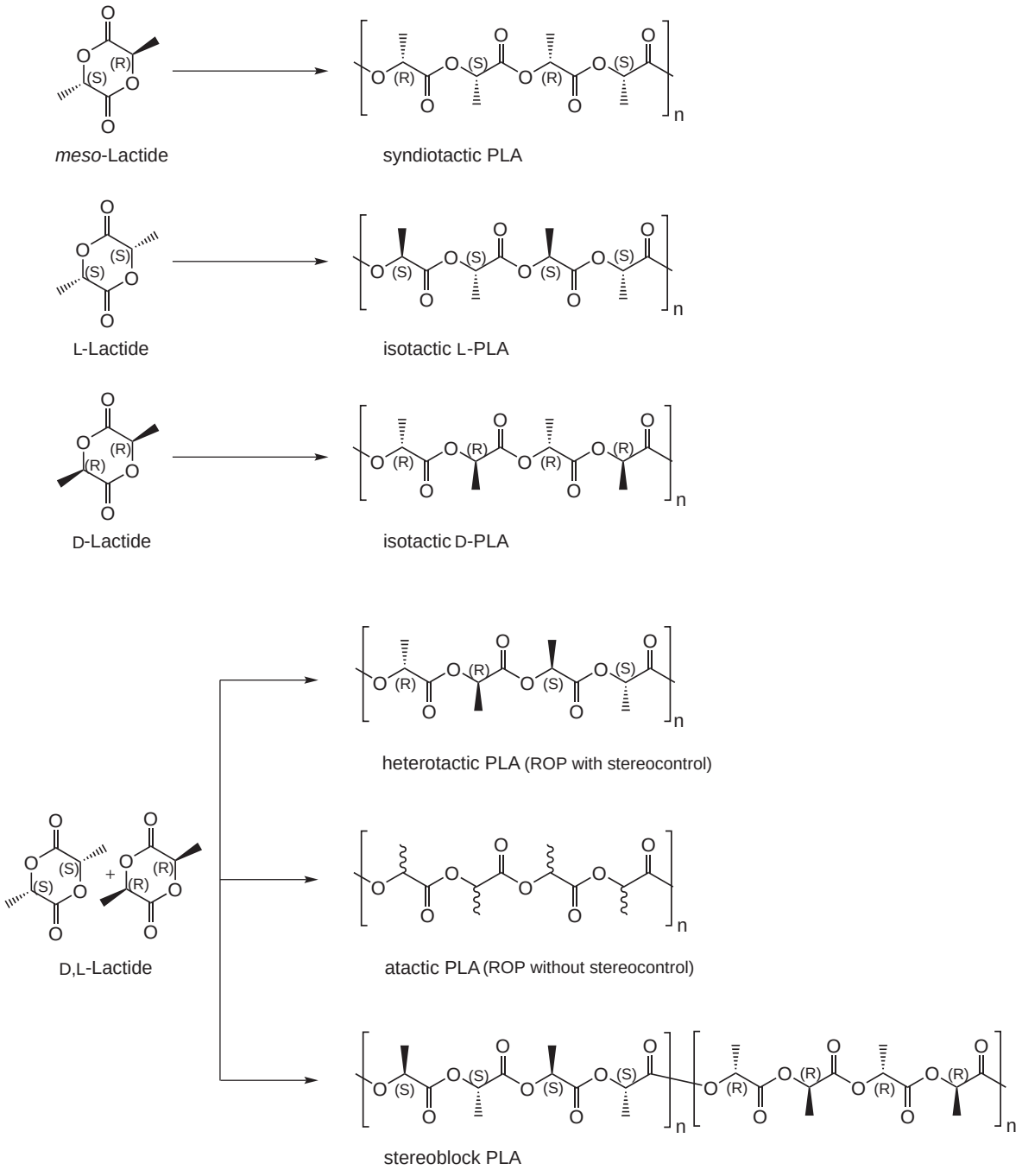

Figure 1.4: Microstructures of polylactide

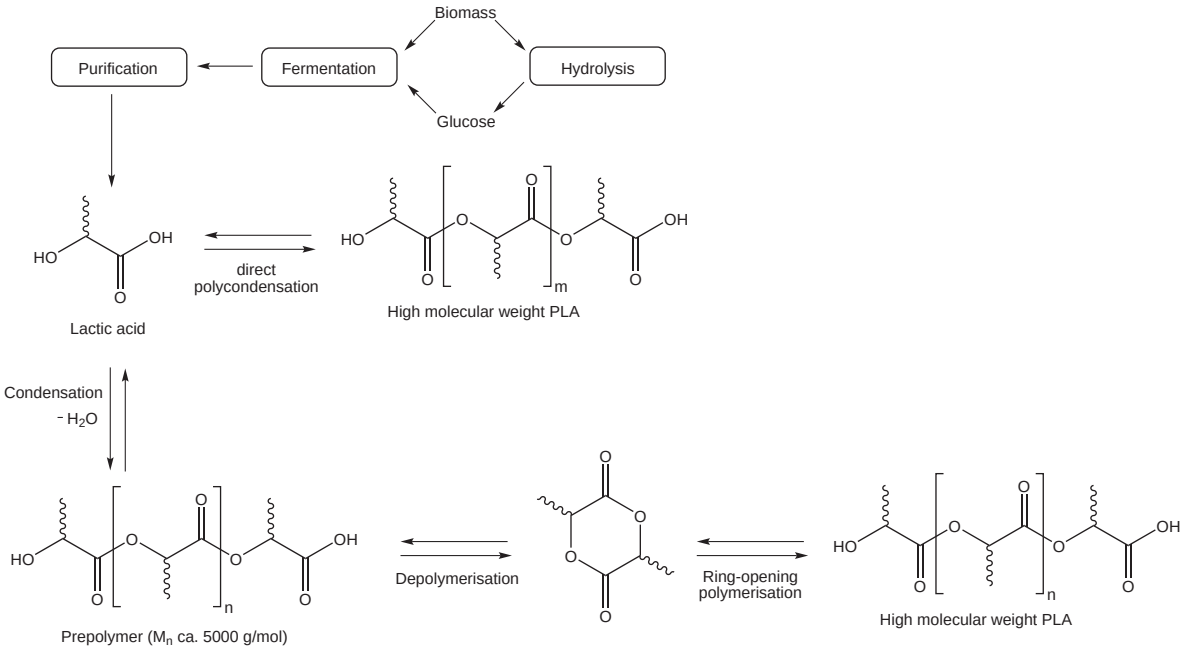

Figure 1.5: Schematic polymerisation routes to PLA

1.2.1 Production of PLA

PLA is available via two polymerisation routes: (1) by direct polycondensation of lactic acid or (2) by ring-opening polymerisation of lactide (see Fig. 1.5). Both processes start with lactic acid which can be obtained by fermentation of carbohydrates from agricultural renewable resources such as corn, sugar beets, agricultural by-products or even agricultural waste.[1,2,23] Due to the fact that if about 5 % of the worldwide annual plastic production were to be replaced by PLA only 0.7 % of the major plant resources for saccharides are needed. Therefore the current feedstock supply is more than adequate to meet foreseeable demand and not to compete against food application.[2]

Direct polycondensation of lactic acid

The direct polycondensation of lactic acid is the oldest technique to obtain PLA and was introduced by Carrothers and coworkers already in 1932.[28] The polymerisation proceeds by the successive reaction of polymer endgroups which results in the gradual growth of polymer chains. To obtain high-molecular weight polymers a high degree of conversion is necessary, and the main increase in molecular weight appears in the later process stages. But step-growth reactions like this are characterised by being equilibrium reactions and therefore the condensation product water has to be removed efficiently. This requires high vacuum, agitation and the percolation of inert gas.[1,2,13,17]

These drawbacks of the direct polycondensation process prevented the efficient production of high-molecular weight polymers for a long period till Mitsui chemicals succeeded in the

establishment of an azeotropic distillation process. A high-boiling solvent (e.g. diphenyl ether, bp 259°C) is used to drive the removal of water in the direct esterification process to obtain high-molecular weight PLA.[1,2]

Ring-opening polymerisation of lactide

High-molecular weight PLA can be directly synthesised by ring-opening polymerisation of lactide. Only low concentration of initiator and relatively low reaction temperatures (< 130°C, in solution) are needed to obtain full conversion of the monomer. By altering the monomer to initiator ratio, the molecular weight of the polymers can be adjusted. In addition, the setting of reaction conditions (e.g. the choice of initiator) allows for a good control of polymerisation and therefore provides tailoring of the properties related to the microstructure and the molecular architecture of the polymer and makes the ROP a precise tool for the production of well-defined polyesters.[1,2,13,17]
Cargill Dow LLC, a 50:50 joint venture of Cargill Incorporated and The Dow Chemical Company, introduced a low-cost continuous process for PLA production on the basis of solvent-free ring-opening polymerisation starting with lactic acid. In the first step, an aqueous solution of lactic acid is polymerised by continuous condensation to produce low molecular weight oligomers, also called prepolymers (Fig.1.5). In the presence of a tin catalyst which enhances the rate and selectivity of intramolecular cyclisation reaction, the prepolymers are depolymerised to lactide. The melt, containing a mixture of lactide stereoisomers and cyclic PLA oligomers, is then purified by distillation. Finally the ring-opening polymerisation, initiated by a tin catalyst, is done in the lactide melt to yield high-molecular weight PLA via a chain-growth reaction. After finished conversion the remaining monomer is removed under vacuum and recycled.[1,2,22,25]

1.2.2 Mechanisms of the ring-opening polymerisation

Depending of the nature of initiator four types of mechanisms are discussed for the ring-opening polymerisation of lactide: 1) the anionic polymerisation mechanism, 2) the cationic polymerisation mechanism, 3) the coordination insertion mechanism and 4) the activated monomer mechanism.

Cationic polymerisation mechanism

The cationic ROP of lactones occurs in the presence of alkylating agents, acylating agents, Lewis acids and protic acids. But the only initiators for which the cationic ROP of lactide was satisfactorily shown are according to Kricheldorf and co-workers triflic acid and methyl triflate.[13,30–33] The mechanism for methyl triflate is depicted in Figure 1.6.
At the beginning of the reaction, the monomer is activated by the methylation of one carbonyl oxygen atom generating a dioxocarbenium ion with an electrophilic activated O-CH bond.

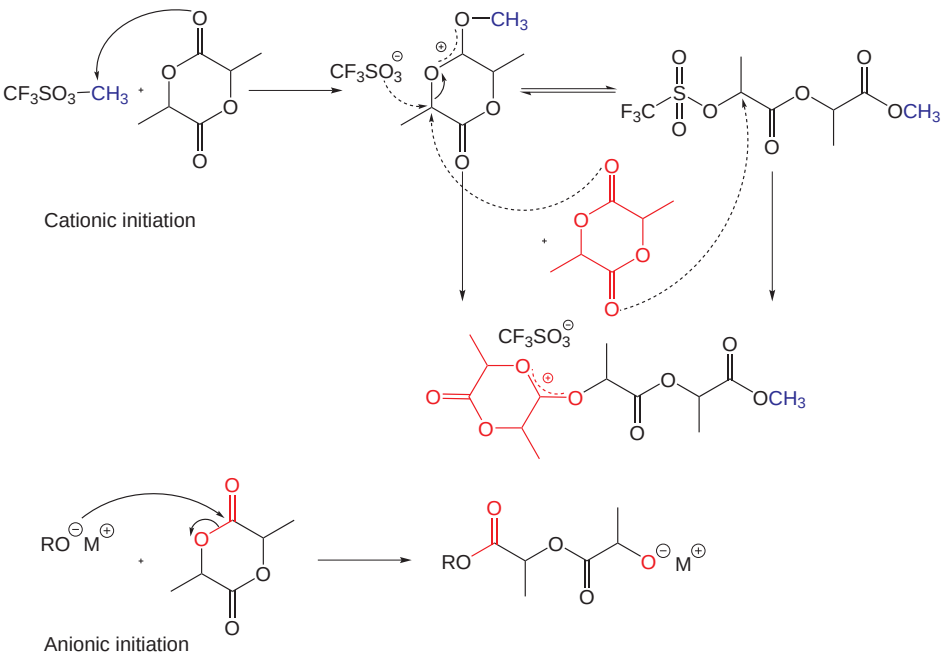

Figure 1.6: Cationic and anionic mechanism for the ROP of lactide[20]

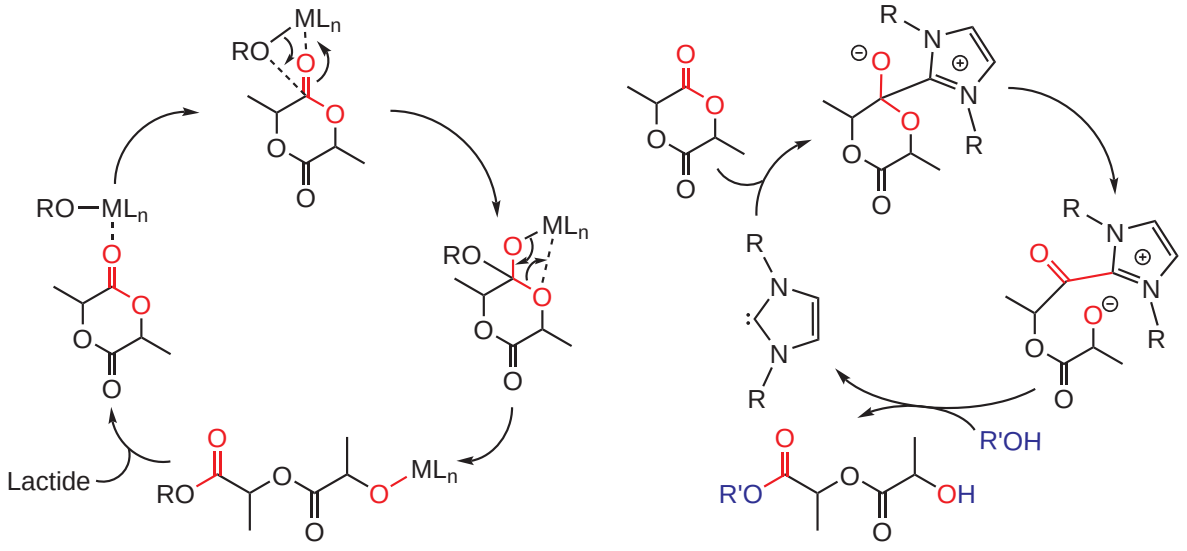

Figure 1.7: Coordination insertion mechanism for metal alkoxide complexes and activated monomer mechanism for organocatalysts and cationic initiators[20,29]

The exact subsequent progress of the reaction is inconsistently depicted in literature. Either the O-CH bond of the dioxocarbenium ion is cleaved by the nucleophilic attack of a second lactide molecule resulting in another electrophilic carbenium ion or the O-CH bond is attacked first by the triflate ion resulting in the ring-cleavage of the lactide molecule followed by the nucleophilic attack of the second lactide. However, in each case the propagation of chain growth proceeds via the subsequent nucleophilic attack of monomer molecules until a monofunctional nucleophil (e.g. water) terminates the reaction.
The cationic polymerisation for chiral monomers like lactide is not an attractive approach due to the high risk of racemisation (each propagation step involves a substitution at the chiral center), which also increases with temperature and the slow conversion rate at lower temperatures, which only yields low to moderate molecular weight polymers.[1,13,17,19,27,29–33]

Anionic polymerisation mechanism

Suitable initiators for the anionic ring-opening polymerisation of lactide are butyllithium and alkali metal oxides. The anionic initiation is shown in Fig. 1.6. First, the nucleophilic anion of the initiator attacks the carbonyl-C atom of the lactide molecule, resulting in the cleavage of the C-O single bond. The resulting alkoxide species continues to propagate as new anion. Although, this polymerisation reaction possesses higher conversion rates in comparison to the cationic ROP, there is still the risk of partial racemisation if the monomer is deprotonated by the initiator or the active chain end.[1,17,19,27,29]

Coordination insertion mechanism

The ROP of lactide occurs in the presence of metal complexes according to the coordination insertion mechanism (Fig. 1.7) which could be confirmed both experimentally by end group analysis and theoretically by density functional theory (DFT) calculations.
In the first step, the lactide is coordinated and thus activated by the Lewis acidic metal center for the subsequent nucleophilic attack of the metal alkoide group. The breaking of the ester C-O bond results in the ring cleavage of lactide while a new metal alkoxide species is generated. This species represents the growing chain, which possesses an ester end group.[17,20,34–39]

Activated monomer mechanism

The activated monomer mechanism is assumed for organocatalysts being strong nucleophiles like N-heterocyclic carbenes (Fig. 1.7) or H-bond donors. This mechanism starts with the nucleophilic attack of the carbene to the lactone. Hence, a tetrahedral intermediate forms and the lactide ring is opened subsequently generating the activated monomer in form of the acylimidazolium alkoxide zwitterion. The latter is protonated by the initiating alcohol or by the chain-end terminated alcohol of the growing polymer, providing an alkoxide that esterifies the acylimidazolium to generate the open-chain ester and the carbene. The probability of accepting

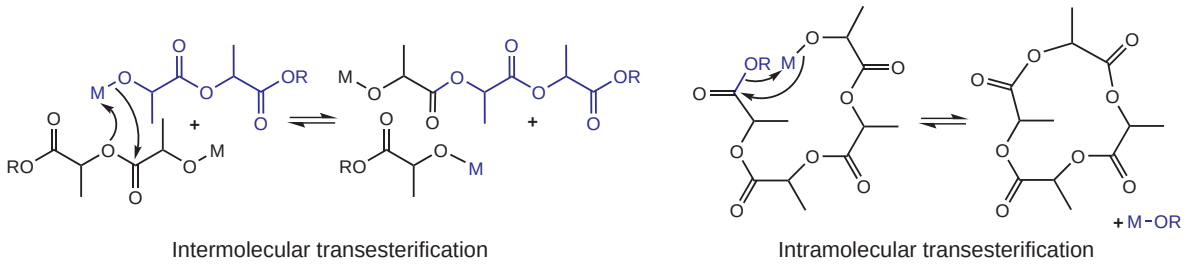

Figure 1.8: Transesterification reactions[20]

the activated monomer is equal for all chains, therefore all chains would grow at the same rate resulting in a living polymerisation.[20,29,40–43]

Side reactions

Controlled polymerisation reactions like the living ROP provide the possibility to predict and to regulate the physical properties of the obtained polymers. However, the living character of ROP can be observed only in the rarest cases due to side reactions like hydrolysis and chain transfer by transesterification (also designated as backbiting reactions). Intermolecular transesterification causes broadening of the molecular weight distribution, whereas intermolecular transesterification generates cyclic oligomers leading to the decrease of averaged molecular weight (see Fig. 1.8).[20]

1.2.3 Initiator systems for the ROP of lactide

During the past decades, various initiator systems have been investigated for the ROP of lactide. The initiator not only dictates the mechanism and therefore significantly influences the molecular weight and the molecular weight distribution but also affects the conversion rate and in some cases controls the stereochemistry of the obtained polymers. General requirements to initiators are well-behaved reaction control, high activity, fast initiation relative to propagation, minimal side reactions (transesterification), high tolerance towards impurities in the monomer, easy handling, colourlessness and odourlessness as well as low costs and toxicity.[44] The ring-opening reagent is often also named as catalyst. In coordination polymerisation reactions this is entitled due to the fact that the reaction takes place at the transition metal containing part of the catalyst. But on the other hand, the catalyst is not left unchanged by the reaction.[45] In the following both terms will be used equally.
The ability to open the lactone ring and to initiate the lactide polymerisation can be found at many combinations of Lewis acids and Lewis bases. In several cases co-initiators like alcohols are utilised to generate the Lewis base in situ. As single-site homogeneous catalysts several metal complexes with metals of the first to fourth group, some lanthanids, as well as iron, zinc, aluminium and tin have been investigated and a wide array of ligand frameworks has been

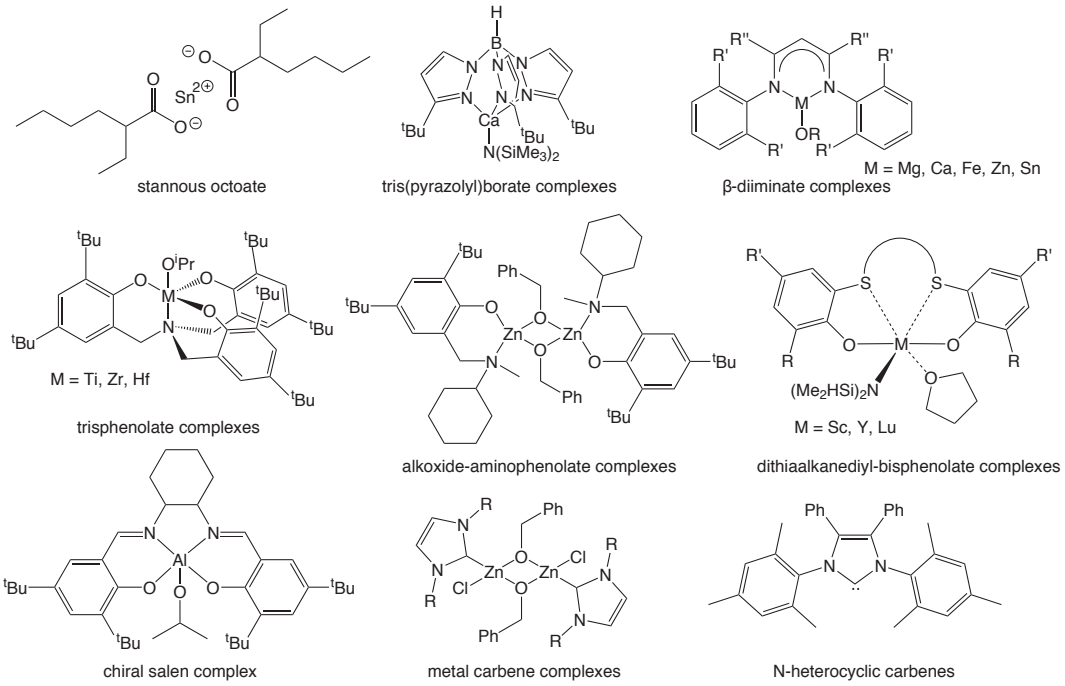

Figure 1.9: Selected initiator systems

employed, generating a library of catalysts. The most commonly used anionic ligand classes include simple alkoxides and carboxylates, β-diiminates, tris(pyrazolyl)borates, phenolates, guanidates, Schiff bases, bis(phosphinimino)methanides and salen ligands. Neutral ligand systems are less represented. Up to now, only complexes of N-heterocyclic carbenes (NHCs) were intensively investigated towards their ability to act as initiators in lactide polymerisation.[46,47] Growing attention has been attracted by organocatalysts.[29] Table 1.2 gives an overview of the most important classes of initiator systems and in Figure 1.9 selected initiators are depicted. Further examples are given in several reviews.[5,17,18,20,29,44,46,47]

For industrial production the most widely used initiator is still tin(II) ethylhexanoate ($SnOct_2$, see Tab. 1.2 No. 1 & 2). It is commercially available, easy to handle, possesses an excellent solubility in the monomer melt and provides PLA with very high molecular weight.[48] $SnOct_2$ is approved by the FDA but since stannous compounds possess critical toxicity properties and the fact that the initiator remains in most processes in the polymer questions the long term large-scale utilisation of this initiators, especially for biomedical and food packaging applications.[17,18,20]

Some of the ligand classes for single-site homogeneous catalysts are able to coordinate various metals and thus provide a wide range of applications. The latter include pure N-donor ligands, O-donor enriched ligands as well as a combination of N- and O- or S- and O-donor ligands. Tridentate N-donor ligands like tris(pyrazolyl)borates are capable of stabilising Mg, Ca, and Zn complexes that possess good ring-opening properties (No. 7).[49–51] A better accessibility to the Lewis acidic metal centre can be provided by the bidentate N-donors β-diiminates (No.

8-12)[24,52] and guanidinates (No. 13, see also Figure 1.18 c+d)[53–55] leading to high activity but at the same time high sensibility towards hydrolysis or decomposition. Complexes stabilised by β-diiminates have been reported for Mg,[24,50,56] Ca,[49,51] Fe,[57] Zn,[24,50,52,56] and Sn.[58]
O-donor enriched ligands like trisphenolates (No. 14) or calixarenes (No. 15) are well suited to build complexes with the highly charged metal ions of the fourth group.[59,60] Many ligand systems offer a combination of different donor functionalities. Amine-phenolates (No. 16 & 17),[61,62] imine-phenolates and Schiff base-phenolate systems (No. 18)[63] possess N- and O-donors whereas 1,ω-dithiaalkanediyl-bridged bisphenolates (No. 19 & 20) feature S- and O-donors for the coordination of rare earth metals and metals of the third group.[64,65]
Beside the catalytic active metal complexes with anionic ligand systems that complete their coordination sphere with further anionic co-ligands like alkoxides, carbanions or amides only a few examples of active initiator classes stabilised by neutral ligands are known to date. The utilisation of zinc complexes with the ligand (S)-N-ethyl-N-phenyl-2-pyrolidinemethanamine was reported by Jeong et al. They could demonstrate that an in situ generated zinc diethyl species initiate the ROP of lactide, but unfortunately the active catalyst could not yet be isolated.[46,78] Preliminary investigations of the reactivity of neutral phosphinimine-containing zinc complexes on a NMR scale show promising results.[79] Tolman and co-workers succeeded in the preparation of highly active but highly sensitive zinc carbene complexes (No. 22).[73] But carbenes themselves also possess excellent initiator properties for the lactide polymerisation (No. 25).[76] In addition to N-heterocyclic carbenes the group of ROP active organocatalysts includes pyridines (No. 23),[74] phosphines (No. 24),[75] guanidines (No. 26, see also Figure 1.18 a),[41] and H-bonding thiourea (No. 27).[77] In the presence of a co-initiating alcohol they show to some extent remarkable conversion rates as well as a good stereocontrol.
Until now several initiator systems have been reported that feature good stereoselection properties in the controlled ring-opening polymerisation of lactide in solution at low temperatures. The stereocontrol of initiators without stereocenters results via a chain-end-control mechanism allowing for the production of heterotactic or isotactic stereoblock polymers from a mixture of D- and L-lactide.[24,52] By application of complexes containing chiral ligands it is possible to obtain isotactic stereoblock polylactide through a site-control mechanism.[72,80] The breakthrough was achieved when the group around Feijen developed an aluminium-salen-alkoxide complex (No. 21) that was able to generate isotactic stereoblock PLA with long isotactic sequences from a D,L-lactide melt.[72] Very recently, Davidson and co-workers succeeded in synthesising a trisphenolate system (No. 14) based on zirconium that could produce heterotactic PLA in bulk at 130°C.[59] These efforts demonstrate the possibility to develop initiators that provide a good control of PLAs microstructure even under industrial applicable conditions.
Beside the organic or inorganic initiator systems, it is also possible to obtain PLA by enzymatic ring-opening polymerisation. Lipase from pseudomonas cepacia (lipase PC) as well as protease (proteinase K) were able to yield PLA. Due to the relatively low catalytic activity and the fact that the reaction took place only at higher temperatures, which are unusual for enzymatic reactions, the latter described system has up to now no industrial relevance.[1,2,48]

Table 1.2: Selective summary of initiator systems for the ROP of lactide and their reactivity

No.	PLA	Initiator (co-catalyst)	Solvents	Temp. in °C	Time	M/I	$(M_n)^a$ in g/mol	Reference
1	L	Sn(II)-octoate	-	100	4.5 h	22	990,000[f]	Pennings et al.[66]
2	L	Sn(II)-octoate (alcohols)	-	200	20 min	33	468,000[e]	Seppälä et al.[67]
3	L	Sn(II)-butoxide	-	120	19 h	1818	968,000	Duda et al.[68]
4	D,L	Zn-dilactate	-	150	96 h	2870	150,000[e]	Schwach et al.[69]
5	D,L	Li-t-butoxide	THF	20	1 h	400	40,000	Kasperczyk[70]
6	D,L	$Al(O^iPr)_3$	-	132	20 h	2085	155,000[d]	Jérôme et al.[71]
Initiators with anionic ligands								
7	D,L	Ca-trispyrazolylborate	THF	25	1 min	200	37,800	Chisholm et al.[49]
8	D,L	Zn-diiminate alkoxides	CH_2Cl_2	20	10 min	100	16,000	Chisholm et al.[56]
			THF		50 min		17,400	
9	D,L	Zn-ethyl-diiminate	CH_2Cl_2	20	20 min	200	63,300	Coates et al.[24]
10	D,L	Mg-diiminate (^{i}PrOH)	CH_2Cl_2	20	2 min	200	29,700	Coates et al.[24]
11	D,L	Fe-diiminate	Toluene	25	20 min	100	37,500	Gibson et al.[57]
12	D,L	Sn-diiminat-alkoxide/amide	Toluene	60	8 h	100	16,000	Gibson et al.[58]
13	D,L	Nd-guanidinate	Toluene	20	14 h	500	54,200	Trifonov et al.[53]
14	D,L	Zr-amine-trisphenolate alkoxide	-	130	6 min	300	32,300	Davidson et al.[59]
15	L	Ti-calixarene	-	130	14 h	2050	42,000[b]	Frediani et al.[60]
16	D,L	Zn-alkoxide-aminophenolate	CH_2Cl_2	25	18 min	1500	130,000[d]	Tolman et al.[61]
17	L	Zn-alkoxide-aminophenolate	CH_2Cl_2	25	2 h	100	15,380	Sobota et al.[62]
18	L	Zn-alkoxide Schiff basephenolate	Toluene	60	4.5 h	150	34,100	Lin et al.[63]
	D,L		CH_2Cl_2	25	24 h	50	9,900	
19	D,L	Y-dithiaalkanediyl-bisphenolate	THF	25	6 h	3000	226,000[d]	Okuda et al.[64]
20	D,L	Sc-dithiaalkanediyl-bisphenolate	THF	25	5 h	300	285,000	Okuda et al.[65]
21	D,L	Al-salen	Toluene	70	48 h	62	2,400[d]	Feijen et al.[72]
			-	130	48 h	200	21,600[d]	
Initiators with neutral ligands								
22	D,L	Zn-carbenes	CH_2Cl_2	25	16 min	200	30,000	Tolman et al.[73]
			-	140	5 min	200	20,000	
Organocatalysts								
23	D,L	4-(dimethylamino)pyridine (PhMeOH)	-	135	20 min	140	17,280	Hedrick et al.[74]
24	D,L	phosphines (PhEtOH)	-	135	24 h	60	6,768	Hedrick et al.[75]
25	D,L	NHCs (1-pyrenebutanol)	CH_2Cl_2	25	1 min	100	13,968[c]	Hedrick et al.[76]
26	L	guanidines (4-pyrenebutanol)	CH_2Cl_2	25	1 min	100	62,600	Hedrick et al.[41]
27	L	thiourea (4-pyrene-1-butanol)	CH_2Cl_2	25	24 h	20	5,200	Hedrick et al.[77]

[a] referred to polystyrene standards, [b] referred to PMMA standards, [c] determined by NMR, [d] absolute values, [e] M_w, [f] M_v

1.3 Guanidines - flexible donor ligands

Almost all catalytic systems used so far for the ring-opening polymerisation of lactide are stabilised by anionic ligands. To achieve high robustness combined with high catalytic activity, in this work neutral multidentate chelate ligands with N-donor functions are used. A neutral ligand class suited for the synthesis of catalytic active complexes are peralkylated guanidines. They show versatile coordination chemistry and offer advantageous donor properties. Despite of their neutral character, guanidines possess due to their effective intra-guanidine delocalisation a high donor strength which is comparable to that of β-diiminates.

1.3.1 Guanidines - Definition and properties

Guanidines are the imido derivates of urea which carry three nitrogen functions - one imine and two amine units. This special assembly is the origin of the most significant characteristic of guanidines - their extremely high basicity. Guanidines show one of the strongest Brønsted basicities under the organic neutral bases which is comparable to the hydroxyl ion (OH^-) and therefore they can be categorised as organic superbases.[81] This unique property originates from the ability to effectively delocalise a positive charge over the CN_3 core moiety after protonation under reversible conditions (Fig. 1.10).[81,82] By this intra-guanidine delocalisation, the resulting compounds possess a considerably enhanced basicity and N-nucleophilicity. The basicity is important for inducing a high Lewis-acidity on the central atom in the case of complexation.
The basicity of guanidines is influenced by their substituents:[82–88] Introduction of single alkyl substituents reduces the basicity due to the annihilation of the equivalence of the resonance structures of the corresponding guanidine cation, whereas multiple substitution leads to the compensation or even to the overcompensation of this effect because of the donor properties of the substituents. The efficiency of delocalisation and therefore the basicity decreases also in the case of full substitution with sterical demanding alkyl groups, which is caused by twisting of the planes of the substituents. Fixing of the guanidine moiety in a ring system consequently increases the basicity. In principle, the implementation of substituents with good donor properties like acceptor and aryl functions leads to the decrease of the basicity of guanidines.
The possibility to define the N-donor strength of the guanidine by introducing various substituents provides the advantage of influencing the coordination behavior of these N-donor

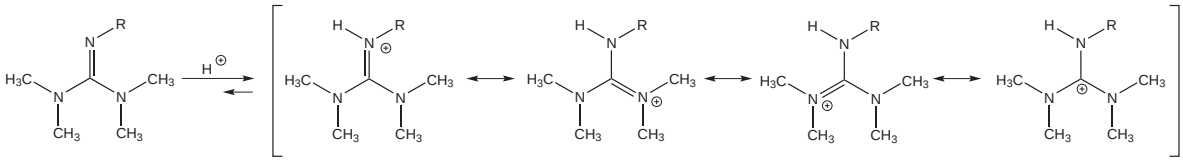

Figure 1.10: Delocalisation of the positive charge in a guanidinium cation

ligands in case of complexation and thus also allows controlling the complex properties.

The class of guanidines includes beside the neutral guanidines $[(R_2N)_2C{=}NR]$, the single negatively charged guanidinates(-1) $[(RN)_2CNR_2]^-$, the double negatively charged guanidinates(-2) $[(RN)_2C{=}NR]^{2-}$ (Fig. 1.11) and the guanidinium cations $[(R_2N)_2C{=}NRH]^+$. With exception of the guanidinium cations, which act in the complexes known so far only as counter ions,[89,90] the other guanidine ligands feature an versatile coordination chemistry and excellent donor properties giving them the opportunity of stabilising different coordination modes and complexes with metal ions of the whole periodic table of the elements.[54,91]

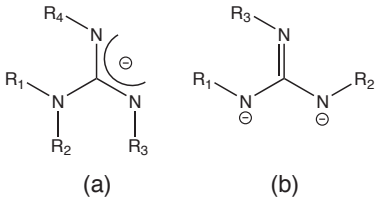

Figure 1.11: Single (a) and double (b) negatively charged guanidinates

1.3.2 Guanidines - Synthesis and modular assembly

The preparation of guanidines can be carried out in various ways. The simplest synthetic pathway to chelating guanidine systems is the reaction of α,ω-dihalide alkanes with guanidine derivates. However, this method does not support many different guanidine compounds and is characterised by long reaction times and the formation of byproducts resulting from side reactions.[92,93] The synthesis done by Bredereck et al. describes the formation of pentaalkyl and aryltetraalkyl guanidines from urea in the presence of phosphorus oxychloride. This method also suffers from long reaction times of up to eight hours.[86,87,94] An interesting preparation technique for the synthesis of penta-substituted guanidines, due to the possibility of providing unsymmetric substituted guanidines, is based on the reaction of isocyanide dichlorides with secondary amines.[84]

The most promising guanidine synthesis was developed by Kantlehner et al. which allows for the formal condensation of a substituted urea with a polyamine. The urea is converted into a strongly electrophilic chloroformamidinium salt which reacts with the amine to pentasubstitued guanidines or bisguanidines in good yields and relatively short reaction times.[95–97] In the first step, the peralkylated urea is converted with phosphorus oxychloride, thionyl chloride or phosgene into the corresponding chloroformamidinium chloride (see Fig. 1.12a). In analogy to the chloromethane-iminium salt intermediates formed in the Vilsmeier reaction[98] they were also referred to as Vilsmeier salts. In the second step, the reaction of the chloroformamidinium chloride with the amine under use of an auxiliary base like triethylamine leads first of all to the formation of the protonated guanidine, the guanidinium chloride. It is subsequently deprotonated with 50% aqueous potassium hydroxide solution and the free guanidine can be obtained as oil, crystals or waxy solid. The triethylammonium chloride arising from the auxiliary base in the course of the reaction can be deprotonated with stoichiometric amounts of sodium hydroxide solution (see Fig. 1.12b).

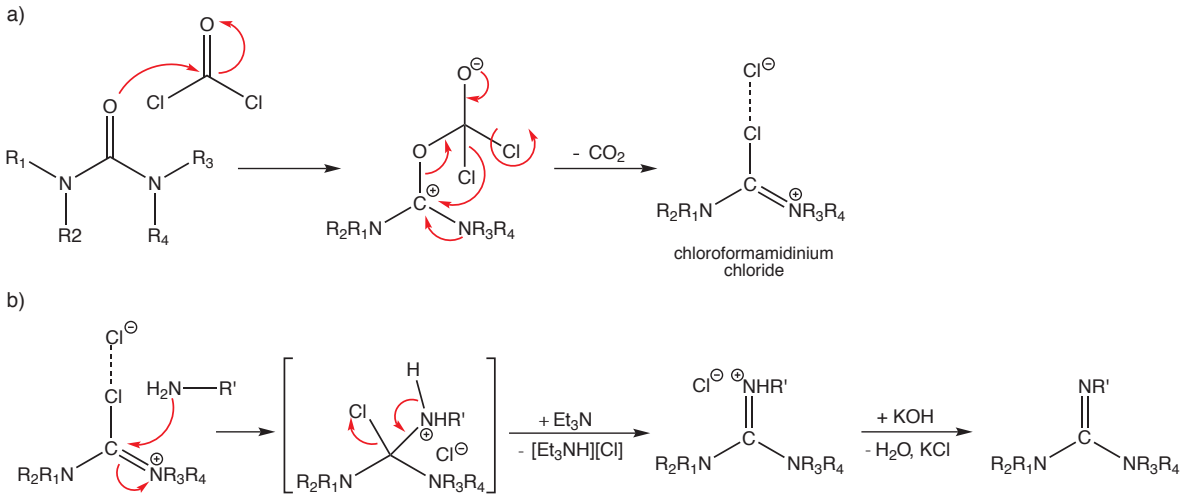

Figure 1.12: Mechanism of (a) the reaction of peralkylated urea with phosgene and (b) of the guanidine synthesis under use of an auxiliary base (triethylamine)

The special features of this synthetic method show their considerable advantages in the modular approach for the synthesis of ligands, developed by Henkel et al.[99,100] It allows combining various guanidine and spacer units in a building block technique and in the recent years a library of peralkylated bisguanidine ligands could be obtained.
Bisguanidines consist of two guanidine units which are combined via an organic spacer (see Fig. 1.13a). They can be synthesised under the above described conditions by the reaction of a bisamine with two equivalents of chloroformamidinium chloride (Fig. 1.14a). To modify the properties of guanidine-based ligands one guanidine moiety can be substituted by an amine group. This changes the electronic environment by replacing one "hard" guanidine function by a "soft" amine donor and simultaneously increases the accessibility to the metal centre in case of complexation by substituting one bulky guanidine by a non-bulky amine unit. These so-called guanidine-amine hybrid ligands combine the excellent donor properties of guanidines with the less steric hindrance of amines (Fig. 1.13b).[101,102] In analogy to the bisguanidines, guanidine-amine hybrid ligands could be obtained analogously by the combination of amine spacers with equimolar amounts of chloroformamidinium chloride (Fig. 1.14b). The flexible modular synthesis protocol of both, bisguanidines and guanidine-amine hybrids, permits the optimal adaption of the ligands to the corresponding applications. In that way, the choice of the spacer influences the denticity, the bite angle and the coordination geometry, whereas the utilisation of different functionalities at the guanidine and at the amine unit can control the σ-donor and π-acceptor properties of the coordinating nitrogen atoms. An overview of the guanidine (G), spacer (Sp) and spacer/amine units is given in Figure 1.15 and 1.16.

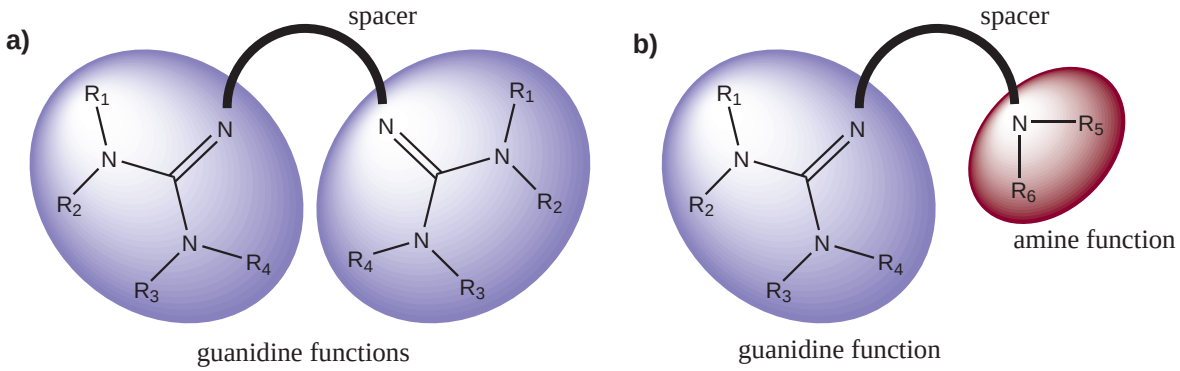

Figure 1.13: Modular framework of bisguanidines (a) and guanidine-amine hybrids (b)

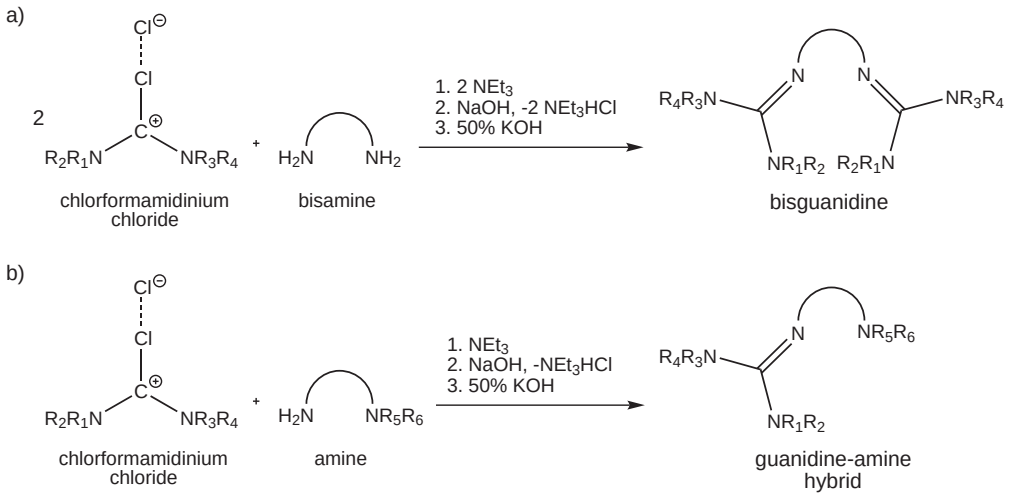

Figure 1.14: Synthesis of (a) a bisguanidine ligand and (b) of a guanidine-amine hybrid ligand

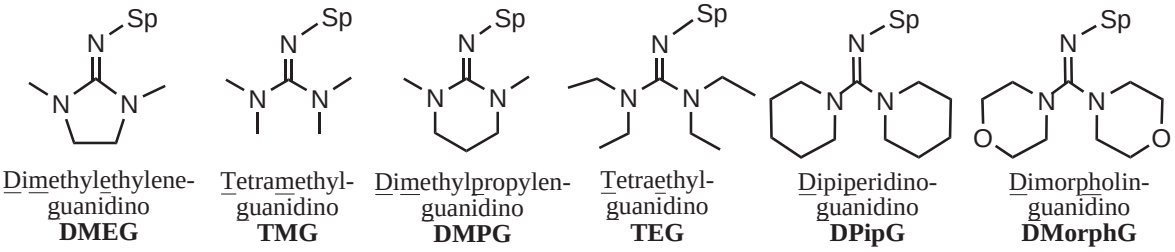

Figure 1.15: Overview of guanidine units

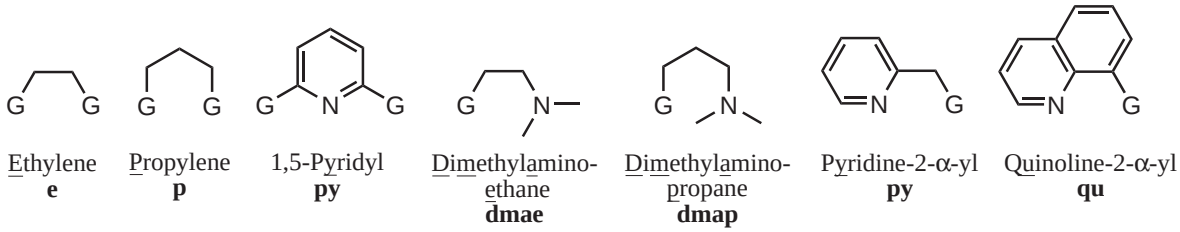

Figure 1.16: Overview of spacer and spacer-amine units

1.3.3 Zinc complexes stabilised by guanidine ligands

Due to their excellent donor properties, guanidine ligands are also suitable for the coordination of zinc and several examples of guanidine zinc complexes have already been reported in the literature.

Bunge et al.[103,104] succeeded in the preparation of the low-coordinate zinc complex [Zn(μ-1,1,3,3-tetraalkylguanidinate)(N($SiMe_3$)$_2$)]$_2$ (Fig. 1.17 a). In this dimeric complex the zinc atoms are bridged via two guanidinate ligands. In the complex ((2-guanidinyl)ethyl-cyclen)zinc(II)diperchlorate synthesised by Kimura et al.[105] the zinc atom is coordinated by four nitrogen atoms of the cyclen ring and possesses a fifth coordination by a guanidine function which is connected to the cyclen ring via an ethylene bridge (Abb. 1.17 b). In the group of Anders[106] chiral zinc guanidine complexes could be obtained by the reaction of N',N"-diisopropyl-(S)-2-(N,N-dialkylaminomethyl)pyrrolidine-1-carboximid-amide with zinc dichloride (see Figure 1.17 c). The first bischelate guanidine zinc complexes were prepared by Henkel et al., Ishikawa et al. and Himmel et al. While the Henkel group uses mostly bisguanidine ligands with aliphatic spacers, like 1,3-bis(N,N,N',N'-tetramethylguanidino)propane (btmgp) which was first synthesised by Pohl et al.[92] (Fig. 1.17 d[107]), Ishikawa[108] and Himmel[109,110] preferred in general the application of bisguanidine ligands with aromatic spacers (for example see Fig. 1.17 e[109]). In the group of Sundermeyer zinc complexes with trisguanidine complexes were synthesised for the first time. They can either coordinate the zinc atom with only two guanidine units[111] or they enclose the zinc atom by all three guanidine functions forming a kind of molecular cage[112] (for acetonitrile(1,1,1-tris{2-[N^2-(1,1,3,3-tetramethylguanidino)]-ethyl}amine)-zinc(II)diperchlorate see Fig. 1.17 f).

These examples do not only show the diversity of guanidine ligands but also the flexibility of the zinc cation concerning its coordination geometry and environment.

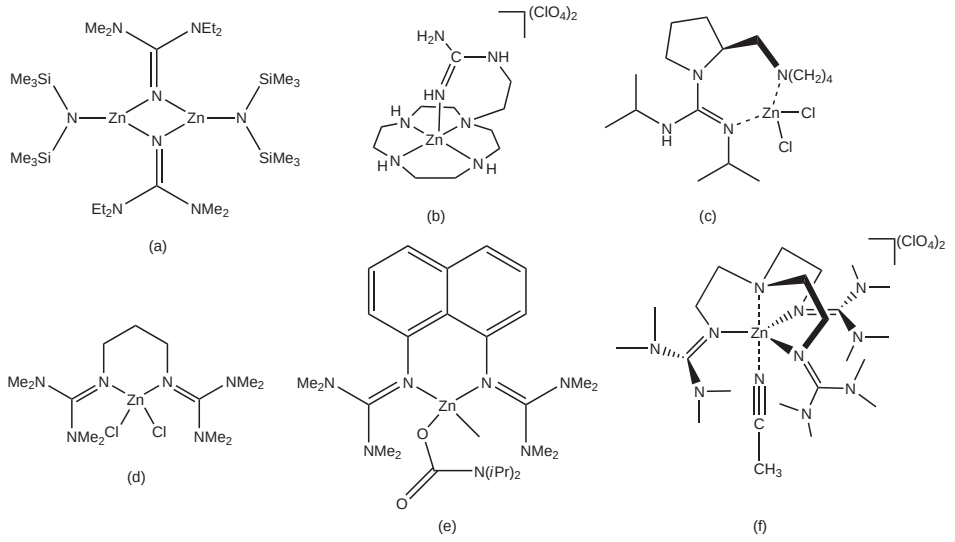

Figure 1.17: Selected zinc guanidine compounds

1.3.4 Guanidines - in the ROP of lactide

In the recent years, several groups demonstrated that guanidine containing compounds act as initiators in the ring-opening polymerisation of lactide, whether as organic molecule or salt or even as metal complex.

Waymouth and co-workers[40–42] investigated the guanidine based organocatalyst 1,5,7-triazabicyclo[4.4.0]dec-5-ene (hppH) (see Fig. 1.18 a), which shows high activity for the controlled solution-phase ROP of cyclic esters in the inert atmosphere of a glove box. This strong guanidine base (pK_a = 26.0 in acetonitrile) provides complete conversion of the monomer within seconds at room temperature for a degree of polymerisation of 100. In the Li[113] group two biogenetic guanidine carboxylates, creatinine acetate and creatinine glycolate, were found to act as single component initiators (Fig. 1.18 b). With initiator concentrations of 1 mol% and reaction times of up to 108 h, the bulk polymerisation at 130°C provides PLA in almost quantitative yields with controlled molecular weights and narrow polydispersities. Bunge et al.[104,114] could demonstrate in preliminary results that dimagnesium and dizinc aryloxides with ethoxide bridges stabilised by 1,1,3,3-tetramethylguanidine (Fig. 1.18 c), which exist as monomer in solution, are ROP active in an argon environment. But most investigations were focused on the application of guanidinate containing complexes. Trifonov et al.[53,115] synthesised bisguanidinate alkoxide complexes of lanthanides, whereas Arnold et al.[116] used monoguanidinate alkoxide complexes of lanthanum for lactide polymerisation.

However, Coles and co-workers[55,117,118] succeeded not only in developing mono- and bisguanidinate zinc complexes but also synthesised active complexes with hpp (for $[Zn(hpp)\{N(SiMe_3)_2\}]_2$ see Fig. 1.18 d). The main disadvantage of guanidinate based catalysts is their high sensitivity that only allows for polymerisations under highly inert reaction conditions which are not applicable for the lactide polymerisation on industrial scale.

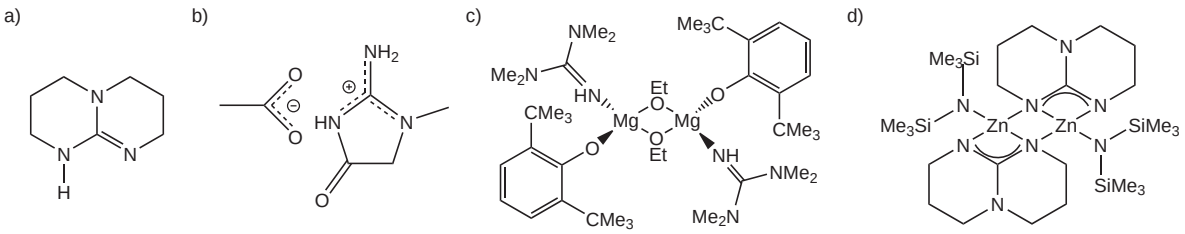

Figure 1.18: Selected guanidine-based initiators for the ROP of lactide

2 Objective and outline

2.1 Objective of this work

Conventional plastics possess excellent properties resulting in a wide variety of applications and since their introduction they revolutionised the quality of human life. Despite the numerous advantages of these materials, there are several drawbacks. Synthetic petrochemical-based polymers are sourced from non-renewable and dwindling fossil resources and their persistence that inhibit their degradation in nature leads either to an accumulation in the environment or to the increase of green house gases in case of combustion.
Modern approaches towards green and sustainable chemistry focus on the substitution of petrochemical-based plastics with biorenewable and biodegradable materials. One of the most auspicious candidates is polylactide due to its favourable chemical and physical properties allowing for processing on existing equipment and providing a wide range of application.
Consequently, the development of new single-site metal catalysts for the ring-opening polymerisation of lactide has seen tremendous growth over the past decade. However, their high polymerisation activity is often combined with high sensitivity which hinders industrial application. For this purposes, there is an exigent need for active initiators that tolerate air, moisture and small impurities in the monomer.

In this thesis the development and preparation of new neutral N-donor stabilised zinc complexes that are suitable for the initiation of lactide polymerisation are targeted.

In order to fulfill industrial requirements the development of an initiator system will be introduced that combines high catalytic activity with great robustness concerning the environment (air, humidity) and impurities in the monomer as well as high thermal stability, low-cost preparation and non-toxicity. For this reason, several neutral chelate ligand classes are investigated in this work such as bisguanidines, imidazolin-2-imine based guanidines, guanidine-amine hybrids, diamines and oxabispidines. Their application shall not only open up a new neutral ligand class for the synthesis of active single-site metal polymerisation catalysts, but also help to overcome the drawbacks of highly sensitive initiators.
Regarding the catalyst design, special emphasis is laid on the discovery of parameters influencing the complex properties (e.g. donor strength, denticity, substituents of the ligand, choice of zinc components). The elucidation of the reaction mechanism is a further challenge that is fo-

cused during this work. These findings will allow for the development of a structure-reactivity relationship leading to tailor-made catalysts with optimised features.
For a systematic investigation of the ligand impact, the modular assembled bisguanidine and guanidine-amine hybrid ligands are best qualified. Their flexible synthesis protocol permits the optimal adaption of compounds to the desired applications. Beside the ligand design, the study of the influence of the anionic component of the zinc salt is another key objective.
A further focus is set on the development of efficient single-site zinc complexes that are able to polymerise different cyclic ester monomers and hence disclose a broad field of applications.

Therefore, the introduction of a new application-oriented catalyst class into the field of the ring-opening polymerisation of cyclic esters, including the investigation of the influencing variables resulting in a structure-reactivity relationship and the elucidation of the polymerisation mechanism, is the main focus of this thesis.

2.2 Outline of the present work

The chapters of the present work are based on each other, but they can be read independently. The first chapter gives a thematic introduction including bioplastics, polylactide and guanidines to set a fundament for the further discussion.
The key objectives of this work are discussed in the Chapters 3 to 9. Chapter 3 provides an overview of the ligands utilised to obtain the corresponding zinc complexes and the synthesis of guanidine and guanidine-amine hybrid ligands as well as the concept of ligand design are presented. The preparation of bisguanidine zinc complexes and their application in lactide polymerisation is described in Chapter 4 whereas Chapter 5 compares the ligand class of imidazolin-2-imine based guanidines with their imidazolidine based guanidine analogues concerning the structural and electronic properties and their effects on the polymerisation activities of the corresponding zinc complexes. Chapter 6 introduces a library of zinc complexes stabilised by guanidine-pyridine ligands and presents the systematic screening of its contents towards the catalytic activity in lactide polymerisation. The identified influencing variables and a structure-reactivity correlation are discussed. The chapter ends with additional tests of the most active catalysts in the ROP of different monomers to evaluate their application range. In Chapter 7 mono- and polydentate guanidine ligands and their impact on the molecular structure as well as on the catalytic performance of their complexes are investigated. Chapter 8 comprehends studies concerning the ability of neutral aromatic and aliphatic ligands to stabilise zinc complexes that act as initiators in ring-opening polymerisation reactions. Chapter 9 deals with the elucidation of the mechanism of lactide polymerisation mediated by guanidine-pyridine zinc complexes using experimental and theoretical studies.

A conclusion of the results and achievements of this work together with an outlook presenting the perspective of further investigations based on this work is given in Chapter 10. Chapter 11 contains the experimental part of this thesis.

3 Ligand synthesis and design

This chapter gives an overview of all ligands that were synthesised or used to obtain the corresponding zinc complexes during this work. The synthesis of guanidines and guanidine-amine hybridligands as well as the concept of ligand design are presented.

3.1 Introduction

In coordination chemistry the ligand design is essential for modelling the features of the corresponding complexes. This permits the optimal adaption of compounds to the desired applications. In the case of guanidines this means that the possibility to define their basicity by introducing various substituents provides the advantage of influencing the coordination behavior of these N-donor ligands during complexation and thus allows controlling the complex properties. In addition, the choice of the spacer influences the denticity, the bite angle and the coordination geometry, whereas the utilisation of different functionalities at the guanidine and at the amine unit can control the σ-donor and π-acceptor properties of the coordinating nitrogen atoms. The size of the substituents also affects the accessibility to the complex centre which can be deciding when complexes are used as catalytic agents.

3.2 Results and discussion

3.2.1 Ligand synthesis

The ligands used within this work are in the majority of cases guanidines, which were prepared by the condensation of chloroformamidinium chlorides with polyamines according to a method introduced by Kantlehner et al. (see Section 1.3.2). The conversion of bisamines with two equivalents of chloroformamidinium chlorides leads to the formation of bisguanidine ligands, whereas the reaction of compounds bearing a secondary amine and another donor function with equimolar amounts of a chloroformamidinium chloride gives guanidine hybrid ligands. In order to synthesise polydentate guanidine ligands, the polyamine has to be reacted with an amount of a chloroformamidinium chloride that corresponds to the number of amine functions. The amines ethylenediamine (e), propylenediamine (p), 8-aminoquinoline

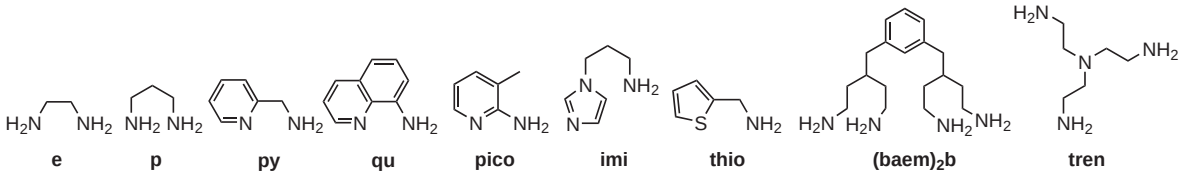

Figure 3.1: Overview of amine precursors

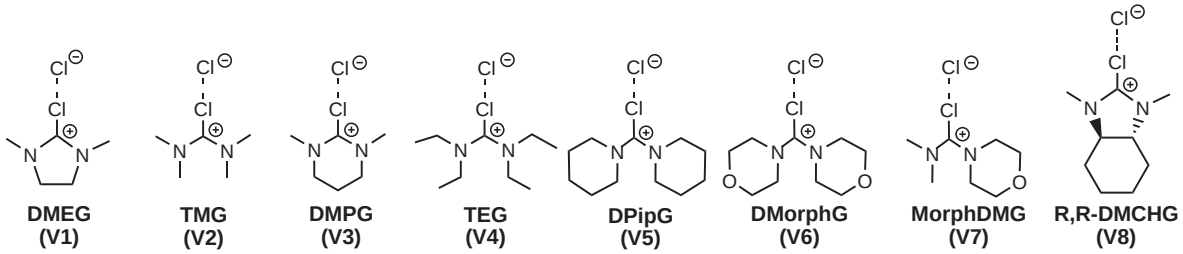

Figure 3.2: Overview of chloroformamidinium chloride precursors

(qu), 2-picolylamine (py), 2-amino-3-picoline (pico), 1-(3-aminopropyl)imidazole (imi), 2-thiophenmethylamine (thio), 2,6-bis[bis(2-aminoethyl)amino]methylbenzene ($(baem)_2b$) and tris(2-aminoethyl)amine (tren) served as spacer or spacer-amine units. As guanidine precursors the chloroformamidinium chlorides N,N,N',N'-dimethylethylenechloroformamidinium chloride (DMEG, **V1**), N,N,N',N'-tetramethylchloroformamidinium chloride (TMG, **V2**), N,N,N',N'-dimethylpropylenechloroformamidinium chloride (DMPG, **V3**), N,N,N',N'-tetraethylchloroformamidinium chloride (TEG, **V4**), N,N,N',N'-dipiperidylchloroformamidinium chloride (DPipG, **V5**), N,N,N',N'-dimorpholinochloroformamidinium chloride (DMorphG, **V6**), N,N,N',N'-morpholinodimethylchloroformamidinium chloride(MorphDMG, **V7**) and (R,R)-N,N,N',N'-dimethylcyclohexenechloroformamidinium chloride (R,R-DMCHG, **V8**) were used. In figure 3.1 and 3.2 the amines and the chloroformamidinium chlorides were summarised, respectively.
The remaining ligands are either commercially available or were provided by other groups in the context of a collaboration.

3.2.2 Bisguanidine and imidazoline based guanidine ligands

In the last few years, the application of bisguanidine ligands in the group of Prof G. Henkel, leading to the development of catalytic active copper complexes for oxidation reactions,[100] encouraged the investigations towards single-site metal catalysts stabilised by neutral bisguanidine ligands. In previous work[101] the bisguanidine ligand N^1,N^2-bis(1,3-dimethylimidazolidin-2-ylidene)ethane-1,2-diamine ($DMEG_2e$, **1**)[119] was used to synthesise zinc complexes and preliminary studies could demonstrate that they possess the potential to initiate the ring-opening polymerisation of lactide. Thus, the ligand as well as its complexes were resynthesised for further studies and the preparation of new complexes. To rate the influence of the guanidine moi-

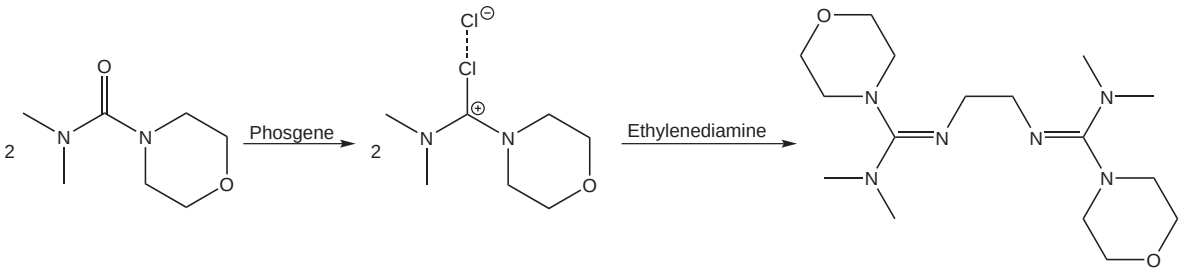

Figure 3.3: Schematic formation of MorphDMG$_2$e (**4**)

ety as well as the spacer unit, the well known bisguanidines 1,2-di[2N-(1,1,3,3-tetramethylguanidino)]ethane (TMG$_2$e, **2**)[111] and 1,3-bis(N,N,N',N'-tetramethylguanidino)propane (btmgp or TMG$_2$p, **3**)[92] were prepared to obtain the corresponding zinc complexes.
In order to influence the stereocontrol of initiators in the lactide polymerisation via chain-end-control, allowing for the production of heterotactic or isotactic stereoblock polymers, the unsymmetric substituted N,N,N',N'-morpholinodimethylchloroformamidinium chloride (MorphDMG, **V7**) was synthesised from the corresponding urea and the conversion with ethylene diamine leads to the formation of the unsymmetric substituted bisguanidine N',N"-(ethane-1,2-diyl)bis(N,N-dimethylmorpholine-4-carboximidamide) (MorphDMG$_2$e, **4**, see Fig. 3.3).
The ligand class of imidazoline based guanidines feature very similar properties compared to imidazolidine based guanidines, but they were regarded to be stronger donors.[120] To elucidate this effect in context of catalytic activity of the corresponding zinc initiators for the lactide polymerisation, the 1,2-bis(imidazolin-2-imino)ethane ligand N^1,N^2-bis(1,3,4,5-tetramethyl-1H-imidazol-2(3H)-ylidene)ethane-1,2-diamine (8MeBL, **5**), provided by the group of Prof. M. Tamm from the Technische Universität Braunschweig, was used to stabilise several zinc complexes that were compared to those of the associated DMEG$_2$e complexes.

3.2.3 Guanidine-amine hybrid ligands

Analogously to the bisguanidine ligand DMEG$_2$e the guanidine-amine hybrid ligands N-(1,3-dimethylimidazolidin-2-yliden)quinolin-8-amine (DMEGqu, **6**),[101,121] 1,1,3,3-tetramethyl-2-(quinolin-8-yl)guanidine (TMGqu, **7**),[101,121,122] N-(1,3-dimethylimidazolidin-2-yliden)pyridin-8-amine (DMEGpy, **14**)[101,121] and 1,1,3,3-tetramethyl-2-((pyridin-2-yl)methyl)guanidine (TMGpy, **15**)[101,121,123] were synthesised during previous studies and some of their zinc complexes showed the potential to initiate the ROP of lactide.[101] Therefore, the ligands as well as their complexes were resynthesised for further studies and the preparation of new complexes.
The ligands based on 8-aminoquinoline and 2-picolylamine show good coordination properties and in many cases relative easily provide single crystals of the corresponding zinc complexes suitable for X-ray diffraction and therefore enable the determination of the solid-state structure which is essential for the postulation of a structure-reactivity relationship. Thus,

these amines were reacted with several chloroforamidinium chlorides to investigate the influence of the guanidine moiety on the ligand properties. For example, the ligands containing TEG and DPipG units exhibit a high sterical demand. However, their complexes do not show favourable crystallisation properties and thus, ligands with DMorphG units were developed. They possess the same sterical demand as DPipG but due to the morpholine rings they show much better crystallisation behavior.
The unsymmetric MorphDMG and the chiral (R,R)-DMCHG guanidine moieties were developed to create ligands that possibly could influence the polymerisation properties of the corresponding zinc initiators during the polymer chain growth resulting in a stereocontrol of the obtained polymer. (R,R)-DMCHG was synthesised by the direct conversion of the enantiomeric pure bismethylated cyclohexanediamine compound. The reaction with 8-aminoquinoline resulted straightforward in the formation of N-((3aR,7aR)-1,3-dimethyl-1H-benzo[d]imidazol-2(3H,3aH,4H,5H,6H,7H,7aH)-ylidene)quinolin-8-amine ((R,R)-DMCHGqu, **13**, see Fig. 3.4).
In addition, various spacer units are utilised to investigate their influence. Ligands based on 2-amino-3-picoline possess a very small bite angle whereas ligands containing 1-(3-aminopropyl)-imidazole and 2-thiophenmethylamine exhibit a different donor functionality beside the guanidine N-donor.
Table 3.1 gives an overview of the synthesised guanidine-amine hybrid ligands.

Table 3.1: Overview of guanidine-amine hybrid ligands

Guanidine moieties	Amine moieties				
	qu	py	pico	imi	thio
DMEG (**V1**)	DMEGqu (**6**)	DMEGpy (**14**)	DMEGpico (**21**)	DMEGimi (**23**)	DMEGthio (**25**)
TMG (**V2**)	TMGqu (**7**)	TMGpy (**15**)	TMGpico (**22**)	TMGimi (**24**)	TMGthio (**26**)
DMPG (**V3**)	DMPGqu (**8**)	DMPGpy (**16**)			
TEG (**V4**)	TEGqu (**9**)	TEGpy (**17**)			
DPipG (**V5**)	DPipGqu (**10**)	DPipGpy (**18**)			
DMorphG (**V6**)	DMorphGqu (**11**)	DMorphGpy (**19**)			
MorphDMG (**V7**)	MorphDMGqu (**12**)	MorphDMGpy (**20**)			
(R,R)-DMCHG (**V8**)	(R,R)-DMCHGqu (**13**)				

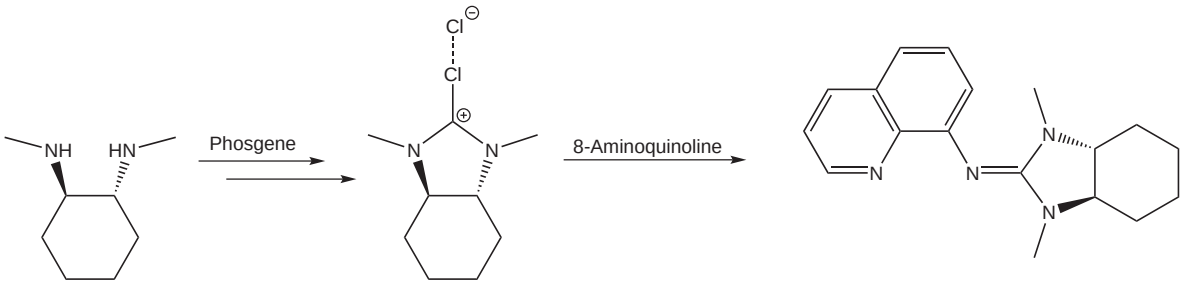

Figure 3.4: Schematic formation of (R,R)-DMCHGqu (**13**)

3.2.4 Polydentate guanidine ligands

In previous investigations it could be demonstrated that polydentate ligands like trispyrazolylborates (see section 1.2.3) are well suited to stabilise catalytic active complexes. In this context, the neutral tetradentate ligands 2,6-bis{[bis(2-aminoethyl)1,3-dimethylimidazolidin-2-ylidene]methyl}benzol ($DMEG_4(baem)_2b$, **27**) and 2,6-bis{[bis(2-aminoethyl)tetramethylguanidino]methyl}benzol ($TMG_4(baem)_2b$, **28**) were synthesised. However, single crystals of the corresponding zinc complexes were only available for the zinc chloride complex of $TMG_4(baem)_2b$. In this structure the ligand does not coordinate one zinc atom fourfold, but two zinc atoms in a bidentate manner. Thus, the tridentate ligands 1,1,1-tris{2-[2N-(1,3-dimethylethylenguanidino)]ethyl}amine ($DMEG_3tren$, **29**)[124] and 1,1,1-tris{2-[N^2-(1,1,3,3-tetramethylguanidino)]ethyl}amine (TMG_3tren, **30**)[112] first described by Sundermeyer et al., were prepared. In order to create a tridentate ligand that possesses a very high steric demand, the ligand 2',2',2"-(2,2',2"-nitrilotris(ethane-2,1-diyl))tris(1,1,3,3-tetraethylguanidine) (TEG_3tren, **31**) was developed.

3.2.5 Amine ligands

In order to elucidate the influence of the guanidine moiety in guanidine-amine hybrid ligands on the catalytic activity of the corresponding zinc complexes, zinc complexes with the pure amine, 8-aminoquinoline (qu, **32**), were prepared. Due to the fact that these complexes are also active initiators in the ROP of lactide, the interest was directed towards simple bischelating amine ligands like 2,2'-bipyridine (bipy, **33**) and 1,10-phenanthroline (phen, **34**), as well as N,N,N',N'-tetramethylethylenediamine (TMEDA, **35**) and N,N,N',N'-tetraethylethylenediamine (TEEDA, **36**) to find new simple and neutral ligands for the development of ROP active single-site metal catalysts. The latter ligands as well as their chiral cyclohexane derivates, (R,R)-N,N,N',N'-tetramethylcyclohexenediamine ((R,R)-TMCDA, **37**) and (R,R)-N,N,N',N'-tetraethylcyclohexenediamine ((R,R)-TECDA, **38**), were provided as corresponding zinc dichloride and zinc dibromide complexes by the group of Prof. C. Strohmann from the Technische Universität Dortmund.
The introduction of chirality centres in the complexes by chiral ligands should allow for the

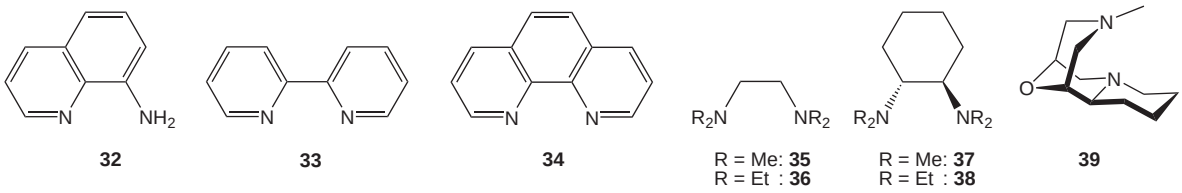

Figure 3.5: Overview of amine ligands

possibility to produce polylactide with a certain stereocontrol. However the chiral cyclohexane ligands could not affect heterotactic enriched PLA, so the chiral tricyclic 9-oxabispidine ligand (1R,2S,9S)-11-methyl-13-oxa-7,11-diazatricyclo[7.3.1.$0^{2,7}$]tridecane (9-oxa, **39**) synthesised by the group of Prof. M. Breuning from the Universität Würzburg was also tested. Figure 3.5 gives an overview of the applied amine ligands.

3.3 Conclusion

In this chapter the ligand classes used to stabilise catalytic active zinc(II) complexes for the ring-opening polymerisation of lactide are introduced. Their variety ranges from bisguanidine and imidazolin-2-imine based guanidine ligands over the very versatile guanidine-amine hybrid ligands to polydentate guanidines and even includes simple and chiral amines. In addition, the synthesis of guanidines and hybrid-guanidines as well as the concept of ligand design are presented.

4 Bisguanidine zinc complexes and their application in lactide polymerisation

A series of bisguanidine stabilised zinc complexes has been synthesised and investigated towards their activity in the bulk polymerisation of D,L-lactide. It could be demonstrated that these compounds are able to act as initiators in lactide polymerisation, and polylactides with molecular weights (M_w) of around 18,000 to 59,000 g/mol were obtained. Variation of the reaction temperature revealed that the molecular weights decrease with increasing temperature. Additionally, the correlation of the intrinsic viscosity with the molecular weight demonstrates that the obtained polymers are linear and structurally homogeneous.

4.1 Introduction

In previous work[101] the bisguanidine ligand N^1,N^2-bis(1,3-dimethylimidazolidin-2-ylidene)-ethane-1,2-diamine ($DMEG_2e$, **1**, Fig. 4.1)[119] was used to synthesise the zinc complexes $[Zn(DMEG_2e)Cl_2]$ (**1a**), $[Zn(DMEG_2e)(CH_3COO)_2]$ (**1b**) and $[Zn(DMEG_2e)_2][CF_3SO_3]_2$ (**1c**). Preliminary studies could demonstrate that they possess the potential to initiate the ring-opening polymerisation of lactide. Thus, the ligand as well as its complexes were resynthesised for further studies and the preparation of new complexes. To rate the influence of the guanidine moiety as well as the spacer unit, the well known bisguanidines 1,2-di[2N-(1,1,3,3-tetramethylguanidino)]ethane (TMG_2e, **2**)[111] and 1,3-bis(N,N,N',N'-tetramethylguanidino)-propane (btmgp or TMG_2p, **3**)[92] (see Fig. 4.1) were prepared to obtain the corresponding zinc complexes. The complex $[Zn(btmgp)Cl_2]$ (**3a**) was prepared in the group of Prof. G. Henkel

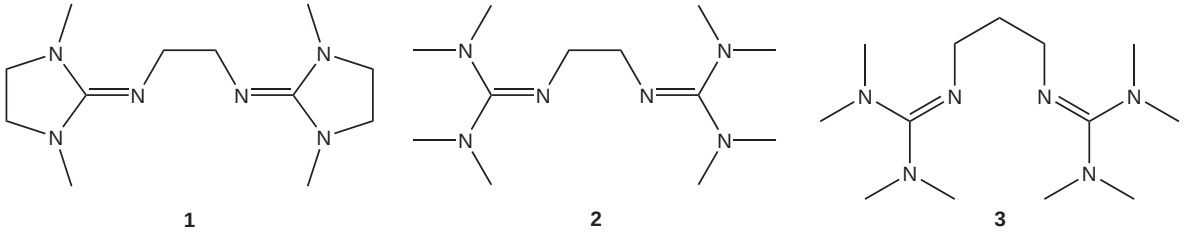

1 2 3

Figure 4.1: Bisguanidine ligands $DMEG_2e$ (**1**), TMG_2e (**2**) and btmgp (**3**).

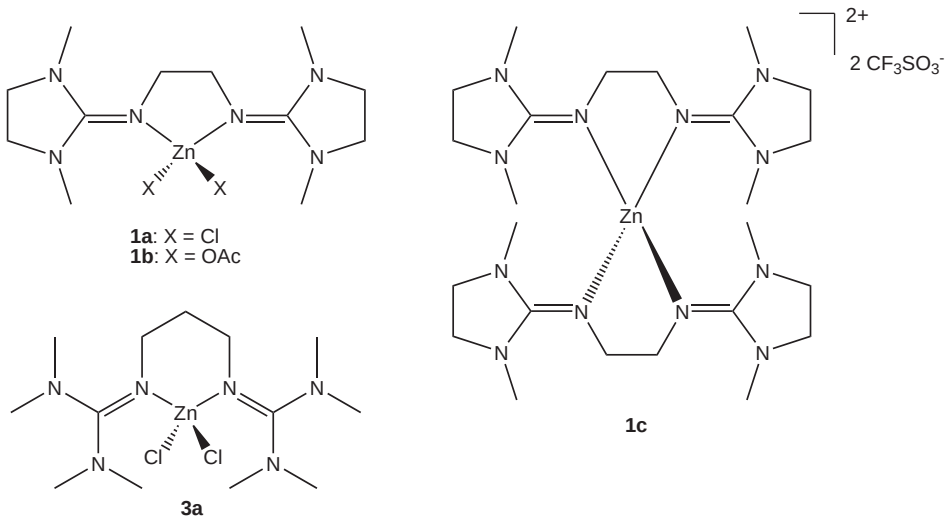

Figure 4.2: Schematic depiction of already reported bisguanidine zinc complexes.

before in context of coordination behaviour studies.[107] A schematic depiction of the already reported bisguanidine zinc complexes is given in Figure 4.2.

4.2 Results and discussion

4.2.1 Complex synthesis

The ligands **1**-**3** were prepared according to literature procedures.[92,111,119] Their reaction with zinc compounds ($ZnCl_2$, $Zn(CH_3COO)_2$, $Zn(CF_3SO_3)_2$, $Zn(C_6H_5COO)_2$) in a dry aprotic solvent (THF, MeCN) generates the bisguanidine zinc complexes **1a**-**3b**. They could be isolated as colourless crystals in yields of 34-98%. Table 4.1 gives an overview of the synthesised compounds. The described zinc complexes are stable towards air and moisture. They can be handled exposed to air without loss of activity. **1a**, **1c**, **1d** and **2a** are stable on air for months, while **1b**, **2b**, **3a** and **3b** are hygroscopic but stable on air for hours up to several days.

Table 4.1: Overview of the synthesised zinc complexes stabilised by bisguanidine ligands.

	$DMEG_2e$ (**1**)	TMG_2e (**2**)	btmgp (**3**)
$ZnCl_2$	$[Zn(DMEG_2e)Cl_2]$ (**1a**)	$[Zn(TMG_2e)Cl_2]$ (**2a**)	$[Zn(btmgp)Cl_2]$ (**3a**)
$Zn(CH_3COO)_2$	$[Zn(DMEG_2e)(CH_3COO)_2]$ (**1b**)	$[Zn(TMG_2e)(CH_3COO)_2]$ (**2b**)	$[Zn(btmgp)(CH_3COO)_2]$ (**3b**)
$Zn(CF_3SO_3)_2$	$[Zn(DMEG_2e)_2][CF_3SO_3]_2$ (**1c**)		
$Zn(C_6H_5COO)_2$	$[Zn(DMEG_2e)(C_6H_5COO)_2]$ (**1d**)		

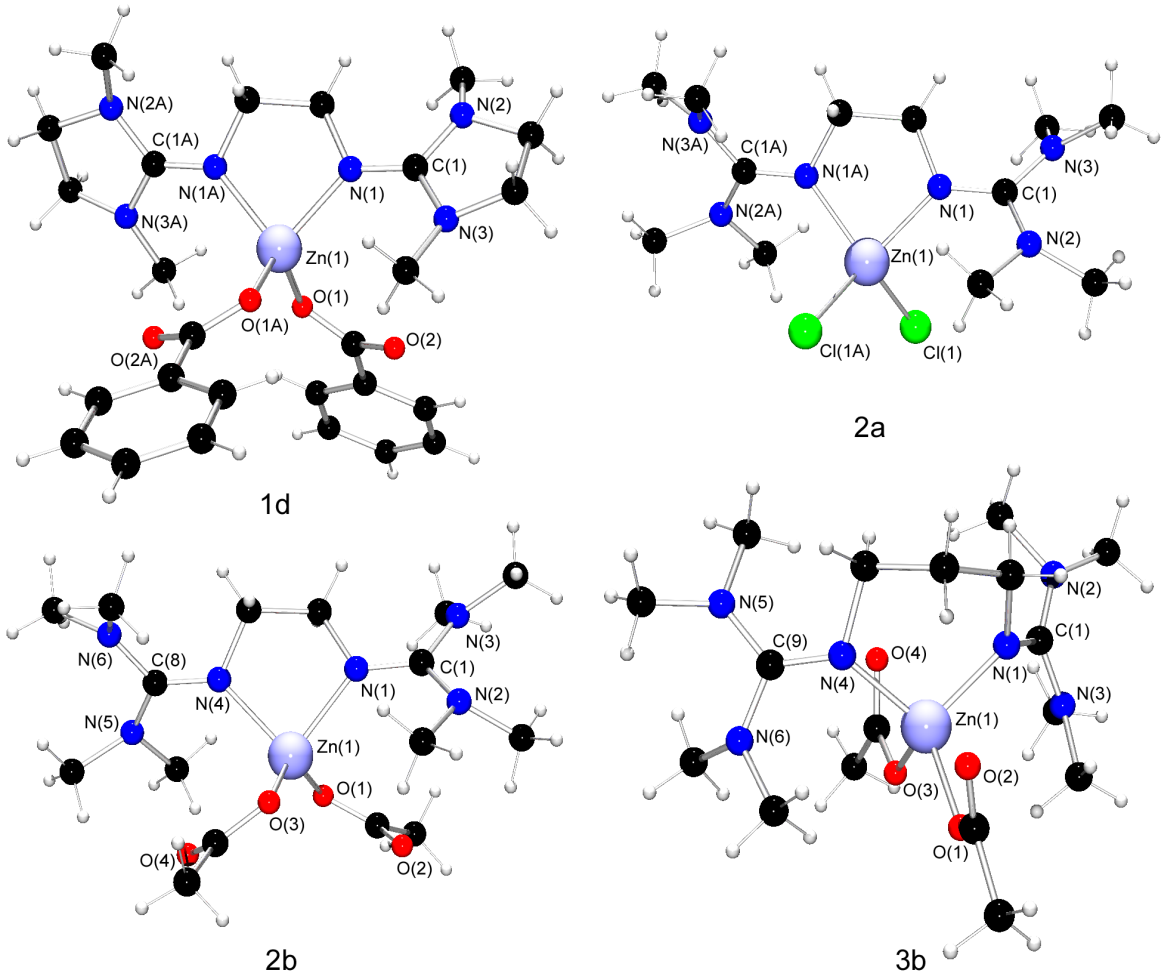

Figure 4.3: Crystal structures of $[Zn(DMEG_2e)(C_6H_5COO)_2]$ (**1d**), $[Zn(TMG_2e)Cl_2]$ (**2a**), $[Zn(TMG_2e)(CH_3COO)_2]$ (**2b**) and $[Zn(btmgp)(CH_3COO)_2]$ (**3b**) as determined at 120 K.

Molecular structures of the compounds **1d**, **2a**, **2b** and **3b** were determined by X-ray crystallography at 120 K (Fig. 4.3). In each complex of the series, except **1c**, the zinc atom is fourfold coordinated generating a distorted tetrahedral coordination environment. Two coordination sites are occupied in a chelating manner by the N-donor atoms of the bisguanidine forming a five- or six-membered heterocycle while the remaining coordination sites are occupied by chloride or acetate or benzoate ions, respectively. In **1c** the zinc atom is coordinated by the N-donor atoms of two $DMEG_2e$ molecules forming a coordination geometry that lies between tetrahedral and square-planar coordination (see Fig. 4.2).
Due to their structural similarity the chloride, acetate and benzoate complexes will be discussed conjoint in groups. Selected bond lengths and angles of the compounds are summarised in Table 4.2 and 4.3.

Complexes with zinc chloride: The structures of the zinc chlorido complexes **1a**, **2a** and **3a** are very similar to each other, especially **1a** and **2a** show only small differences. The two Zn-Cl distances in **1a** (2.260(2) Å) and **2a** (2.258(1) Å) are due to symmetric reasons equal in length whereas in **3a** one distance is slightly longer (2.233(1) vs. 2.306(1) Å). **1a** and **2a** exhibit with values of 2.038(2) and 2.042(1) Å Zn-N bonds of the same length. The corresponding values of **3a** turn out to be smaller (1.997(2), 2.008(2) Å), whereas the lengths of the C=N bond of the guanidine moieties are identical in all three complexes (av. 1.310 Å). As mentioned before, the zinc atom in each complex is coordinated in a tetrahedral manner. However, the bite angles of 86.2(1) (**1a**), 85.0 (1) (**2a**) and 97.0(1) (**3a**) are too small for a ideal-typic tetrahedral geometry, resulting in a distortion. This distortion is reflected in the angle between the ZnN_2 and the $ZnCl_2$ plane (**1a**: 74.5, **2a**: 70.6, **3a**: 89.0°) which is 90° in a tetrahedron. Thus, the flexible propylene spacer of the btmgp ligand in **3a** leads only to a slight distortion compared to those observed for **1a** and **2a**.

Table 4.2: Selected bond lengths [Å] and angles [°] of **1a**,[101] **2a** and **3a**.[107]

	1a	**2a**	**3a**
Zn-N	2.038(2)	2.042(1)	1.997(2), 2.008(2)
Zn-Cl	2.260(1)	2.258(1)	2.233(1), 2.306(1)
C_{gua}-N_{gua}	1.309(3)	1.309(2)	1.307(3), 1.316(3)
C_{gua}-N	1.381(3), 1.354(3)	1.365(2), 1.366(2)	1.354(3), 1.363(3), 1.356(3), 1.356(3)
N-Zn-N	86.2(1)	85.0(1)	97.0(1)
$\angle(ZnCl_2, ZnN_2)$	74.5	70.6	89.0

Complexes including zinc acetate and zinc benzoate: The complexes **1b**, **2b**, **3b** and **1d** are also very similar. This is for example reflected in the Zn-O and C_{gua}-N_{gua} distances. Their values are each equal, both in the complexes themselves and within the complex group (Zn-O: av. 1.967, C_{gua}-N_{gua}: av. 1.308 Å). The distances between the zinc atom and the N-donor atoms differ slightly and increase from **3b** (av. 1.999 Å) over **1b** (av. 2.025 Å) and **1d** (2.055(2) Å) to **2b** (av. 2.068 Å). The bite angles of the coordinated bisguanidines strongly depend on their spacer unit. In complexes with the ethylene bridged ligands the bite angle is substantially smaller (**1b**: 86.2(1), **2b**: 84.4(1), **1d**: 85.7(1)°) than in the complex with the propylene bridge (**3b**: 100.2(1)°). This effect is also reflected in the angle between the ZnN_2 and the ZnO_2 plane. The corresponding value of **3b** is with 86.3° higher than those for **1b** (76.3°) and **2b** (80.4°). But the highest value is observed for **1d** (88.1°) due to the coordination of the sterical demanding benzoate ligands.

Table 4.3: Selected bond lengths [Å] and angles [°] of **1b**,[101] **2b**, **3b** and **1d**.

	1b	**2b**	**3b**	**1d**
Zn-N	2.011(2), 2.038(2)	2.051(2), 2.085(2)	1.998(2), 2.000(2)	2.055(2)
Zn-O	1.969(2), 1.956(2)	1.971(2), 1.975(2)	1.967(2), 1.968(2)	1.961(2)
C_{gua}-N_{gua}	1.308(2), 1.305(2)	1.301(2), 1.312(2)	1.307(3), 1.307(3)	1.316(3)
C_{gua}-N	1.367(3), 1.371(3), 1.364(3), 1.368(3)	1.367(2), 1.381(2), 1.364(3), 1.369(2)	1.353(4), 1.368(3), 1.360(3), 1.365(3)	1.370(3), 1.364(3)
N-Zn-N	86.2(1)	84.4(1)	100.2(1)	85.7(1)
$\measuredangle(ZnO_2, ZnN_2)$	76.3	80.4	86.3	88.1

4.2.2 Polymerisation activity

In preliminary studies **1a**, **1b** and **1c** could demonstrate that they possess the potential to initiate the ring-opening polymerisation of lactide. Thus, these complexes were extensively investigated towards their polymerisation properties. For this purpose, D,L-lactide and the initiator (I/M ratio 1:500 or 1:1000) were heated to 135°C, 150°C and 165°C. After a reaction time of 24 or 48 h, the polymer melt was dissolved in dichloromethane, and then the polylactide was precipitated in cold ethanol, isolated and dried in vacuum at 50°C. In order to specify the catalytic activity of the complexes, the polymer yield was determined and the molecular weights as well as the polydispersity of the obtained PLA were measured by gel permeation chromatography (see Table 4.4). The tacticity was analysed by homonuclear decoupled ^{1}H NMR spectroscopy. In general, the monomer conversion as well as the weight averaged molar mass values (M_w) of the corresponding polymer are higher for **1a** than for **1b** and **1c**. At the standard temperature for lactide polymerisations, which is 150 °C,[125] **1c** shows the best results for M_w (32,000-38,000 g/mol) and the highest yields. The acetate complex **1b** exhibits a weaker performance. This indicates an effect of the anionic component of the zinc salt on the catalytic activity of the corresponding zinc complex. Interestingly, an increase in reaction time from 24 to 48 h results in a decrease of conversion and molecular weight. Similar observations were reported by Chisholm et al.[126] and Schwach et al.,[127] who considered side reactions like the interchain or intrachain transesterification as well as the chain-transfer reaction to be responsible for this effect. In this context, it is expected that a decrease of reaction temperature would lead to minor side reaction effects.[126,127] The experimental results (see Figure 4.4) support this hypothesis. At 135 °C, **1a** and **1b** provide considerably larger polymers than at higher temperatures, with M_w values up to 59,000 g/mol. Thus, the values of molecular weights achieved by the present procedure decreased with increasing temperature. Only in the case of **1c** this temperature effect is not pronounced, because a maximum for the degree of polymerisation is reached at 150 °C.
In order to study the structural characteristics of the synthesised polymers, the intrinsic viscosities were correlated with the molecular weight M of the polymers. As outlined in Figure 4.5, all polymer samples exhibited an unique trend. For polymers large enough, this correlation is described by the Mark-Houwink equation:[128] $[\eta] = K \cdot M^{\alpha}$.

Table 4.4: Polymerisation of D,L-lactide by **1a**-**3b**

Initiator		Temp. [°C]	Time[a] [h]	M/I	Yield [%]	M_w [g/mol]	PD[b]	P_r[c]
None		165	24	-	0	-	-	
$[Zn(DMEG_2e)Cl_2]$	**1a**	135	24	500	82	59,000	1.7	
$[Zn(DMEG_2e)Cl_2]$	**1a**	150	24	500	79	38,000	1.7	0.50
$[Zn(DMEG_2e)Cl_2]$	**1a**	150	24	1000	70	33,000	1.6	
$[Zn(DMEG_2e)Cl_2]$	**1a**	150	48	500	67	33,000	1.6	
$[Zn(DMEG_2e)Cl_2]$	**1a**	165	24	500	61	34,000	1.6	
$[Zn(DMEG_2e)(CH_3COO)_2]$	**1b**	135	24	500	63	35,000	1.6	
$[Zn(DMEG_2e)(CH_3COO)_2]$	**1b**	150	24	500	69	24,000	1.6	0.50
$[Zn(DMEG_2e)(CH_3COO)_2]$	**1b**	150	24	1000	86	28,000	1.8	
$[Zn(DMEG_2e)(CH_3COO)_2]$	**1b**	150	48	500	66	18,000	1.6	
$[Zn(DMEG_2e)(CH_3COO)_2]$	**1b**	165	24	500	46	22,000	1.5	
$[Zn(DMEG_2e)_2][CF_3SO_3]_2$	**1c**	135	24	500	82	37,000	1.7	
$[Zn(DMEG_2e)_2][CF_3SO_3]_2$	**1c**	150	24	500	83	38,000	1.6	0.50
$[Zn(DMEG_2e)_2][CF_3SO_3]_2$	**1c**	150	24	1000	93	34,000	1.9	
$[Zn(DMEG_2e)_2][CF_3SO_3]_2$	**1c**	150	48	500	83	32,000	1.7	
$[Zn(DMEG_2e)_2][CF_3SO_3]_2$	**1c**	165	24	500	51	23,000	1.6	
$[Zn(DMEG_2e)(C_6H_5COO)_2]$	**1d**	150	24	500	80	27,000	1.7	0.50
$[Zn(TMG_2e)Cl_2]$	**2a**	150	24	500	87	45,000	1.9	0.53
$[Zn(TMG_2e)Cl_2]$	**2a**	150	48	500	92	39,000	1.8	
$[Zn(TMG_2e)(CH_3COO)_2]$	**2b**	150	24	500	87	24,000	1.9	0.49
$[Zn(TMG_2e)(CH_3COO)_2]$	**2b**	150	48	500	81	22,000	1.7	
$[Zn(btmgp)Cl_2]$	**3a**	150	24	500	71	26,000	1.7	n.d.
$[Zn(btmgp)Cl_2]$	**3a**	150	48	500	64	26,000	1.6	
$[Zn(btmgp)(CH_3COO)_2]$	**3b**	150	24	500	46	20,000	1.6	n.d.
$[Zn(btmgp)(CH_3COO)_2]$	**3b**	150	48	500	47	18,000	1.5	

[a] Reaction times were not necessarily optimised; [b] PD = M_w/M_n where M_n is the number-average molar mass;

[c] From analysis of the ^1H homonuclear decoupled NMR spectrum using the equation $P_r^2 = 2$ [sis].[24]

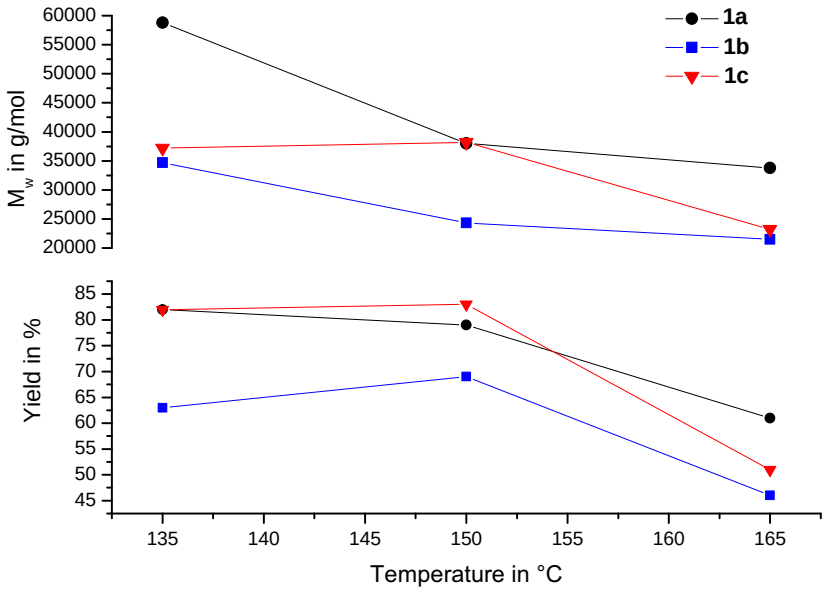

Figure 4.4: Dependence of weight-averaged molar mass (M_w) and yield vs. reaction temperature for the three initiator systems **1a**-**1c**.

The linear behaviour and unique trend of all examined polymers indicates that the obtained PLA samples are structurally homogeneous and linear. Hence, the structure of the polymers reported herein is independent of the initiator used and the averaged values for the Mark-Houwink constants at 35 °C in THF were calculated to be α = 0.59 and K = 0.068. Further values for different temperatures and solvents were reported by Rafler et al.[129] and Schindler and Harper.[130]

The bisguanidine zinc complexes **1d**-**3b** were also screened regarding their activity in the solvent-free polymerisation of lactide. In contrast to **1a**-**1c**, they were only tested at the standard conditions (M/I = 500, T = 150°C, see Table 4.4).

It could be proven that all tested bisguanidine zinc complexes possess catalytic activity in the ROP of lactide. The activity of **1d** is higher than those of the corresponding zinc acetate complex **1b**. The obtained yield lies in the same range of those of **1c**, but the M_w values are smaller. The complexes stabilised by TMG_2e, **2a** and **2b**, show by trend a slightly better performance than their $DMEG_2e$ stabilised analogues. In contrast, the btmgp analogues provide PLA in lower yields and with lower M_w values than the complexes with ethylene bridged ligands. This may be also due to the fact that the latter complexes are slightly hygroscopic and therefore not as stable as the other complexes.

The P_r values of 0.49 or 0.53 imply that in general the complex structure of the investigated zinc guanidine compounds shows no ability to affect the tacticity of the formed polymer.

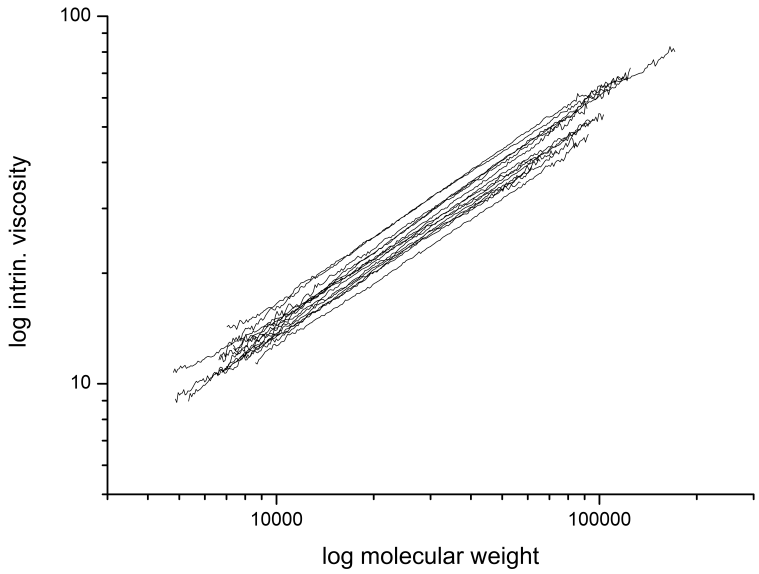

Figure 4.5: Mark-Houwink plot of PLA obtained by **1a**-**1c**. The calculated mean value for α is 0.59 and for K is 0.068 at 35 °C in THF.

4.3 Conclusion

This chapter deals with the synthesis and complete characterisation of aliphatic bisguanidine-stabilised zinc complexes that were proven to be active initiators in the ring-opening polymerisation of D,L-lactide. PLAs with molecular masses (M_w) of around 18,000-59,000 g/mol could be obtained. In complexes with the same bisguanidine ligand the activity of the initiator depends on the anionic component of the zinc salt. Complexes with zinc triflate and zinc dichloride seem to be the most auspicious candidates for application in the ROP of lactide. The catalytic activity of complexes including the same anionic component of the zinc salt increases from btmgp via $DMEG_2$e to TMG_2e.

By changing the reaction temperature it could be shown that lower temperatures allow side reactions to be avoided during the polymerisation and thus give higher molecular masses. Moreover, the Mark-Houwink correlation demonstrates that the obtained polymers are linear and homogeneous. Compared to other systems, the guanidine zinc complexes possess an advantageous combination of properties: they are nontoxic, comparably stable and give PLAs with good M_w values at industrial conditions. This makes the guanidine zinc systems a promising class of catalysts for the ring-opening polymerisation of D,L-lactide.

5 New insights into the lactide polymerisation with neutral N-donor stabilised zinc complexes: Comparison of imidazoline vs. imidazolidine based guanidine complexes

Two imidazoline based guanidine zinc complexes [Zn(8MeBL)Cl_2] (**5a**) and [Zn(8MeBL)$(OAc)_2$] (**5b**) were synthesised, completely characterised and investigated for their activity in the solvent-free ring-opening polymerisation of D,L-lactide. It could be shown that these compounds are able to act as efficient initiators in the lactide polymerisation, and polylactides with molecular weights (M_w) of around 23,000-55,000 g/mol could be obtained. **5a** and **5b** exhibit an advantageous combination of robustness towards humidity and high activity in the polymer melt. A comparative DFT study on **5a** and **5b** and their imidazolidine counterparts revealed that the two complex series possess a strikingly similar electronic structure. Although the imidazoline containing ligand is more basic, its zinc complexes have only a slightly higher positive charge on the zinc atom in comparison to the corresponding imidazolidine based guanidine complexes. Accordingly, their activity in the initiation of the ring-opening polymerisation is increased which is directly related to the Lewis acidity of the zinc atom. These findings provide more insight into the mechanism of the lactide polymerisation with neutral N-donor stabilised zinc complexes.

5.1 Introduction

Targeting a controlled activity of robust initiators in the ROP of D,L-lactide, the research was extended towards further neutral guanidine-type ligand classes like the imidazoline based guanidines.[131–133] Bisguanidine ligands, in general, attain their unique properties from their ability to delocalise a positive charge over the guanidine moiety (see Fig. 5.1a). The enhanced basicity and nucleophilicity of their compounds is caused by this delocalisation. In bisguani-

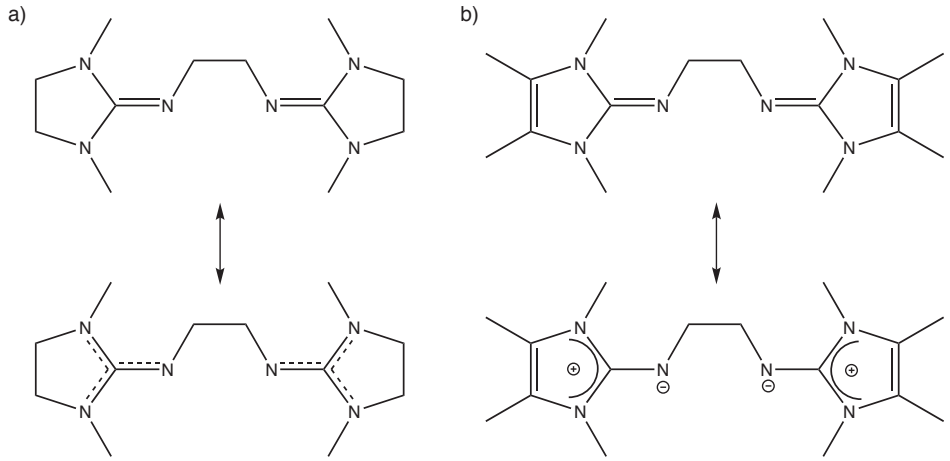

Figure 5.1: (a) The imidazolidine based bisguanidine ligand $DMEG_2e$ (**1**)[119] and (b) the imidazoline based bisguanidine ligand 8MeBL (**5**)[132] and their resonance structures.

dines which contain unsaturated substituents, e.g. the imidazoline based guanidines, the electron density can be effectively delocalised in the imidazole rings inducing a strong polarisation of the exocyclic C=N bond (Fig. 5.1b).[134] Thus, this ligand family is typically regarded to be a stronger donor compared to guanidines containing saturated substituents.[120]
The basicity is important for inducing a high Lewis acidity on the zinc atom. For the lactide ROP with zinc guanidine systems, the correlation was found that complexes with greater positive charge on the zinc atom exhibit a greater catalytic activity (see Section 6.1). Furthermore, the ligand class of imidazoline based guanidines has shown to be able to coordinate a great variety of metals in several coordination modes.[131–133,135–137] For a direct comparison of their zinc chemistry and the polymerisation activity of the corresponding zinc complexes, the two bischelating ligands $DMEG_2e$ (**1**)[119] and 8MeBL (**5**)[132] were chosen for the comparative studies because of their structural similarity (Fig. 5.1). This similarity allows the electronic attributes that promote lactide polymerisation by neutral N-donor stabilised zinc complexes to be elucidated. The 1,2-bis(imidazolin-2-imino)ethane ligand N^1,N^2-bis(1,3,4,5-tetramethyl-1H-imidazol-2(3H)-ylidene)ethane-1,2-diamine (8MeBL, **5**) was provided by the group of Prof. M. Tamm from the Technische Universität Braunschweig.
Herein, the synthesis and characterisation of the first zinc imidazoline bisguanidine complexes is presented. An extensive DFT based comparative discussion concentrates on their structural and electronic similarities and differences to their imidazolidine counterparts. The imidazoline based bisguanidine zinc complexes proved to be active initiators in D,L-lactide bulk polymerisation, and polylactides with molecular weights (M_w) up to 55,000 g/mol and polydispersities (M_w/M_n) around 2 could be obtained.

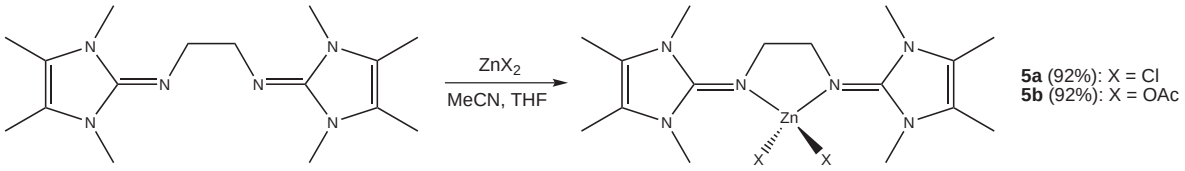

Figure 5.2: Synthesis of zinc complexes **5a** and **5b** stabilised by the imidazolin-2-imine based guanidine ligand.

5.2 Results and discussion

5.2.1 Complex syntheses

The imidazoline bisguanidine ligand 8MeBL (**5**) was synthesised by the reaction of the imidazolin-2-imines[120] Imine^{Me} with 1,2-ethyleneditosylate and subsequent deprotonation with KO^{t}Bu in high yields.[132] The reaction of **5** with the zinc salts $ZnCl_2$ and $Zn(CH_3COO)_2$ in a dry, aprotic solvent (MeCN, THF) resulted straightforwardly in the formation of the corresponding zinc complexes [Zn(8MeBL)Cl_2] (**5a**) and [Zn(8MeBL)$(OAc)_2$] (**5b**) (Fig. 5.2). They could both be isolated as colourless crystals in good yields of 92 %. Single crystals of the complexes were obtained by cooling the saturated solution slowly to room temperature. The isolated crystalline solids are stable towards moisture and air. They can be handled and stored in air for several days, whereas the corresponding imidazoline type guanidines and zinc salts are sensitive towards hydrolysis or rather hygroscopic.
The molecular structures of the compounds **5a** and **5b** (Fig. 5.3 and 5.4) were determined by X-ray crystallography. In these complexes, the zinc atom is fourfold coordinated by the two N-donor atoms of the imidazoline ligand and two chlorine ions or two acetate ions, respectively. In order to compare the structural properties of the zinc complexes stabilised by imidazoline based guanidine ligands, these complexes are discussed together with their imidazolidine counterparts [Zn($DMEG_2e$)Cl_2] (**1a**) and [Zn($DMEG_2e$)$(OAc)_2$] (**1b**) which are already described in Chapter 4.

5.2.2 Comparative discussion of the molecular structures in the crystal

The crystal structures of all four zinc complexes are very similar. Selected bond lengths and angles of the compounds are collected in Table 5.1. In all the complexes the zinc atom is fourfold coordinated, whereby two coordination sites are occupied in a chelating manner by the N-donor atoms of the guanidine ligands to form a five-membered heterocycle. The distances between the zinc atom and the N-donor atoms do not differ very much. Their values are ranging from 2.005(1) to 2.038(2) Å. In **1a** the Zn-Cl distances are equal in length (2.260(1) Å) due to symmetry. In **5a** one Zn-Cl bond is longer than the other. The longer bond measures 2.277(1) Å and the shorter 2.241(1) Å and thus their averaged value fits very well with the Zn-Cl distance of **1a**. In the diacetato complexes the distances of the Zn atom and the coordinated O

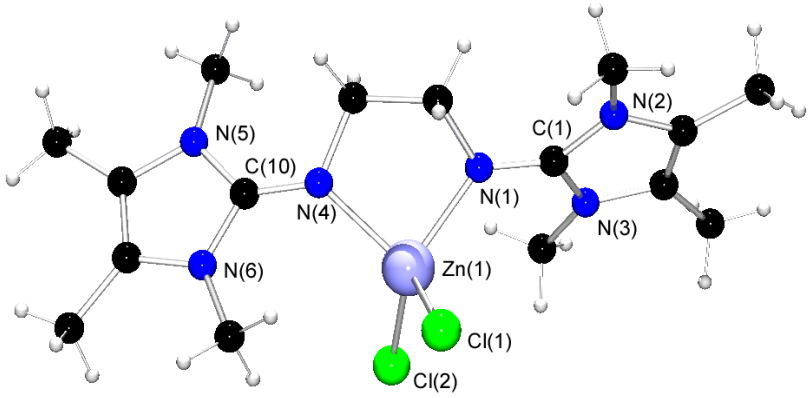

Figure 5.3: Crystal structure of $[Zn(8MeBL)Cl_2]$ (**5a**) as determined at 120 K.

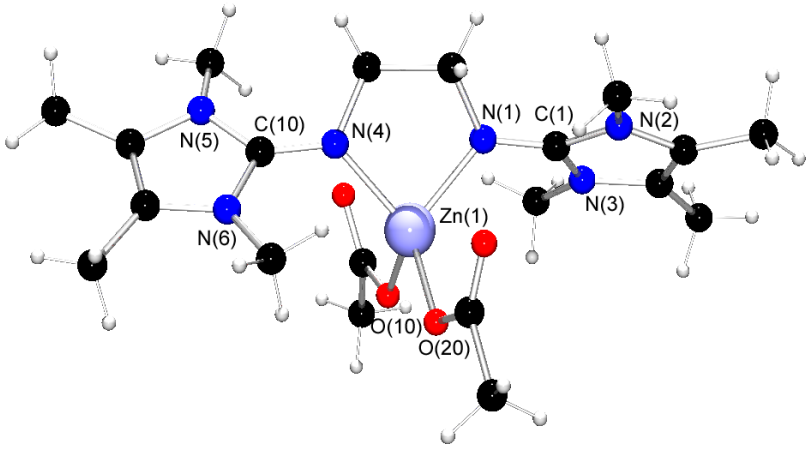

Figure 5.4: Crystal structure of $[Zn(8MeBL)(OAc)_2]$ (**5b**) as determined at 120 K.

atom are equal within the limits of significance (av. 1.961 Å). The different electronic character of the imidazoline and the imidazolidine based guanidine ligands is reflected in the C_{gua}-N_{gua} distances. In **5a** and **5b**, the positive charge is delocalised in the N_2C_3-heterocycle leading to longer C_{gua}-N_{gua} bonds (av. 1.320 Å) whereas in the imidazolidine bisguanidine zinc complexes **1a** and **1b** the positive charge is delocalised over the guanidine CN_3 backbone resulting in slightly shorter C_{gua}-N_{gua} distances (av. 1.307 Å). This different delocalisation behaviour is also observed by regarding the angles between the $C_{gua}N_3$ and the $N_{ring}C_3$ planes. Whereas those values of **5a** and **5b** are with av. 5.6 and 6.3° quite small indicating the planarity of the N_2C_3-heterocycle caused by the high delocalisation of the positive charge, the values of **1a** and **1b** are with av. 15.5 and 14.9° significantly higher. This shows the stronger deviation of the heterocycle atoms from the ring plane and therefore the tendency of imidazolidine guanidine systems not to delocalise the positive charge over the heterocycle but over the guanidine moiety.

In all four complexes, the coordination geometry of the zinc atom is dictated by the bite angles of the chelating ligands which possess an averaged value of 85.9° and therefore differ considerably from the angle expected for an ideal-typic tetrahedron (109.47°). This leads to a distorted tetrahedral coordination geometry which is also reflected in the angle between the ZnX_2 (X = Cl, OAc) and the ZnN_2 planes. In ideal-typic tetrahedral coordination geometry it is 90°, but in the complexes **5a** and **5b** described here these angles are with 82.1(1) (**5a**) and 84.9(1)° (**5b**) slightly smaller. However, in the imidazolidine guanidine zinc complexes **1a** and **1b** these angles are with 74.5(1) and 76.6(1)° even smaller than in the imidazoline complexes.

Table 5.1: Selected bond lengths (Å) and bond angles (°) of **5a**, **5b** and their imidazolidine counterparts **1a** and **1b**.

	5a	**1a**	**5b**	**1b**
Zn-N	2.019(1), 2.032(1)	2.038(2)	2.005(1), 2.006(1)	2.011(2), 2.038(2)
Zn-X (X = Cl^-, OAc^-)	2.241(1), 2.277(1)	2.260(1)	1.955(1), 1.965(1)	1.956(2), 1.969(2)
C_{gua}-N_{gua}	1.321(2), 1.318(2)	1.309(3)	1.323(2), 1.318(2)	1.308(2), 1.305(2)
C_{gua}-N_{ring}	1.367(2), 1.362(2), 1.373(2), 1.366(2)	1.381(3), 1.354(3)	1.362(2), 1.364(2), 1.360(2), 1.367(2)	1.367(3), 1.371(3), 1.364(3), 1.368(3)
N-Zn-N	85.4(1)	86.2(1)	85.9(1)	86.2(1)
∠(ZnX_2, ZnN_2)	82.1(1)	74.5(1)	84.9(1)	76.3(1)
∠($C_{gua}N_3$, ZnN_2)	56.4(1) 26.5(1)	22.4(1)	87.7(1) 24.8(1)	39.8(1) 28.1(1)
∠($C_{imine}N_3$, $N_{ring}C_3$) (av.)	5.6	15.5	6.3	14.9

5.2.3 DFT calculations

The structural trends described above are discussed under consideration of gas phase DFT calculations. The electronic structures of the zinc complexes **5a**, **5b** and their imidazolidine counterparts **1a** and **1b** have been examined using the B3LYP hybrid DFT functional[138–140] or the M05-2X functional[141] in combination with the 6-31g(d) basis set, implemented by the Gaussian 03 suite of programs.[142] Geometry optimisations were performed using the coordinates from X-ray data as starting points. The results of the optimisations are presented in Table 5.2 and 5.3.

For both functionals, the computed complex structures are in good agreement with their solid state structures. By trend, the Zn-N distances are predicted 0.01 to 0.03 Å too long. This ten-

Table 5.2: Summary of key geometric parameters of the calculated structures of **5a** and **1a** (bond lengths in Å and angles in °).

	5a		**1a**	
	B3LYP/6-31g(d)	M05-2X /6-31g(d)	B3LYP/6-31g(d)	M05-2X /6-31g(d)
Zn-Cl	2.302; 2.259	2.252; 2.285	2.322; 2.354	2.270
Zn-N_{gua}	2.041	2.033; 2.038	2.029; 2.031	2.045
C_{gua}-N_{gua}	1.322; 1.317	1.311; 1.318	1.308; 1.306	1.301
C_{gua}-N_{ring}	1.376; 1.384	1.371; 1.366	1.384; 1.364	1.359
	1.369; 1.371	1.359	1.389; 1.365	1.376
N-Zn-N	84.7	84.2	84.6	83.5
O-Zn-O	117.6	118.7	119.3	120.0
∠(ZnO_2, ZnN_2)	79.3	76.7	74.0	69.3
∠($C_{gua}N_3$, ZnN_2)	68.0; 30.4	64.3; 33.9	52.2; 34.6	49.9; 49.9
∠($C_{gua}N_3$, $N_{ring}C_3$)	6.0	6.0	14.0	15.7

Table 5.3: Summary of key geometric parameters of the calculated structures of **5b** and **1b** (bond lengths in Å and angles in °).

	5b		**1b**	
	B3LYP/6-31g(d)	M05-2X /6-31g(d)	B3LYP/6-31g(d)	M05-2X /6-31g(d)
Zn-O	1.947	1.955	1.939	1.941
Zn-N_{gua}	2.025	2.027	2.046	2.036
C_{gua}-N_{gua}	1.315	1.309	1.302	1.297
C_{gua}-N_{ring}	1.372	1.365	1.384	1.367
	1.377	1.369	1.388	1.383
N-Zn-N	85.8	85.3	86.5	85.4
O-Zn-O	78.9	100.9	76.8	99.3
∠(ZnO_2, ZnN_2)	78.8	62.7	81.0	69.1
∠($C_{gua}N_3$, ZnN_2)	51.9; 52.1	49.4; 49.4	37.2; 37.2	36.0; 36.1
∠($C_{gua}N_3$, $N_{ring}C_3$)	6.2	5.0	15.0	12.6

dency has been observed quite frequently for such systems.[143,144] The Zn-Cl distances are better described by the M05-2X functional in comparison to the solid-state structure. The Zn-O distances in **5b** and **1b** are predicted too short by both functionals. Remarkably, the B3LYP functional describes the C=N bonds of all four complexes more accurately than the M05-2X functional. For B3LYP, the deviation from the solid-state data averages to 0.003 Å whereas for M05-2X the corresponding values deviate about 0.008 Å.

The tetrahedral coordination environments and the guanidine ligand bite angles in **5a**, **5b**, **1a** and **1b** are correctly described by both functionals. It has to be noted that the B3LYP functional describes the angles between the ZnN_2 and the ZnX_2 planes slightly better for the four complexes than the M05-2X functional compared to those found in the solid state. The coordination of the acetate ions in the complexes **5b** and **1b** is in good agreement as well. The calculated values for the twist of the NC_3 unit against the ZnX_2 plane gives an ambiguous picture: for **5a**, both functionals describe the difference between the "sides" of the complex qualitatively cor-

Table 5.4: Mulliken and NBO charges in electron units (charge of electron is equal to -1) of **5a** and **1a** (basis set: 6-31g(d)).

	5a				**1a**			
	Mulliken		**NBO**		**Mulliken**		**NBO**	
	B3LYP	M05-2X	B3LYP	M05-2X	B3LYP	M05-2X	B3LYP	M05-2X
Zn	+0.677	+0.638	+1.529	+1.019	+0.669	+0.609	+1.526	+1.014
Cl	-0.556	-0.543	-0.815	-0.664	-0.545	-0.535	-0.807	-0.657
	-0.540	-0.535	-0.823	-0.649	-0.545	-0.535	-0.810	-0.657
N_{gua}	-0.698	-0.710	-0.838	-0.810	-0.670	-0.688	-0.800	-0.763
	-0.688	-0.713	-0.851	-0.791	-0.664	-0.688	-0.809	-0.763
C_{gua}	+0.801	+0.832	+0.656	+0.692	+0.820	+0.817	+0.697	+0.724
	+0.818	+0.814	+0.657	+0.690	+0.822	+0.817	+0.693	+0.724
N	-0.526	-0.554	-0.387	-0.397	-0.477	-0.491	-0.492	-0.499
	-0.508	-0.576	-0.424	-0.420	-0.455	-0.491	-0.450	-0.466
	-0.538	-0.551	-0.415	-0.399	-0.481	-0.516	-0.488	-0.499
	-0.514	-0.564	-0.388	-0.430	-0.455	-0.516	-0.449	-0.466

Table 5.5: Mulliken and NBO charges in electron units (charge of electron is equal to -1) of **5b** and **1b** (basis set: 6-31g(d)).

	5b				**1b**			
	Mulliken		**NBO**		**Mulliken**		**NBO**	
	B3LYP	M05-2X	B3LYP	M05-2X	B3LYP	M05-2X	B3LYP	M05-2X
Zn	+0.854	+0.859	+1.627	+1.288	+0.816	+0.838	+1.631	+1.289
Cl	-0.610	-0.627	-0.890	-0.853	-0.616	-0.630	-0.908	-0.860
	-0.610	-0.627	-0.890	-0.853	-0.616	-0.630	-0.908	-0.860
N_{gua}	-0.699	-0.702	-0.845	-0.805	-0.671	-0.689	-0.787	-0.762
	-0.700	-0.702	-0.845	-0.805	-0.671	-0.689	-0.787	-0.762
C_{gua}	+0.791	+0.797	+0.666	+0.683	+0.828	+0.832	+0.692	+0.719
	+0.791	+0.797	+0.666	+0.683	+0.828	+0.832	+0.692	+0.719
N	-0.528	-0.574	-0.398	-0.425	-0.485	-0.497	-0.461	-0.494
	-0.509	-0.574	-0.419	-0.403	-0.454	-0.497	-0.479	-0.473
	-0.528	-0.543	-0.398	-0.425	-0.485	-0.521	-0.461	-0.494
	-0.509	-0.543	-0.419	-0.403	-0.454	-0.521	-0.479	-0.473

rect, in contrast to **1a**, where the twist is predicted considerably too high (22° in solid-state, 34 and 52° for B3LYP, 50° for M05-2X). For **5b** and **1b**, the twist is described reasonably. It might be that this twist is also influenced by packing forces in the crystal. Notably, the accordance between theory and experiment for the angles between the $C_{gua}N_3$ and the $N_{ring}C_3$ planes in the four complexes is very good for both functionals.
For a more detailed analysis of the electronic structure the Mulliken charges and the NBO charges have been determined. The Mulliken charge of each atom was calculated by a Mulliken population analysis. The NBO charges of each atom was calculated by a natural bond orbital analysis.[145,146] The resulting charges are summarised in Table 5.4 and 5.5. These charges do not represent absolute charges but the trends among the complexes give an impression of electronic effects. The advantage of NBO charges over Mulliken charges lies in their greater independence of the basis sets.[147]
In comparison of the imidazoline guanidine stabilised complexes **5a** and **5b** with the imidazolidine guanidine complexes **1a** and **1b**, the charges of the guanidine N atom of the imidazolines are predicted to be in average 0.025 (Mulliken charge) or 0.045 (NBO charge) more negative. Concomitantly, the positive charge on the zinc atom is slightly increased (≈ 0.01 Mulliken charge, less than 0.01 NBO charge). In addition, the positive charge on the guanidine C atoms is slightly higher in the imidazoline guanidine systems. This effect is due to a better delocalisation of the positive charge within imidazole ring systems. Interestingly, the differences between the Mulliken charge distribution in tetramethylguanidine and dimethylethyleneguanidine groups are more pronounced than the differences between imidazolines and imidazolidine based guanidines discussed herein (see Section 6.1). In summary, the imidazoline guanidine complexes should show an slightly enhanced Lewis acidity of the zinc atoms compared to their imidazolidine counterparts and therefore act as good initiators for the lactide polymerisation.

5.2.4 Polymerisation activity

As reported in Chapter 4, guanidine zinc complexes possess catalytic activity in the ring-opening polymerisation of D,L-lactide and offer the advantage of acceptable or even high stability towards air and moisture. It is observed that in most cases active catalysts feature high Mulliken charges at the N-donor atoms which lead to an improved Lewis acidity of the zinc atom (see section 6.1). The zinc complexes stabilised by imidazoline based guanidine ligands are expected to be more active catalysts in comparison to the corresponding zinc bisguanidine complexes containing imidazolidine moieties due to the higher basicity of the imidazolines. Following DFT analysis, in these ligands the positive charge is strongly delocalised in the imidazoline rings and thus the zinc centre in these complexes should exhibit a stronger Lewis acidity leading to good catalytic properties. Therefore, the imidazoline based guanidine zinc complexes were investigated concerning their activity in the bulk polymerisation of D,L-lactide.

For the polymerisation procedure the monomer D,L-lactide and the initiator (I/M ratio 1:500) were heated at 150°C. It has to be noted that the monomer was used as purchased without further purification. After the reaction time of 24 h or 48 h, the melt was dissolved in dichloromethane, and then the PLA was precipitated in cold ethanol, isolated and dried under vacuum at 50°C. In order to rate the catalytic activity of the complexes, the polymer yield was defined and the molecular weights as well as the polydispersity of the obtained PLA were determined by gel permeation chromatography (see Table 5.6). The tacticity and the probability of heterotactic enchainment (P_r) were analysed by homonuclear decoupled ^{1}H NMR spectroscopy.[24]
The complexes **5a** and **5b** were found to initiate the ring-opening polymerisation of D,L-lactide and show in general similar results to the corresponding imidazolidine bisguanidine zinc complexes **1a** and **1b**. In the case of **5a** and **5b**, the yields are slightly higher than for **1a** and **1b**. The dichloro complex **5a** affords higher molecular weights than its counterpart **1a**, and they both generate higher M_w values than the diacetato complexes, whose values are in the same range. Whereas the extension of reaction time from 24 to 48 h leads in the case of **5a** to a slight increase of molecular weight, in polymerisations initiated with **5b**, **1a** and **1b** a decrease of molecular weight can be observed which may be caused by side reactions such as interchain or intrachain transesterification resulting in a chain-transfer reaction.[126,127] The P_r values of 0.50 or 0.53 imply that the complex structure shows no ability to affect the tacticity of the formed polymer.
The catalytic study supports the findings of the DFT calculations: the imidazoline based guanidines feature a slightly higher positive charge at the zinc atom and more negative charges at the guanidine N atoms, such that a slightly higher catalytic activity had to be expected. A continuation of this thought implies that systems with exceedingly high Lewis acidity on the zinc atom

Table 5.6: Polymerisation of D,L-lactide in the presence of the imidazoline zinc complexes **5a** and **5b**, as well as the imidazolidine zinc complexes **1a** and **1b**.

Initiator		Time[a] [h]	Yield [%]	M_w [g/mol]	PD[b]	P_r[c]
[Zn(8MeBL)Cl_2]	**5a**	24	85	51,000	2.0	0.53
[Zn(8MeBL)Cl_2]	**5a**	48	89	55,000	1.9	
[Zn(DMEG$_2$e)Cl_2]	**1a**	24	79	38,000	1.7	0.50
[Zn(DMEG$_2$e)Cl_2]	**1a**	48	67	33,000	1.6	
[Zn(8MeBL)($CH_3COO)_2$]	**5b**	24	88	24,000	2.0	0.50
[Zn(8MeBL)($CH_3COO)_2$]	**5b**	48	85	23,000	2.1	
[Zn(DMEG$_2$e)($CH_3COO)_2$]	**1b**	24	69	24,000	1.6	0.50
[Zn(DMEG$_2$e)($CH_3COO)_2$]	**1b**	48	66	18,000	1.6	

Reaction conditions: catalyst (0.2 mol%), 150 °C; [a] reaction times were not necessarily optimised; [b] PD = M_w/M_n where M_n is the number-average molar mass; [c] from analysis of the ^{1}H homonuclear decoupled NMR spectrum using the equation $P_r{}^2 = 2$ [sis].[24]

and great basicity on the N-donor function are excellent initiators for the ROP of lactide. All these findings are in good accordance with the coordination-insertion mechanism proposed for the lactide polymerisation with transition metal alkoxide complexes.[5,20,25,44,47,148] In this mechanism, the pre-coordination of the substrate lactide to the metal centre is crucial for the subsequent ring-opening step. The co-ligands which are usually alkoxides act then as nucleophiles and open the lactide ring.[5,20,25,44,47] It has to be remarked that the complexes **5a**, **5b**, **1a** and **1b** initiate the ROP of lactide without any addition of alkoxide or other co-catalysts. It is proposed that the highly nucleophilic guanidine N-donor systems act as ring-opening agents.

5.3 Conclusion

In this chapter the synthesis and complete characterisation of the first examples of imidazoline based guanidine zinc complexes is reported. The structural and theoretical analysis revealed that the dichloro and diacetato complexes of the ligand 8MeBL are very similar to those of the corresponding imidazolidine based guanidine $DMEG_2e$. DFT calculations with B3LYP and M05-2X functionals in combination with the 6-31g(d) basis set were in good agreement with the solid-state structures. A charge distribution analysis using Mulliken and NBO charges exhibited that the complexes containing the imidazoline moieties possess more negative charge on the guanidine N atoms and slightly more positive charge on the zinc atom than their imidazolidine counterparts. Notably, **5a** and **5b** were active in the solvent-free polymerisation of lactide. The resulting poly-D,L-lactide could be obtained with yields of app. 85 % and molecular weights (M_w) of up to 55,000 g mol^{-1} with a polydispersity of 2. This is consistent with the slightly higher activity of **5a** and **5b** in the ROP of lactide compared to the activity of **1a** and **1b**. Hence, the strategy of using neutral, strongly nucleophilic ligand systems for the stabilisation of catalytically active and environmentally benign zinc complexes has again been positively evaluated.

In summary, these findings lead to two mechanistic evidences: (a) enhanced Lewis acidity of the zinc centre directly correlates with the enhanced polymerisation activity and (b) by using exclusively neutral N-donor ligands for the stabilisation of the catalysts, it is proven that anionic (co-)ligands are not necessary prerequisites for the nucleophilic lactide-opening step.

6 Systematic screening of a library of zinc complexes stabilised by guanidine-pyridine ligands

In order to develop highly active initiators for the ring-opening polymerisation of lactide, a library of zinc complexes stabilised by guanidine-pyridine ligands was provided by combining various zinc compounds with different ligands. The obtained complexes were screened towards their catalytic activity to identify influencing variables and to build up a structure-reactivity correlation which is indispensable for the rating of catalytic potential of new complexes and for the creation of improved catalysts.
By variation of the anionic component of the zinc salts, its impact on the molecular structure as well as on the catalytic properties of the corresponding complexes was investigated. Furthermore, new guanidine-pyridine ligands were developed by combining various chloroformamidinium chlorides with 8-aminoquinoline and 2-picolylamine in order to analyse the influence of the guanidine unit in the ligand stabilising the initiator complexes on their ability to promote the polymerisation of lactide.
Finally, the most auspicious candidates were also tested in the ring-opening polymerisation of different monomers to allow the evaluation of their application range.

6.1 Air-stable and highly active zinc complexes stabilised by DMEGqu, TMGqu, DMEGpy and TMGpy

The synthesis of the zinc complexes stabilised by guanidine-pyridine hybrid ligands $[Zn(DMEGqu)_2(CF_3SO_3)][CF_3SO_3]$ (**6c**), $[Zn(TMGqu)_2(CF_3SO_3)][CF_3SO_3]$ (**7c**), $[Zn(TMGpy)Cl_2]$ (**15a**) and $[Zn(TMGpy)(CH_3COO)_2]$ (**15b**) is reported. These zinc complexes were completely characterised and together with the complexes developed before, $[Zn(DMEGqu)Cl_2]$ (**6a**), $[Zn(TMGqu)Cl_2]$ (**7a**), $[Zn(DMEGpy)Cl_2]$ (**14a**), $[Zn(DMEGqu)(CH_3COO)_2]$ (**6b**), $[Zn(TMGqu)(CH_3COO)_2]$ (**7b**) and $[Zn(DMEGpy)(CH_3COO)_2]$ (**14b**), screened towards their activity in the ring-opening polymerisation of D,L-lactide. They proved to be active initiators in lactide bulk polymerisation,

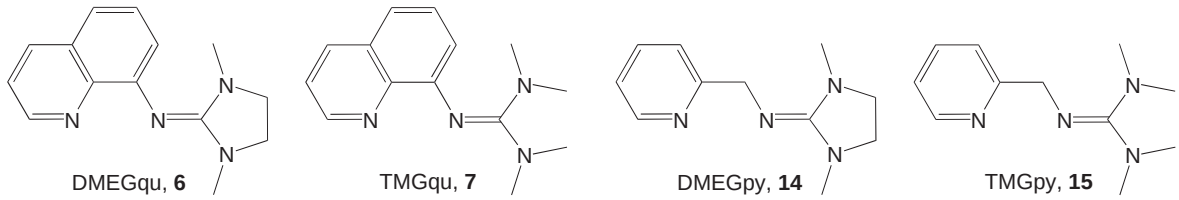

Figure 6.1: Guanidine-pyridine hybrid ligands.[101,121]

and polylactides with molecular weights (M_w) up to 176,000 g/mol could be obtained. They combine high activity with robustness towards moisture and air.
The influence of reaction temperature and of the anionic component of the zinc salt on the activity of the catalyst, as well as the occurrence of undesired side reactions, was investigated. By correlating these findings with the structural study on the zinc complexes a structure-reactivity relationship for the zinc catalysts could be deduced. This study was accompanied by DFT calculations. The bis-chelate triflate complexes **6c** and **7c**, supported by quinoline-guanidine ligands **6** and **7**, exhibit by far the highest reactivity. Systematic comparison of these complexes with their mono-chelate counterparts and their bisguanidine analogues allows the attributes that promote polymerisation by neutral guanidine ligand systems to be elucidated: accessibility to the zinc centre and Lewis acidity.

6.1.1 Introduction

As reported in Chapter 4, zinc guanidine complexes combine great potential as active catalysts in the ROP of D,L-lactide with acceptable stability. To improve the activity of guanidine-based zinc complexes the ligand system was modified by substituting one guanidine moiety by an amine group. This changes the electronic environment by replacing one "hard" guanidine function by a "soft" pyridine donor and simultaneously increases accessibility to the zinc centre by substituting one bulky guanidine by a non-bulky pyridine unit. These guanidine-amine hybrid ligands combine the excellent donor properties of guanidines with additional coordination space for pre-coordination of substrates, and their modular synthesis protocol, which combines different spacer and guanidine groups, permits flexible ligand design (see Chapter 3). The use of quinolyl and pyridyl units leads to the guanidine-pyridine hybrid ligands N-(1,3-dimethylimidazolidin-2-yliden)quinolin-8-amine (DMEGqu, **6**), 1,1,3,3-tetramethyl-2-(quinolin-8-yl)guanidine (TMGqu, **7**), N-(1,3-dimethylimidazolidin-2-yliden)pyridin-8-amine (DMEGpy, **14**) and 1,1,3,3-tetramethyl-2-[(pyridin-2-yl)methyl]guanidine (TMGpy, **15**), which were synthesised during previous studies and are depicted in Fig. 6.1.[101,121] These ligands were used to obtain the zinc complexes [Zn(DMEGqu)Cl_2] (**6a**), [Zn(TMGqu)Cl_2] (**7a**), [Zn(DMEGpy)Cl_2] (**14a**), [Zn(DMEGqu)($CH_3COO)_2$] (**6b**), [Zn(TMGqu)($CH_3COO)_2$] (**7b**) and [Zn(DMEGpy)($CH_3COO)_2$] (**14b**) (see Fig. 6.2). In preliminary studies, some of them showed the potential to initiate the ROP of lactide.[101]

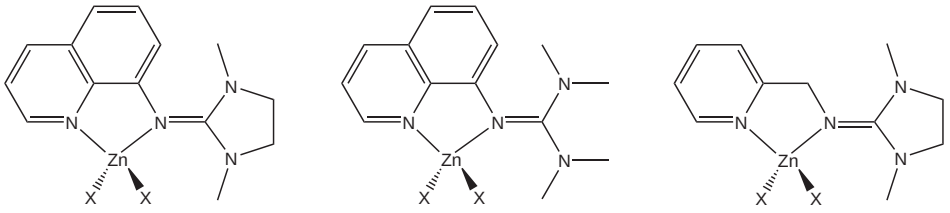

Figure 6.2: Schematic depiction of already reported guanidine-pyridine hybrid zinc complexes.

Hence, new zinc complexes stabilised by these ligands were prepared and characterised and the whole series of zinc complexes was screened for their catalytic activities in the polymerisation of lactide. The study extensively correlates experimental results with DFT calculations to evaluate the reactivity. Furthermore, it is shown that the classical conflict between stability and activity can be compensated by an integrated approach.

6.1.2 Results and discussion

Synthesis of the zinc complexes

The guanidine-pyridine hybrid ligands DMEGqu, TMGqu, DMEGpy and TMGpy were synthesised by condensation of N,N,N',N'-tetramethylchloroformamidinium chloride (TMG, **7**) and N,N'-dimethylethylenechloroformamidinium chloride (DMEG, **6**) with 8-aminoquinoline and 2-picolylamine in high yields of up to 98%.[101,121] Their reaction with zinc salts ($ZnCl_2$, $Zn(CH_3COO)_2$, $Zn(CF_3SO_3)_2$) in a dry, aprotic solvent (MeCN, THF) resulted in straightforward formation of the zinc complexes **6a**-**15b** (see Table 6.1). They could be isolated as colourless (**14a**, **15a**, **14b**, **15b**) or yellow crystals (**6a**, **7a**, **6b**, **7b**, **6c** and **7c**) in yields of 64-99%. Single crystals of the complexes were obtained either by cooling a saturated solution slowly to room

Table 6.1: Overview of the synthesised zinc complexes of guanidine-pyridine hybrid ligands.

	$ZnCl_2$	$Zn(CH_3COO)_2$	$Zn(CF_3SO_3)_2$
DMEGqu (**6**)	$[Zn(DMEGqu)Cl_2]$ (**6a**)[a]	$[Zn(DMEGqu)(CH_3COO)_2]$ (**6b**)[a]	$[Zn(DMEGqu)_2(CH_3SO_3)][CH_3SO_3]$ (**6c**)
TMGqu (**7**)	$[Zn(TMGqu)Cl_2]$ (**7a**)[a]	$[Zn(TMGqu)(CH_3COO)_2]$ (**7b**)[a]	$[Zn(TMGqu)_2(CH_3SO_3)][CH_3SO_3]$ (**7c**)
DMEGpy (**14**)	$[Zn(DMEGpy)Cl_2]$ (**14a**)[a]	$[Zn(DMEGpy)(CH_3COO)_2]$ (**14b**)[a]	-[b]
TMGpy (**15**)	$[Zn(TMGpy)Cl_2]$ (**15a**)	$[Zn(TMGpy)(CH_3COO)_2]$ (**15b**)	-[b]

[a] These complexes have been reported before;[101] [b] these complexes could not be structurally characterised.

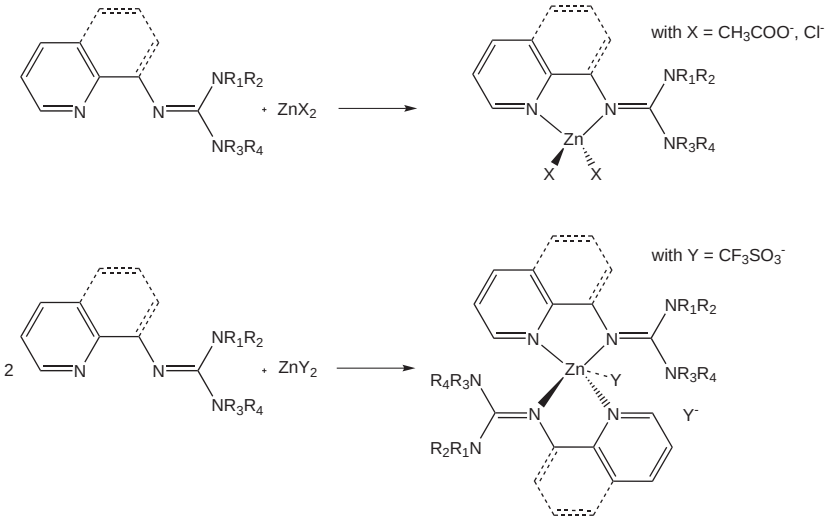

Figure 6.3: Schematic depiction of the general complex synthesis.

temperature or by slow diffusion of diethyl ether into the solution. The resulting crystals provide high stability towards moisture and air. They can be handled and stored in air without loss of activity, whereas the corresponding guanidine-pyridine hybrid ligands and zinc salts are sensitive towards hydrolysis or rather hygroscopic.
The crystal structures of $[Zn(DMEGqu)_2(CF_3SO_3)][CF_3SO_3]$ (**6c**), $[Zn(TMGqu)_2(CF_3SO_3)][CF_3SO_3]$ (**7c**), $[Zn(TMGpy)Cl_2]$ (**15a**) and $[Zn(TMGpy)(CH_3COO)_2]$ (**15b**) (Figures 6.4-6.6) were determined by X-ray crystallography and compared to those of the known complexes. In the complexes with zinc chloride and zinc acetate, the zinc atom is fourfold coordinated by the two N-donor atoms of the guanidine-pyridine hybrid ligands and two chlorine ions or two acetate ions, respectively. However, in the complexes with zinc triflate, the zinc atom is fourfold coordinated by two chelate ligands (Figure 6.3). The above-described zinc complexes formed independently of the molar ratio of the starting materials. Due to their structural similarity, the complexes containing zinc chloride, zinc acetate and zinc triflate will be discussed conjoint in groups.
Complexes with zinc chloride: The structures of the zinc chloride complexes $[Zn(DMEGqu)Cl_2]$ (**6a**), $[Zn\ (TMGqu)Cl_2]$ (**7a**), $[Zn(DMEGpy)Cl_2]$ (**14a**) and $[Zn(TMGpy)Cl_2]$ (**15a**) are very similar to each other. Selected bond lengths and angles of the compounds are collected in Table 6.2. In all complexes each zinc atom is fourfold coordinated, whereby two coordination sites are occupied in a chelating manner by the N-donor atoms of the guanidine-pyridine hybrid ligands to form a five-membered heterocycle. The two Zn-Cl bonds in **14a** are equal in length (av. 2.240 Å), but in **15a**, **6a** and **7a** one bond is longer than the other. In these complexes the longer Zn-Cl bond measures 2.236 Å (av.) and the shorter one 2.215 Å (av.). The distances between the zinc atom and the N-donor atoms of the guanidine-pyridine hybrid ligands differ due to the different coordination properties of the N-donor atoms. In **14a**, **6a** and **7a** the corresponding lengths are equal with an amount of

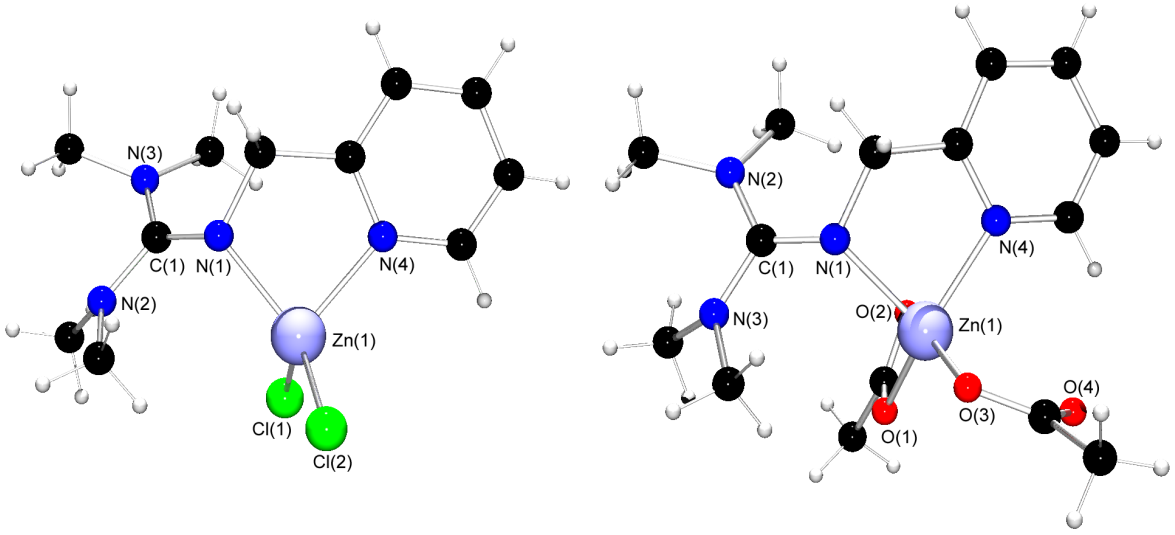

Figure 6.4: Crystal structure of $[Zn(TMGpy)Cl_2]$ (**15a**) and $[Zn(TMGpy)(CH_3COO)_2]$ (**15b**) as determined at 153 and 120 K.

2.045 Å (av.) for Zn-N_{py} and 2.036 Å (av.) for Zn-N_{gua}, but in **15a** the Zn-N_{py} bond is 0.02 Å (2.065(2) Å) longer and the Zn-N_{gua} bond 0.03 Å (2.009(2) Å) shorter than the average values of the other complexes. The C_{gua}-N_{gua} double bonds range in length from 1.317(1) to 1.335(2) Å and show the tendency of being slightly shorter for pyridine ligands. Remarkably, in all four complexes the ligands have the same bite angle of 82.8° (av.), which differs considerably from the tetrahedral angle (109.47°). This leads to a distorted tetrahedral coordination geometry of the zinc atom. This is also reflected in the angle between the $ZnCl_2$ and ZnN_2 planes. In ideal tetrahedral coordination geometry it is 90°, but in the present complexes these angles are 83.4(1) (**14a**), 85.1(1) (**15a**), 84.4(1) (**6a**) and 79.3(1)° (**7a**).

To evaluate the influence of the guanidine-pyridine hybrid ligands on the structure, complexes **6a**-**15a** were compared with the already reported bipyridine compounds $[Zn(bipy)Cl_2]$ (**33a**)[149] and $[Zn(phen)Cl_2]$ (**34a**)[150] as well as the bisguanidine complex $[Zn(DMEG_2e)Cl_2]$ (**1a**).[101] The Zn-Cl bonds in the bipyridine complexes are of different length, just as in **6a**, **7a** and **15a**. The longer ones ($[Zn(bipy)Cl_2]$: 2.210(1) Å, $[Zn(phen)Cl_2]$: 2.207(3) Å) conform to the shorter bond of **15a**, **6a** and **7a**, whereas the other ones are 0.017 Å shorter [$[Zn(bipy)Cl_2]$: 2.198(1) Å, $[Zn(phen)Cl_2]$: 2.198(3) Å]. The Zn-Cl bonds in the bisguanidine complex are equal, and with values of 2.260(1) Å they are longer than those in all the other complexes. The Zn-N_{gua} distances of $[Zn(DMEG_2e)Cl_2]$ (2.038(2) Å) correspond to those in **14a**, **6a** and **7a**, and the Zn-N_{py} bond lengths in $[Zn(bipy)Cl_2]$ (2.064(2), 2.053(2) Å) and $[Zn(phen)Cl_2]$ (2.072(7) and 2.050(7) Å) to those of **7a**-**14a**. The bite angles of the bipyridine ligands are slightly smaller ($[Zn(bipy)Cl_2]$: 80.3(1)°, $[Zn(phen)Cl_2]$: 80.4(3)°), and the bite angle of the guanidine ligand ($[Zn(DMEG_2e)Cl_2]$: 86.2(1)° is slightly widened. The C_{gua}-N_{gua} bond length of the bisguanidine complex of 1.309(3) Å is smaller than the average length of the corresponding bond in the complexes **6a**-**15a**.

Table 6.2: Selected bond lengths (Å) and bond angles (°) of **6a**, **7a**, **14a** and **15a**.

	6a	**7a**	**14a**	**15a**
Zn-N_{py}	2.045(1)	2.044(1)	2.047(1)	2.065(2)
Zn-N_{gua}	2.039(1)	2.034(1)	2.036(1)	2.009(2)
Zn-Cl	2.212(1)	2.217(1)	2.237(1)	2.215(1)
	2.234(1)	2.238(1)	2.243(1)	2.235(1)
C_{gua}-N_{gua}	1.327(2)	1.335(2)	1.317(2)	1.317(3)
C_{gua}-N	1.355(2)	1.347(2)	1.375(2)	1.356(3)
	1.352(2)	1.357(2)	1.362(2)	1.360(3)
N-Zn-N	82.6(1)	82.3(1)	83.7(1)	82.6(1)
∠($ZnCl_2$, ZnN_2)	84.4(1)	79.3(1)	83.4(1)	85.1(1)
∠($C_{gua}N_3$, ZnN_2)	53.4(1)	55.9(1)	18.9(1)	48.6(1)
∠($C_{gua}N_3$, NC_3) (av.)	12.6	29.5	9.8	33.7
Structural parameter ρ	0.98	0.99	0.96	0.97

Complexes with zinc acetate: The crystal structures of [Zn(DMEGqu)$(CH_3COO)_2$] (**6b**), [Zn(TMGqu)$(CH_3COO)_2$] (**7b**), [Zn(DMEGpy)$(CH_3COO)_2$] (**14b**) and [Zn(TMGpy)$(CH_3COO)_2$] (**15b**) were obtained by reaction of zinc acetate with **6**, **7**, **14** and **15**. Table 6.3 lists selected bond lengths and angles. Crystals of **14b** contain two crystallographically independent molecules per asymmetric unit with the same molecular composition but different structural properties, denoted by **14b-1** and **14b-2**. In **14b-2** a twisting in the guanidine moiety can be observed that may be the reason for the different bond lengths and angles compared to **14b-1**. However, the packaging effects leading to the differentiation of these structures are surprisingly strong.

The zinc atoms of all complexes are fourfold coordinated by the N-donor atoms of the guanidine-pyridine hybrid ligands and by the oxygen atoms of two acetate ions. The coordination geometry of the zinc atom can be best described as a distorted tetrahedron. The bite angles of the coordinated ligands, which range from 80.9 to 83.6°, are notably smaller than the tetrahedral angle. The distorted geometry is also reflected in the angle between the ZnO_2 and ZnN_2 planes, which exhibit on average a deviation of 11° from the ideal tetrahedral arrangement. In **14b-1** and **7b** the two Zn-O bond lengths are equal (av. 1.949 and 1.955 Å), whereas the other complexes contain one shorter (**14b-2**: 1.952(1); **15b**: (1.934(2); **6b**: 1.950(1) Å) and one longer bond (**14b-2**: 2.005(1); **15b**: 1.978(2); **6b**: 2.021(1) Å). The Zn-N bonds show no apparent influence of the kind of N-donor, as was found for the chlorido complexes. In **14b-1** the two bond lengths are equal (av. 2.037 Å). In the complexes with a DMEG guanidine unit the Zn-N_{gua} bond is longer than the Zn-N_{py} bond, whereas in those with a TMG guanidine unit the Zn-N_{gua} bond is shorter than the Zn-N_{py} bond. The C_{gua}=N_{gua} double bond lengths range from 1.310(2) to 1.344(2) Å. By trend the C_{gua}=N_{gua} bonds in the quinoline ligands are apparently 0.02 Å longer than those in the pyridine ligands.

Table 6.3: Selected bond lengths (Å) and bond angles (°) of **6b**, **7b**, **14b-1**, **14b-2** and **15b**.

	6b	**7b**	**14b-1**	**14b-2**	**15b**
Zn-N_{py}	2.048(1)	2.080(1)	2.036(2)	2.058(2)	2.062(2)
Zn-N_{gua}	2.106(1)	2.054(1)	2.038(2)	2.075(2)	2.044(2)
Zn-O	1.950(1)	1.951(1)	1.946(1)	1.952(1)	1.934(2)
	2.021(1)	1.958(1)	1.952(1)	2.005(1)	1.978(2)
C_{gua}-N_{gua}	1.336(2)	1.344(2)	1.313(2)	1.310(2)	1.321(4)
C_{gua}-N	1.336(2)	1.343(2)	1.367(2)	1.375(2)	1.365(4)
	1.364(2)	1.348(2)	1.348(2)	1.368(2)	1.358(4)
N-Zn-N	80.9(1)	81.3(1)	83.6(1)	81.8(1)	82.7(1)
∠(ZnO_2, ZnN_2)	78.4(1)	85.8(1)	76.3(1)	73.1(1)	82.8(1)
∠($C_{gua}N_3$, ZnN_2)	48.1(1)	55.4(1)	14.3(1)	41.0(1)	43.0(1)
∠($C_{gua}N_3$, NC_3) (av.)	11.3	27.1	9.4	15.5	33.3
Structural parameter ρ	0.99	1.00	0.97	0.96	0.97

The acetato complexes stabilised by guanidine-pyridine hybrid ligands can be compared with the already reported bipyridine complex [Zn_2(1,1,2,2-tetrakis(2-pyridyl)-ethane)$(OAc)_4$][151] and the bisguanidine complex [Zn($DMEG_2e$)$(OAc)_2$] (**1b**)[101] to quantify the influence of the guanidine-pyridine hybrid ligands on the structure of the complex. The Zn-O distances of the pyridyl complex (1.946(2), 1.974(2) Å) and the bisguanidine complex (1.969(2), 1.956(2) Å) lie in the same range as those in **6b**-**15b**. One Zn-N_{py} bond of the pyridyl complex (2.119(2) Å) is slightly longer than the average bond length of the zinc acetato complexes stabilised by guanidine-pyridine hybrid ligands, whereas the other (2.094(2) Å) lies in the same range. One of the Zn-N_{gua} bonds in the bisguanidine complex (2.011(2) Å) is slightly shorter than the average in **6b**-**15b**, whereas the other (2.038(2) Å) fits well to the average. The C_{gua}-N_{gua} bonds do not differ much (1.308(2), 1.305(2) Å). All tetrahedrally coordinated zinc complexes with guanidine-pyridine hybrid ligands show twisting of the guanidine plane (CN_3) with respect to the coordination plane (N-Zn-N) to avoid steric interactions. The angles between the ZnN_2 and ZnO_2 planes increase with increasing sterical demand of the guanidine-pyridine hybrid ligand in the order DMEGpy⟶ TMGpy⟶ DMEGqu⟶ TMGqu. Complex **14b-2** also fits the trend, although it differs by about 27° from **14b-1**.

Complexes with zinc triflate: The structures of zinc triflate complexes [Zn$(DMEGqu)_2(CF_3SO_3)$][CF_3SO_3] (**6c**) and [Zn$(TMGqu)_2(CF_3SO_3)$][CF_3SO_3] (**7c**) exhibit a different coordination of the zinc atom compared to the complexes of zinc chloride and zinc acetate (Figures 6.5 and 6.6, Table 6.4). Each Zn atom is sixfold coordinated, whereby four coordination sites are occupied in a bis-chelating manner by the N-donor atoms of two guanidine-pyridine hybrid ligands. The remaining coordination sites are occupied by two oxygen atoms of one triflate anion, while the other triflate anion is far away from the complex centre and acts as counterion. The asymmetric unit contains Λ and Δ isomers of the complex

cation of **7c**; thus, in the following only one structure is discussed.
The distances between the zinc atom and the pyridine donor atom are identical in each complex cation (**6c**: av. 2.090; **7c**: av. 2.062 Å) and significantly longer than the corresponding Zn-N_{gua} bond lengths (**6c**: av. 2.042; **7c**: av. 2.021 Å). The C_{gua}=N_{gua} bonds are also identical and exhibit an average value of 1.346 Å. The distances between the zinc and oxygen atoms in **7c** (2.684(3) and 2.698(3) Å) are very long but smaller than the sum of the van der Waals radii of 2.79 Å. The cationic complex unit of **6c** exhibits one short (2.452(7) Å) and one long Zn-O bond (2.700(7) Å). These long bonds indicate weak coordination, which is a prerequisite for coordination of a lactide molecule. The coordination geometry of the zinc centre can be best described as a distorted trigonal bipyramid in which the apical positions are occupied by the pyridine nitrogen atoms of the ligands. The equatorial sites are occupied by the guanidine nitrogen donors and the oxygen atoms of the triflate anion, which act as one equatorial donor. The metal atom lies in the trigonal plane in both complexes. The fact that the N atoms of the two aromatic systems reside in the apical positions is in accordance with the properties of the two types of N atoms. Guanidine ligands have stronger donating properties than pyridine ligands, and this leads to a decrease in the Zn-N_{gua} bond length (bond to an equatorial side). The distortion of the coordination geometry is reflected in the angle between two axial sites: In trigonal-bipyramidal coordination the angle is 180°, but it is diminished to 172.0(1)° in **6c** and to 161.1(1)° in **7c**. The angle between the two nitrogen atoms in equatorial position (**6c**: 122.3(1)°, **7c**: 128.0(1)°) is near to the undistorted angle (120°). However, the angle between an equatorial and an axial site differs from the ideal value (90°) because of the fixed value for the bite angle (av. 81.5°) and leads to another slight distortion. This distortion minimises the interactions between the sterically demanding guanidine residues and the aromatic parts.

Table 6.4: Selected bond lengths (Å) and bond angles (°) of **6c** and **7c**.

	6c	**7c**
Zn-N_{py}	2.089(3), 2.091(3)	2.052(3), 2.071(3)
Zn-N_{gua}	2.035(3), 2.049(3)	2.031(3), 2.011(3)
Zn-O	2.452(7), 2.700(7)	2.684(3), 2.698(3)
C_{gua}-N_{gua}	1.345(5), 1.340(5)	1.357(5), 1.342(5)
C_{gua}-N	1.344(5), 1.337(5), 1.340(5), 1.343(5)	1.329(5), 1.352(5), 1.344(5), 1.338(5)
N-Zn-N	81.4(1), 80.5 (1)	82.1(1), 81.9(1)
N_{py}-Zn-N_{py}	172.0(1)	161.3(1)
N_{gua}-Zn-N_{gua}	122.3(1)	128.0(1)
∠(ZnN_2, ZnN_2)	60.6(1)	58.9(1)
∠($C_{gua}N_3$, ZnN_2)	55.0(2), 59.4(1)	56.0(1), 52.9(2)
∠($C_{gua}N_3$, NC_3) (av.)	9.0	28.0
Structural parameter ρ	1.00	1.01

The structural motif of a trigonal bipyramid was already described for a cobalt complex of the ligand DMEGqu (**6**).[121]
A further effect is torsion of the $ZnN_{2,ligand}$ and $ZnN_{2,ligand'}$ plane by 60.6(1)° in **6c** and 58.9(1)° in **7c** with respect to each other. The angles between the $C_{gua}N_3$ and ZnN_2 planes in **6c** (55.0(2) and 59.4(1)°) are similar to those in **7c** (56.0(1) and 52.9(2)°), because in both complexes the metal centre is comparably crowded and the steric interactions should be reduced.

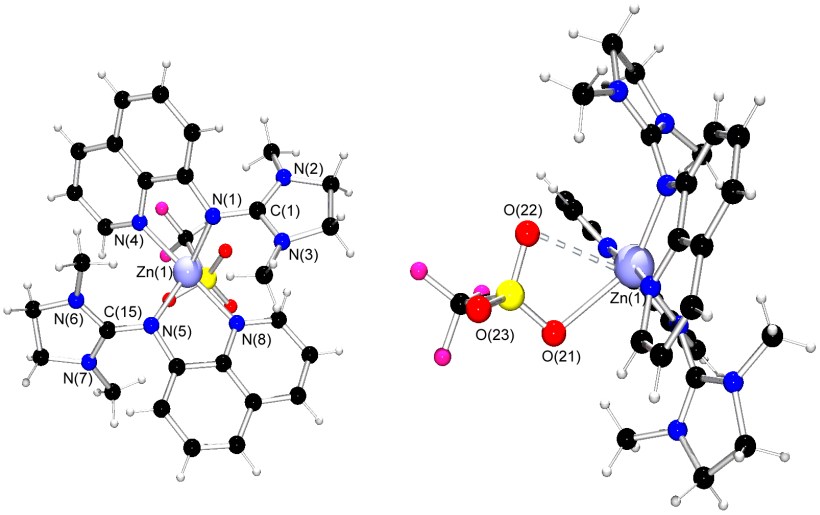

Figure 6.5: Molecular structure of $[Zn(DMEGqu)_2(CF_3SO_3)]^+$ in crystals of $[Zn(DMEGqu)_2(CF_3SO_3)][CF_3SO_3]$ (**6c**) as determined at 120 K.

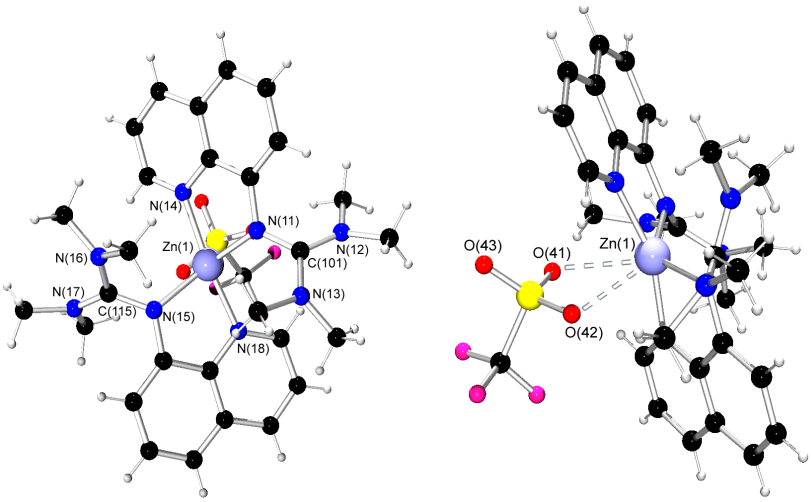

Figure 6.6: Molecular structure of $[Zn(TMGqu)_2(CF_3SO_3)]^+$ in crystals of $[Zn(TMGqu)_2(CF_3SO_3)][CF_3SO_3]$ (**7c**) as determined at 120 K.

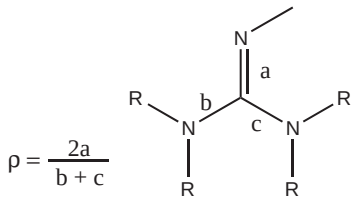

Figure 6.7: Calculation of the structural parameter ρ.

Structural influence of the guanidine unit: In all reported zinc complexes with guanidine-pyridine hybrid ligands twisting within the guanidine moiety can be observed which is characteristic for peralkylated guanidine units.[121,152] This twisting is a result of the interplay between the electronic effect of the intra-guanidine conjugation (driving towards planarity) and the evasion of the alkyl substituents. The average angle between the $C_{gua}N_3$ and NC_3 plane is 30.3° for TMG and 11.3° for DMEG. Twisting within TMG is more distinct because of the free rotation of the methyl groups connected to the amine function, whereas in DMEG twisting is hindered by the rigid ethylene bridge between the amine groups of the guanidine moiety. Delocalisation of the positive charge within the guanidine unit and the resultant levelling of the C-N bond lengths can be expressed by the structural parameter ρ (see Fig. 6.7).[100,153,154] A ρ value of 1 means complete delocalisation of the positive charge and total bond levelling. The ρ values of the chlorido complexes increase from **14a** (0.96), **15a** (0.97), **6a** (0.98) to **7a** (0.99). The general trend that delocalisation in complexes with quinoline ligands is higher than in those with pyridine ligands is also found for the acetato complexes. The ρ values for the corresponding pyridine complexes are 0.96 (**14b-2**) and 0.97 (**14b-1**, **15b**), whereas those of the quinoline complexes of 0.99 (**6b**) and 1.00 (**7b**) are considerably higher. Besides this trend in the structural parameter ρ, the C=N bonds in quinoline containing complexes are about 0.02 Å longer than those in the pyridine containing complexes. The bis-chelate complexes **6c** and **7c** show complete delocalisation of the positive charge in the guanidine unit. Altogether these complexes show a high degree of delocalisation.

A correlation between the twisting of the guanidine unit with respect to the chelate plane and the levelling of the C-N bonds was found. Interestingly, the only exception is **14b-2**. The more the guanidine unit twists out of the chelate plane to minimise the disadvantageous interaction with sterically demanding groups, the higher the ρ value and the greater the delocalisation and bond levelling. A possible explanation is that the guanidine unit leaves the conjugation of the aromatic system (quinoline or pyridine) by twisting and acts as isolated donor.

Ligand effect: Structural discussion of 6 and its zinc complexes: Due to the possibility to prepare single crystals of the pure ligand DMEGqu (**6**) suitable for X-ray diffraction, the molecular structure (Fig. 6.8) could be determined. The comparison of key geometric parameters of the free ligand with those of the complexes thereof (**6a**, **6b** and **6c**) allows for the examination of the influence of **6** during complexation. The key geometric parameters are summarised in Table 6.5.

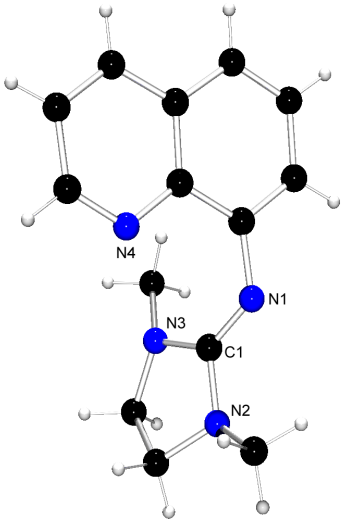

Figure 6.8: Molecular structure of DMEGqu (**6**) as determined at 120 K.

It is intriguing to what extent the C-N bonds in the guanidine residue change during complexation. In the free ligand the distance between C_{gua} and N_{gua} is shorter than the other C-N bonds in the guanidine unit and therefore it is regarded as double bond whereas the others are single bonds. When the ligand coordinates the metal atom the positive charge of the Lewis acid zinc(II) is partially transferred to the Lewis base guanidine where it is delocalised over the three nitrogen atoms. This can be observed in all three complexes as convergence of the C-N distances due to the elongation of the C_{gua}-N_{gua} bond and the shortening of the C_{gua}-N bonds. This distance levelling is also an indicator for the delocalisation of the positive charge within the guanidine function and can be rated by ρ. Complexation leads to a significant increase of ρ and adopts with $\rho = 1$ (which denotes complete delocalisation) the highest value for the zinc triflate containing complex **6c**.
A twisting within the guanidine moiety can be observed which is characteristic for peralkylated guanidine units. This twisting is a result of the interplay between the electronic effect of the intra-guanidine conjugation (driving towards planarity) and the evasion of the alkyl substituents. In the ligand as well as in all three complexes the angle between the $C_{gua}N_3$ and NC_3 plane adopts values which lie in the typical range of DMEG units and are smaller the closer the ρ value is to one.

DFT calculations

The structural trends described above were investigated by gas-phase DFT calculations. The electronic structures of zinc complexes **6a**-**7c** and **14a**-**15b** were examined by using B3LYP density functional theory and the 6-31G(d) and 6-31G+(d) basis sets, implemented in the Gaussian 03 suite of programs.[142] Geometry optimisations were performed by using the coordinates from X-ray data as starting point in case of **6a**-**7c** and **14a**-**15b**. The results of the optimisa-

Table 6.5: Summary of key geometric parameters from the structures of **6** and the complexes thereof (bond lengths in Å and angles in °).

	6	**6a**	**6b**	**6c**
C_{gua}-N_{gua}	1.283(3)	1.327(2)	1.336(2)	1.345(5), 1.340(5)
C_{gua}-N	1.384(2)	1.355(2)	1.336(2)	1.344(5), 1.337(5)
	1.378(3)	1.352(2)	1.364(2)	1.340(5), 1.343(5)
C_{ar}-N_{gua}	1.394(2)	1.402(2)	1.398(2)	1.405(5), 1.414(5)
$\angle$ ($C_{gua}N_3$, $N_{gua}C_{ar2}$)	65.2(1)			
$\angle$ ($C_{gua}N_3$, ZnN_2)		53.4(1)	48.1(1)	55.0(2), 59.4(1)
$\angle$ ($C_{gua}N_3$, NC_3) (av.)	12.3	12.6	11.3	9.0
Structural parameter ρ	0.93	0.98	0.99	1.00

tions are presented in Tables A.1-A.6 (see Appendix).
For the 6-31G(d) basis set, the computed structures of the complexes are in good agreement with their solid-state structures, whereas the 6-31G+(d) basis set generally yields too long bond lengths. The soft donating character of pyridine and guanidine units is significantly overestimated by this diffuse basis set, as has been observed in several cases.[143] For most complexes, the predicted Zn-N distances are about 0.03 Å too long, which is a known tendency for such systems.[143,144] Hence, ligands **6**, **7**, **14**, **15** and the model ligand HGqu were examined with B3LYP density functional theory and only the 6-31G(d) basis set (Table A.6 in the Appendix and Figure 6.9). The tetrahedral coordination environments in **6a**-**7b** and **14a**-**15b** are correctly described by both basis sets. Special emphasis is placed on the angles between the ZnN_2 and the ZnX_2 planes, which are in good accordance with those found in the solid state. The coordination of the acetate ions in the complexes **6b**-**15b** is in good agreement as well. Interestingly, for the acetato complexes, contacts of the benzyl or quinoline spacer hydrogen atoms to the acetate oxygen atoms are found, which were confirmed by DPFGSE-NOE NMR measurements in solution. For acetato complex **14b**, two conformers were found in the solid state. Their differences in Zn-N_{py} and Zn-N_{gua} bond lengths are reflected qualitatively in the DFT calculations, too. Their calculated energy difference of 1.4 kcalmol^{-1} explains their coexistence in the single crystal.
The bis-chelate complexes **6c** and **7c** are correctly described as well: the trigonal-bipyramidal coordination is well reflected in the N_{py}-Zn-N_{py} angles (169.5 for **6c** and 167.8° for **7c**) which describe the apical sites. Moreover, the η^2 binding mode of the triflate anion and the Zn-O bond lengths are in good agreement with the X-ray structures. In comparison with the solid-state structures, the calculated C=N guanidine "double-bond" lengths are extremely close to the X-ray data. Especially the differences between the four coordinating ligands are well reflected: for TMGqu and DMEGqu complexes this bond is generally about 1.335 Å long, whereas for TMGpy and DMEGpy complexes it is shortened to about 1.317 Å. Concomitantly, the tendency

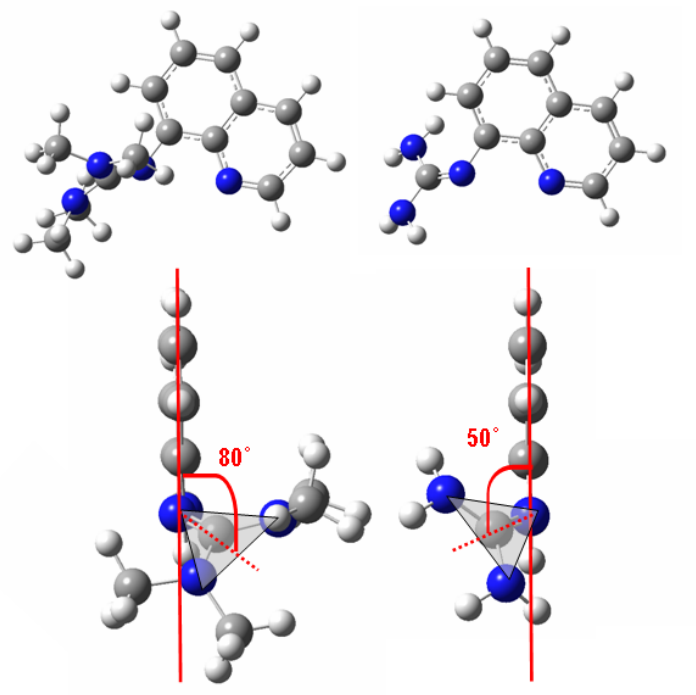

Figure 6.9: Comparison of the calculated structure of TMGqu (7, l) with the model ligand HGqu (r) [RB3LYP(6-31G(d))].

for the structural parameter ρ is correctly predicted: the quinoline-containing systems exhibit a slightly higher ρ (0.98-0.99) than the pyridine systems (0.94-0.96), which is in good accordance with the solid-state structures. Moreover, particularly the fact that the guanidine units twist with respect to the chelate plane in dependence on the ligand in complexes **6a**-**15b** could be reproduced by DFT calculations. The following trend could be deduced: quinoline systems exhibit a contact between the guanidine substituents and the ortho position. To avoid steric hindrance, the whole guanidine unit twists by 45° with respect to the chelate plane. Simultaneously, the levelling within the guanidine unit increases up to $\rho = 1$ because the guanidine moiety leaves conjugation with the aromatic system. In the pyridine systems, the spacer is more flexible and allows other ways of avoiding steric hindrance between guanidine substituents and the rest of the ligand molecule, which results in a smaller twist angle accompanied by a smaller ρ value. As the same trend was found experimentally, it cannot be related to packing effects but to intrinsic forces within the complexes.
The DFT analysis of the ligands and a model ligand without substituents (HGqu) shows that the focus on the steric interactions is only one aspect of this twisting effect (Figure 6.9). Even without substituents, twisting of up to 50° occurs. The aromatic influence is crucial for the guanidine system: the analysis of the Mulliken charges of the ligands (Table 6.9) reveals that the guanidine N_{imine} atom is significantly more negatively charged in quinoline ligands and complexes than in pyridine ones. Furthermore, the guanidine double bonds in the quinoline

ligands are calculated to have an average length of 1.287 Å (pyridine-guanidine ligands: 1.283 Å), which is longer than the values for reported aliphatic guanidines (1.277 Å)[155] but in the range of aromatic guanidines (1.282 Å).[156] In aromatic guanidines, rotation around the C=N bonds is facilitated by the interaction with the aromatic system, which is manifested in coalescence behaviour for the corresponding guanidine substituents.[99] Thus, it is understandable that the C=N bonds are longer and the C-N bonds shorter than in the pyridine systems where the guanidine moiety is bound to the benzyl group and not directly to the aromatic ring. Hence, in the quinoline systems the ρ value must be higher than in the pyridine systems for electronic reasons.

For a more detailed analysis of the electronic structure, the Mulliken charges were determined for the ligands and their complexes (Tables 6.6-6.9). These do not represent absolute charges but the trends among the complexes give an impression of electronic effects. A pronounced effect is the difference between the DMEG and TMG groups. As the geometry optimisations predict, the intra-guanidine twist is significantly smaller in the DMEG groups (12°) because of the ethylene backbone, which geometrically restricts intra-guanidine torsion. In all analysed complexes, the imine N atom in DMEG groups is around 0.05 more negatively charged than that in TMG groups. At the same time, the corresponding amine N atoms in the DMEG-containing systems are slightly more negatively charged, and the central guanidine C atoms are considerably more positively charged than those in the TMG-containing systems. This result is in good accordance with the theoretical calculations on TMG- and DMEG-containing ligands performed by Tamm et al.[120]

An important result of this analysis is the remarkable positive charge on the zinc atom in the bis-chelate complexes of 1.004 (**6c**) and 0.994 (**7c**) in comparison to around 0.68 for the chlorido complexes and about 0.87 for the acetato complexes. This finding documents the higher Lewis acidity of the zinc atom in **6c** and **7c** compared to **6a**-**15b**.

Table 6.6: Mulliken charges in electron units (charge of electron is equal to -1) of **6a**, **7a**, **6b** and **7b** (RB3LYP/6-31G(d)).

	6a	**7a**	**6b**	**7b**
Zn	+0.692	+0.697	+0.881	+0.886
N_{py}	-0.644	-0.641	-0.657	-0.650
N_{gua}	-0.781	-0.745	-0.788	-0.755
C_{gua}	+0.806	+0.684	+0.812	+0.706
N_{amine}	-0.451	-0.403	-0.434	-0.411
	-0.458	-0.409	-0.454	-0.392
X=Cl, OAc	-0.502	-0.501	-0.610	-0.606
	-0.536	-0.530	-0.602	-0.606

Table 6.7: Mulliken charges in electron units (charge of electron is equal to -1) of **6c** and **7c** (RB3LYP/6-31G(d)).

	6c	**7c**
Zn	+1.004	+0.994
N_{py}	-0.638, -0.641	-0.655, -0.619
N_{gua}	-0.811, -0.792	-0.736, -0.771
C_{gua}	+0.800, +0.757	+0.648, +0.645
N_{amine}	-0.447, -0.448,	-0.399, -0.399,
	-0.443, -0.448	-0.395, -0.392
O	-0.617, -0.621	-0.601, -0.668

Table 6.8: Mulliken charges in electron units (charge of electron is equal to -1) of **14a**, **15a**, **14b** and **15b** (RB3LYP/6-31G(d)).

	14a	**14b-1**	**14b-2**	**15a**	**15b**
Zn	+0.682	+0.860	+0.872	+0.667	+0.862
N_{py}	-0.571	-0.579	-0.598	-0.566	-0.580
N_{gua}	-0.675	-0.659	-0.673	-0.622	-0.615
C_{gua}	+0.823	+0.796	+0.811	+0.696	+0.680
N_{amine}	-0.458	-0.449	-0.449	-0.404	-0.422
	-0.475	-0.469	-0.478	-0.423	-0.405
X=Cl, OAc	-0.516	-0.600	-0.608	-0.494	-0.618
	-0.518	-0.618	-0.612	-0.530	-0.597

Table 6.9: Mulliken charges of ligands **6**, **7**, **14** and **15** (RB3LYP/6-31G(d)).

	6	**7**	**14**	**15**
N_{py}	-0.501	-0.490	-0.473	-0.460
N_{gua}	-0.598	-0.525	-0.544	-0.469
C_{gua}	+0.756	+0.613	+0.722	+0.606
N_{amine}	-0.455	-0.419	-0.478	-0.417
	-0.461	-0.421	-0.454	-0.424

NMR spectroscopy

Since twisting of the guanidine plane relative to the coordination plane in the solid-state and in the gas-phase DFT calculations was observed, the configuration in solution was investigated. Temperature-dependent ^{1}H NMR spectra of complexes **6a**-**7c** and the free ligands **6** and **7** were measured to determine whether it is possible to stop rotation of the C=N bond. In the case of a frozen rotation, DPFGSE-NOE NMR spectra should determine whether there is a NOE contact between the hydrogen atom of the quinoline carbon atom in ortho position to the guanidine moiety and a hydrogen atom of the methyl groups of the guanidine unit. However, even at -90°C the rotation of the C=N bond is still present, so no preferred configuration is ascertainable.

Polymerisation activity

The above described series of zinc complexes stabilised by guanidine-pyridine hybrid ligands was investigated towards their activity in bulk polymerisation of D,L-lactide. The ligand design strategy focuses on two points. First, improving accessibility to the zinc centre for the pre-coordination of substrates requires the substitution of one bulky guanidine by a non-bulky pyridine unit. Second, the electronic environment is modified by replacing one "hard" guanidine N-donor group by the "soft" N donor of the pyridine unit.
For the polymerisation procedure, the monomer D,L-lactide and the zinc initiator (I/M ratio 1:500 or 1:1000) were heated at 130 or 150°C. After a reaction time of 24 h or 48 h, the melt was dissolved in dichloromethane, and then the PLA was precipitated in cold ethanol, isolated and dried under vacuum at 50°C. To rate the catalytic activity of the complexes, the polymer yield was determined, and the molecular weights and polydispersity of the obtained PLA were investigated by gel permeation chromatography (see Table 6.10). As reference experiments, the polymerisation activity of zinc salts, the pure ligands and tin octoate were tested (see Table 6.11).
The polymerisation activities of zinc complexes with guanidine-pyridine hybrid ligands depend on the nature of the anionic component of the zinc salt in the complex and on whether the coordinated ligand contains a pyridine or a quinoline unit.
The zinc chloride complexes **6a** and **7a**, both containing a quinoline unit, show no ability to catalyse the polymerisation of D,L-lactide, but the corresponding complexes **14a** and **15a**, both exhibiting a pyridine unit, demonstrate good or very good polymerisation properties. In the case of the acetate-containing complexes **6b**-**15b** it is also detected that complexes containing a pyridine unit in the coordinated ligand are more active than the corresponding complexes based on quinoline ligands. Though the catalytic properties of the complexes with a coordinated pyridine ligand that additionally contain chlorido ligands are more favourable than those that contain acetate instead of chloride. In the case of complexes with a coordinated quinoline ligand it is the other way round. However, the most auspicious candidates for highly active catalysts in the ROP of D,L-lactide are triflate-containing complexes **6c** and **7c**. They combine

Table 6.10: Polymerisation of D,L-lactide initiated by guanidine-pyridine zinc complexes.

Initiator	Temp. [°C]	Time[a] [h]	Yield [%]	M_w [g/mol]	PD[b]	Pr[c]
6a	130	24	0	-	-	-
6a	150	24	0	-	-	-
6a	150	48	0	-	-	-
7a	130	24	0	-	-	-
7a	150	24	0	-	-	-
7a	150	48	0	-	-	-
14a	130	24	55	67,000	2.0	
14a	150	24	74	44,000	2.2	0.57
14a	150	48	88	46,000	2.1	
15a	130	24	73	94,000	2.2	
15a	150	24	83	54,000	2.1	0.56
15a⋆	150	24	67	62,000	2.3	
15a	150	48	91	48,000	2.2	
6b	130	24	7	14,000	2.7	
6b	150	24	36	12,000	2.4	0.49
6b	150	48	58	17,000	2.0	
7b	130	24	0	-	-	
7b	150	24	2	12,000	2.0	
7b	150	48	41	19,000	2.1	0.50
14b	130	24	58	22,000	2.5	
14b	150	24	76	21,000	2.4	0.51
14b	150	48	73	19,000	2.5	
15b	130	24	78	27,000	2.1	
15b	150	24	73	13,000	2.0	0.50
15b	150	48	63	11,000	2.3	
6c	130	24	67	176,000	2.0	
6c	150	24	92	162,000	2.1	0.56
6c⋆	150	24	80	154,000	2.3	
6c	150	48	93	157,000	2.0	
7c	130	24	95	106,000	1.9	
7c	150	24	93	155,000	2.2	0.58
7c⋆	150	24	94	153,000	2.3	
7c	150	48	93	102,000	2.1	

Reaction conditions: Catalyst (0.2 mol%, *0.1 mol%); [a] reaction times were not necessarily optimised; [b] PD = M_w/M_n where M_n is the number-average molar mass; [c] from analysis of the ^{1}H homonuclear decoupled NMR spectrum using the equation $P_r{}^2 = 2$ [sis].[24]

almost quantitative yields with high molecular weights up to 176,000 g/mol. Their outstanding catalytic activities result presumably from their structural properties (accessibility to the zinc centre) and enhanced Lewis acidity. Seemingly, the weak coordination of the triflate anion favours attachment of lactide and therefore accelerates the reaction.

Regarding the M_w values of the obtained polymers it is remarkable that the experimental values ($M_{w,exp.}$) differ significantly from the theoretical values ($M_{w,theor.}$). In the case of **14b** and **15b**, the $M_{w,exp.}$ values are with e.g. 21,000 g/mol smaller than the corresponding theoretical value with 55,000 g/mol. These findings indicate that in the polymerisation reactions mediated by **14b** and **15b** side reactions occur which terminate the chain growth but release the catalyst still active. In contrast, the polymers obtained by **6c** and **7c** possess $M_{w,exp.}$ values that are significantly higher than the $M_{w,theor.}$ values (e.g. $M_{w,exp.}$ = 162,000 ; $M_{w,theor.}$ = 66,000 g/mol). A possible explanation is that the initiation rate of the polymerisation is slower than the propagation rate so that only a fraction of the used complexes starts growing chains and actually initiate the ROP.

The comparison of the guanidine-pyridine zinc system with the bisguanidine zinc system to evaluate the strategy of substitution of one guanidine by a pyridine unit reveals at first sight no obvious trend. The zinc bisguanidine complexes $[Zn(DMEG_2e)Cl_2]$ (**1a**), $[Zn(DMEG_2e)(CH_3COO)_2]$ (**1b**) and $[Zn(DMEG_2e)_2][CF_3SO_3]_2$ (**1c**) exhibit higher polymerisation activities than **6a**, **6b**, **7a**, **7b**, **14b** and **15b**, but **14a** and **15a** show higher and **6c** and **7c** much higher activities. To classify the polymerisation activity of the guanidine-pyridine zinc system, the standard catalyst for industrial PLA production, tin octoate, was examined under the same reaction conditions. The tin compound leads to almost quantitative yields but the molecular weights of the obtained polymers (47,000-80,000 g/mol, see Table 6.11) are lower than those for **15a** and significantly smaller than those for **6c** and **7c**.

In addition, not only the structure of the used catalyst is important for the polymerisation process but also the reaction conditions are relevant. In most cases the lower temperature of 130°C leads to higher molecular masses but slightly lower yields. Increasing the reaction time from 24 to 48 h often does not improve the conversion, nor does it increase the molecular weight of the obtained polymers. On the contrary, a decrease in yield and molecular weight can be observed in several cases. This effect was already reported for polymerisation experiments conducted with bisguanidine complexes (Chapter 4), which may be caused by side reactions such as interchain or intrachain transesterification resulting in a chain-transfer reaction.[126,127]

To exclude the possibility that the complexes decompose in the polymer melt and the single components are the real initiators in the ring-opening polymerisation of lactide, the catalytic properties of the guanidine-pyridine hybrid ligands **6**, **7**, **14** and **15** and zinc salts $ZnCl_2$, $Zn(CH_3COO)_2$ and $Zn(CF_3SO_3)_2$ were tested (Table 6.11). The catalytic activities of the guanidine-pyridine hybrid ligands are markedly lower than those of the examined complexes. In a different context, guanidines have already been reported as effective organocatalysts for the ring-opening polymerisation of cyclic esters.[40–42] Ligand **14** is almost inactive and **6**, **7** and **15** reach an average yield of only 35% with molecular weights of 9,000 g/mol at 150°C and 48 h

polymerisation time; under the other conditions they show no polymerisation activity at all.

Table 6.11: Polymerisation of D,L-lactide initiated by **6**, **7**, **14**, **15**, $ZnCl_2$, $Zn(CH_3COO)_2$, $Zn(CF_3SO_3)_2$ and $SnOct_2$.

Initiator	Temp. [°C]	Time [h]	Yield [%]	M_w [g/mol]	PD[a]
6	130	24	0	-	-
6	150	24	0	-	-
6	150	48	47	9,000	1.9
7	130	24	0	-	-
7	150	24	0	-	-
7	150	48	32	9,000	2.4
14	130	24	0	-	-
14	150	24	0	-	-
14	150	48	< 1	-	-
15	130	24	0	-	-
15	150	24	0	-	-
15	150	48	26	9,000	2.0
$ZnCl_2$	130	24	0	-	-
$ZnCl_2$	150	24	42	34,000	2.4
$ZnCl_2$	150	48	85	45,000	2.4
$Zn(CH_3COO)_2$	130	24	42	134,000	2.1
$Zn(CH_3COO)_2$	150	24	69	130,000	2.1
$Zn(CH_3COO)_2$	150	48	84	117,000	2.2
$Zn(CF_3SO_3)_2$	130	24	0	-	-
$Zn(CF_3SO_3)_2$	150	24	0	-	-
$Zn(CF_3SO_3)_2$	150	48	0	-	-
$SnOct_2$	130	24	100	80,000	1.9
$SnOct_2$	150	24	98	47,000	1.9
$SnOct_2$	150	48	93	37,000	2.0

Reaction conditions: Catalyst (0.2 mol%); [a] PD = M_w/M_n where M_n is the number-average molar mass.

It is noteworthy that zinc chloride is inactive at 130°C but at 150°C gives results that are comparable to or worse than those of **14a**. Complex **15a** always shows better polymerisation activity than zinc chloride. On the other hand, the catalytic performance of zinc acetate is higher than those of all examined complexes containing zinc acetate. Interestingly, zinc triflate shows no catalytic activity at all in the ROP of lactide although the most active zinc complexes of guanidine-pyridine hybrid ligands contain this zinc salt. Nevertheless, all results show no in-

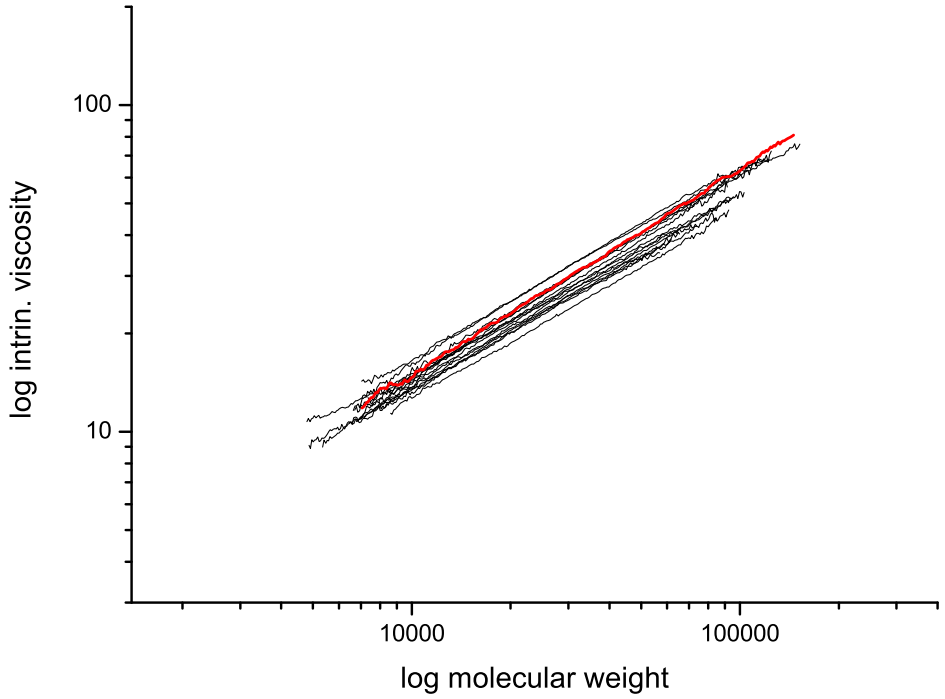

Figure 6.10: Mark-Houwink plot of selected PLAs obtained by ROP with zinc based catalysts (black lines) and stannous octoate (red line). The calculated mean values of α and K in THF at 35°C are 0.59 and 0.067, respectively.

dication that the complexes decompose in the polymer melt and that the single components may be the true initiators in the ring-opening polymerisation of lactide.

The structural characteristics of the synthesised polymers were studied by correlating their intrinsic viscosities with the molecular weight M. For polymers large enough, this correlation is described by the Mark-Houwink equation:[128] $[\eta] = K \cdot M^{\alpha}$.

Figure 6.10 shows Mark-Houwink plots of selected PLAs obtained by ROP with **6b**, **6c**, **7b**, **7c**, **14a**-**15b**, $ZnCl_2$, $Zn(CH_3COO)_2$, $Sn(Oct)_2$ and bisguanidine complexes **1a**, **1b** and **1c**. All plots show linear behaviour and the identical trends for all examined polymers indicate that the obtained PLA samples are structurally homogeneous and linear. Hence, the structure of the examined polymer is independent of the used initiator. The averaged values for the Mark-Houwink constants of the obtained polymers at 35°C in THF were calculated to α = 0.59 and K = 0.067. These values agree with those described in Chapter 4 for PLAs obtained with bisguanidine zinc complexes. Comparable values for different temperatures and solvents have already been reported.[19,129,130]

Especially complexes **6c** and **7c** are highly active polymerisation catalysts applicable in the

current industrial practice. They tolerate air, moisture and impurities in lactide and are soluble in organic solvents and molten lactide. The obtained polymers have high molecular masses and a relatively narrow molecular weight distribution. Intriguingly, the ROP of lactide is catalysed without the presence of a co-initiator such as alcohols.[5,47] Furthermore, no alkoxide groups are required to attack the carbonyl group of lactide. The enhanced Lewis acidity of the zinc atoms is presumably the more important factor for the coordination and activation of lactide.

6.1.3 Conclusion

The synthesis and complete characterisation of zinc complexes stabilised by guanidine-pyridine hybrid ligands was reported. They proved to be active initiators in the ring-opening polymerisation of D,L-lactide with only few exceptions. Polylactides with molecular weights (M_w) up to 176,000 g/mol and in almost quantitative yields could be obtained. These values represent a significant augmentation over bisguanidine zinc complexes and corroborate the strategy of building up N-donor ligands with different donor strengths and substituents with varied sterical demand. In complexes with the same guanidine ligand the activity of the initiator depends on the anionic component of the zinc salt.
Zinc triflate complexes turned out to be excellent catalysts for ROP of lactide. A possible explanation is that flexible coordination of one triflate anion to the zinc centre facilitates precoordination of the lactide molecule, while the higher positive charge at the zinc centre in comparison to the tetrahedral complexes offers higher Lewis acidity for activation of lactide.
The reported class of zinc complexes offers a number of advantages: straightforward catalyst synthesis, easy and robust handling, high polymer yields and homogeneous polymers with high molecular mass.
Moreover, the Mark-Houwink correlation demonstrates that the polymers obtained with the guanidine zinc complexes and the industrial standard $SnOct_2$ are linear and structurally indistinguishable.

6.2 Tracking the structure-reactivity relationship of zinc guanidine-quinoline hybrid complexes initiating lactide polymerisation

Three zinc guanidine-pyridine hybrid complexes $[Zn(TMGqu)_2(CH_3SO_3)][CH_3SO_3]$ (**7e**), $[Zn(DMEGqu)(CH_3SO_3)_2]$ (**6e-1**) and $[Zn(DMEGqu)_2(CH_3SO_3)][CH_3SO_3]$ (**6e-2**) were synthesised, completely characterised and investigated on their activity in the solvent-free ring-opening polymerisation of D,L-lactide. It was proven that the bis-chelate trigonal-bipyramidally coordinated compounds **7e** and **6e-2** are able to act as initiators in lactide polymerisation. The tetrahedral complex **6e-1** does not initiate lactide polymerisation. In an integrated approach

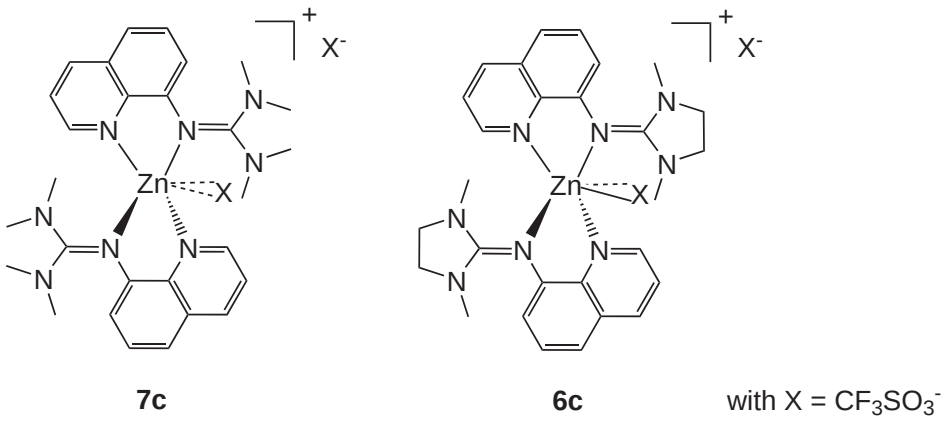

Figure 6.11: $[Zn(TMGqu)_2(CF_3SO_3)][CF_3SO_3]$ (**7c**) and $[Zn(DMEGqu)_2(CF_3SO_3)][CF_3SO_3]$ (**6c**).

of structural studies and DFT calculations, the active complexes **7e** and **6e-2** were analysed towards their structural and electronical prerequisites in comparison to their more active triflate analogues **7c** and **6c**. The influence of coordination strength of the anionic component on the charge distribution within the complex and on the substrate accessibility to the zinc centre is highlighted as crucial factor for the polymerisation initiation. As result, it is shown that the mesylate complexes **7e** and **6e-2** have less positive charge on the zinc atom and the mesylate is stronger bound than the corresponding triflate in the triflate complexes **7c** and **6c**. Consequently, the reactivity of the complexes is directly correlated to the coordinational behaviour of the anionic component.

6.2.1 Introduction

Zinc guanidine-pyridine hybrid complexes were found to be excellent and environmentally benign initiators in the solvent-free ROP of D,L-lactide. The most auspicious candidates were the bis-chelate complexes $[Zn(TMGqu)_2(OTf)][OTf]$ (**7c**) and $[Zn(DMEGqu)_2(OTf)][OTf]$ (**6c**) (see Fig. 6.11 and Section 6.1).
Their outstanding catalytic activity compared to those of other guanidine-pyridine hybrid zinc complexes results from their structural properties and enhanced Lewis acidity. Seemingly, the weak coordination of the triflate anion allows a good accessibility to the zinc centre which favours coordination of lactide and therefore accelerates the reaction. In addition, it was found that complexes with greater positive charge on the zinc atom exhibit a greater catalytic activity. To elucidate the structural and electronical influences on the structure-reactivity relationship of zinc guanidine-pyridine complexes in the polymerisation of D,L-lactide three different complexes with the slightly stronger coordinating anion mesylate were synthesised. They were investigated concerning the structural and electronical influence of the anionic component on the polymerisation activity.

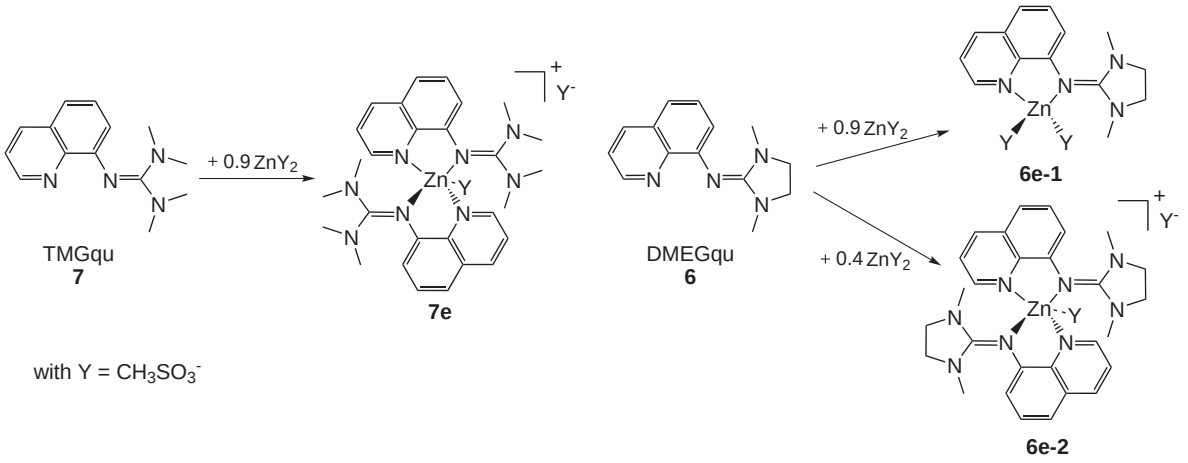

Figure 6.12: Complex synthesis of **7e**, **6e-1** and **6e-2** in dependence of molar ratio.

6.2.2 Results

Synthesis of the zinc complexes

The reaction of TMGqu and DMEGqu with zinc mesylate (molar ratio ligand to zinc salt 1.1 : 1) in a dry, aprotic solvent (MeCN, THF) resulted in straightforward formation of zinc complexes $[Zn(TMGqu)_2(CH_3SO_3)][CH_3SO_3]$ (**7e**) and $[Zn(DMEGqu)(CH_3SO_3)_2]$ (**6e-1**). Complex
$[Zn(DMEGqu)_2(CH_3SO_3)][CH_3SO_3]$ (**6e-2**) can be obtained if an excess of DMEGqu (molar ratio ligand to zinc salt 2.5 : 1) is used (see Fig. 6.12). They could be isolated as yellow crystals in yields of 96-99%. Single crystals of the complexes were obtained either by cooling a saturated solution slowly to room temperature or by slow diffusion of diethyl ether into the solution. The resulting crystals have high stability towards moisture and air.

Structure of the zinc complexes

The crystal structures of **7e**, **6e-1** and **6e-2** (Figures 6.13-6.15) were determined by X-ray crystallography. In the complexes **7e** and **6e-2** the zinc atom is fourfold coordinated by the nitrogen atoms of two chelate ligands and possesses an additional contact to one oxygen atom of one mesylate ion, while the other mesylate ion is far away from the complex centre and acts as counterion. Contrastingly, in complex **6e-1** the zinc atom is twofold coordinated by the two N-donor atoms of the DMEGqu ligand and the remaining coordination sites are occupied by two oxygen atoms of two mesylate ions (Fig. 6.14). Selected bond lengths and angles of the compounds are collected in Table 6.12.
In the bis-chelate complexes **7e** and **6e-2** the coordination geometry of the zinc centre can be best described as trigonal-bipyramidal. The axial positions are occupied by the pyridine nitrogen atoms and in the equatorial plane the guanidine nitrogen atoms as well as one oxygen

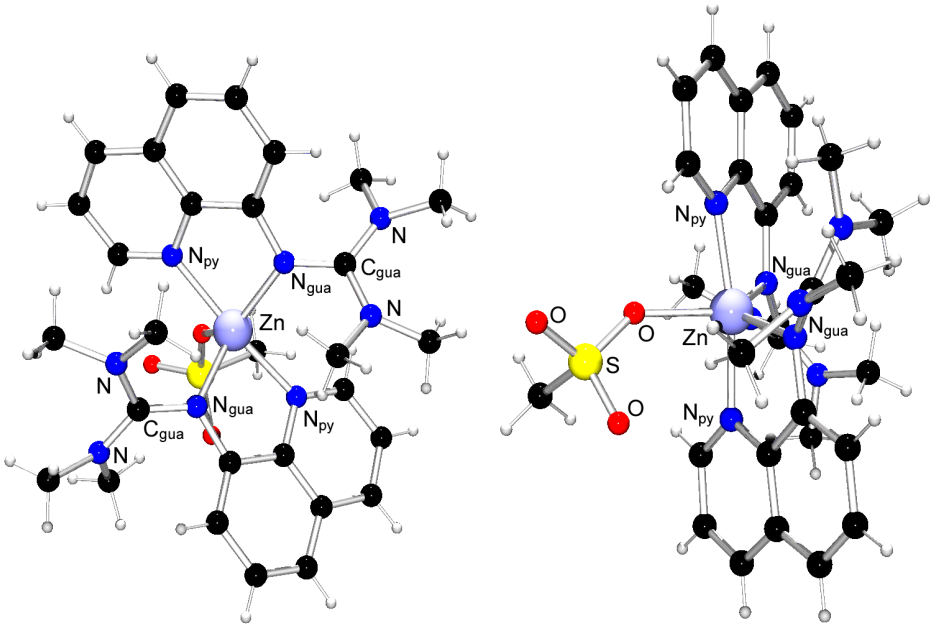

Figure 6.13: Molecular structure of $[Zn(TMGqu)_2(CH_3SO_3)]^+$ in crystals of $[Zn(TMGqu)_2(CH_3SO_3)][CH_3SO_3]$ (**7e**) as determined at 120 K (depicted in two different orientations).

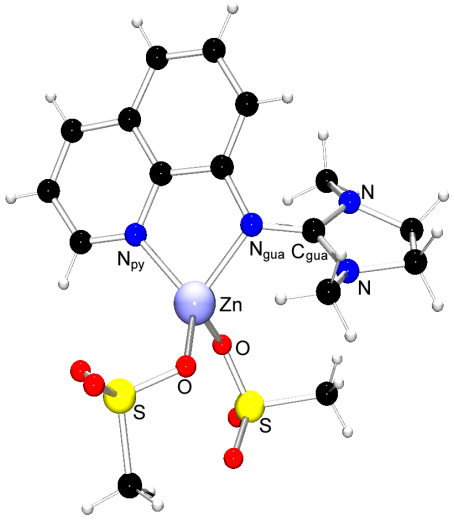

Figure 6.14: Crystal structure of $[Zn(DMEGqu)(CH_3SO_3)_2]$ (**6e-1**) as determined at 120 K.

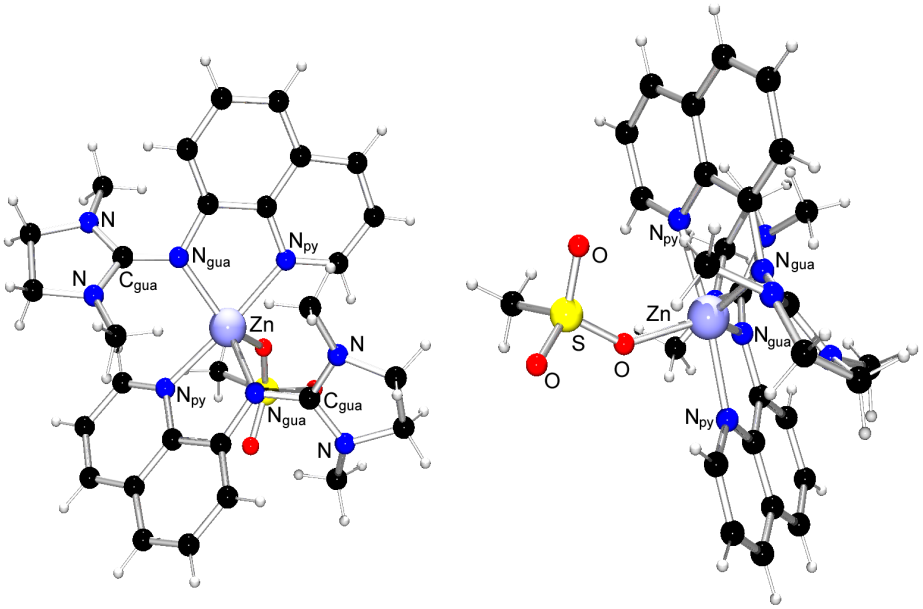

Figure 6.15: Molecular structure of $[Zn(DMEGqu)_2(CH_3SO_3)]^+$ in crystals of $[Zn(DMEGqu)_2(CH_3SO_3)][CH_3SO_3]$ (**6e-2**) as determined at 120 K (depicted in two different orientations).

atom of the mesylate ion are located around the zinc atom. The angle between the guanidine nitrogen atoms and the zinc atom is with 121.5° (av.) in accordance with the value expected for an ideal-typic trigonal-bipyramid which is 120°. The bite angles of the chelate ligands with an averaged value of 80.1° (90°) and the angle between the pyridine nitrogen atoms and the zinc centre with 171.3° (av.) (180°) are each to small and therefore leading to a distortion of the structure. In complex **6e-1** the coordination geometry of the zinc centre is dictated by the bite angles of the chelate ligand which possesses a value of 83.6° and therefore differs considerably from the angle expected for an ideal-typic tetrahedron (109.47°). This leads to distorted tetrahedral coordination geometry.

The distances between the zinc atom and the pyridine donor atom are in the same range in each complex (**7e**: av 2.096; **6e-1**: 2.031; **6e-2**: av 2.088 Å) and significantly longer than the corresponding Zn-N_{gua} bond lengths (**7e**: av 2.061; **6e-1**: 2.017; **6e-2**: av 2.063 Å). It is noticeable that the Zn-N bonds in the tetrahedral complex **6e-1** are in general shorter than the corresponding bonds in the bipyramidal complexes due to the smaller coordination number. This effect is also reflected in the distances between the zinc atom and the oxygen atom(s). In **6e-1** it is significantly shorter (av. 1.947 Å) than in the complexes **7e** and **6e-2** (**7e**: 2.103; **6e-2**: 2.072 Å).

The distances between the nitrogen and the carbon atoms of the guanidine function are in all three complexes very alike and lie in the range of 1.330 to 1.354 Å which is indicative for good delocalisation in this moiety.

The angle between the $C_{gua}N_3$ and the NC_3 plane shows the characteristic twisting within the guanidine moiety which can be found for all peralkylated guanidine units.[152] This twisting is a result of the interplay between the electronic effect of the intraguanidine conjugation (driving towards planarity) and the evasion of the alkyl substituents. The angles average a higher value for TMGqu (29.6°) than in DMEGqu (11.8 and 9.6°) because twisting within TMG is more distinct due to the free rotation of the methyl groups connected to the amine function, whereas in DMEG twisting is hindered by the rigid ethylene bridge between the amine groups of the guanidine moiety.

Table 6.12: Selected bond lengths (Å) and bond angles (°) of **7e**, **6e-1** and **6e-2**.

	7e	**6e-1**	**6e-2**
Zn-N_{gua}	2.043(1), 2.079(1)	2.017(1)	2.053(3), 2.072(3)
Zn-N_{py}	2.088(1), 2.103(1)	2.031(1)	2.087(3), 2.089(3)
Zn-O	2.103(1)	1.937(1), 1.956(1)	2.072(3)
C_{gua}-N_{gua}	1.354(2), 1.342(2)	1.337(2)	1.341(5), 1.330(5)
C_{gua}-N_{amine}	1.344(2), 1.346(2), 1.348(2), 1.350(2)	1.354(2), 1.343(2)	1.327(5), 1.335(5), 1.352(5), 1.338(5)
N_{gua}-Zn-N_{gua}	121.1(1)	-	121.8(1)
N_{gua}-Zn-N_{py} (bite)	80.8(1), 79.2(1)	83.6(1)	80.9(1), 79.3(1)
N_{py}-Zn-N_{py}	170.7(1)	-	171.8(1)
∠ ($C_{gua}N_3$, NC_3) (av.)	29.6	11.8	9.6

DFT calculations

The structural trends described above are discussed under consideration of gas phase DFT calculations. The electronic structures of the zinc complexes **7e**, **6e-1** and **6e-2** have been examined using the B3LYP hybrid DFT functional[138–140] in combination with the 6-31g(d) basis set, implemented by the Gaussian 03 suite of programs.[142] Geometry optimisations were performed using the coordinates from X-ray data as starting points. The results of the optimisations are presented in Table 6.13.

The computed complex structures are in good agreement with their solid state structures. By trend, the Zn-N distances are predicted 0.01 to 0.05 Å too long. This tendency has been observed quite frequently for such systems (see section 6.1).[143,144] In contrast, the Zn-O distances in **7e** and **6e-2** are predicted around 0.5 Å too short, thus over-estimating the donor strength of the mesylate. For this reason, the donor strength of the N donor might be under-estimated. The trigonal-bipyramidal coordination in **7e** and **6e-2** is correctly described with regard to the critical angles like the bite angles and the N_{gua}-Zn-N_{gua} and N_{py}-Zn-N_{py} angles.

Complex **6e-1** seems to represent a more complicated case: the Zn-N distances are predicted clearly too long whereas one of the Zn-O distances is predicted slightly too short. Concomitantly, the coordination of the mesylate anions is not correctly described: in the solid-state,

Table 6.13: Summary of key geometric parameters of the calculated structures of **7e**, **6e-1** and **6e-2** (RB3LYP/6-31G(d), bond lengths in Å and angles in °).

	7e	**6e-1**	**6e-2**
Zn- N_{gua}	2.140, 2.077	2.111	2.136, 2.089
Zn-N_{py}	2.127, 2.147	2.057	2.120, 2.142
Zn-O	2.054	1.929, 2.056, 2.271	2.029
C_{gua}-N_{gua}	1.344, 1.345	1.329	1.338, 1.338
C_{gua}-N_{amine}	1.367, 1.356 1.363, 1.356	1.375, 1.348	1.359, 1.351 1.353, 1.365
N_{gua}-Zn-N_{gua}	116.8	-	116.4
N_{gua}-Zn-N_{py} (bite)	78.4, 79. 7	80.5	78.4, 79.6
N_{py}-Zn-N_{py}	165.9	-	169.7
$\angle$ ($C_{gua}N_3$, NC_3)	30.9	11.5	8.7

Table 6.14: Mulliken charges in electron units (charge of electron is equal to -1) of **7e**, **6e-1** and **6e-2** (RB3LYP/ 6-31g(d)).

	7e	**6e-1**	**6e-2**
Zn	+0.968	+0.899	+0.974
N_{gua}	-0.741, -0.756	-0.788	-0.791, -0.798
N_{py}	-0.633, -0.607	-0.663	-0.619, -0.636
O	-0.686	-0.678, -0.698	-0.682
C_{gua}	+0.668, +0.653	0.792	+0.773, +0.773
N_{amine}	-0.399, -0.394, -0.394, -0.407	-0.435, -0.457	-0.445, -0.444 -0.448, -0.440

both anions act a monodentate ligands with short Zn-O bonds (1.937(1) and 1.956(1) Å) whereas the DFT predicts one monodentate mesylate donor and the other mesylate as bidentate donor. In fact, the donor strength of the mesylate is stronger in reality.

For a more detailed analysis of the electronic structure the Mulliken charges have been determined. The resulting charges are summarised in Table 6.14. These charges do not represent absolute charges but the trends among the complexes give an impression of electronic effects. The comparison between the bis-chelate complex cations **7e** and **6e-2** and the tetrahedral complex **6e-1** reveals that the zinc atom is significantly more positively charged in the bis-chelates. This effect goes along with the great positive charge found for the bis-chelate triflate systems **7c** and **6c** (Section 6.1). The guanidine N atoms are more negatively charged in the DMEG-containing ligands in **6e-1** and **6e-2** which is in accordance with the results for similar TMG and DMEG complexes. The greater negative charge on the guanidine N atoms in **6e-1** and **6e-2** is consequentially accompanied by greater positive charges on the guanidine C atoms in **6e-1** and **6e-2**.

Polymerisation activity

The guanidine-pyridine zinc complexes **7e**, **6e-1** and **6e-2** were investigated towards their activity in the bulk polymerisation of D,L-lactide according to the standard procedure (0.2 mol% catalyst, 150°C). In order to rate the catalytic activity of the complexes, the polymer yield was defined and the molecular weights as well as the polydispersity of the obtained PLA were determined by gel permeation chromatography (see Table 6.15). In contrast to earlier studies, the reaction time was extended because after 24 h the yield was too small to give reasonable results.
It was found that the complexes **7e** and **6e-2** initiate the ring-opening polymerisation of D,L-lactide and provide very similar results whereas the tetrahedral complex **6e-1** shows even after 48 h no polymerisation activity. However, the comparison of the results of the bis-chelate mesylate complexes to those of the corresponding triflate complexes demonstrates clearly that the polymerisation activity decreases dramatically if the complexes contain the mesylate anion instead of the triflate ion. Application of **7c** and **6c** leads in half reaction time to polymers with a three times higher yield and more than five times higher molecular weights. The smaller PD values in the case of **7e** and **6e-2** may be due to the smaller yield.

Table 6.15: Polymerisation of D,L-lactide in the presence of the guanidine zinc complexes **7e**, **6e-1** and **6e-2**, as well with **7c** and **6c**.

Initiator		Time [h]	Yield [%]	M_w [g/mol]	PD[a]
$[Zn(TMGqu)_2(CH_3SO_3)][CH_3SO_3]$	(**7e**)	48	33	28,000	1.6
$[Zn(DMEGqu)(CH_3SO_3)_2]$	(**6e-1**)	48	0	-	-
$[Zn(DMEGqu)_2(CH_3SO_3)][CH_3SO_3]$	(**6e-2**)	48	29	28,000	1.5
$[Zn(TMGqu)_2(CF_3SO_3)][CF_3SO_3]$	(**7c**)	24	93	155,000	2.2
$[Zn(DMEGqu)_2(CF_3SO_3)][CF_3SO_3]$	(**6c**)	24	92	162,000	2.1

Reaction conditions: Catalyst (0.2 mol%), 150 °C.

[a] PD = M_w/M_n where M_n is the number-average molar mass.

6.2.3 Discussion

The investigations reveal a high dependence of the polymerisation activity of the zinc complexes on their structural and electronical properties. The comparison of the mesylate complexes **7e** and **6e-2** to their more active triflate analogues (Section 6.1) **7c** and **6c** allows to elucidate the influence of coordination strength of the anionic component on the charge distribution within the complex and on the substrate accessibility to the zinc centre as crucial factors for the polymerisation initiation. An overview of the compared complex features is

given in Table 6.16. For reasons of clarity, only the features of the DMEGqu containing complexes **6e-1**, **6e-2** and **6c** are listed. The bis-chelate complexes **7e** and **6e-2** are structurally and electronically very similar to each other and consequently show almost the same polymerisation activity, indicating that the properties of the guanidine function have the same effect in this case.

Table 6.16: Correlation of structural and electronical properties of **6e-1**, **6e-2** and **6c** with their ROP activity.

Complex	*Bond length*	*Mulliken Charge*		*ROP activity*	
	Zn-O	Zn^{2+}	av. N_{gua}	Yield	M_w
6e-1	1.937, 1.956 Å	+0.899	-0.788	0	-
6e-2	2.072 Å	+0.974	-0.795	29 %	28,000 g/mol
6c	2.700, 2.452 Å	+1.004	-0.837	92 %	162,000 g/mol

The tetrahedral zinc mesylate complex **6e-1** was found to be inactive under the given conditions. It is remarkable that the initiator activity increases from **6e-1** over **6e-2** to **6c** with increasing Zn-O distance and decreasing bond strength. This effect reinforces our hypothesis that the anion acts as placeholder for the monomer. Hence, the weak coordination of the triflate anion allows a good accessibility to the zinc centre which favours coordination of lactide and therefore accelerates the reaction. The slightly stronger donating property of the mesylate anion prevents fast coordination of the lactide.
In addition, the electronic properties of the complexes influence their activity as well. The positive charge at the zinc atom increases in the same direction as the polymerisation activity: from **6e-1** over **6e-2** to **6c**. So it was demonstrated that a great positive charge at the zinc atom promotes the ability to initiate the lactide polymerisation. In addition, it is proposed that the highly nucleophilic guanidine donor system acts as ring-opening agent. With regard to these influences, it is obvious that the polymerisation presented here proceeds without the presence of alkoxides or alcohols which are traditionally necessary.[5,13,20,25,44,47,148,157]
In summary, in the case of guanidine-pyridine hybrid zinc complexes an auspicious initiator for the polymerisation of lactide should be a bis-chelate complex with additional very long or weak Zn-O bonds which possesses a high positive charge at the zinc atom.

6.2.4 Conclusion

The synthesis and complete characterisation of three zinc guanidine-pyridine hybrid complexes $[Zn(TMGqu)_2(CH_3SO_3)][CH_3SO_3]$ (**7e**), $[Zn(DMEGqu)(CH_3SO_3)_2]$ (**6e-1**) and $[Zn(DMEGqu)_2(CH_3SO_3)][CH_3SO_3]$ (**6e-2**) were reported. They were investigated towards their activity in the solvent-free ring-opening polymerisation of D,L-lactide and it was proven that the bis-chelate trigonal-bipyramidally coordinated compounds **7e** and **6e-2** are able to act

as initiators for lactide polymerisation. Polylactides with molecular weights (M_w) of around 28,000 g/mol could be obtained with relatively narrow polydispersities. The tetrahedral complex **6e-1** does not initiate lactide polymerisation under the given conditions.
In an integrated approach of structural studies and DFT calculations, the activity of the complexes **7e** and **6e-2** was correlated with their structural and electronical prerequisites in comparison to their more active triflate analogues **7c** and **6c**. The investigations reveal that the coordination strength of the anionic component has a significant impact on two issues of the polymerisation initiation: the charge distribution within the complex (especially the positive charge on the zinc atom) influences the attraction towards the substrate lactide and the accessibility to the zinc centre regulates the substrate coordination. DFT analysis shows that the mesylate complexes **7e** and **6e-2** exhibit less positive charge on the zinc atom and the mesylate is stronger bound than the corresponding triflate in the triflate complexes **7c** and **6c**. Consequently, the reactivity of the complexes is directly correlated to the coordinational behaviour of the anionic component.

6.3 Zinc complexes with guanidine-pyridine hybrid ligands: Anion effect and catalytic activity

The guanidine-pyridine ligands DMEGqu (**6**), TMGqu (**7**) and DMEGpy (**14**) were reacted with zinc benzoate, zinc acetyl acetonate, zinc bromide, zinc tetrafluoroborate and zinc D,L-lactate in order to obtain the corresponding complexes. The anion effect on the molecular structure and the catalytic activity of these complexes were investigated.

6.3.1 Introduction

In the last two sections it could be demonstrated that the anionic component of the zinc complexes, developed to initiate the ROP of lactide, strongly influences not only the molecular structure of the corresponding complex but also has a high impact on its catalytic properties. For further investigations of this anion effect the guanidine-pyridine ligands DMEGqu (**6**), TMGqu (**7**) and DMEGpy (**14**) were reacted with different zinc compounds to obtain the according complexes. Zinc benzoate ($Zn(C_6H_5COO)_2$, $Zn(OBz)_2$) and zinc acetylacetonate ($Zn(C_5H_7O_2)_2$, $Zn(acac)_2$) were chosen because they possess good coordination properties and provide in case of coordination Zn-O bonds which may support the insertion of lactide molecules. Zinc bromide ($ZnBr_2$) was used to investigate the influence of the halide in comparison to zinc dichloride complexes. Due to the fact that the quite weak or non-coordinating anion triflate provides highly active zinc complexes, zinc tetrafluoroborate ($Zn(BF_4)_2$) was applied as well because of its weak coordination properties. In addition the preparation of complexes containing zinc lactate ($Zn(C_3H_5O_3)_2$, $Zn(Lac)_2$) was aspired. DFT calculations in the context of mechanistic studies (see Chapter 9) revealed that in guanidine-pyridine systems the

ring-opening of the first lactide molecule is the most energy-intensive step and therefore defines the reaction rate. This step may be avoided if a lactate moiety is already coordinated to the zinc atom.

6.3.2 Results and discussion

Synthesis of the zinc complexes

The preparation of zinc complexes stabilised by guanidine-pyridine hybrid ligands was conducted by simple stirring of the educts in a dry, aprotic solvent (MeCN, THF). An overview of the obtained compounds in given in Table 6.17. They could be isolated as yellow (**6d**, **7d**, **6f**, **7f**, **6g** and **6h**) or colourless crystals (**14d**) in yields of 86-99%. Single crystals of the complexes were obtained either by cooling a saturated solution slowly to room temperature or by slow diffusion of diethyl ether into the solution. The resulting crystals provide high stability towards moisture and air.

Table 6.17: Overview of prepared zinc complexes.

	DMEGqu (**6**)	TMGqu (**7**)	DMEGpy (**14**)
$Zn(OBz)_2$	$[Zn_2(DMEGqu)(OBz)_4]$ (**6d**)	$[Zn(TMGqu)(OBz)_2]$ (**7d**)	$[Zn(DMEGpy)(OBz)_2]$ (**14d**)
$ZnBr_2$	$[Zn(DMEGqu)Br_2]$ (**6f**)	$[Zn(TMGqu)Br_2]$ (**7f**)	
$Zn(acac)_2$	$[Zn(DMEGqu)(acac)_2]$ (**6g**)		
$Zn(BF_4)_2$	$[Zn(DMEGqu)_2(BF_4)][BF_4]$ (**6h**)		
$Zn(D,L\text{-}Lac)_2$	[Zn(DMEGqu)(D,L-Lac)] (**6i**)		

Structure of the zinc complexes

The lactate containing complex $[Zn(DMEGqu)(D,L\text{-}C_3H_5O_3)_2)]$ (**6i**) was only available as crystal powder, but its composition could be identified by means of NMR, IR and MS measurements as well as elemental analysis (see Fig. 6.16). The crystal structures of $[Zn_2(DMEGqu)(C_6H_5COO)_4]$ (**6d**), $[Zn(TMGqu)(C_6H_5COO)_2]$ (**7d**), $[Zn(DMEGpy)(C_6H_5COO)_2]$ (**14d**), $[Zn(DMEGqu)Br_2]$ (**6f**), $[Zn(TMGqu)Br_2]$ (**7f**), $[Zn(DMEGqu)(C_5H_7O_2)_2]$ (**6g**) and $[Zn(DMEGqu)_2(BF_4)][BF_4]$ (**6h**) were determined by X-ray crystallography (see Fig. 6.17-6.19).

Complexes with zinc benzoate and zinc acetylacetonate: The complexes prepared of zinc benzoate **6d**, **7d** and **14d** include the same anionic component. However, their molecular structures are quite different from each other (see Fig. 6.17).

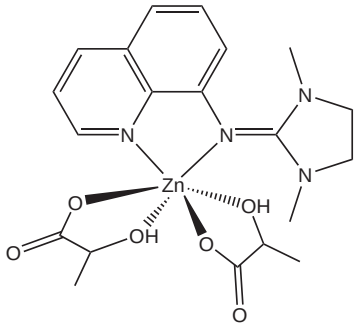

Figure 6.16: Schematic structure of [Zn(DMEGqu)(D,L-Lac)$_2$)] (**6i**).

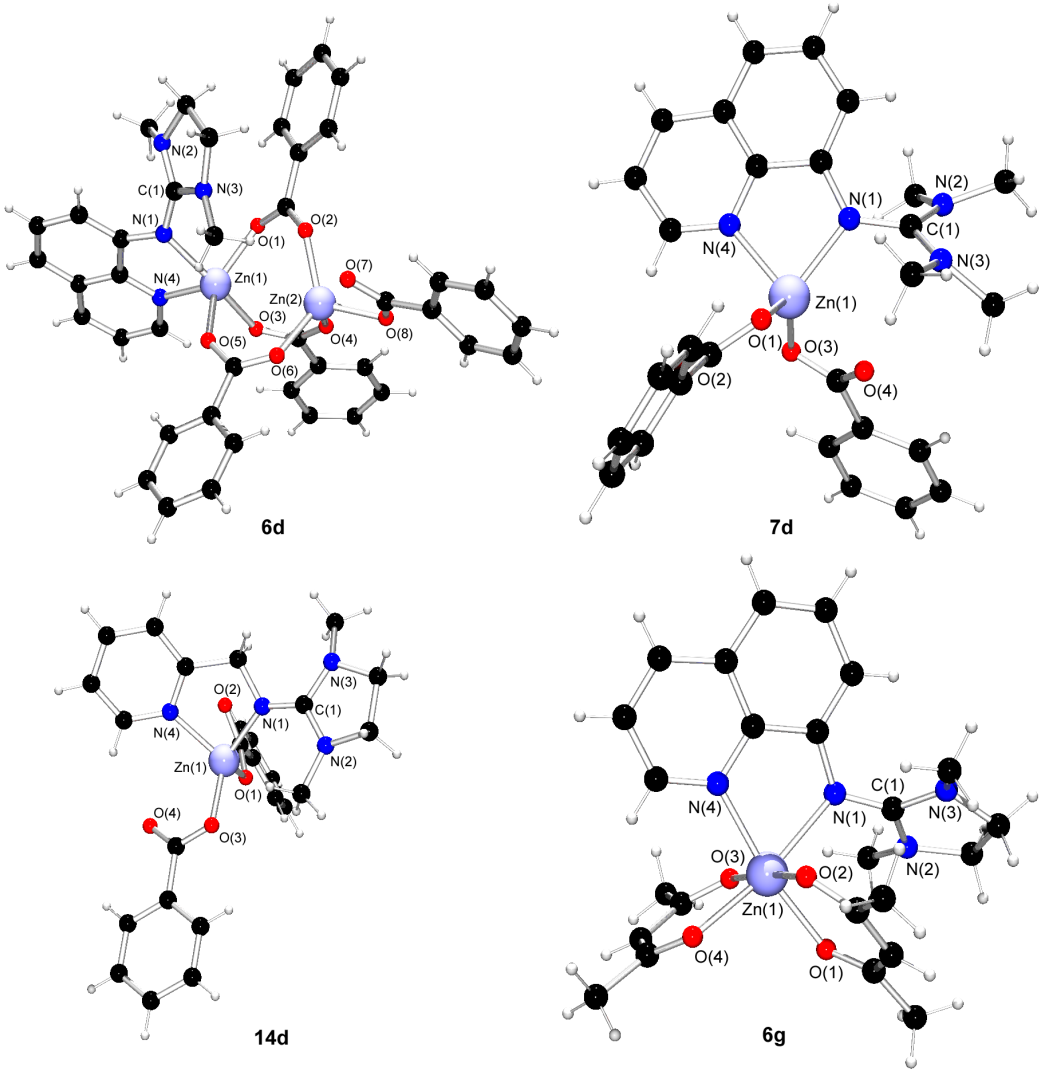

Figure 6.17: Crystal structures of [Zn_2(DMEGqu)($C_6H_5COO)_4$] (**6d**), [Zn(TMGqu)($C_6H_5COO)_2$] (**7d**), [Zn(DMEGpy)($C_6H_5COO)_2$] (**14d**) and [Zn(DMEGqu)($C_5H_7O_2)_2$] (**6g**) as determined at 120 K.

Complex **6d** possesses a dinuclear structure where one zinc atom is coordinated in a trigonal bipyramidal manner by the two N-donors of the guanidine ligand and three oxygen atoms of three benzoate ligands that act as η^2-bridge between the two zinc atoms. The Zn-N_{gua} bond is with 2.154(3) Å longer than the Zn-N_{py} bond which possesses a length of 2.055(3) Å. This difference in bond lengths is reflected in the coordination geometry where the N_{gua} atom occupy the axial position and the N_{py} atom one of the equatorial positions in the trigonal bipyramid. The second zinc atom exhibits a tetrahedral coordination geometry in which three coordination sites are occupied by the oxygen atoms of the η^2-bridging benzoates and the remaining coordination site is occupied by an oxygen atom of a mono-coordinating benzoate ligand. The Zn-O bond lengths depend on their coordination mode. The Zn-O length of the oxygen atoms in the equatorial positions of the trigonal bipyramid are with 2.002(2) and 2.009(2) Å shorter than the corresponding value of the oxygen atom in the axial position which is 2.082(2) Å. The Zn-O bonds of the ZnO_4 tetrahedron are with an average value of 1.970 Å almost equal in length.

Complexes **7d** and **14d** possess a mononuclear structure with a distorted tetrahedral coordination environment at the zinc atom. The latter is coordinated in a chelating manner by the two N-donor atoms of the guanidine ligands. In each complex the Zn-N_{py} distances possess with 2.077(2) (**7d**) and 2.058(2) Å (**14d**) higher values than the Zn-N_{gua} distances (**7d**: 2.056(2); **14d**: 2.026(2) Å). The remaining coordination sites are taken by the oxygen atoms of benzoate ligands. Though, in **14d** both benzoates act as mono-coordinating ligand, in **7d** one of them coordinates the zinc atom with both oxygen atoms acting as one donor. The Zn-O bond length of the bi-coordinating benzoate ligand exhibit with 2.096(2) and 2.248(2) Å higher values compared to those of the mono-coordinating benzoate ligands which increase from 1.945(1) over 1.961(1) in **14d** to 1.973(1) Å in **7d**.

Complex **6g** which is prepared of zinc acetylacetonate exhibits a distorted octahedral coordination geometry at the zinc atom. The latter is coordinated by the N-donor atoms of ligand **6** (Zn-N_{py}: 2.116(2); Zn-N_{gua}: 2.249(2) Å) and four O-donor atoms of two acetylacetonate lig-

Table 6.18: Selected bond lengths (Å) and bond angles (°) of **6d**, **7d**, **14d** and **6g**.

	6d	**7d**	**14d**	**6g**
Zn-N_{py}	2.055(3)	2.077(2)	2.058(2)	2.116(2)
Zn-N_{gua}	2.154(3)	2.056(2)	2.026(2)	2.249(2)
Zn-O	2.002(2), 2.009(2), 2.082(2), 1.953(2), 1.969(2), 1.971(2), 1.987(2)	1.973(1), 2.096(2), 2.248(2)	1.945(1), 1.961(1)	2.042(2), 2.085(2), 2.092(2), 2.094(2)
C_{gua}-N_{gua}	1.334(4)	1.342(2)	1.318(2)	1.319(3)
C_{gua}-N	1.355(4), 1.354(4)	1.350(2), 1.342(2)	1.344(2), 1.376(2)	1.344(3), 1.369(3)
N_{gua}-Zn-N_{amine} (bite)	79.2(1)	80.7(1)	82.8(1)	75.8(1)
∠(ZnO_2, ZnN_2)	-	-	80.8	-

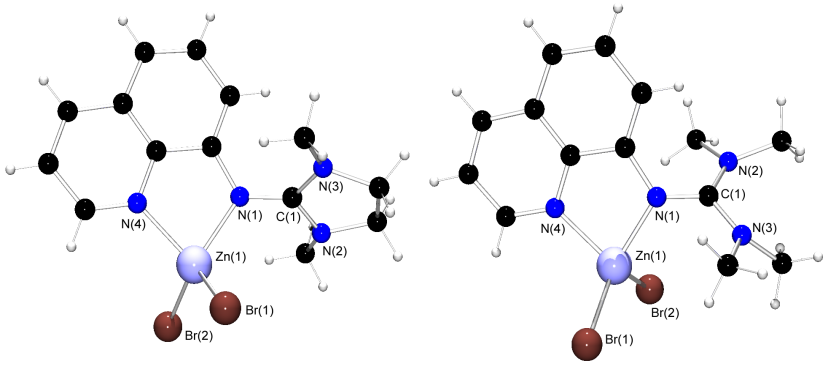

Figure 6.18: Crystal structures of [Zn(DMEGqu)Br_2] (**6f**, l) and [Zn(TMGqu)Br_2] (**7f**, r) as determined at 120 K.

ands (Zn-O: 2.042(2)-2.094 Å). The Zn bond lengths (Zn-O, Zn-N) in the octahedron are due to its geometry longer than those in the tetrahedral complexes and the bite angle of the ligand is smaller (**6d**: 79.1(1); **7d**: 80.7(1); **14d**: 82.8(1); **6g**: 75.8(1)°).
The C-N bonds in the guanidine moiety are in **6d** and **7d** within the precision of measurements equal in length (**6d**: av. 1.348; **7d**: 1.345 Å), whereas in **14d** and **6g** all three C-N bond lengths show different values. The C_{gua}-N_{gua} bond possesses with 1.318(2) (**14d**) and 1.319(3) Å (**6g**) in each complex the smallest C-N values. The C_{gua}-N bonds are with 1.344(2) and 1.376(2) Å for **14d** and 1.344(3) and 1.369(3) Å for **6g** significantly longer. Selected bond lengths and angles of the zinc complexes including anionic components with O-donors are collected in Table 6.18.
Complexes with zinc bromide: Complexes **6f** and **7f** are very similar to their chlorido analogues **6a** and **7a**. Their zinc atom is coordinated in a tetrahedral manner by two N atoms of guanidine-pyridine hybrid ligands and two bromide atoms (Fig. 6.18). The coordination of the different halides Br and Cl shows no significant influence of the crystal structures of the corresponding complexes (see Tab. 6.19). The Zn-N bonds of all four complexes are within

Table 6.19: Selected bond lengths (Å) and bond angles (°) of **6f**, **7f**, **6a** and **7a**.

	6f	**7f**	**6a**	**7a**
Zn-N_{py}	2.048(2)	2.042(2)	2.045(1)	2.044(1)
Zn-N_{gua}	2.038(2)	2.028(2)	2.039(1)	2.034(1)
Zn-Br (Zn-Cl)	2.352(1), 2.374(1)	2.349(1), 2.375(1)	2.212(1), 2.234(1)	2.217(1), 2.238(1)
C_{gua}-N_{gua}	1.343(3)	1.340(2)	1.327(2)	1.335(2)
C_{gua}-N	1.349(3), 1.336(3)	1.343(2), 1.354(2)	1.355(2), 1.352(2)	1.347(2), 1.357(2)
N_{gua}-Zn-N_{amine} (bite)	82.1(1)	82.5(1)	82.6(1)	82.3(1)
∠(Zn$Br(Cl)_2$, ZnN_2)	83.1	80.7	84.4(1)	79.3(1)

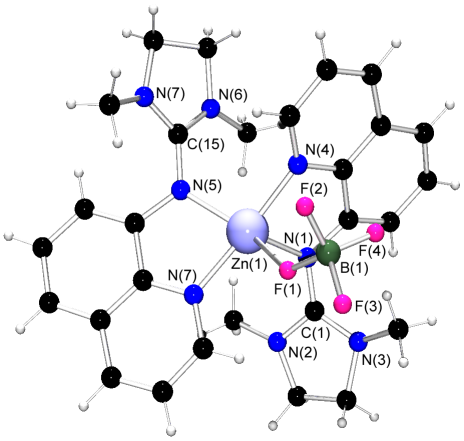

Figure 6.19: Crystal structure of $[Zn(DMEGqu)_2(BF_4)]^+$ in crystals of $[Zn(DMEGqu)_2(BF_4)][BF_4]$ (**6h**) as determined at 120 K.

the precision of measurements each equal in length (Zn-N_{gua}: av. 2.035; Zn-N_{py}: av. 2.045 Å). Only the Zn-Br bonds are in average 0.138 Å longer than the Zn-Cl bonds due to the bigger bromide atoms.

Complex with zinc tetrafluoroborate: In complex **6h** the zinc atom is fourfold coordinated by the nitrogen atoms of two chelate ligands and possesses an additional contact to one fluorine atom of one tetrafluoroborate ion, while the other tetrafluoroborate ion is far away from the complex centre and acts as counterion (Fig. 6.19). This structure motif can also be found in the zinc triflate and zinc mesylate complexes **6c** and **6e-2** described above. Selected bond lengths and angles of the complexes **6h**, **6c** and **6e-2** are collected in Table 6.20.

The coordination geometry of the zinc atom can also be described as trigonal-bipyramidal. The axial positions are occupied by the pyridine nitrogen atoms (Zn-N_{py}: av. 2.032 Å) and in the equatorial plane the guanidine nitrogen atoms (Zn-N_{gua}: av. 2.021 Å) as well as the fluorine atom of one tetrafluoroborate ion are located around the zinc atom. The angle between the guanidine nitrogen atoms and the zinc atom is with 112.7(1)° smaller than the value expected for an ideal-typic trigonal-bipyramid (120°). The bite angles of the chelate ligands with an averaged value of 82.8° (90°) and the angle between the pyridine nitrogen atoms and the zinc centre with 156.6(2)° (180°) are each to small and therefore leading to a distortion of the structure. The C-N bonds of the guanidine moieties are with an averaged value of 1.341 Å within the precision of measurements equal in length indicating a good delocalisation of electron density.

The Zn-F distance is of high interest concerning the catalytic activity of complex **6h** due to the fact that the long or weak Zn-O bond in **6c** and **6e-2** were considered responsible for their catalytic properties. With a value of 2.435(3) Å the Zn-F bond lies between those of the corresponding Zn-O bond in **6c** (av. 2.576 Å) and **6e-2** (2.072(3) Å). Thus, the ability of **6h** to initiate the ROP of lactide should lie between those of **6c** and **6e-2**.

Table 6.20: Selected bond lengths (Å) and bond angles (°) of **6h**, **6c** and **6e-2**.

	6h	**6c**	**6e-2**
Zn-N_{py}	2.031(4), 2.032(4)	2.089(3), 2.091(3)	2.053(3), 2.072(3)
Zn-N_{gua}	2.038(4), 2.004(4)	2.035(3), 2.049(3)	2.087(3), 2.089(3)
Zn-F (Zn-O)	2.435(3)	2.452(7), 2.700(7)	2.072(3)
C_{gua}-N_{gua}	1.334(5), 1.349(5)	1.345(5), 1.340(5)	1.341(5), 1.330(5)
C_{gua}-N_{amine}	1.335(6), 1.353(5), 1.330(6), 1.346(6)	1.344(5), 1.337(5), 1.340(5), 1.343(5)	1.327(5), 1.335(5), 1.352(5), 1.338(5)
N_{gua}-Zn-N_{amine} (bite)	83.5(2), 82.0(2)	81.4(1), 80.5 (1)	80.9(1), 79.3(1)
∠(ZnN_2, ZnN_2)	59.7	60.6(1)	60.3

Polymerisation activity

To investigate the anion effect on the catalytic activity of the complexes, **6d**, **7d**, **14d**, **6f**, **7f**, **6g** and **6h** were tested as initiators in the solvent-free polymerisation of D,L-lactide according to the standard procedure (0.2 mol% catalyst, 150°C). The polymer yield was defined and the molecular weights as well as the polydispersity of the obtained PLA were determined by gel permeation chromatography (see Table 6.21).

The dinuclear complex **6d** shows good catalytic performance with yields up to 89 % and molecular weights that conform to the theoretical values (e.g. $M_{w,exp}$ = 63,000 g/mol; $M_{w,theor.}$ = 61,000 g/mol). In comparison to **6d**, the mononuclear complex **7d** possesses less activity. Only after 48 h it provides PLA in low yields. On the contrary, **14d** that is also a mononuclear complex produces polymers in respectable yields but with slightly lower molecular weights. Due to the fact that pure zinc acetate also exhibits the ability to initiate the lactide polymerisation, the pure zinc benzoate was tested as well. It could be demonstrated that zinc benzoate itself possesses catalytic activity comparable to those of **14d** but lower than those of **6d**.

The structural similarity of the zinc bromide complexes **6f** and **7f** with their zinc chloride analogues **6a** and **7a** is also reflected in their catalytic performance. **6f** and **7f** show as well as **6a** and **7a** even after 48 h no ability to initiate the ROP of lactide.

Complex **6g**, including zinc acetylacetonate, exhibits a behaviour similar to that of **14d**. PLAs were obtained in good yields but with comparably low molecular weights (e.g. $M_{w,exp}$ = 20,000 g/mol; $M_{w,theor.}$ = 51,000 g/mol). This effect may be a hint for chain termination reactions.

The catalytic activity of **6h** can be compared to those of **6d** but the M_w values are significantly higher. These results fit very well with the prediction. Due to the value of the zinc distance to the weak coordinating ligand, the activity of **6h** was predicted slightly lower than those of **6c**. These findings support the hypothesis that in bis-chelate complexes the coordination strength of the anionic component has a significant impact on the polymerisation initiation.

The attempt to improve the catalytic properties of guanidine-pyridine based zinc complexes by introducing lactate ligands to the coordination sphere, did not provide the desired results.

Table 6.21: Polymerisation of D,L-lactide in the presence of **6d**, **7d**,**14d**, **6f**, **7f**, **6g**, **6h** and zinc benzoate

Initiator		Time[a] [h]	Yield [%]	M_w [g/mol]	PD[b]	Pr[c]
$[Zn_2(DMEGqu)(C_6H_5COO)_4]$	**6d**	24	85	63,000	1.8	0.52
$[Zn_2(DMEGqu)(C_6H_5COO)_4]$	**6d**	48	89	60,000	1.8	
$[Zn(TMGqu)(C_6H_5COO)_2]$	**7d**	24	0	-	-	-
$[Zn(TMGqu)(C_6H_5COO)_2]$	**7d**	48	16	23,000	1.6	
$[Zn(DMEGpy)(C_6H_5COO)_2]$	**14d**	24	74	28,000	1.8	0.50
$[Zn(DMEGpy)(C_6H_5COO)_2]$	**14d**	48	81	25,000	2.0	
$Zn(C_6H_5COO)_2$		24	77	123,000	1.8	
$Zn(C_6H_5COO)_2$		48	86	107,000	1.9	
$[Zn(DMEGqu)Br_2]$	**6f**	24	0	-	-	-
$[Zn(DMEGqu)Br_2]$	**6f**	48	0	-	-	-
$[Zn(TMGqu)Br_2]$	**7f**	24	0	-	-	-
$[Zn(TMGqu)Br_2]$	**7f**	48	0	-	-	-
$[Zn(DMEGqu)(C_5H_7O_2)_2]$	**6g**	24	71	20,000	2.0	0.50
$[Zn(DMEGqu)(C_5H_7O_2)_2]$	**6g**	48	80	22,000	1.9	
$[Zn(DMEGqu)_2(BF_4)][BF_4]$	**6h**	24	84	119,000	1.9	0.51
$[Zn(DMEGqu)_2(BF_4)][BF_4]$	**6h**	48	87	100,000	1.8	
$[Zn(DMEGqu)(D,L\text{-}C_3H_5O_3)_2)]$	**6i**	24	0	-	-	-
$[Zn(DMEGqu)(D,L\text{-}C_3H_5O_3)_2)]$	**6i**	48	29	11,000	1.5	

Reaction conditions: Catalyst (0.2 mol%), 150 °C; [a] reaction times were not necessarily optimised; [b] PD = M_w/M_n where M_n is the number-average molar mass; [c] From analysis of the ^{1}H homonuclear decoupled NMR spectrum using the equation $P_r^2 = 2$ [sis].[24]

Complex **6i** shows a weak performance as initiator in the ROP of lactide. However, these findings mean not obligatory that **6i** possesses less catalytic potential. During the polymerisation tests the melt colour turned from light yellow to deep brown, indicating that the complex was decomposed. This thermal instability is also reflected in the low melting point (60°C).
In summary, it was demonstrated that the kind of anionic component used to prepare the initiator influences its molecular structure as well as its thermal stability and hence has high impact on the catalytic activity.

6.3.3 Conclusion

In this section guanidine-pyridine zinc complexes were prepared including various zinc salts in order to elucidate the anion effect which was observed during previous studies (see section 6.1 and 6.2). In the case of guanidine-quinoline ligands, complexes with weak coordinating anions like triflate and tetrafuoroborate possess high potential as active initiators in the lactide polymerisation whereas halide complexes show no catalytic activity. The use of lactate ligands to overcome the energy barrier of the first ring-opening step was limited due to the low thermal stability of the corresponding complex. In general, it could be demonstrated that the choice of anionic component, used to prepare the initiator, defines the molecular structure, the charge distribution and the thermal stability of the complex and therefore its properties. Thus, the anion effect plays an important role in context of catalyst design.

6.4 Zinc complexes with guanidine-pyridine hybrid ligands: Guanidine effect and catalytic activity

Two series of new guanidine-pyridine ligands were developed by combining various chloroformamidinium chlorides with 8-aminoquinoline and 2-picolylamine. The latter as well as the pure 8-aminoquinoline were reacted with zinc chloride, zinc acetate and zinc triflate to prepare the corresponding complexes which were tested as initiators in the solvent-free ring-opening polymerisation of D,L-lactide. The guanidine effect on the catalytic activity of the obtained zinc complexes was investigated.

6.4.1 Introduction

During the previous sections it could be demonstrated that the catalytic properties of initiators belonging to the class of guanidine-pyridine zinc complexes strongly depend on the anionic component of the zinc salt as well as on the kind of pyridine unit in the ligand stabilising the complexes. In this section the impact of the guanidine unit in the ligand stabilising the initiator complexes on their ability to promote the polymerisation of lactide is investigated.
The modular synthesis protocol of guanidine-pyridine hybrid ligands allows for the easy variation of pyridine-spacer and guanidine units (see Section 1.3.2) and thus permits the optimal adaption of the ligands to the corresponding applications. In order to investigate the influence of the guanidine unit in guanidine-pyridine hybrid ligands on the catalytic activity of the corresponding zinc complexes, two series of new guanidine-pyridine ligands were developed by combining various chloroformamidinium chlorides with 8-aminoquinoline and 2-picolylamine. These two spacer-pyridine units were chosen due to the fact that ligands based on 8-aminoquinoline and 2-picolylamine show good coordination properties and in many cases relative easily provide single crystals of the corresponding zinc complexes suitable for X-

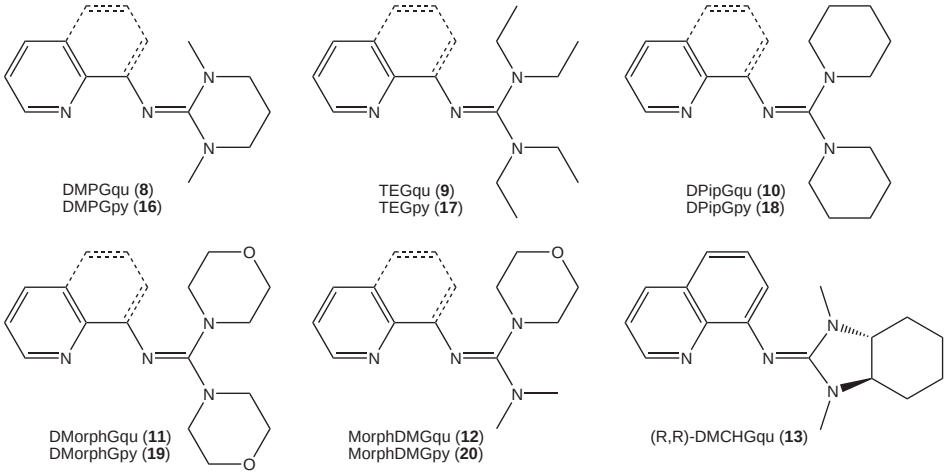

Figure 6.20: Overview of synthesised guanidine-pyridine hybrid ligands.

ray diffraction and therefore enable the determination of the solid-state structure. In addition, zinc complexes with the pure amine, 8-aminoquinoline (qu, **32**), were prepared to generate complex analogues without guanidine moiety.

6.4.2 Results and discussion

Synthesis of guanidine-pyridine hybrid ligands and their zinc complexes

The guanidine-pyridine hybrid ligands DMPGqu (**8**), TEGqu (**9**), DPipGqu (**10**), DMorphGqu (**11**), MorphDMGqu (**12**) and (R,R)-DMCHGqu (**13**) were synthesised by condensation of chloroformamidinium chlorides **V3**-**V8** with 8-aminoquinoline in high yields of up to 98%. Analogously DMPGpy (**16**), TEGpy (**17**), DPipGpy (**18**), DMorphGpy (**19**) and MorphDMGpy (**20**) were prepared by reacting **V3**-**V7** with 2-picolylamine (see Chapter 3). Figure 6.20 gives an overview of the synthesised guanidine-pyridine hybrid ligands.
The guanidine moieties were chosen due to their different properties. DMPG is very similar to DMEG but possesses a six-membered ring instead of five-membered ring. The guanidine substituents in TEG are compared to those in TMG about one CH_2 unit elongated. This makes TEG a guanidine unit with flexible hydrocarbon arms resulting in a high steric demand. DPipG and DMorphG exhibit due to their piperidine and morpholine rings, respectively, also a high steric demand. The unsymmetric MorphDMG and the chiral (R,R)-DMCHG guanidine moieties were developed to create ligands that possibly could influence the polymerisation properties of the corresponding zinc initiators during the polymer chain growth resulting in a stereocontrol of the obtained polymer.
In order to obtain the corresponding zinc complexes, the ligands **8**-**13**, **16**-**20** and **32** were reacted with zinc chloride, zinc acetate and zinc triflate in a dry, aprotic solvent (MeCN, THF). Single crystals of the complexes were obtained either by cooling a saturated solution slowly to

Table 6.22: Overview of prepared zinc complexes.

	$ZnCl_2$	$Zn(OAc)_2$	$Zn(OTf)_2$
DMPGqu (**8**)	[Zn(DMPGqu)Cl_2] (**8a**)	[Zn(DMPGqu)$(OAc)_2$] (**8b**)	-[a]
TEGqu (**9**)	[Zn(TEGqu)Cl_2] (**9a**)	-[a]	-[a]
DPipGqu (**10**)	-[a]	[Zn(DPipGqu)$(OAc)_2$] (**10b**)	-[a]
DMorphGqu (**11**)	[Zn(DMorphGqu)Cl_2] (**11a**)	[Zn(DMorphGqu)$(OAc)_2$] (**11b**)	[Zn(DMorphGqu)$_2$][OTf]$_2$ (**11c**)
MorphDMGqu (**12**)	[Zn(MorphDMGqu)Cl_2] (**12a**)	[Zn(MorphDMGqu)$(OAc)_2$] (**12b**)	-[a]
(R,R)-DMCHGqu (**13**)	-[a]	-[a]	-[a]
qu (**32**)	[Zn(qu)Cl_2] (**32a**)	-[a]	[Zn(qu)$_2$$(OTf)_2$] (**32c**)
DMPGpy (**16**)	-[a]	-[a]	-[a]
TEGpy (**17**)	[Zn(TEGpy)Cl_2] (**17a**)	-[a]	-[a]
DPipGpy (**18**)	-[a]	-[a]	-[a]
DMorphGpy (**19**)	[Zn(DMorphGpy)Cl_2] (**19a**)	[Zn(DMorphGpy)$(OAc)_2$] (**19b**)	-[a]
MorphDMGpy (**20**)	[Zn(MorphDMGpy)Cl_2] (**20a**)	-[a]	-[a]

[a] These complexes have not been isolated and characterised until now.

room temperature or by slow diffusion of diethyl ether into the solution. The resulting crystals provide, as typical for guanidine-pyridine zinc complexes, high stability towards moisture and air. Table 6.22 gives an overview of the complexes that could be isolated and characterised. In general it was found that the quinoline ligands possess better crystallisation properties than pyridine ligands and those with flexible bulky residues like TEG and DPipG show poor packing abilities. Interestingly, DMorphG ligands which include also steric demanding residues exhibit much better crystallisation behavior. Unfortunately, the complexes containing zinc triflate, which were predicted to have good catalytic potential, are very difficult to isolate as pure products. In addition, the reaction of **8** with zinc acetate in the presence of chloride ions resulted in the formation of the mixed-coordination complex [Zn(DMPGqu)(Cl)(OAc)] (**8a/b**, Fig. 6.24).

Structure of the zinc complexes

The complexes [Zn(MorphDMGqu)Cl_2] (**12a**) and [Zn(qu)Cl_2] (**32a**) were only available as crystal powder, but their composition could be identified by means of NMR, IR and MS mea-

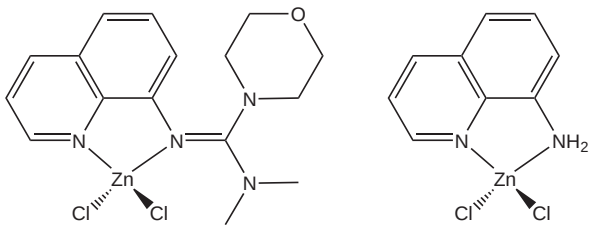

Figure 6.21: Schematic structures of [Zn(MorphDMGqu)Cl_2] (**12a**, l) and [Zn(qu)Cl_2] (**32a**, r).

surements as well as elemental analysis (see Fig. 6.21). The solid-state structures of the remaining complexes (Figures 6.22-6.26) were determined by X-ray crystallography. In the complexes with zinc chloride and zinc acetate, the zinc atom is fourfold coordinated by the two N-donor atoms of the guanidine-pyridine hybrid ligands and two chlorine ions or two acetate ions, respectively. In the complexes with zinc triflate, the zinc atom is fourfold coordinated by two chelate ligands.

Due to their structural similarity the complexes containing zinc chloride, zinc acetate and zinc triflate will be discussed conjoint in groups.

Complexes with zinc chloride: In the chlorido complexes **8a**, **9a**, **11a**, **17a**, **19a** and **20a** the zinc atom exhibit a distorted tetrahedral coordination geometry (see Fig. 6.22 and 6.23). The Zn-N bond lengths in each complex, except **11a**, differ due to the different coordination properties of the N-donor atoms. In **8a**, **9a**, and **20a** the Zn-N_{py} bonds are only 0.02, 0.03 and 0.02 Å longer than the Zn-N_{gua} bonds, whereas in **17a** and **19a** the bond lengths differ with difference values of 0.07 Å considerably from each other. The Zn-Cl bonds are also not equal in length (av. 2.212 and 2.243 Å). The distortion of the coordination environment is mainly generated by the bite angles of the guandine ligands. Their values ranging from 81.6(1) to 83.4(1)° are each smaller than the tetrahedral angle. The degree of distortion reflected by the angle between the ZnN_2

Table 6.23: Selected bond lengths (Å) and bond angles (°) of **8a**, **9a**, **11a**, **17a**, **19a** and **20a**.

	8a	**9a**	**11a**	**17a**	**19a**	**20a**
Zn-N_{py}	2.042(2)	2.055(1)	2.053(2)	2.077(2)	2.072(3)	2.045(8)
Zn-N_{gua}	2.027(2)	2.029(1)	2.047(2)	2.005(2)	2.005(3)	2.022(9)
Zn-Cl	2.224(1), 2.253(1)	2.208(1), 2.234(1)	2.210(1), 2.246(1)	2.204(1), 2.245(7)	2.207(1), 2.239(1)	2.220(3), 2.242(3)
C_{gua}-N_{gua}	1.356(2)	1.356(2)	1.332(3)	1.316(3)	1.319(4)	1.324(12)
C_{gua}-N	1.338(2), 1.341(2)	1.348(2), 1.349(2)	1.357(3), 1.346(3)	1.353(3), 1.367(3)	1.372(4), 1.348(4)	1.362(13), 1.362(13)
N-Zn-N	83.4(1)	81.8(1)	81.6(1)	82.0(1)	83.0(1)	82.2(4)
∠ ($ZnCl_2$, ZnN_2)	87.3	87.5	85.0	83.9	89.8	82.1
Structural parameter ρ	1.01	1.01	0.99	0.97	0.97	0.97

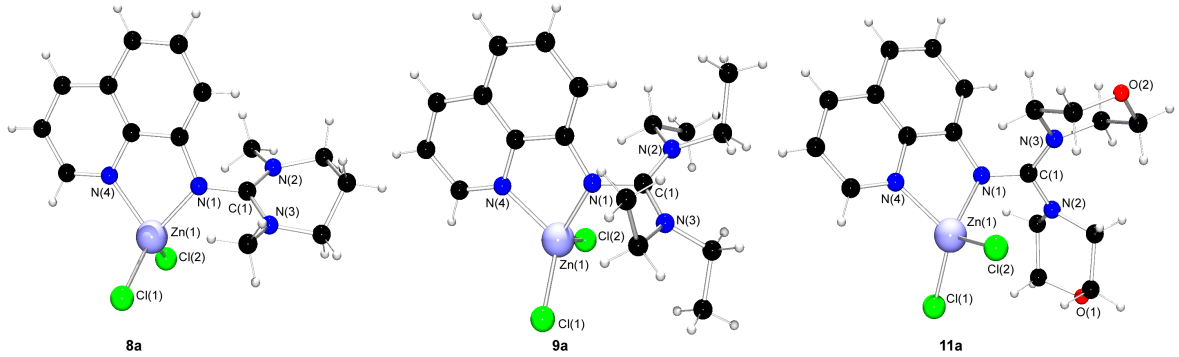

Figure 6.22: Crystal structures of $[Zn(DMPGqu)Cl_2]$ (**8a**), $[Zn(TEGqu)Cl_2]$ (**9a**) and $[Zn(DMorphGqu)Cl_2]$ (**11a**) as determined at 120 K.

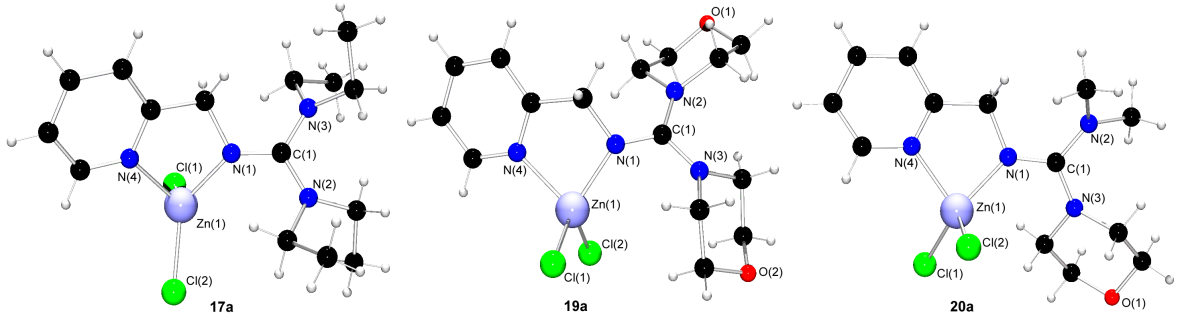

Figure 6.23: Crystal structures of $[Zn(TEGpy)Cl_2]$ (**17a**), $[Zn(DMorphGpy)Cl_2]$ (**19a**) and $[Zn(MorphDMGpy)Cl_2]$ (**20a**) as determined at 120 K.

and the $ZnCl_2$ planes varies between the complexes (**8a**: 87.3, **9a**: 87.5, **11a**: 85.0, **17a**: 83.9, **19a**: 89.8, **20a**: 82.1°) and is less distinct in **19a**. Regarding the guanidine moiety of the complexes, it is noticeable that in **8a** and **9a** the C_{gua}-N_{gua} bond is slightly longer than the C_{gua}-N bonds whereas in the remaining complexes the reverse case can be observed. Selected bond lengths and angles are collected in Table 6.23.

Complexes with zinc acetate: The crystal structures of **8b**, **10b**, **11b**, **12b** and **19b** are depicted in Figure 6.24 and 6.25 and Table 6.24 lists selected bond lengths and angles.

The zinc atom of each complex is coordinated by the N-donor atoms of the guanidine-pyridine hybrid ligand and by the oxygen atoms of two acetate ions. The coordination mode of the oxygen atoms varies between the different complexes. In **8b** both oxygen atoms of both acetate ions act as donors and coordinate to the zinc atom. In the other complexes one oxygen donor of each acetate ion clearly coordinates the metal. The other one exhibits indeed a higher distance to the zinc atom than the latter, but it is orientated in direction to the zinc so that a contact can be assumed. It is observed that the shorter one Zn-O bond is, the longer is the other one, whereas the approaching of the Zn-O bond lengths indicates the participation of both acetate O-donors in the coordination. However, the coordination geometry of the zinc centre can

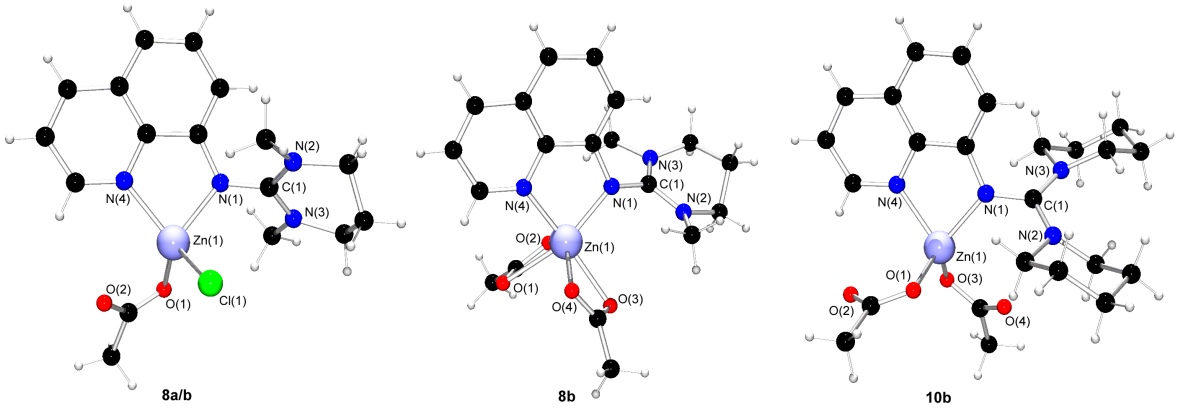

Figure 6.24: Crystal structures of [Zn(DMPGqu)(Cl)(OAc)] (**8a/b**), [Zn(DMPGqu)$(OAc)_2$] (**8b**) and [Zn(DPipGqu)$(OAc)_2$] (**10b**) as determined at 120 K.

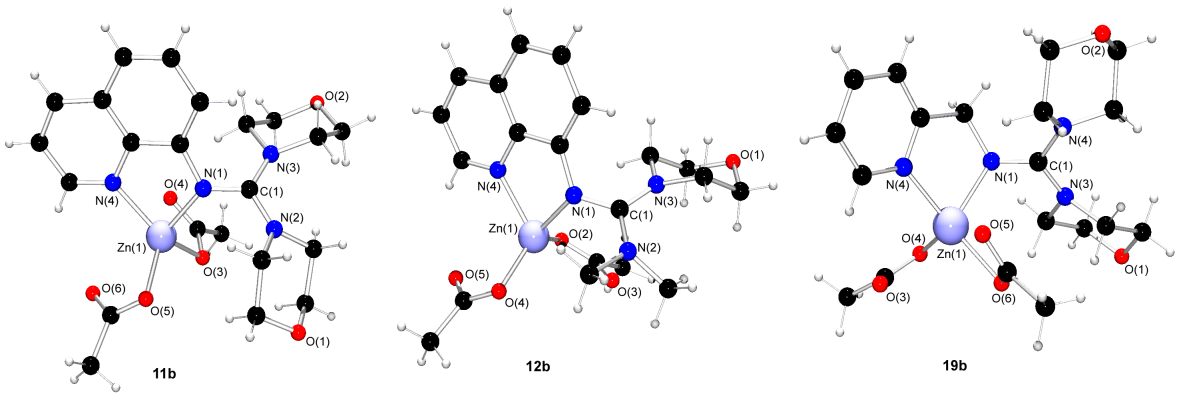

Figure 6.25: Crystal structures of [Zn(DMorphGqu)$(OAc)_2$] (**11b**), [Zn(MorphDMGqu)$(OAc)_2$] (**12b**) and [Zn(DMorphGpy)$(OAc)_2$] (**19b**) as determined at 120 K.

Table 6.24: Selected bond lengths (Å) and bond angles (°) of **8b**, **10b**, **11b**, **12b** and **19b**.

	8b	**10b**	**11b**	**12b**	**19b**
Zn-N_{py}	2.091(2)	2.097(2)	2.073(3)	2.090(4)	2.100(2)
Zn-N_{gua}	2.061(2)	2.040(2)	2.059(3)	2.030(3)	2.063(2)
Zn-O	2.097(2), 2.121(2), 2.226(2), 2.355(2)	1.953(2), 1.975(2)	1.998(3), 2.003(3)	1.950(3), 1.989(3)	2.015(1), 2.063(2)
C_{gua}-N_{gua}	1.351(2)	1.345(2)	1.347(4)	1.356(5)	1.315(2)
C_{gua}-N	1.341(3), 1.338(2)	1.342(2), 1.357(2)	1.344(4), 1.365(4)	1.332(6), 1.343(6)	1.374(2), 1.358(3)
N-Zn-N	80.6(1)	80.5(1)	81.4(1)	81.1(2)	80.5(1)
∠(ZnO_2, ZnN_2)	-	89.3	75.5	85.0	77.4
Structural parameter ρ	1.01	1.00	0.99	1.01	0.96

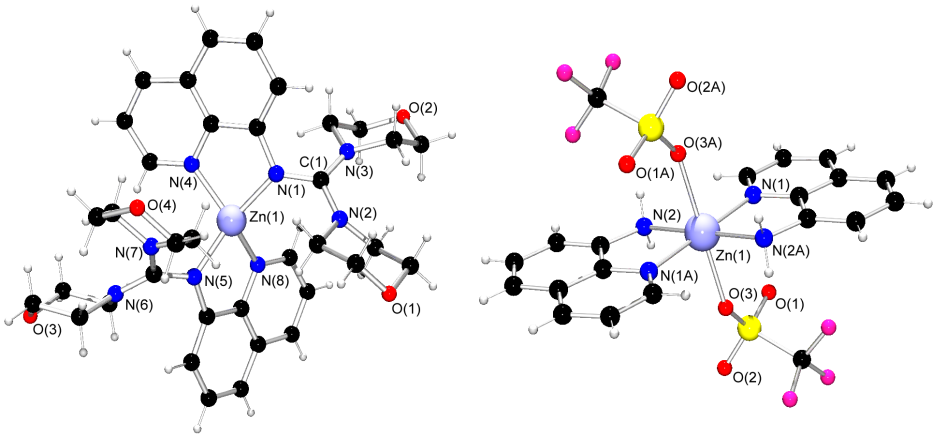

Figure 6.26: Molecular structures of $[Zn(DMorphGqu)_2]^{2+}$ in crystals of $[Zn(DMorphGqu)_2][CF_3SO_3]_2$ (**11c**, l) and $[Zn(qu)_2(CF_3SO_3)_2]$ (**32c**, r) as determined at 120 K.

be best described as a distorted tetrahedron, where the acetate ions act, independent of their coordination mode, as one donor.

The bite angles of the coordinated ligands, ranging from 80.5 to 81.4°, are notably smaller than the tetrahedral angle and account for the distortion of the structure. The trend that the Zn-N_{py} distances are longer than the corresponding Zn-N_{gua} bond length can also be found in the group of acetate containing zinc complexes. The C-N bonds in the guanidine function lie in general in the same range demonstrating a good delocalisation in this moiety. Just in **19b** the C_{gua}-N_{gua} bond is clearly shorter than the C_{gua}-N bonds.

Complexes with zinc triflate: The complexes containing zinc triflate show due to the different steric demand of their ligands different molecular structures (see Fig. 6.26 and Tab. 6.25). In **32c** the zinc atom is coordinated in a chelating manner by the N-donor atoms of two 8-aminoquinoline ligands forming a square-planar coordination environment. In addition, one oxygen atom of the triflate ions coordinates the zinc atom from each site of the plane generating a stretched octahedron. The bulky DMorphG residues in **11c** would not allow for such coordination. Here the zinc atom is also coordinated in a chelating manner by the N-donor atoms of two ligand molecules. But both triflate ions are far away from the reaction centre and act only as counterion which is an important difference to the structure motifs of **6c** and **7c**. The coordination geometry of the zinc ion is highly distorted and lies between tetrahedral and square-planar coordination to minimise the interactions of the sterically demanding guanidine residues. This is also reflected in the angle between the ZnN_2 planes (62.9°), which is between the tetrahedral (90°) and the square-planar coordination (0°). A similar structure motif was also found for the bisguanidine complex **1c** (see Chapter 4).

Table 6.25: Selected bond lengths (Å) and bond angles (°) of **11c** and **32c**.

	11c	**32c**
Zn-N_{py}	2.010(3), 2.027(3)	2.080(2), 2.080(2)
Zn-N_{gua} / Zn-N_{amine}	1.982(3), 2.000(3)	2.109(2), 2.109(2)
Zn-O		2.291(2), 2.291(2)
C_{gua}-N_{gua}	1.346(5), 1.347(4)	
C_{gua}-N	1.349(5), 1.357(4), 1.351(4), 1.349(4)	
N-Zn-N	84.4(1), 83.4(1)	81.6(1), 81.6(1)
∠ (ZnN_2, ZnN_2)	62.9	0.0
Structural parameter ρ	0.99, 1.00	

Polymerisation activity

To investigate the guanidine effect on the catalytic activity of the complexes, they were tested as initiators in the solvent-free polymerisation of D,L-lactide according to the standard procedure (0.2 mol% catalyst, 150°C). The polymer yield was defined and the molecular weights as well as the polydispersity of the obtained PLA were determined by gel permeation chromatography (see Table 6.26). The tacticity was analysed by homonuclear decoupled ^{1}H NMR spectroscopy.[24]

Regarding the polymerisation results, it is obvious that under the given conditions there seems to be no clear trend concerning the guanidine impact on the catalytic activity. Zinc chloride complexes with ligands based on quinoline show no, or in the case of **9a** only weak catalytic performance. Those with ligands based on pyridine, show good activity independent of the kind of guanidine moiety. And remarkably, the zinc dichlorido complex **32a** also possess the ability to initiate the lactide polymerisation effectively, even if it does not contain a guanidine function. The investigation of the acetate containing complexes shows similar results. Their activity among each other is very alike and seems not to depend on the guanidine unit in the ligand.

In the case of **19b** PLAs in good yields were obtained that possess significantly lower molecular weights than they should have according to the theory (e.g. $M_{w,exp.}$ = 33,000 g/mol; $M_{w,theor.}$ = 53,000 g/mol). This effect was also observed for **14b** and **15b** (see Section 6.1). The triflate complex **32c** shows also good catalytic activity and the achieved yields are even higher than those of **32a** but the molecular weights are comparably low. **11c** altogether provides a good performance including high yields with molecular weights that are only slightly higher than the theoretical values (e.g. $M_{w,exp.}$ = 79,000 g/mol; $M_{w,theor.}$ = 64,000 g/mol).

By comparing the performance of the complexes **8a** and **8b** with those of **8a/b** the anion effect can be demonstrated again. The catalytic activity of the mixed complex lies in between those of the alike coordinated compounds.

Table 6.26: Polymerisation of D,L-lactide initiated by guanidine-pyridine zinc complexes.

Initiator		Time[a] [h]	Yield [%]	M_w [g/mol]	PD[b]	Pr[c]
$[Zn(DMPGqu)Cl_2]$	**8a**	48	0	-	-	-
$[Zn(TEGqu)Cl_2]$	**9a**	24	0	-	-	-
$[Zn(TEGqu)Cl_2]$	**9a**	48	17	31,000	2.0	0.55
$[Zn(DMorphGqu)Cl_2]$	**11a**	48	0	-	-	-
$[Zn(MorphDMGqu)Cl_2]$	**12a**	48	0	-	-	-
$[Zn(TEGpy)Cl_2]$	**17a**	24	77	64,000	2.1	0.54
$[Zn(TEGpy)Cl_2]$	**17a**	48	87	64,000	1.9	
$[Zn(DMorphGpy)Cl_2]$	**19a**	24	51	48,000	1.6	0.57
$[Zn(DMorphGpy)Cl_2]$	**19a**	48	78	60,000	1.8	
$[Zn(MorphDMGpy)Cl_2]$	**20a**	24	72	55,000	1.8	0.56
$[Zn(MorphDMGpy)Cl_2]$	**20a**	48	80	53,000	1.8	
$[Zn(qu)Cl_2]$	**32a**	24	71	70,000	1.8	0.54
$[Zn(qu)Cl_2]$	**32a**	48	83	79,000	1.9	
$[Zn(DMPGqu)(CH_3COO)Cl]$	**8a/b**	24	18	14,000	1.7	
$[Zn(DMPGqu)(CH_3COO)_2]$	**8b**	24	36	25,000	1.7	
$[Zn(DMPGqu)(CH_3COO)_2]$	**8b**	48	60	33,000	1.8	
$[Zn(DMorphGqu)(CH_3COO)_2]$	**11b**	24	10	16,000	1.5	
$[Zn(DMorphGqu)(CH_3COO)_2]$	**11b**	48	51	24,000	1.7	0.49
$[Zn(MorphDMGqu)(CH_3COO)_2]$	**12b**	24	4	16,000	1.7	
$[Zn(MorphDMGqu)(CH_3COO)_2]$	**12b**	48	29	22,000	1.7	0.49
$[Zn(DMorphGpy)(CH_3COO)_2]$	**19b**	24	74	33,000	1.8	0.49
$[Zn(DMorphGpy)(CH_3COO)_2]$	**19b**	48	81	30,000	1.8	
$[Zn(qu)_2(CF_3SO_3)_2]$	**32c**	24	85	45,000	1.7	0.50
$[Zn(qu)_2(CF_3SO_3)_2]$	**32c**	48	86	49,000	1.8	
$[Zn(DMorphGqu)_2][CF_3SO_3]_2$	**11c**	24	89	79,000	1.9	0.57
$[Zn(DMorphGqu)_2][CF_3SO_3]_2$	**11c**	48	92	64,000	1.9	

Reaction conditions: Catalyst (0.2 mol%), 150 °C; [a] reaction times were not necessarily optimised; [b] PD = M_w/M_n where M_n is the number-average molar mass; [c] From analysis of the ^1H homonuclear decoupled NMR spectrum using the equation $P_r^2 = 2$ [sis];[24]

A possible impact of the complexes on the tacticity and thus on the microstructure of the obtained PLA was investigated by determination of the probability of heterotactic enchainment rated by the P_r values. The polymers produced by **9a**, **17a**, **32a**, **11b**, **12b**, **19b** and **32c** show no ability to control the tacticity. In the case of **19a**, **20a** and **11c** with P_r values of 0.56-0.57 a slight heterotactic bias was observed. This effect also depends on the anionic compound in the zinc complexes, due to the fact that the lowest P_r values (0.49) are provided by the acetato complexes whereas the corresponding chlorido and triflato complexes possess higher values. Regarding the chlorido complexes, it seems that the guanidine moiety possesses a certain impact on the heterotactic enchainment. However, due to the very low overall effect the impact of the guanidine moiety cannot be clarified.

6.4.3 Conclusion

To elucidate the influence of the guanidine unit in guanidine-pyridine hybrid ligands on the catalytic activity of the corresponding zinc complexes, two series of new guanidine-pyridine ligands were developed by combining various chloroformamidinium chlorides with 8-aminoquinoline and 2-picolylamine. The latter as well as the pure 8-aminoquinoline were reacted with zinc chloride, zinc acetate and zinc triflate to obtain the corresponding complexes which were tested as initiators in the solvent-free ring-opening polymerisation of D,L-lactide. Under the given conditions no clear trend concerning the guanidine impact on the catalytic activity could be observed. The impact of the guanidine moiety on the grade of heterotactic enchainment cannot be clarified due to the very low overall effect.
In addition, the complexes stabilised by the pure amine, **32a** and **32a**, were proven to be active initiators in the lactide polymerisation, although they do not possess a guanidine function.

6.5 Ring-opening polymerisation of cyclic esters: Evaluating the application range of guanidine-pyridine zinc complexes

In order to evaluate the application range of guanidine-pyridine zinc complexes, their most auspicious candidates, the bis-chelate complexes **6c** and **7c**, were investigated towards their ability to act as initiators in the ring-opening polymerisation of various cyclic esters.

6.5.1 Introduction

The physical properties, hydrolysis and biodegradation behavior of polylactide can be controlled not only by altering the averaged molecular weight and its distribution, to meet also the requirements of specific applications it is even possible to modify the properties of PLA by tailoring of macromolecular architecture and microstructure (see Section 1.2).

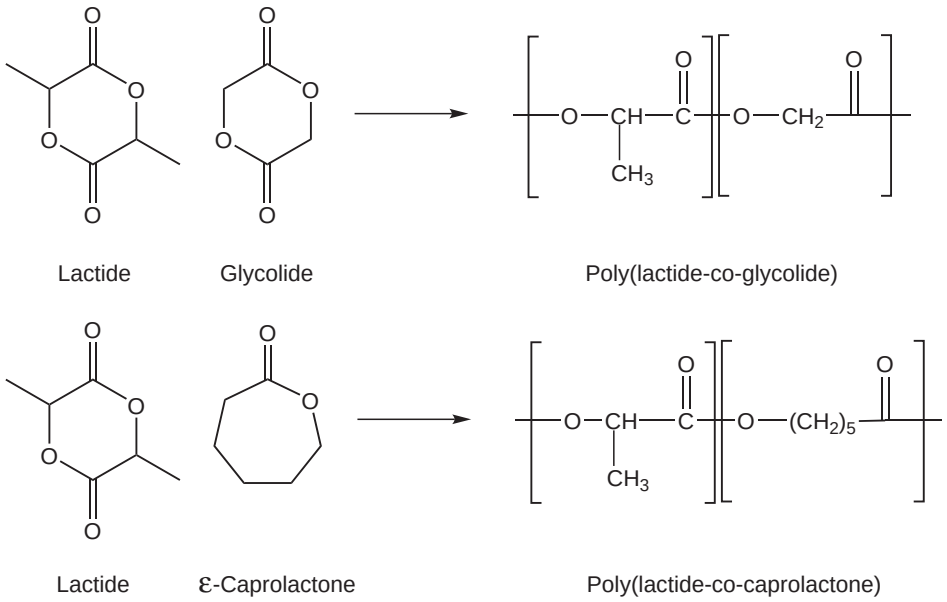

Figure 6.27: Monomers and repeating units of polylactide-copolymers.[158]

Lactide itself exists in different enantiomeric forms whose homopolymers possess different properties compared to those of their copolymers. Optical pure isotactic D- or L-PLA is a semi-crystalline, hard and rather brittle material with typical melting points of 170 to 180°C, whereas D,L-PLA is an amorphous, transparent polymer with a softening point observed around 60°C.[13,19,25,27] Thus, PLA with tailor-made properties is obtained either by copolymerisation of different enantiomeric forms of lactide or by copolymerisation of lactide with similar cyclic monomers like ε-caprolactone and glycolide.[6,16] The chemical structure of cyclic monomers and the resulting PLA-copolymers are presented in Figure 6.27. For an overview of PLA microstructures see Figure 1.4 in Chapter 1.
Initiators suited for the preparation of polylactide-copolymers also have to be active initiators in the homopolymerisations of the corresponding monomers. In order to investigate the qualification for copolymerisation applications and to evaluate the application range of guanidine-pyridine zinc complexes, their most auspicious candidates, the bis-chelate complexes **6c** and **7c**, were investigated towards their ability to act as initiators in the ring-opening polymerisation of D-lactide, L-lactide, glycolide and ε-caprolactone.

6.5.2 Results and discussion

The complexes **6c** and **7c** were tested for their ability to initiate the ring-opening polymerisation of pure D- and L-lactide according to the standard procedure for D,L-lactide. In order to rate the catalytic activity of the complexes, the polymer yield was defined and the molecular weights as well as the polydispersity of the PLA were determined by gel permeation chromatography (see Table 6.27). The microstructure of the obtained PLA samples was investigated by

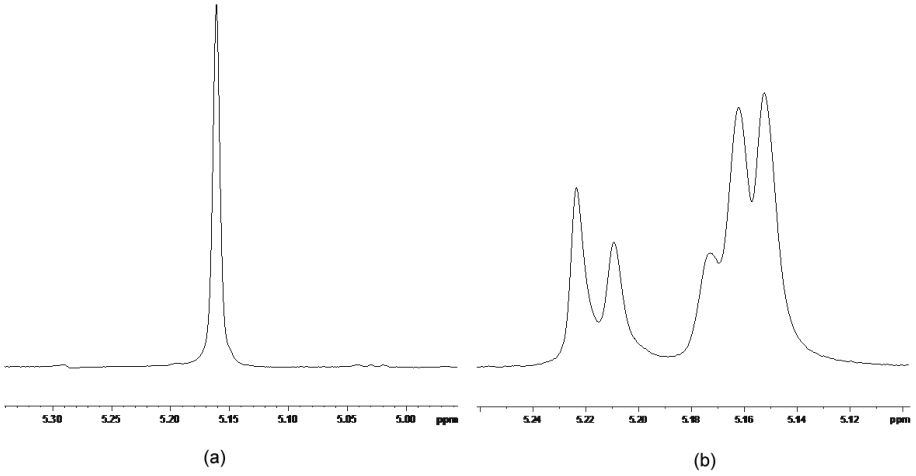

Figure 6.28: Detail of homonuclear decoupled ^{1}H NMR spectra for poly(L-lactide) (a) and for atactic poly(D,L-lactide) with P_r = 0.56 (b).

homonuclear decoupled ^{1}H NMR spectroscopy.[24,159]

6c and **7c** both proved to be highly active initiators for lactide polymerisation, independent of the used monomer. They provide D- and L-PLA in almost quantitative yields and with molecular weights up to 137,000 g/mol. In the homonuclear decoupled ^{1}H NMR of the obtained polymer samples just one sharp peak can be observed (e.g. Fig. 6.28a) indicating that the investigated polymers possess an isotactic microstructure. For comparison Figure 6.28 depicts details of homonuclear decoupled ^{1}H NMR spectra for isotactic poly(L-lactide) and for the atactic poly(D,L-lactide).

At high temperatures undesired racemisation of the pure stereoisomer is reported for anionic and cationic polymerisation mechanisms. This racemisation leads to an atactic polymer. In the case of the coordination insertion mechanism racemisation does not occur.[19,80] Since only isotactic polymers were observed, no racemisation took place in either cases reported here. This observation is consistent with the assumption of a coordination-insertion mechanism active for the guanidine/zinc systems (see Chapter 9).

For glycolide polymerisation tests the monomer (used without further purification) and the initiator (I/M ratio 1:500) were heated for 45 min at 150°C. It could be observed that in the solvent-free polymerisation of glycolide with **6c** and **7c** the viscosity of the polymer melt increases very fast so that several minutes after the melting the melt became solid. Therefore the polymerisation procedures were stopped after 45 min. Then, the melt was dissolved in hexafluoroisopropanol, and the polyglycolide (PGA) was precipitated in cold ethanol, isolated and dried under vacuum at 50°C. The yield was determined. Due to the fact that pure PGA is only soluble (although not very good) in hexafluoroisopropanol, NMR measurements or gel permeation chromatography were not applicable. Even though the bulk polymerisation seems not to be suited for the production of polyglycolide, it could be demonstrated that **6c** and **7c**

Table 6.27: Ring-opening polymerisation of cyclic esters initiated by **6c** and **7c**.

Monomer	Initiator		Time[a] [h]	Yield [%]	M_w [g/mol]	PD[d]
L-Lactide	$[Zn(DMEGqu)_2(CF_3SO_3)][CF_3SO_3]$	**6c**	24	92	103,000	1.5
	$[Zn(TMGqu)_2(CF_3SO_3)][CF_3SO_3]$	**7c**	24	99	92,000	2.2
D-Lactide	$[Zn(DMEGqu)_2(CF_3SO_3)][CF_3SO_3]$	**6c**	24	96	137,000	1.9
	$[Zn(TMGqu)_2(CF_3SO_3)][CF_3SO_3]$	**7c**	24	97	117,000	1.8
Glycolide	$[Zn(DMEGqu)_2(CF_3SO_3)][CF_3SO_3]$	**6c**	0.75	28	-	-
	$[Zn(TMGqu)_2(CF_3SO_3)][CF_3SO_3]$	**7c**	0.75	60	-	-
ε-Caprolactone	$[Zn(DMEGqu)_2(CF_3SO_3)][CF_3SO_3]$	**6c**	24	19[b]	19,000[c]	1.2
	$[Zn(DMEGqu)_2(CF_3SO_3)][CF_3SO_3]$	**6c**	48	35[b]	29,000[c]	1.4
	$[Zn(TMGqu)_2(CF_3SO_3)][CF_3SO_3]$	**7c**	24	69[b]	38,000[c]	1.6
	$[Zn(TMGqu)_2(CF_3SO_3)][CF_3SO_3]$	**7c**	48	89[b]	44,000[c]	1.6

Reaction conditions: Catalyst (0.2 mol%), 150 °C; [a] reaction times were not necessarily optimised; [b] conversion determined by NMR; [c] referred to polystyrene standards; [d] PD = M_w/M_n where M_n is the number-average molar mass.

are also able to polymerise glycolide. By trend, the catalytic activity of **7c** is here higher than that of **6c**.

The polymerisation procedure for the preparation of polycaprolactone (PCL) is in general consistent with the standard procedure for D,L-lactide. But due to the fact that PCL is obtained as fine precipitate which can be isolated only by centrifugation, the conversion of the monomer was determined by NMR measurements of dried samples from the dichloromethane solution. Gel permeation chromatography provided the molecular weights as well as the polydispersity referred to polystyrene standards (Table 6.27).

The complexes **6c** and **7c** both initiate the ROP of ε-caprolactone but in the case of **7c** considerably higher yields and PCLs with higher molecular weights could be obtained.

6.5.3 Conclusion

It could be demonstrated that the guanidine-pyridine zinc complexes **6c** and **7c** are also well suited for the general application in the polymerisation of cyclic esters and therefore possess also high potential for the copolymerisation of lactide.

The monomers D- and L-lactide were converted into the polymers in almost quantitative yields and with molecular weights up to 137,000 g/mol. The PLAs obtained were isotactic in each case. A racemisation could not be observed and thus the hypothesis of a coordination insertion mechanism is supported (see Chapter 9). The polymerisation of glycolide and ε-caprolactone indicate that **7c** provides even better catalytic performance than **6c**. These findings were in accordance with the kinetic studies described in Chapter 9.

6.6 Conclusion

A library of zinc complexes stabilised by guanidine-pyridine ligands was developed and the complexes were screened towards their activity in the solvent-free ring-opening polymerisation of D,L-lactide. They proved to be active initiators with only few exceptions. Polylactides with molecular weights (M_w) up to 176,000 g/mol and in almost quantitative yields could be obtained. These results represent a significant augmentation over bisguanidine zinc complexes and corroborate the strategy of building up N-donor ligands with different donor strengths and substituents with varied sterical demand.
In complexes with the same N-donor ligand, the anionic component of the zinc salt has a significant impact on the activity of the corresponding initiator. It defines the molecular structure, the charge distribution and the thermal stability of the complex and therefore its properties. The charge distribution within the complex (especially the positive charge on the zinc atom) influences the attraction towards the substrate lactide and the accessibility to the zinc centre regulates the substrate coordination. Consequently, the reactivity of the complexes is directly correlated to the coordination behaviour of the anionic component and the anion effect plays an important role in context of catalyst design. A clear trend concerning the guanidine impact on the catalytic activity could not be observed under the given conditions. Similarly, the influence of the guanidine moiety on the grade of heterotactic enchainment cannot be clarified due to the very low overall effect.
Guanidine-pyridine zinc complexes including zinc triflate were proven to be excellent catalysts in ROP of lactide. The flexible coordination of one triflate anion to the zinc centre is considered responsible for their outstanding activity. It facilitates pre-coordination of the lactide molecule, while the higher positive charge at the zinc centre in comparison to the tetrahedral complexes offers higher Lewis acidity for activation of lactide. This argument was supported by studies on the corresponding complexes with zinc mesylate. In addition, it was demonstrated that the triflate complexes are also well suited for the general application in the polymerisation of cyclic esters like D-lactide, L-lactide, glycolide and ε-caprolactone and therefore possess also high potential for the copolymerisation of lactide.
In summary, zinc complexes of guanidine-pyridine hybrid ligands exhibit an advantageous combination of properties: they are non-toxic, can be stored in air without loss of activity and they do not need co-catalysts like alkoxides to give PLAs with high M_w values under industrially attractive conditions. This bundle of properties makes the guanidine/zinc systems an excellent and application-oriented class of catalysts for the ring-opening polymerisation of lactide.

7 Zinc complexes with mono- and polydentate behaving guanidine ligands and their application in lactide polymerisation

Mono- and polydentate behaving guanidine ligands and their corresponding zinc complexes were prepared and investigated towards the influence of these special ligand classes on the molecular structures of the complexes as well as their performance in the ring-opening polymerisation of lactide.

7.1 Zinc complexes with monodentate behaving guanidine-pyridine hybrid ligands and their application in lactide polymerisation

The influence of different spacer units on the molecular structures and the properties of the corresponding complexes is investigated using the example of the guanidine-pyridine ligands DMEGpico (**21**) and TMGpico (**22**). They, as well as their complexes $[Zn(DMEGpico)_2Cl_2]$ (**21a**), $[Zn(TMGpico)_2Cl_2]$ (**22a**) and $[(TMGpico)_2Zn_3(CH_3COO)_6]$ (**22b**) were synthesised and characterised. **21a** and **22a** were proven to be active initiators in the ROP of lactide. However, the comparison of their catalytic activity with that of complexes including similar ligands with longer spacer units did not show a dependence between spacer unit or molecular structure and the polymerisation behaviour for this class of compounds.

7.1.1 Introduction

In order to investigate the influence of different spacer units on the molecular structures and the properties of the corresponding complexes, the ligands N-(1,3-dimethylimidazolidin-2-ylidene)-3-methylpyridin-2-amine (DMEGpico, **21**) and 1,1,3,3-tetramethyl-2-(3-methylpyri-

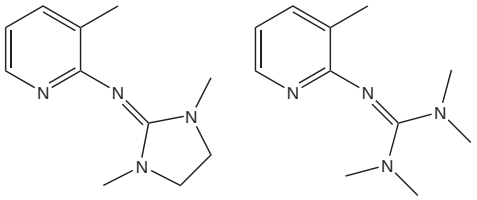

Figure 7.1: Schematic structure of DMEGpico (**21**) and of TMGpico (**22a**).

din-2-yl)guanidine (TMGpico, **22**) as well as their chlorido and acetato complexes were synthesised and completely characterised. The amine 2-amino-3-picoline which possesses only one C building block between the N-donor functions was chosen as spacer-amine component due to its high structural similarity to 2-picolylamine (py) which offers a C_2 spacer and was used to prepare the ligands DMEGpy (**14**) and TMGpy (**15**). The obtained chlorido complexes were tested for their ability to act as initiators in the ROP of lactide and their activity is compared to those of the chlorido complexes stabilised by the similar ligands, DMEGpy and TMGpy, which possess longer spacer units.

7.1.2 Results and Discussion

Ligand and complex syntheses

The syntheses of the guanidine-pyridine hybrid ligands DMEGpico (**21**) and TMGpico (**22**) were carried out by the condensation of 2-amino-3-picoline with the chloroformamidinium chlorides DMEG (**V1**) and TMG (**V2**), respectively. Figure 7.1 depicts the schematic structure of **21** and **22**. Their reaction with equimolar amounts of zinc salts ($ZnCl_2$, $Zn(CH_3COO)_2$) in a dry, aprotic solvent (MeCN, THF) resulted in straightforward formation of the zinc complexes $[Zn(DMEGpico)_2Cl_2]$ (**21a**), $[Zn(TMGpico)_2Cl_2]$ (**22a**) and $[(TMGpico)_2Zn_3(CH_3COO)_6]$ (**22b**) in yields of 67-98%. Colourless single crystals of the complexes were obtained by slow diffusion of diethyl ether in a saturated solution.
The molecular structures of **21a**, **22a** and **22b** were determined by X-ray crystallography (Fig. 7.2 and 7.3). The molecular structures of **22a** exhibit two molecules per asymmetric unit. Due to their high similarity in the following only one structure is discussed as **22a**.
In all three complexes, the ligands **21** and **22** which both possess guanidine as well as pyridine N-donor atoms, coordinate the zinc atom only by the pyridine donor and thus act as monodentate ligands. The N_{gua} is with an average value of 2.854 Å too far away from the zinc centre to support interaction. This coordination behaviour is affected by the close distance of the N-donor atoms generating a very small bite.
In the chlorido complexes $[Zn(DMEGpico)_2Cl_2]$ (**21a**) and $[Zn(TMGpico)_2Cl_2]$ (**22a**) the zinc center is twofold coordinated by two N_{py} atoms of two guanidine-pyridine ligands and the remaining coordination sites are occupied by two chlorido ions resulting in a distorted tetra-

Table 7.1: Selected bond lengths (Å) and bond angles (°) of **21a** and **22a**.

	21a	**22a**
Zn-N_{py}	2.039(3), 2.055(3)	2.036(2), 2.049(2)
Zn-Cl	2.285(1), 2.286(1)	2.277(1), 2.278(1)
C_{gua}-N_{gua}	1.294(4), 1.292(5)	1.301(2), 1.299(2)
C_{gua}-N	1.376(5), 1.375(5), 1.374(5), 1.369(5)	1.363(2), 1.370(2), 1.362(2), 1.381(2)
N-Zn-N	112.9(1)	115.3(1)
Cl-Zn-Cl	108.4(1)	107.5(2)
∠ ($ZnCl_2$, ZnN_2)	82.4	83.2
Structural parameter ρ	0.94, 0.94	0.95, 0.95

Table 7.2: Selected bond lengths (Å) and bond angles (°) of **22b**.

	22b
Zn-N_{py}	2.016(3)
Zn-O	1.962(2), 1.983(2), 1.989(2), 2.062(2), 2.082(3), 2.126(2)
C_{gua}-N_{gua}	1.307(5)
C_{gua}-N	1.350(5), 1.365(5)
O-Zn-O	104.2(1), 105.5(1), 102.5(1), 180.0, 87.8(1), 92.2(1), 180.0, 91.1(1), 89.0(1), 88.2(1), 91.8(1), 180.0
Structural parameter ρ	0.96

hedral coordination (Fig. 7.2 and Tab. 7.1). The Zn-N_{py} bond lengths of the two coordinated ligands differ slightly from each other (**21a**: 2.039(3), 2.055(3); **22a**: 2.036(2), 2.049(2) Å) whereas the Zn-Cl bonds are equal in length (**21a**: 2.285(1), 2.286(1); **22a**: 2.277(1), 2.278(1) Å). In the guanidine moiety of DMEGpico and TMGpico the C_{gua}-N_{gua} bond is with a difference of av. 0.08 (**22a**) or av. 0.07 Å (**22a**) significantly shorter than the C_{gua}-N bonds compared to similar complexes like [Zn(DMEGpy)Cl_2] (**14a**) and [Zn(TMGpico)Cl_2] (**15a**) in which the ligands coordinate the zinc atom also by the guanidine donor atom. In the latter case, the charge transfer generated by the coordination leads to the delocalisation of electron density over the guanidine function and to the levelling of bond length.

The same effect was also observed for the guanidine moieties in the zinc acetato complex [Zn_3(TMGpico)$_2$(CH_3COO)$_6$] (**22b**, Fig. 7.3). This complex possesses a trinuclear solid-state structure in which two Zn atoms are each coordinated by the pyridine N-donor atom of ligand **22** and three oxygen atoms of three acetato bridging ligands resulting in a distorted tetrahedral

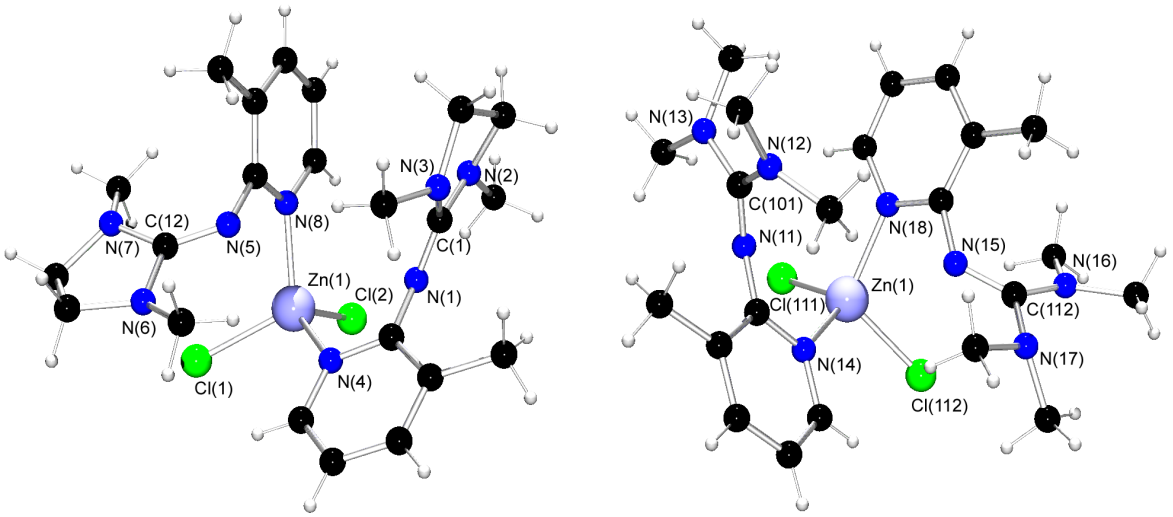

Figure 7.2: Crystal structure of $[Zn(DMEGpico)_2Cl_2]$ (**21a**, l) and of $[Zn(TMGpico)_2Cl_2]$ (**22a**, r) as determined at 120 K.

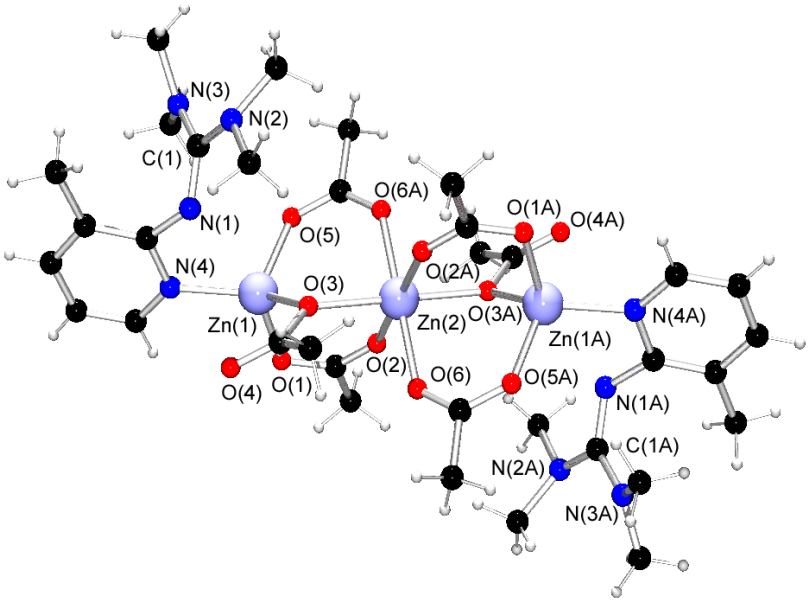

Figure 7.3: Molecular structure of $[Zn_3(TMGpico)_2(CH_3COO)_6]$ (**22b**) as determined at 120 K.

coordination environment. Each of the bridging ligands connects each Zn atom with a third Zn atom located between them. Consequently, the latter shows an octahedral coordination environment where each corner is occupied by an acetato oxygen atom. Interestingly, in each case two acetato ligands bridge the Zn atoms via two oxygen functions but the third acetato ligand connects the metal atoms via only one oxygen atom of the acetate group. This structure motif is very similar to that found for $[Zn_3(bipy)_2(CH_3COO)_6]$ (**33b**, see Section 8.1). The values for the Zn-O bonds in **22b** depend on the coordination mode of the acetato ligands. The Zn-O bonds at the terminal zinc atoms are in average with 1.978 Å generally shorter than those belonging to the ZnO_6 octahedron (av. 2.090 Å). Selected bond lengths and angles are summarised in Table 7.2.

Polymerisation activity

Based on mechanistic studies on the ring-opening polymerisation of lactide mediated by guanidine-pyridine zinc complexes (Chapter 9) it is proposed that the guanidine function of the coordinated ligand plays a key role during the first ring-opening step. Possibly the uncoordinated guanidine functions close to the reaction centre in **21a** and **22a** support the polymerisation reaction and enhance the catalytic activity. Therefore, the chlorido complexes **21a** and **22a** were tested for their ability to initiate the ring-opening polymerisation of D,L-lactide according to the standard procedure (0.2 mol% catalyst, 150°C). In order to rate the catalytic activity of the complexes, the polymer yield, the molecular weights as well as the polydispersity of the PLA were determined (see Table 7.3). The tacticity was analysed by homonuclear decoupled ^{1}H NMR spectroscopy.[24]

21a and **22a** show independent of the coordinated ligand almost the same catalytic activity. Only the width of the molecular weight distribution is for **21a** slightly higher. Their yields are quite high, but the experimental observed M_w values are smaller than the calculated ones (e.g. $M_{w,exp.}$ = 37,000; $M_{w,theor.}$ = 57,000 g/mol). Compared to the chlorido complexes containing the ligands DMEGpy and TMGpy, which possess a spacer one CH_2 unit longer than in

Table 7.3: Polymerisation of D,L-lactide initiated by **21a** and **22a**.

Initiator		Time[a] [h]	Yield [%]	M_w [g/mol]	PD[b]	Pr[c]
$[Zn(DMEGpico)_2Cl_2]$	**21a**	24	79	37,000	1.9	
$[Zn(DMEGpico)_2Cl_2]$	**21a**	48	84	34,000	1.9	
$[Zn(TMGpico)_2Cl_2]$	**22a**	24	78	36,000	1.7	0.52
$[Zn(TMGpico)_2Cl_2]$	**22a**	48	82	35,000	1.7	

Reaction conditions: Catalyst (0.2 mol%), 150 °C; [a] reaction times were not necessarily optimised; [b] PD = M_w/M_n where M_n is the number-average molar mass; [c] From analysis of the ^{1}H homonuclear decoupled NMR spectrum using the equation $P_r{}^2 = 2$ [sis];[24]

DMEGpico and TMGpico, their catalytic performance lies in the same range. Just complex **15a** shows higher activity. Hence, it could not be demonstrated that the uncoordinated guanidine function near the reaction centre supports the polymerisation reaction.

7.1.3 Conclusion

The guanidine-pyridine ligands DMEGpico (**21**) and TMGpico (**22**) as well as their chlorido and acetato complexes $[Zn(DMEGpico)_2Cl_2]$ (**21a**), $[Zn(TMGpico)_2Cl_2]$ (**22a**) and $[Zn_3(TMGpico)_2(CH_3COO)_6]$ (**22b**) were synthesised and characterised. Due to their short spacer unit, **21** and **22** act as monodentate ligands by coordinating the zinc atoms via the pyridine N-donor atom. The chlorido complexes were proven to be active initiators in the ROP of lactide. An impact of the ligand spacer on the complex properties concerning the initiation of lactide polymerization as well as an increase in catalytic activity due to the uncoordinated guanidine function next to the reaction centre could not be observed in the case of **21** and **22**.

7.2 Zinc complexes with polydentate tris- and tetraguanidine ligands and their application in lactide polymerisation

Due to the fact that polydentate ligands were proven to be well suited ligand classes to stabilise catalytic active complexes, $DMEG_4(baem)_2b$ (**27**), $TMG_4(baem)_2b$ (**28**) and TEG_3tren (**31**) were synthesised. The chlorido complexes including polydentate ligands $[(TMG_4(beam)_2b)(ZnCl_2)_2]$ (**28a**), $[Zn(DMEG_3tren)Cl][Cl]$ (**29a**) and $[Zn(TMG_3tren)Cl][Cl]$ (**30a**) were prepared and tested for their ability to polymerise lactide.

7.2.1 Introduction

Polydentate ligands like trispyrazolylborates (see Section 1.2.3) are well suited to stabilise catalytic active complexes. In this context, the novel neutral tetradentate guanidine ligands 2,6-bis{[bis(2-aminoethyl)1,3-dimethylimidazolidin-2-ylidene]methyl}benzol ($DMEG_4(baem)_2b$, **27**) and 2,6-bis{[bis(2-aminoethyl)tetramethyl-guanidino]methyl}benzol ($TMG_4(baem)_2b$, **28**) as well as the tridentate ligands 1,1,1-tris{2-[2N-(1,3-dimethylethylenguanidino)]ethyl}amine ($DMEG_3tren$, **29**)[124] and 1,1,1-tris{2-[N^2-(1,1,3,3-tetramethylguanidino)]ethyl}amine (TMG_3tren, **30**),[112] first described by Sundermeyer et al., were synthesised. In order to create a tridentate ligand that possesses a very high steric demand, the ligand 2',2',2"-(2,2',2"-nitrilotris(ethane-2,1-diyl))tris(1,1,3,3-tetraethylguanidine) (TEG_3tren, **31**) was developed. Their reaction with zinc chloride gave the corresponding zinc complexes which were investigated towards their catalytic activity in the ROP of lactide.

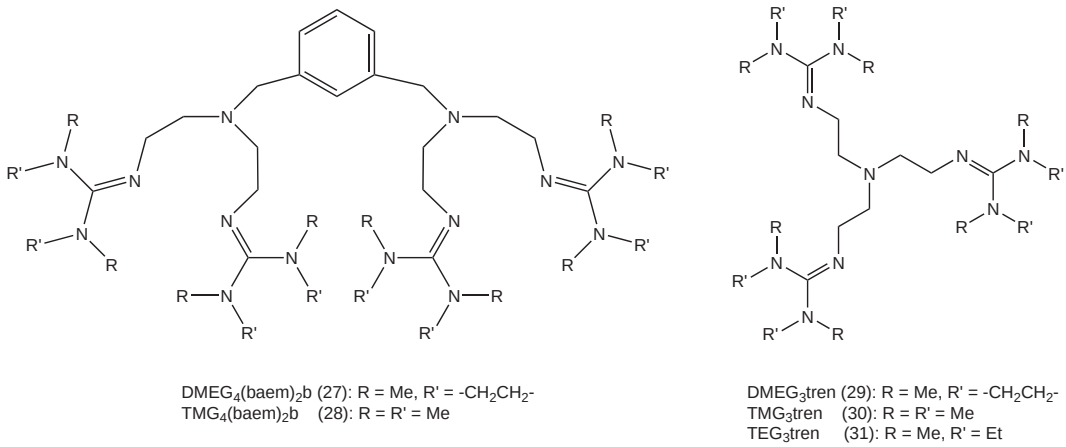

Figure 7.4: Schematic structure of polydentate guanidine ligands.

7.2.2 Results and Discussion

Ligand and complex syntheses

The tetradentate ligands $DMEG_4(baem)_2b$ (**27**) and $TMG_4(baem)_2b$ (**28**) were prepared by the reaction of four equivalents of chloroformamidinium chloride with the tetramine 2,6-bis{[bis(2-aminoethyl)amino]methyl}benzene. The latter is accessible in a three step synthesis starting with the protection of the amine functions of 1,5-diamino-3-azapentane as phthalimids according to Miranda et al.[160] In the next step two equivalents of the 1,5-phthalimido-3-azapentane were added to 2,6-bis(bromo-methyl)benzene to give the protected tetramine 2,6-bis{[bis(2-phthalimidoethyl)amino]methyl}benzene.[161] The removal of the protecting groups occurs by simple acidic cleavage[161] and 2,6-bis{[bis(2-aminoethyl)amino]methyl}benzene was obtained in almost quantitative yields.

The tridentate ligands $DMEG_3tren$ (**29**) and TMG_3tren (**30**) were prepared according to literature procedures described by Sundermeyer et al.[112,124] To achieve a tridentate ligand with high steric demand, tris(2-aminoethyl)amine was reacted with three equivalents of the chloroformamidinium chloride TEG (**V4**) to give TEG_3tren (**31**). A schematic depiction of the polydentate ligands **27**-**31** is given in Figure 7.4.

The complexes $[(TMG_4(beam)_2b)(ZnCl_2)_2]$ (**28a**), $[Zn(DMEG_3tren)Cl][Cl]$ (**29a**) and $[Zn(TMG_3tren)Cl][Cl]$ (**30a**) were obtained as colourless crystal solids in yields of 36-77 % by stirring of the polydentate ligands with $ZnCl_2$ in dry THF. Single crystals of **28a** and **29a** were prepared by slow diffusion of ethyl ether in an acetonitrile solution of the complexes and their solid-state structures were determined by X-ray crystallography (Fig. 7.5 and 7.6). The crystal structures of **28a** exhibit two molecules per asymmetric unit. Due to their high similarity, in the following only one structure is discussed as **28a**. The crystals of **30a** were strongly disordered and not suited for X-ray measurements. But the reaction of **30** with $ZnCl_2$ in the presence of triflate ions resulted in the formation of single crystals of $[Zn(TMG_3tren)Cl][CF_3SO_3]$ which possess the same structure motif as **30a** and are discussed in the following as **30a*** (see Fig. 7.6).

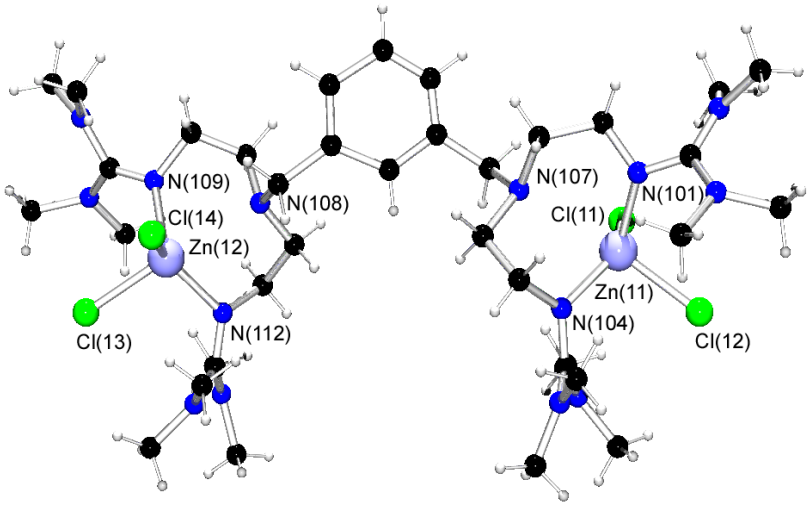

Figure 7.5: Crystal structure of $[(TMG_4(beam)_2b)(ZnCl_2)_2]$ (**28a**) as determined at 120 K.

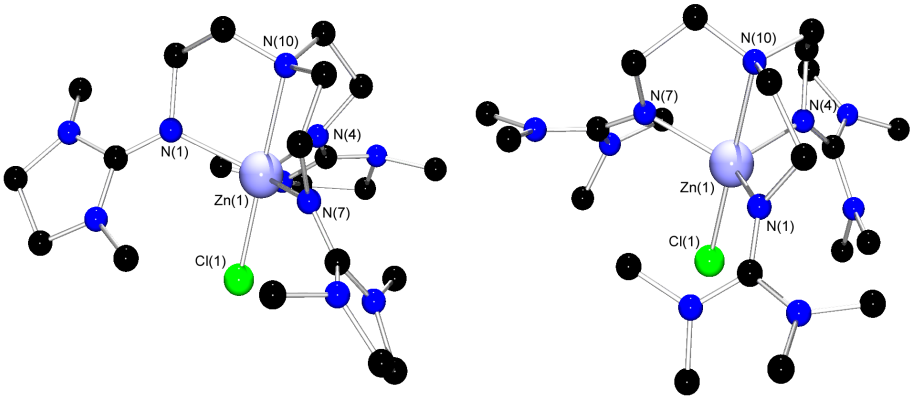

Figure 7.6: Molecular structure of $[Zn(DMEG_3tren)Cl]^+$ in crystals of $[Zn(DMEG_3tren)Cl][Cl]$ (**29a**) and $[Zn(TMG_3tren)Cl]^+$ in crystals of $[Zn(TMG_3tren)Cl][CF_3SO_3]$ (**30a***) as determined at 120 K. Hydrogen atoms were obmitted due to reasons of clearity.

The polydentate ligand $TMG_4(beam)_2b$ in **28a** does not coordinate one zinc atom fourfold, but two zinc atoms in a bidentate manner. The remaining coordination sites are occupied in each case by two chlorine atoms resulting in a distorted tetrahedral coordination geometry. The Zn-N_{gua} distances are in each tetrahedron within the precision of measurements equal in length (av. 2.024 Å), whereas each tetrahedron exhibit one shorter (av. 2.302 Å) and one longer (av. 2.350 Å) Zn-Cl bond. Regarding the C-N bond lengths in the guanidine moiety, there is no clear trend observed within the precision of measurements.

The complexes **29a** and **30a*** exhibit a trigonal-bipyramidal coordination geometry. The equatorial plane is defined by the N-donor atoms of the guanidine moieties (Zn-N_{gua}: av. 2.078 (**29a**); av. 2.086 Å (**30a***)), whereas the axial positions are taken by the amine nitrogen atom (Zn-N: 2.339(2) (**29a**); 2.336(3) Å (**30a***)) and the chlorido ligand (Zn-Cl: 2.332(2) (**29a**); 2.356(1) Å (**30a***)), respectively. The second chlorine atom or the triflate ion is far away from the metal centre and acts as counter ion. Hence, the zinc atom is located in a molecular pocket formed by the N-donor ligands. This structure motif was e.g. also observed for the complexes $[Mn(TMG_3tren)Cl][Cl]$ and $[Zn(TMG_3tren)(CF_3SO_3)][CF_3SO_3]$ prepared by Sundermeyer et al.[112,162] The C_{gua}-N_{gua} bonds are in each guanidine moiety with av. 1.311 (**29a**) and av. 1.313 Å (**30a***) equal in length and significantly shorter than the C_{gua}-N bonds (**29a**: av. 1.364; **30a***: av. 1.364 Å). The kind of guanidine moiety shows no impact on the structure properties of the obtained complexes.

Selected bond lengths and angles of **28a**, **29a** and **30a*** are summarised in Table 7.4.

Table 7.4: Selected bond lengths (Å) and bond angles (°) of **28a**, **29a** and **30a***.

	28a	**29a**	**30a***
Zn-N_{gua}	2.001(10), 2.041(11), 2.012(10), 2.043(10)	2.074(2), 2.076(2), 2.084(2)	2.075(3), 2.085(3), 2.098(3)
Zn-N		2.339(2)	2.336(3)
Zn-Cl	2.301(3), 2.333(4), 2.302(4), 2.366(4)	2.332(1)	2.356(1)
C_{gua}-N_{gua}	1.332(15), 1.314(15), 1.310(17), 1.273(16)	1.307(2), 1.312(2), 1.313(2)	1.310(4), 1.316(4), 1.314(4)
C_{gua}-N	1.365(16), 1.305(16), 1.342(15), 1.353(15), 1.322(17), 1.385(17), 1.402(15), 1.356(15)	1.373(2), 1.350(2), 1.365(2), 1.380(2), 1.341(2), 1.376(2)	1.349(4), 1.372(4), 1.367(4), 1.360(4), 1.362(4), 1.372(4)
N-Zn-N	117.7(4), 118.1(4)		
Cl-Zn-Cl	104.1(1), 101.5(1)		
∠($ZnCl_2$, ZnN_2)	82.3, 83.1		

Polymerisation activity

The chlorido complexes **28a**, **29a** and **30a** were tested for their ability to initiate the ring-opening polymerisation of D,L-lactide according to the standard procedure (0.2 mol% catalyst calculated relative to the zinc centres, 150°C). In order to rate the catalytic activity of the complexes, the polymer yield, the molecular weights as well as the polydispersity of the PLA were determined (see Table 7.5). The tacticity was analysed by homonuclear decoupled ^{1}H NMR spectroscopy.[24]

One idea concerning the preparation of zinc complexes stabilised by polydentate guanidine ligands was that the arms coordinating the zinc atom may release the metal atom easily when a substrate molecule approaches and that the guanidine function of the free arm supports the polymerisation reaction and enhance the catalytic activity (cf. Chapter 9). It is also supposable that the structure motif of a molecular pocket may influence the polymerisation behaviour.

In contrast to these suggestions, the complexes **29a** and **30a** show neither an enhanced polymerisation activity compared to other zinc guanidine systems nor can an impact on the microstructure be observed. Independent of the different ligands coordinated, they provide the same catalytic performance. PLAs were produced in respectable yields of around 70 % but the obtained chain length is smaller than it is in theory (e.g. $M_{w,exp.}$ = 22,000; $M_{w,theor.}$ = 50,000 g/mol). The chlorido complex **28a** including tetrahedral coordinated zinc centres exhibits with yields of around 84 % higher polymerisation activity than **29a** and **30a**. However, the M_w values of the produced polymer are also smaller than the theoretical values. This observation indicates the occurrence of side reaction leading to chain transfer or truncation. The polymerisation activity of **29a** and **30a** may be affected by the high steric hindrance of the guanidine units that hinder the accessibility to the zinc centre and therefore the coordination and activation of lactide molecules. An impact on the stereo preference during the polymerisation due to this high steric demand could not be observed for **29a** and **30a** (P_r = 0.53; 0.52).

Table 7.5: Polymerisation of D,L-lactide initiated by **28a**, **29a** and **30a**.

Initiator		Time[a] [h]	Yield [%]	M_w [g/mol]	PD[b]	Pr[c]
[(TMG_4(beam)$_2$b)($ZnCl_2$)$_2$]	**28a**	24	81	36,000	1.9	0.54
[(TMG_4(beam)$_2$b)($ZnCl_2$)$_2$]	**28a**	48	86	33,000	1.9	
[Zn($DMEG_3$tren)Cl][Cl]	**29a**	24	72	21,000	1.8	0.53
[Zn($DMEG_3$tren)Cl][Cl]	**29a**	48	70	22,000	1.8	
[Zn(TMG_3tren)Cl][Cl]	**30a**	24	71	22,000	1.9	0.52
[Zn(TMG_3tren)Cl][Cl]	**30a**	48	69	21,000	1.8	

Reaction conditions: Catalyst (0.2 mol%), 150 °C; [a] reaction times were not necessarily optimised; [b] PD = M_w/M_n where M_n is the number-average molar mass; [c] From analysis of the ^{1}H homonuclear decoupled NMR spectrum using the equation $P_r{}^2$ = 2 [sis];[24]

7.2.3 Conclusion

In this section the synthesis of the polydentate ligands $DMEG_4(baem)_2b$ (**27**), $TMG_4(baem)_2b$ (**28**) and TEG_3tren (**31**) is reported. The zinc complexes stabilised by **28**, $DMEG_3tren$ (**29**) and TMG_3tren (**30**) were prepared and tested for their catalytic activity in the ring-opening polymerisation of D,L-lactide. They were all proven to be active initiators in lactide polymerisation but influences characteristic for polydentate initiator systems like enhanced polymerisation activity or impact on the PLA microstructure could not be observed.

7.3 Conclusion

In summary, the monodentate acting guanidine-pyridine ligands DMEGpico (**21**) and TMGpico (**22**) as well as the polydentate guanidine ligands $DMEG_4(baem)_2b$ (**27**), $TMG_4(baem)_2b$ (**28**) and TEG_3tren (**31**) were synthesised and completely characterised. The zinc complexes $[Zn(DMEGpico)_2Cl_2]$ (**21a**), $[Zn(TMGpico)_2Cl_2]$ (**22a**), $[(TMGpico)_2Zn_3(CH_3COO)_6]$ (**22b**), $[(TMG_4(beam)_2b)(ZnCl_2)_2]$ (**28a**), $[Zn(DMEG_3tren)Cl][Cl]$ (**29a**) and $[Zn(TMG_3tren)Cl][Cl]$ (**30a**) were obtained as colourless crystals and the chlorido complexes were tested towards their ability to initiate the ring-opening polymerisation of D,L-lactide. They all were proven to be active initiators although a characteristic polymerisation behaviour compared to other zinc guanidine systems could not be observed. Hence, the different ligands classes have crucial impact on the molecular structure of the corresponding complexes but this ligand effect has not the desired influence on the lactide polymerisation activity.

8 Zinc complexes stabilised by neutral aromatic and aliphatic amine ligands and their application in the ring-opening polymerisation of lactide

Encouraged by the unexpected catalytic activity of zinc complexes stabilised by the amine 8-aminoquinoline, neutral aliphatic and aromatic diamines as well as oxabispidines were investigated towards their ability to stabilise zinc complexes that act as active initiators in lactide polymerisation. Further focus was laid on the question whether the stereogenic information in the complexes including the chiral ligands **37**, **38** and **39** is able to control the tacticity and thus the microstructure of the resultant PLA.

8.1 New challenge for classics: Neutral zinc complexes stabilised by 2,2'-bipyridine and 1,10-phenanthroline and their application in the ROP of lactide

The zinc acetato and triflato complexes of 2,2'-bipyridine and 1,10-phenanthroline were prepared and completely characterised. The whole series (including the already described dichlorido complexes and the ligands themselves) were screened for their catalytic activity in the solvent free ring-opening polymerisation of D,L-lactide. The acetato and triflato complexes were found to be active initiators and polylactides could be obtained in almost quantitative yields or with high molecular weights, up to 145,000 g/mol.

8.1.1 Introduction

To find new neutral ligands for the development of ROP active single-site metal catalysts interests were focused on 2,2'-bipyridine (bipy, **33**) and 1,10-phenanthroline (phen, **34**), some of the most widely used bidentate ligands in coordination chemistry (Fig. 8.1). They are commercially

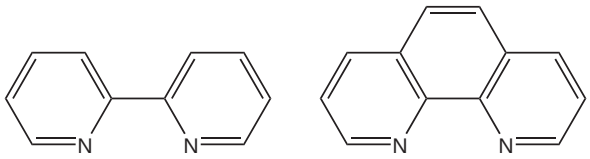

Figure 8.1: Bidentate ligands 2,2'-bipyridine (bipy, **33**, l) and 1,10-phenanthroline (phen, **34**, r)

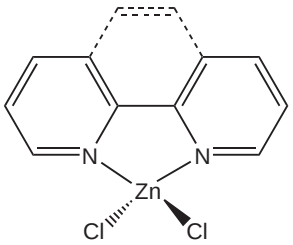

Figure 8.2: Schematic depiction of $[Zn(bipy)Cl_2]$ (**33a**) and $[Zn(phen)Cl_2]$ (**34a**)[149,150]

available, easy to handle and due to their favourable donor properties they are able to stabilise complexes with a wide range of transition metals. To date several zinc complexes containing **33** and **34** were synthesised,[163–175] but none has been tested for their ability to initiate the ring-opening polymerisation of cyclic lactones. Herein the synthesis and characterisation of four novel zinc actetate and triflate complexes stabilised by 2,2'-bipyridine and 1,10-phenanthroline are reported. They together with already described chloride complexes (Fig. 8.2)[149,150] and the ligands themselves were screened for their catalytic activity in the solvent-free ROP of D,L-lactide.

8.1.2 Results and Discussion

Complex syntheses

The zinc complexes **33a**[149] and **34a**[150] were prepared according to literature procedures. $[Zn_3(bipy)_2(CH_3COO)_6]$ (**33b**), $[Zn_2(phen)_2(CH_3COO)_4]$ (**34b**), $[Zn(bipy)_2(CF_3SO_3)_2]$ (**33c**) and $[Zn(phen)_2(CF_3SO_3)_2]$ (**34c**) were obtained as colourless crystal solids in 88-98% yield by simple stirring of **33** and **34** with $Zn(OAc)_2$ and $Zn(OTf)_2$ in a dry aprotic solvent (THF/MeCN) (see Fig. 8.3). Single crystals were prepared either by cooling a saturated solution slowly to room temperature or by slow diffusion of diethyl ether into the solution. The molecular structures of **33b**-**34c** (Fig. 8.4-8.6) were determined by X-ray crystallography. The crystals obtained show a high stability towards moisture and air. They can be handled and stored in air, whereas the corresponding zinc salts are sensitive towards hydrolysis and are rather hygroscopic.

The chlorido complexes **33a** and **34a** exhibit simple tetrahedral coordination geometry, where the zinc atom is fourfold coordinated by the two N-donor atoms of the chelating ligand and two chlorides, respectively (Fig. 8.2). The acetato complexes **33b** and **34b** possess an oligonu-

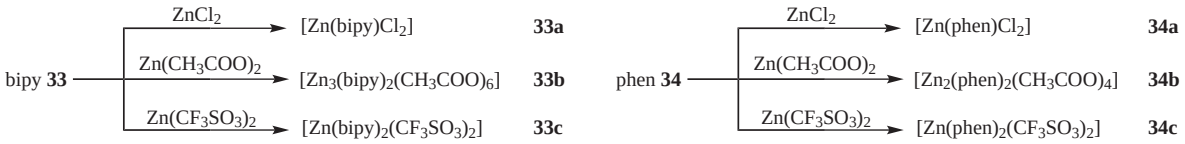

Figure 8.3: Schematic synthesis of **33a**-**34c**

clear structure. In **33b**, two Zn atoms are surrounded by the N-donor atoms of **33** and three oxygen atoms of three acetato bridging ligands connecting each Zn atom with a third Zn atom located between them. Consequently, the latter shows an octahedral coordination environment whereat each corner is occupied by an acetato oxygen atom. Interestingly, in each case two acetato ligands bridge the Zn atoms via two oxygen functions but the third acetato ligand connects the metal atoms via only one oxygen atom of the acetate group. This structure motif is very similar to that found for $[Zn_3(TMGpico)_2(CH_3COO)_6]$ (**22b**, see Section 7.1). **34b** is a binuclear species that is also bridged by acetato ligands. Each Zn atom is coordinated by the N-donors of **34** in a chelating manner, and two oxygen atoms of two acetato ligands connecting them both and generating an eight-membered heterocycle. To complete the trigonal bipyramidal coordination sphere of each metal atom the fifth coordination site is occupied by a non-bridging acetato ligand. The zinc triflato complexes **33c** and **34c** are mononuclear and exhibit an analogous structure motif. Each zinc atom is surrounded by the four N-donor atoms of two chelate ligands and two oxygen atoms of two triflato ligands generating an octahedral coordination environment.

Due to the rigid structure of **33** and **34**, the bite angles of the described complexes differ slightly, ranging from 75.8(1) to 79.3(1)° but showing slightly higher values for the triflato complexes. Regarding the Zn-N bond length, it is notable that in all complexes, except **33b**, one of the bonds is with a difference of 0.010 (**33c**), 0.024 (**34c**) and 0.104 Å (**34b**) longer than the other. Their absolute values range from 2.102(1) to 2.210(2) Å. The values for the Zn-O bonds in **33b**

Table 8.1: Selected bond lengths [Å] and angles [°] of **33b**, **34b**, **33c**, and **34c**.

	1b	**2b**	**1c**	**2c**
Zn-N	2.143 (2), 2.148(2)	2.104(2), 2.208(2), 2.104(2), 2.210(2)	2.102(1), 2.112(1)	2.102(1), 2.126(1)
Zn-O	2.018(2), 2.019(2), 1.992(1), 2.071(2), 2.102(1), 2.161(1)	1.981(2), 2.004(2), 2.096(2), 1.984(2), 2.003(2), 2.078(2)	2.191(1)	2.189(1)
N-Zn-N	75.8(1)	76.7(1) 77.0(1)	78.1(1)	79.3(1)
O-Zn-O	98.0(1), 98.0(1), 99.3(1) 180.0, 93.0(1), 87.0(1), 90.1(1), 89.9(1), 87.9(1), 92.1(1), 180.0, 180.0	117.3(1), 95.9(1), 100.2(1), 116.4(1), 97.7(1), 96.3(1),	83.3(1)	83.6(1)
$\measuredangle(ZnN_2, ZnN_2)$			82.0(1)	85.0(1)

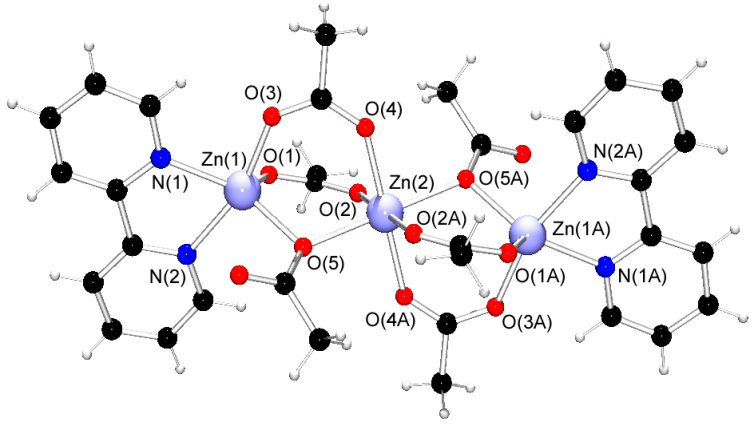

Figure 8.4: Crystal structure of $[Zn_3(bipy)_2(CH_3COO)_6]$ (**33b**) as determined at 120 K.

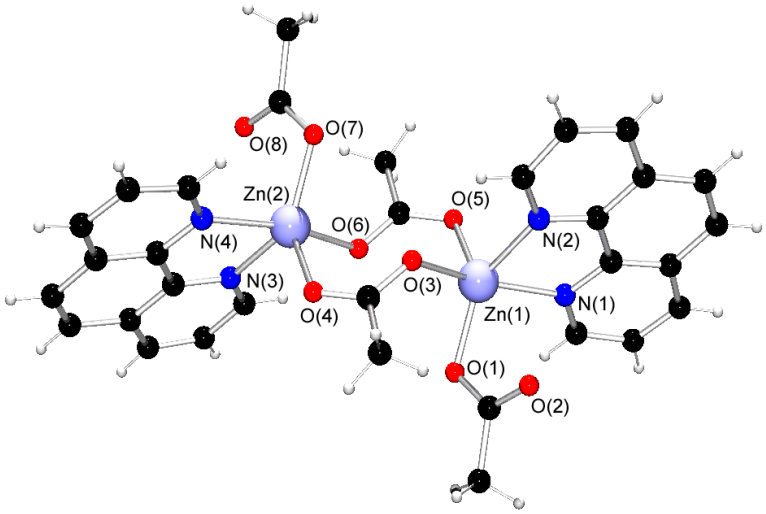

Figure 8.5: Crystal structure of $[Zn_2(phen)_2(CH_3COO)_4]$ (**34b**) as determined at 120 K.

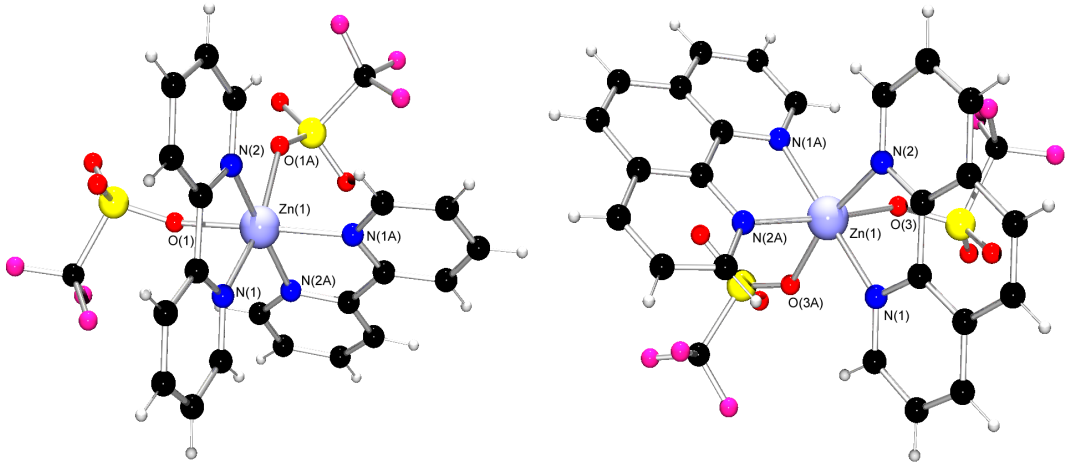

Figure 8.6: Crystal structure of $[Zn(bipy)_2(CF_3SO_3)_2]$ (**33c**) and of $[Zn(phen)_2(CF_3SO_3)_2]$ (**34c**) as determined at 120 K.

and **34b** depend on the coordination mode of the acetato ligands. In **33b** the Zn-O bonds between the bridging acetato ligands and the zinc atoms that are also coordinated by the pyridine ligands are in average with 2.010 Å generally shorter than those belonging to the ZnO_6 octahedron (av. 2.111 Å). In **34b** the non-bridging acetato ligand possesses the shortest Zn-O value with av. 1.983 Å. The value for the bridging ligand, whose oxygen atom is occupying the equatorial coordination site of the trigonal bipyramid, is with av. 2.004 Å longer than the latter Zn-O bond length, but not as long as the Zn-O bond belonging to the oxygen atom occupying the axial coordination site of the trigonal bipyramid (av. 2.087 Å). Due to their similar structure, the Zn-O bond lengths of **33c** (2.191(1) Å) and **34c** (2.189(1) Å) possess equal values. Selected bond lengths and angles are summarised in Table 8.1.

Polymerisation activity

The complexes **33a** to **33c** and **34a** to **34c**, as well as the ligands **33** and **34** were tested for their ability to initiate the ring-opening polymerisation of D,L-lactide according to the standard procedure (0.2 mol% catalyst, 150°C). In order to rate the catalytic activity of the complexes, the polymer yield was determined and the molecular weights as well as the polydispersity of the PLA were determined by gel permeation chromatography (see Table 8.2). The tacticity was analysed by homonuclear decoupled ^{1}H NMR spectroscopy.[24]

Table 8.2: Polymerisation of D,L-lactide in the presence of bipy, phen and their corresponding zinc complexes.

Initiator		Time[a] [h]	Yield [%]	M_w [g/mol]	PD[b]	P_r^c
bipy	**33**	48	0	-	-	-
$[Zn(bipy)Cl_2]$	**33a**	48	0	-	-	-
$[Zn_3(bipy)_2(CH_3COO)_6]$	**33b**	24	95	80,000	1.8	0.50
$[Zn_3(bipy)_2(CH_3COO)_6]$	**33b**	48	93	68,000	1.7	-
$[Zn(bipy)_2(CF_3SO_3)_2]$	**33c**	24	12	75,000	1.6	-
$[Zn(bipy)_2(CF_3SO_3)_2]$	**33c**	48	57	145,000	1.9	0.59
phen	**34**	48	0	-	-	-
$[Zn(phen)Cl_2]$	**34a**	48	0	-	-	-
$[Zn_2(phen)_2(CH_3COO)_4]$	**34b**	24	94	56,000	1.7	0.50
$[Zn_2(phen)_2(CH_3COO)_4]$	**34b**	48	89	45,000	1.9	-
$[Zn(phen)_2(CF_3SO_3)_2]$	**34c**	24	0	-	-	-
$[Zn(phen)_2(CF_3SO_3)_2]$	**34c**	48	21	87,000	2.0	0.61

Reaction conditions: Catalyst (0.2 mol%), 150°C; [a] reaction times were not necessarily optimised; [b] PD = M_w/M_n where M_n is the number-average molar mass; [c] from analysis of the ^{1}H homonuclear decoupled NMR spectrum using the equation $P_r^2 = 2$ [sis].[24]

The pure ligands as well as the chloride complexes show even after 48 h no catalytic activity whereas the zinc acetato and zinc triflato complexes possess the ability to produce PLA. Due to the fact that the acetate containing complexes provide polymers with significantly higher molecular weights and higher yields as their triflate containing analogues, it is obvious that the catalytic activity strongly depends on the character of the anionic component of the zinc complex. This strong dependence is also reported in previous studies by using zinc guanidine-pyridine complexes (Section 6). In addition, the complexes stabilised by **33** exhibit a higher activity than those stabilised with **34**. The extension of reaction time from 24 to 48 h leads in the case of **33c** and **34c** to an increase of yield and molecular weight, whereas in polymerisations initiated with **33b** and **34b** a decrease of molecular weight can be observed which may be caused by side reactions such as interchain or intrachain transesterification resulting in a chain-transfer reaction.[126,127] It is also remarkable that the molecular weights of the polymers obtained by utilising **33c** and **34c** were significantly high in relation to the obtained yield. These PLA samples also show with P_r values of 0.59 and 0.61 a slight heterotactic enchainment whereas the values of samples obtained by using **33b** and **34b** (0.50) imply that the complex structure shows no ability to affect the tacticity of the formed polymer.

8.1.3 Conclusion

In this chapter the synthesis and complete characterisation of four novel zinc complexes stabilised by the neutral bisdentate ligands, 2,2'-bipyridine and 1,10-phenanthroline are reported, that were proven to be active initiators in the solvent-free ring-opening polymerisation of D,L-lactide. They provide PLAs in almost quantitative yields or with high molecular weights up to 145,000 g/mol. This combined with commercial availability, high robustness resulting in an easy handling and their favourable donor properties clearly demonstrate the high potential of this neutral ligand class for the development of excellent and application-oriented single-site metal catalysts for the ROP of lactide.

8.2 Simple diamine zinc complexes as efficient catalysts in the lactide polymerisation

Zinc(II) halide complexes stabilised by simple diamine ligands are investigated towards their application as initiators in the lactide polymerisation. They offer high stability and facile synthesis, but also good efficiency.

8.2.1 Introduction

Encouraged by the successful development of catalytic active zinc complexes stabilised by the aromatic bisamine ligands 2,2'-bipyridine and 1,10-phenanthroline (Chapter 8.1), the focus is expanded to simple aliphatic diamine ligands.
The facile chelating and commercially available nitrogen ligand, N,N,N',N'-tetramethylethylenediamine (TMEDA, **35**) is applied in many fields of coordination chemistry[176–180] and its ethyl-substituted analogue N,N,N',N'-tetraethylethylenediamine (TEEDA, **36**) has already been reported to accelerate anionic ethylene polymerisation.[181,182] These ligands, as well as their chiral cyclohexane derivatives N,N,N',N'-tetramethylcyclohexanediamine ((R,R)-TMCDA, **37**) and N,N,N',N'-tetraethylcyclohexanediamine ((R,R)-TECDA, **38**) (Figure 8.7) were investigated towards their ability to stabilise zinc halide complexes suitable as initiators for the solvent-free ROP of lactide.[181,182]

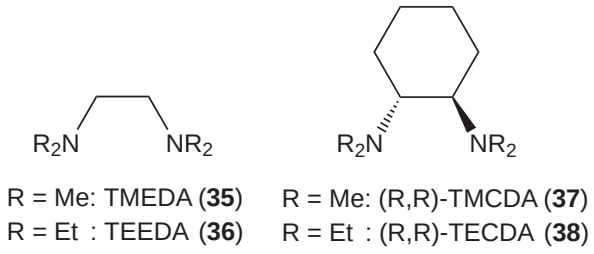

Figure 8.7: Simple diamine and chiral diaminocyclohexane ligands

8.2.2 Results and discussion

The zinc halide complexes were synthesised by the reaction of amine and an equivalent amount of zinc(II) bromide/chloride in the group of Prof. C. Strohmann from the Technische Universität Dortmund and were provided in the context of a collaboration. Compound **35f** has already been reported before.[183]
The zinc bromide complexes **35f**-**38f** as well as the zinc chloride complexes **37a** and **38a** are highly air stable and non-sensitive towards humidity and can be stored without any precautions for months. In all structures the zinc atom exhibits a distorted tetrahedral coordination sphere. Figure 8.8 schematically displays the prepared diamine complexes.

R = Me: [Zn(TMEDA)Br_2] (**35f**)
R = Et : [Zn(TEEDA)Br_2] (**36f**)

R = Me, X = Cl: [Zn((R,R)-TMCDA)Cl_2] (**37a**)
R = Me, X = Br: [Zn((R,R)-TMCDA)Br_2] (**37f**)
R = Et , X = Cl: [Zn((R,R)-TECDA)Cl_2] (**38a**)
R = Et , X = Br: [Zn((R,R)-TECDA)Br_2] (**38f**)

Figure 8.8: Schematic depiction of the zinc(II) bromide and chloride complexes **35f**-**38f**.

The crystalline compounds were investigated towards their activity to initiate the ring-opening polymerisation of D,L-lactide according to the standard procedure (0.2 mol% catalyst, 150°C). In order to rate the catalytic activity of the complexes, the polymer yield was defined and the molecular weights as well as the polydispersity (PD) of the obtained PLA were determined by gel permeation chromatography (see Table 8.3). The tacticity of selected polymer samples was analysed by homonuclear decoupled ^{1}H NMR spectroscopy.[24] A reaction time of 48 h was chosen for **35f**, **36f**, **37f** and **37a** because after 24 h the yield was too small to give reasonable results.

The simple TMEDA complex **35f** does not show any activity, even after a reaction time of 48 h. However, the complexes **36f** - **38f** initiate the ring-opening polymerisation of D,L-lactide

Table 8.3: Polymerisation of D,L-lactide initiated by **35f**-**38f**, as well as **37a** and **38a**.

Initiator		Time[a] [h]	Yield [%]	M_w [g/mol]	PD[b]	P_r[c]
[Zn(TMEDA)Br_2]	**35f**	24	0	-	-	-
		48	0	-	-	-
[Zn(TEEDA)Br_2]	**36f**	48	56	58,000	1.9	n.d.
[Zn((RR)-TMCDA)Br_2]	**37f**	48	20	25,000	1.5	n.d.
[Zn((RR)-TECDA)Br_2]	**38f**	24	92	133,000	1.9	0.55
		48	91	113,000	1.9	n.d.
[Zn((RR)-TMCDA)Cl_2]	**37a**	48	27	38,000	1.6	0.57
[Zn((RR)-TECDA)Cl_2]	**38a**	24	89	99,000	2.1	n.d.
		48	93	84,000	1.9	n.d.

Reaction conditions: Catalyst (0.2 mol%), 150 °C; [a] reaction times were not necessarily optimised; [b] PD = M_w/M_n where M_n is the number-average molar mass; [c] From analysis of the ^{1}H homonuclear decoupled NMR spectrum using the equation $P_r^2 = 2$ [sis].[24]

whereas the halogen influence is small. The most successful candidates for highly active catalysts in the ROP of lactide are the TECDA-containing complexes **38a** and **38f**. They combine almost quantitative yields with high molecular weights up to 133,000 g/mol, which lie in the range suitable for industrial applications (lower limit 40,000 g/mol).[184] The polydispersities of 1.5 to 2.1 show that during the reaction transesterifications take place resulting in chain-transfer reactions.[126,127] The P_r values of the complexes containing a chiral ligand show with 0.57 (**37a**) or 0.55 (**38f**) only a slight heterotactic bias and imply that the complex structures provide under the given conditions no or only a very slight ability to affect the tacticity of the formed polymer. The observed efficiency of some of the simple diamine complexes is surprising but the increased activity from TMEDA (**35**) to TECDA (**38**) via TMCDA (**37**) and TEEDA (**36**) may be due to several effects and has to be elucidated in further studies.

8.2.3 Conclusion

A series of highly stable diamine zinc complexes was screened towards its application as catalysts in the lactide polymerisation. Especially the TECDA complexes **38f** and **38a** showed an unexpected activity with high yields and molecular weights. The presented catalysts convince by the combination of efficiency and stability which often are in conflict with each other.

8.3 Lactide Polymerisation with 9-oxabispidine zinc complexes

The zinc dichlorido and zinc diacetato complexes of the chiral tricyclic 9-oxabispidine (1R,2S,9S)-11-methyl-13-oxa-7,11-diazatricyclo[7.3.1.$0^{2,7}$]tridecane (9-oxa, **39**) were prepared and characterised by X-ray crystallography. The latter complex was found to catalyse the solvent-free polymerisation of D,L-lactide to give atactic polylactide.

8.3.1 Introduction

In the ongoing search for new zinc complexes with neutral N-donor ligands as initiators for the solvent-free ROP of lactide the attention was drawn to chiral tertiary amines since their stereochemical information might influence the tacticity of the PLA and, thus, the physical and

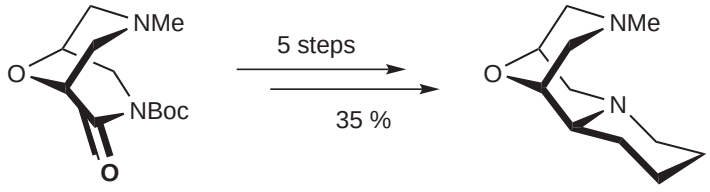

Figure 8.9: The tricyclic 9-oxabispidine (9-oxa, **39**) and the imide precursor.[185]

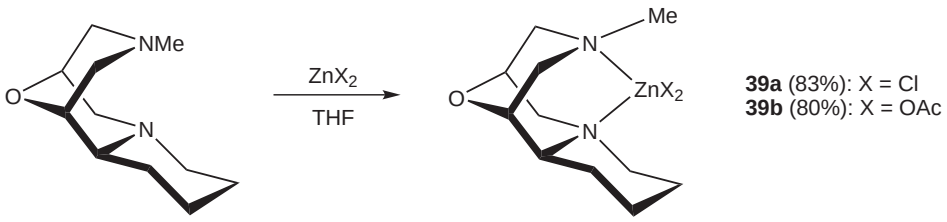

Figure 8.10: Formation of the chiral zinc complexes **39a** and **39b** from **39**.

mechanical properties. Furthermore, by using a neutral diamine an enhanced stability of the resulting catalyst complex is targeted. As the chiral diamine the newly developed tricyclic 9-oxabispidine (1R,2S,9S)-11-methyl-13-oxa-7,11-diazatricyclo[7.3.1.$0^{2,7}$]tridecane (9-oxa, **39**) (Fig. 8.9) is chosen, which is for example accessible in a few steps from the imide precursor (1R,5S)-tert-butyl 7-methyl-2-oxo-9-oxa-3,7-diazabicyclo[3.3.1]nonane-3-carboxylate.[185–188] This ligand was supplied by Breuning and co-workers within the scope of a collaboration. The high potential of 9-oxa in asymmetric synthesis was recently shown in the Pd^{II}-catalysed kinetic resolution of secondary alcohols giving selectivity factors of up to 19.[185] In this chapter, the synthesis and characterisation of the first zinc complexes of 9-oxa, their activity in the ROP of D,L-lactide and their impact on the tacticity of the obtained polymers are reported.

8.3.2 Results and discussion

Complex syntheses

The chiral zinc complexes **39a** and **39b** were obtained as colourless crystals in 80-83% yield by simple stirring of 9-oxa with $ZnCl_2$ and $Zn(OAc)_2$ in dry THF (Fig. 8.10). The obtained complexes are stable towards moisture and air for several days. Single crystals were prepared either by cooling a saturated solution slowly to room temperature or by slow diffusion of pentane into the solution. The molecular structures of **39a** and **39b**, determined by X-ray crystallography, are shown in Figure 8.11. In both complexes, the zinc atom is fourfold coordinated in a slightly distorted tetrahedral manner by the N-donor atoms of the oxabispidine 9-oxa and the two chloride or acetate ions, respectively. The bite angles of 89° in **39a** and of 88° in **39b** are slightly too small for an ideal-typic tetrahedral geometry. These resulting distortions are also reflected in the angle between the $ZnCl_2$ and the ZnN_2 plane in **39a** (81°) and the ZnO_2 and the ZnN_2 plane in **39b** (78°), which would be 90° in a tetrahedron.

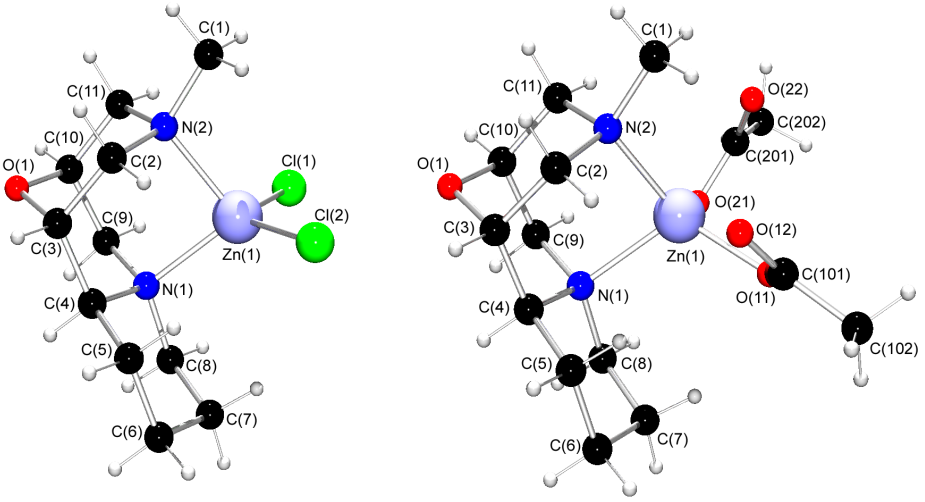

Figure 8.11: Molecular structures of $[Zn(9\text{-oxa})Cl_2]$ (**39a**, l) and $[Zn(9\text{-oxa})(OAc)_2]$ (**39b**, r) as determined at 120 K. Selected bond lengths (Å) and angles (°): **39a:** Zn(1)-N(1) 2.077(2), Zn(1)-N(2) 2.070(2), Zn(1)-Cl(1) 2.208(1), Zn(1)-Cl(2) 2.223(1), N(1)-Zn(1)-N(2) 88.89(7), Cl(1)-Zn(1)-N(2) 117.57(2); **39b:** Zn(1)-N(1) 2.121(3), Zn(1)-N(2) 2.073(3), Zn(1)-O(11) 1.933(2), Zn(1)-O(21) 2.014(2), N(1)-Zn(1)-N(2) 88.3(1), O(11)-Zn(1)-O(21) 106.6(1).

Polymerisation activity

The activity of the complexes **39a** and **39b** was studied on the bulk polymerisation of D,L-lactide (Table 8.4). The reactions were carried out with 0.2 mol-% of **39a** or **39b** at 150 °C according to the standard procedure. The molecular weight and polydispersity of PLA were determined by gel permeation chromatography, the tacticity and the probability of heterotactic enchainment (P_r) was analysed by homonuclear decoupled ^{1}H NMR spectroscopy.[24]
As also found before for zinc guanidine complexes (see Chapter 6), the activity of **39a** and **39b** strongly depended on the anionic component of the zinc salt. While the dichlorido complex **39a** did not initiate the polymerisation of lactide, polylactides with weight-average molecular

Table 8.4: Polymerisation of lactide in the presence of the 9-oxa zinc complexes **39a** and **39b**.

Initiator		Yield [%]	M_w [g/mol]	PD^a	$P_r{}^b$
$[Zn(9\text{-oxa})Cl_2]$	**39a**	0	-	-	-
$[Zn(9\text{-oxa})(OAc)_2]$	**39b**	29	21,000	1.93	0.50

Reaction conditions: Catalyst (0.2 mol%), 150 °C, 48 h; ^{a} PD = M_w/M_n where M_n is the number-average molar mass; ^{b} From analysis of the ^{1}H homonuclear decoupled NMR spectrum using the equation $P_r{}^2$ = 2 [sis].[24]

weights of up to 21,000 g/mol were obtained with the corresponding diacetato complex **39b**. Thus, the latter catalyst required no common co-catalysts (alcohols or anionic compounds like alkoxides) in order to initiate the ring-opening polymerisation under industrially applicable conditions. The P_r value of 0.50 implies that the stereogenic information in **39b** is not able to control the tacticity of the resultant PLA.

8.3.3 Conclusion

The novel zinc complexes **39a** and **39b** which possess the 9-oxabispidine 9-oxa (**39**) as a chiral ligand were synthesised und structurally characterised. Compound **39b** promotes the ROP of D,L-lactide without co-catalysts like alkoxides but the stereogenic information in **39b** is not able to control the tacticity of the resultant PLA.

8.4 Conclusion

In this chapter the synthesis of catalytic active zinc complexes based on rather simple aliphatic and aromatic diamines as well as oxabispidines is reported. Hence, it was proven that these ligand classes are also suited to provide initiators for the ROP of lactide. They combine the advantageous properties of a simple assembly, low cost production and high activity. However, the stereogenic information in complexes with the chiral ligands **37**, **38** and **39** is not able to control the tacticity of the resultant PLA under the chosen conditions. It seems that the impact on the polymer microstructure is even higher for steric demanding ligands.

9 Elucidation of the mechanism of lactide polymerisation mediated by guanidine-pyridine zinc complexes

The experimental and theoretical studies on the mechanism of lactide polymerisation with the guanidine-pyridine zinc complexes $[Zn(DMEGqu)_2(CF_3SO_3)][CF_3SO_3]$ (**6c**) and $[Zn(TMGqu)_2(CF_3SO_3)][CF_3SO_3]$ (**7c**) reveal that the polymerisation proceeds via a coordination-insertion mechanism. The guanidine functions of the coordinated ligand support the first ring-opening step and thus allow the ROP without additional co-catalysts like alcohols or alkoxides.

9.1 Introduction

The elucidation of the mechanism of lactide polymerisation in the presence of single-site metal catalysts allows for a deeper understanding of the reaction parameters and therefore supports the development of new initiators with optimised features.
Since the guanidine-pyridine zinc complexes **6c** and **7c** are the most auspicious candidates as initiators for lactide polymerisation, their polymerisation reactions as well as their obtained polymers were investigated to collect information in regard to their mechanism. With these findings a mechanism is proposed and evaluated by DFT calculations.

9.2 Results and discussion

9.2.1 Experimental Studies

Kinetic studies on the bulk polymerisation

In order to determine the kinetics of the solvent free ring-opening polymerisation of lactide mediated by **6c** and **7c**, homogenised samples of a mixture of D,L-lactide and the initiator (0.02mol%) were heated at 150°C. After the respective reaction time, the polymer melt was dissolved in dichloromethane. From this solution samples were taken, dried in vacuo and

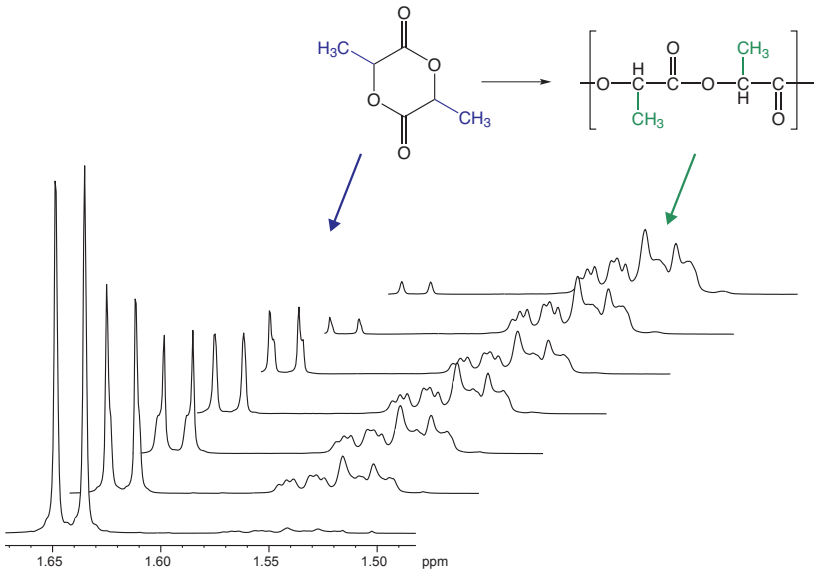

Figure 9.1: Reaction monitoring by ^{1}H NMR measurements in the case of **6c**.

used for the determination of conversion by NMR spectroscopy and of the molecular weights as well as their distribution by GPC. Figure 9.1 depicts the reaction monitoring by ^{1}H NMR measurements.

The kinetic studies (Fig. 9.2) demonstrate that the reaction mediated by **6c** proceeds up to 80% conversion within the first 8 h, but complete conversion is only obtained after 24 h. The reaction mediated by **7c** is significantly faster with 95% conversion achieved within the first 4 h. These findings clearly demonstrate that **7c** provides a higher catalytic activity in the ROP of lactide than **6c** and support those indications found for the polymerisation of glycolide and ε-caprolactone (see Section 6.5).

Logarithmic plotting of the kinetic data (Fig. 9.3) revealed that the reaction proceeds in a controlled manner.[189,190] The linear dependence of $\ln(B)$ with conversion C and time t that shows the polymerisation obeys first-order kinetics is given by

$$\ln B = \ln\left(\frac{1}{1-C}\right) = k_p[I]_0 t.$$

The linearity of the plots indicates that there is no termination reaction or that the number of growing chains is constant throughout polymerisation.[190] With regard to polydispersities around 2, transesterification reactions seem to occur in the course of the reaction which broadens the distribution after the first polymerisation steps. Nevertheless, theses reactions can be regarded as living polymerisations according to a definition given by Penczek et al.:[189] "Living polymerization takes place when a given set of macromolecules, born at initiation, retain their

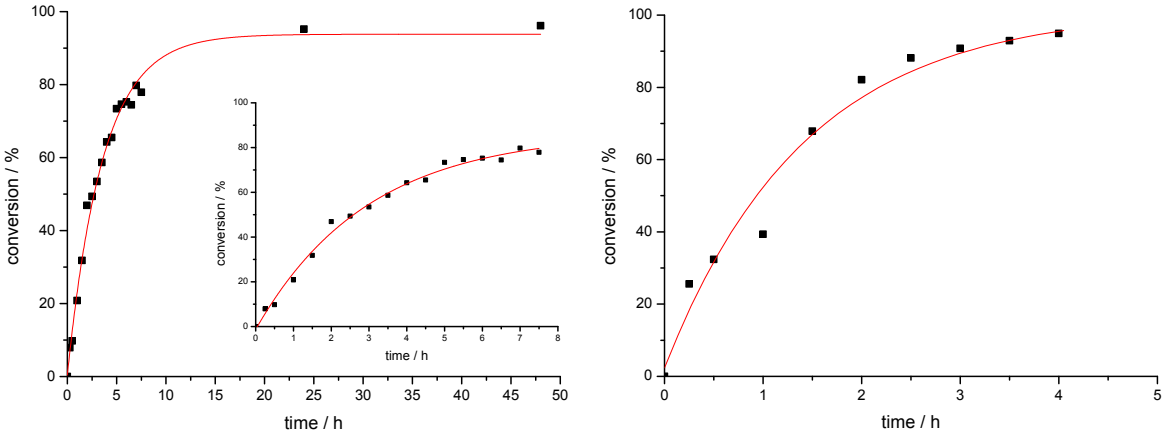

Figure 9.2: Dependence of lactide conversion vs. time for **6c** (l) and **7c** (r) at 150°C.

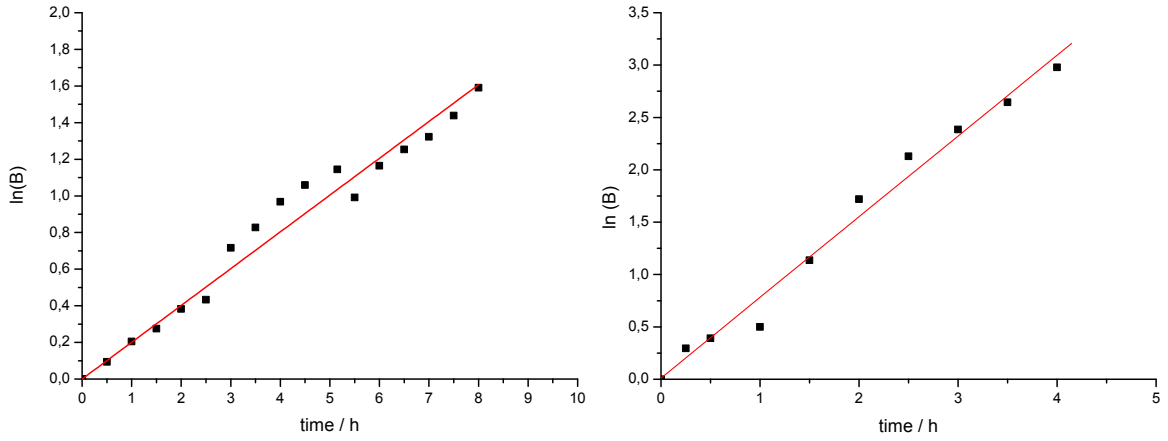

Figure 9.3: Dependence of ln(B) vs. time for **6c** (l) and **7c** (r) at 150°C.

activity at least to the complete monomer conversion for the reason that irreversible deactivation (termination) and irreversible transfer (so called degenerative) are absent. Polymerization of cyclic esters is very often called living. This is justified whenever deactivation and transfer are reversible."

Ring-opening reactions mediated by **6c** and **7c** are performed in a controlled manner without the presence of alkoxides or alcohols. Thus, the highly basic guanidine function is proposed to take the role as nucleophilic reagent and to open the lactide molecule during a coordination-insertion mechanism.

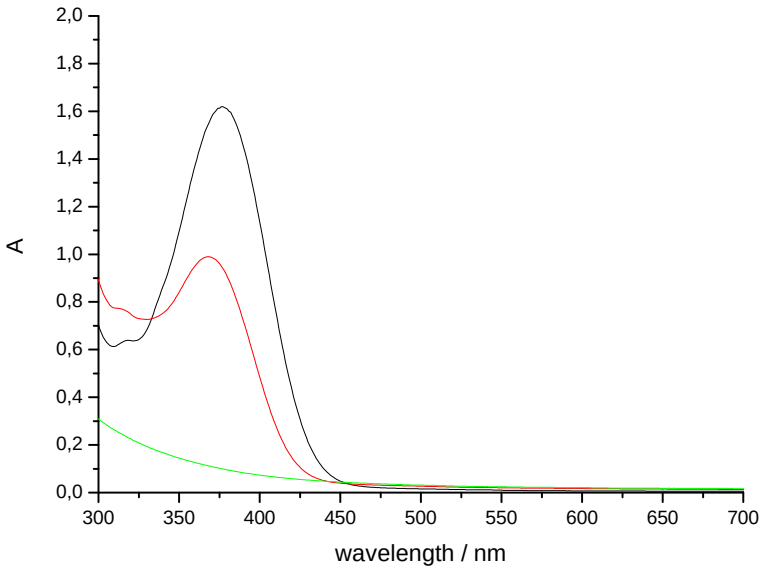

Figure 9.4: UV/Vis absorption of PLA samples obtained with **6c** (black line), **7c** (red line) and $SnOct_2$ (green line).

UV/Vis absorption studies of the polylactide

An intriguing feature of the obtained polylactide samples is their slightly yellowish colour. They show absorption features in the UV range which are not present in samples produced using $SnOct_2$ (Figure 9.4).
The guanidine ligands themselves have intense absorptions at 347 (8800 $Lmol^{-1}cm^{-1}$) and 371 (1320 $Lmol^{-1}cm^{-1}$) nm for DMEGqu and TMGqu, respectively.[121] This π-$\pi^\star$ transition of the aromatic quinoline system can be found in the polymer samples as well. In samples polymerised with **6c**, the absorption of DMEGqu appears at 377 nm, whereas the absorption of TMGqu in samples polymerised with **7c** appears at 368 nm. Remarkably, the distinct intensity difference of the two ligands shows up in the UV absorption spectra of the corresponding polymer samples as well.
This effect is a hint that the guanidine ligand of the initiating complex (or a derivate of it) remains in the polymer, possibly attached to the polymer chain ends.

EDX measurements

The results of the UV/Vis measurements led to the conclusion that parts of the complexes remain in the polymer samples. By means of energy dispersive X-ray spectroscopy, it can be traced if zinc from residual zinc or zinc complexes remains in the polymer. Measurements at an acceleration voltage of 15 keV on 2 mm thick polymer samples gave within the limit of detection (10^{10} atoms in 1000 μm^3) no zinc signal.

Hence, it is assumed that only the guanidine ligands remain in the polymer and the zinc is washed out during the work-up process.

Fluorescence studies of the polylactide

Guided by the UV absorption of the PLA samples, fluorescence measurements of the guanidine ligands and the PLA samples were performed (Figure 9.5). With the same trend as found for the UV absorption, the fluorescence signals of the ligands show up at 500 (DMEGqu) and 510 nm (TMGqu). Notably, the DMEGqu ligand has the double fluorescence intensity compared to TMGqu. This intensity difference can be retrieved in the fluorescence of the solid-state emission spectra of the PLA samples as well: the samples produced by using DMEGqu complex (PLA-**6c**) emit with double intensity compared to the TMGqu samples (PLA-**7c**). The emission wavelength is slightly blue-shifted to 491 (DMEGqu) and 486 nm (TMGqu).
Due to the PLA production process, the ligand might be precipitated accidentally with the PLA. In order to clarify this question, a PLA sample was worked up in several cycles of dissolution in dichloromethane and precipitation in ethanol. After each step the polymer was dried and samples for the fluorescence measurements were taken. Figure 9.7 depicts the course of the integral fluorescence intensities for this series of samples. Within the limit of accuracy, the fluorescence remains maintained over six cycles. A small amount of ligand seems to be washed out, but 80 % of the original intensity remains even after six cycles. This can be regarded as a

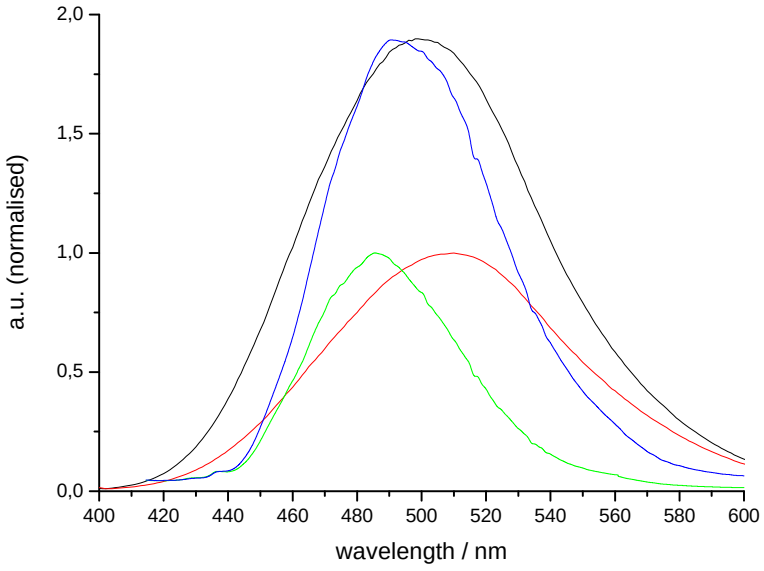

Figure 9.5: Fluorescence of the guanidine ligands (in MeCN, c = 10^{-5} mol/L) and the corresponding PLA samples (0.095 μm) (black line: **6**; red line: **7**; blue line: PLA-**6c**; green line: PLA-**7c**).

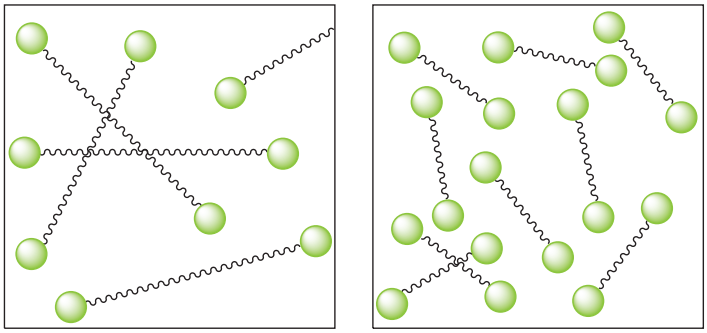

Figure 9.6: Schematic depiction of the fluorophore density of polymer samples in dependence of chain length.

proof that the guanidine ligand is chemically bound to the polymer and after polymerisation remains as end group.
As an additional experiment to support the "end group" hypothesis the fluorescence intensity of samples with different molecular weight was investigated. If the fluorescent part remains at the chain end, longer chains show less fluorescence intensity per mass unit compared to those with shorter chains (Fig. 9.6).
Figure 9.8 illustrates the measured dependence of the fluorescence intensity on the chain length: the polymer sample with the chain length of 260,000 g/mol shows the smallest normalised intensity whereas the polymer sample with a chain length of 36,000 g/mol shows the highest fluorescence intensity. The sample with app. six times longer chains has an integral intensity which is six times smaller. This inverse relation shows again that the ligands act as end groups.

Racemisation behaviour

In Section 6.5, it was demonstrated that the polymerisation of pure D- and L-lactide mediated by **6c** and **7c** at 150°C provides the formation of isotactic PLA. Undesired racemisation leading to atactic polymers as it is reported for anionic and cationic polymerisation reactions[19,80] was not observed. The lack of racemisation at higher temperatures supports the proceeding via a coordination-insertion mechanism.

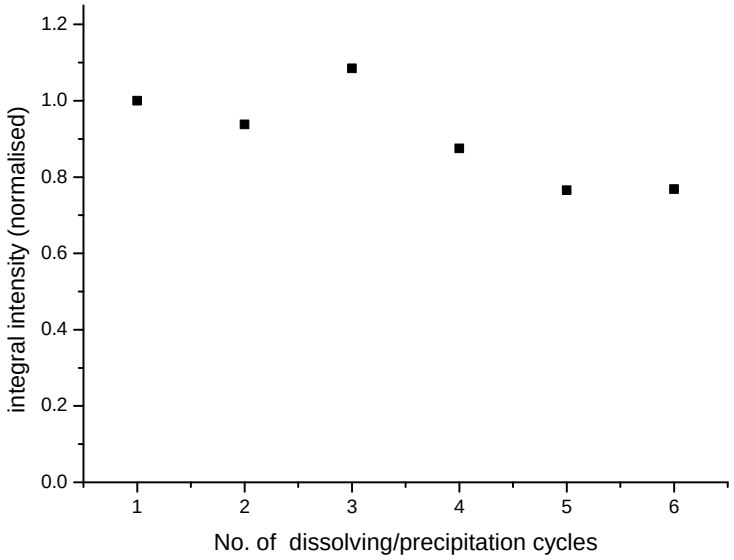

Figure 9.7: Tracing of the fluorescence upon dissolving and precipitating.

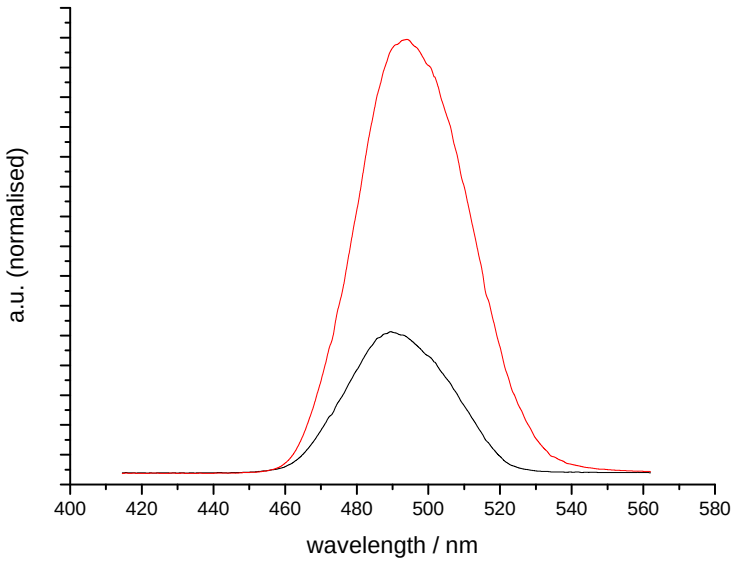

Figure 9.8: Fluorescence spectra for the PLA-**6c** samples with M_w of 260,000 (black line) and 36,000 g/mol (red line).

Discussion

The experimental studies revealed several points indicating that for the guanidine-pyridine zinc systems a special variant of the coordination-insertion mechanism is active:

- The progress of the polymerisation conversion obeys first-order kinetics.
- UV spectra of the polymers trace an intense absorption originating from residual guanidine ligand.
- EDX spectroscopy shows that no zinc remains in the polymer within the limit of detection.
- The polymer samples show intense fluorescence and the fluorescence spectra of samples of different catalysts reflect the absorption and emission intensity difference of the guanidine ligands very well.
- Further fluorescence experiments demonstrate that the guanidine ligand cannot be washed out during the work-up of the polymer samples and that the fluorescence intensity is reciprocally related to the chain length.
- Furthermore, no racemisation occurs during the polymerisation of pure D- and L-lactide which is a hint that the reaction does not exhibit an anionic or cationic mechanism but proceeds via a coordination-insertion mechanism.

9.2.2 Theoretical studies

Proposed mechanism

Guided by the idea that the basic guanidine is able to open the lactide ring nucleophilically, the following mechanistic model was developed according to the general coordination-insertions mechanism (Figure 9.9). In the first step, the lactide replaces the triflate ion and coordinates via one of the carbonyl oxygen atoms ($O_{Carbonyl}$) to the zinc centre (**M1**) resulting in transition state **M2 TS**. The guanidine N atom (N_{Gua}) transfers electron density to the carbonyl C atom ($C_{Carbonyl}$) on the reverse side of the lactide molecule leading to the formation of a bond (nucleophilic attack). Simultaneously, the $C_{Carbonyl}$-$O_{Alkoxide}$ bond in the lactide molecule breaks. By reorientation of the opened lactide molecule, the currently formed alcoholate anion is able to coordinate to the zinc centre (**M3**). During further reorganisation steps, the N-donor atoms of the ligand are released from the zinc atom and remain at the end of the new-built chain (**M4**).
The chain propagation proceeds by the coordination of a further lactide molecule to the zinc centre of this new species. In contrast to the first ring-opening step, the next lactide molecule is opened by the coordinated alcoholate anion of the growing chain. Instead of a $C_{Carbonyl}$-N_{Gua} bond a $C_{Carbonyl}$-$O_{Alkoxide}$ bond is tied.

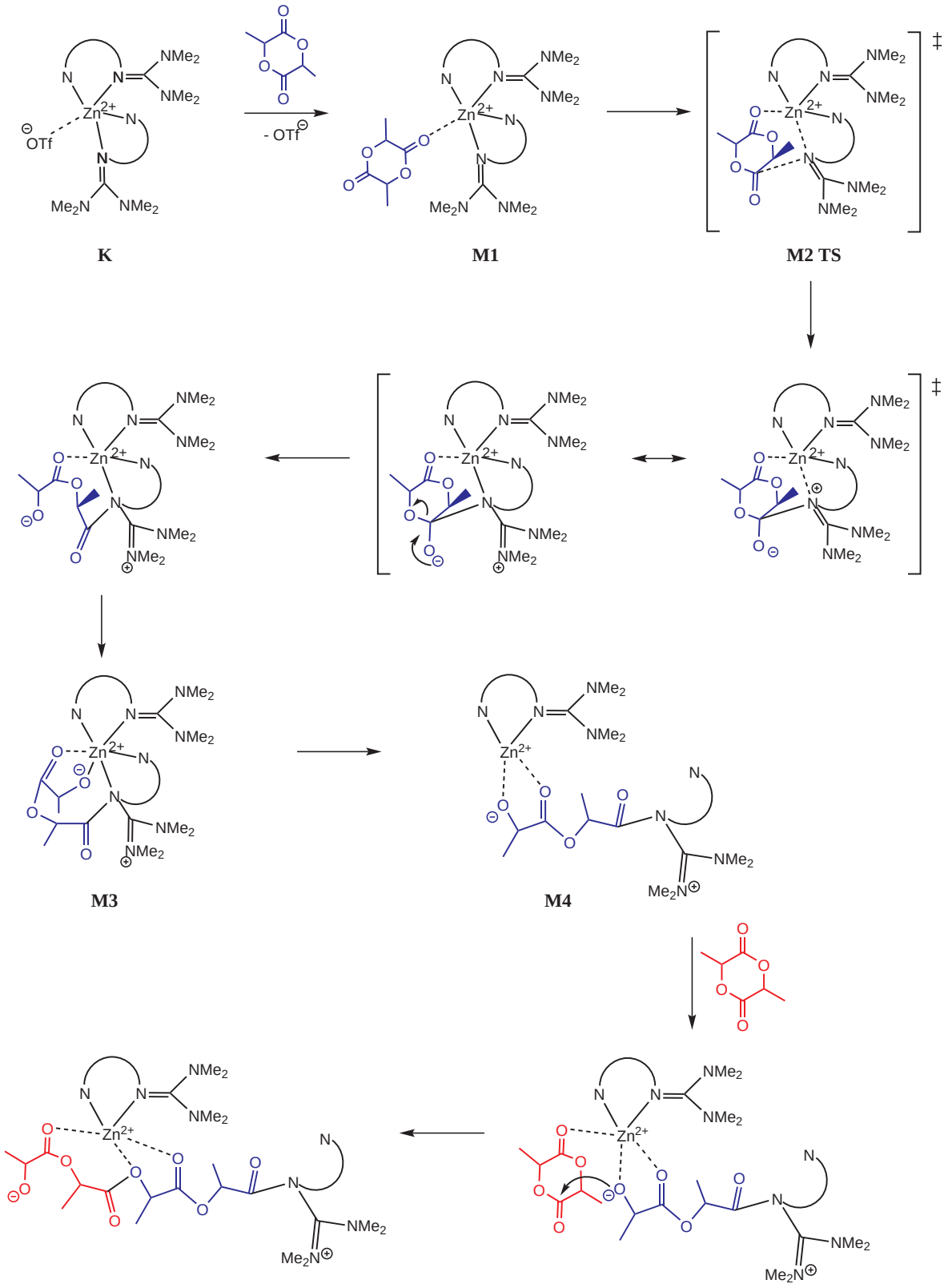

Figure 9.9: Proposed DFT based mechanism for the ROP of lactide.

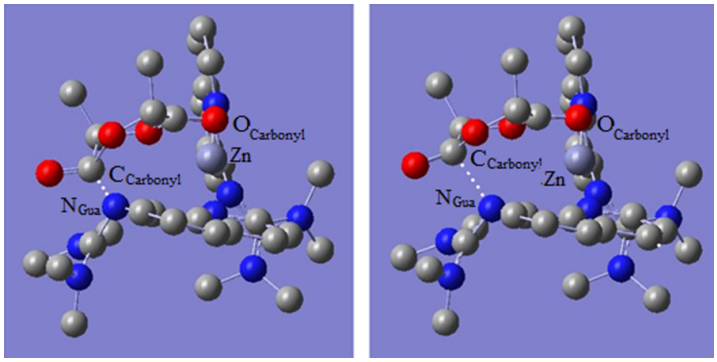

Figure 9.10: Vibration of the calculated transition state **M2 TS** with negative frequency.

Mechanistic calculations

As demonstrated in previous studies (Chapter 6), gas phase DFT calculations using the B3LYP density functional theory and the 6-31G(d) basis sets are able to describe guandine zinc complexes reasonably. For computational work on the ring-opening polymerisation,[191] this combination of functional and basis set was chosen as well.[37,38,192,193] The starting point of the mechanistic calculations (**M1**) was obtained by substitution of a triflate ion in complex **7c** by a lactide molecule (built up in GaussView).
On the basis of Synchronous Transit-Guided Quasi-Newton (STQN) calculations[147] the transition state was searched. Finally, the state **M2 TS** was found which possesses only one negative frequency which is characteristic for a transition state. This vibration at -61.2 cm^{-1} is a stretching vibration between the $C_{Carbonyl}$ and N_{Gua} atoms whereby the $C_{Carbonyl}$-$O_{Alkoxide}$ distance is simultaneously changed (Figure 9.10). During this vibration a rehybridisation of the $C_{Carbonyl}$ atoms from sp^2 to sp^3 can be observed.
In order to study the crucial transition state **M2 TS**, the dependence of the $C_{Carbonyl}$-N_{Gua} distance on the length of the adjacent $C_{Carbonyl}$-$O_{Alkoxide}$ lactide bond is investigated by DFT calculations (Figure 9.11 and 9.12). In a grid search, the distance between $C_{Carbonyl}$ and N_{Gua} is reduced stepwise and the structure of the transition state is optimised for each case. This analysis showed that the $C_{Carbonyl}$-$O_{Alkoxide}$ bond length increases to the same extent at which the $C_{Carbonyl}$ and the N_{Gua} atoms approach each other. Hence, the nucleophilic ring-opening is

Table 9.1: Atom distances (in Å) of the calculated transition state **M2 TS** in comparison.

	Zn-$O_{Carb.}$	$C_{Carb.}$-N_{Gua}	$C_{Carb.}$-$O_{Alkoxide}$	$C_{Carb.}$-$O_{Carb.}$
given educt structure	2.16	1.70	1.46	1.24
given product structure	2.09	1.43	1.55	1.27
after lactide insertion (**M4**)	-	1.43	-	1.21
free lactide	-	-	1.34	1.20
calculated transition state (**M2 TS**)	2.11	1.71	1.51	1.24

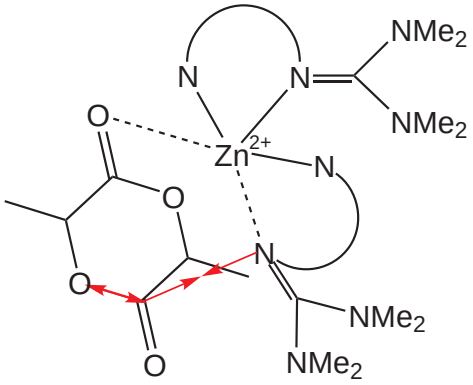

Figure 9.11: Variation of the $C_{Carbonyl}$-N_{Gua}-bond length.

a result of the $C_{Carbonyl}$-N_{Gua} bond formation. Furthermore, it can be observed that the N_{Gua} atom of the lactide bonding ligand withdraws from the zinc centre the shorter the $C_{Carbonyl}$-N_{Gua} distance becomes.

In Table 9.1 geometric key parameters of the given and calculated geometries are summarised in comparison to the parameters of the free lactide molecule and the end state **M4** of the first insertion step. The $C_{Carbonyl}$-N_{Gua} distance is with 1.71 Å significantly longer than in a covalent bond (1.43 Å after lactide insertion) and the $C_{Carbonyl}$-$O_{Alkoxide}$ distance in the lactide molecule is with 1.51 Å considerably longer than in the free lactide (1.34 Å[194]) which is due to the fact that this bond is currently broken. In **M2 TS** the guanidine group of the lactide binding ligand

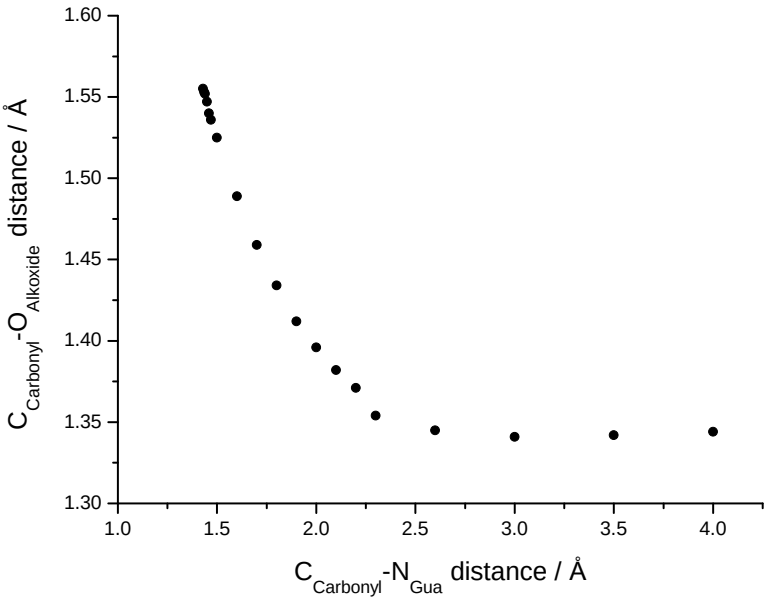

Figure 9.12: $C_{Carbonyl}$-$O_{Alkoxide}$-distances upon variation of the $C_{Carbonyl}$-N_{Gua}-distance.

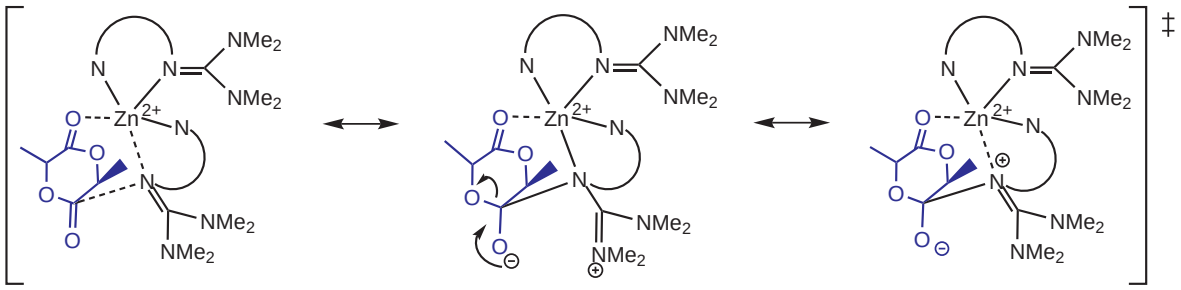

Figure 9.13: Mesomeric forms of the transition state **M2 TS**.

coordinates no longer the zinc atom (Zn-N_{Gua}: 3.82 Å). In the transition state, the $C_{Carbonyl}$-$O_{Carbonyl}$-distance is longer than in the free lactide or in the end state **M4**. This is a hint that in the transition state a partial single bond is formed between these two atoms which is in accordance with the rehybridisation of the $C_{Carbonyl}$ atom (Figure 9.13).

In summary, the first ring-opening step mediated by guanidine-pyridine zinc systems can be theoretically described by the energy profile depicted in Figure 9.14. The energy level increases after lactide coordination due to the approaching of $C_{Carbonyl}$ and N_{Gua} resulting in the transition state **M2 TS** on the highest energy level. After ring-opening, the energy decreases by coordination and reorientation of the opened lactide chain to the energy level of the final state. The first insertion step is overall endothermic (ΔH = +13.8 kcal/mol).

The energy level of the transitions state **M2 TS** with a value of ΔE(**M2 TS**) = 86.5 kcal/mol seems to be comparatively high for an actual proceeding reaction - even at 150°C.

This result is in accordance with experimental findings concerning the molecular weight of the obtained polymers (Section 6.1). It was found that the experimental M_w values for PLA-**6c** and PLA-**7c** are significantly higher than the theoretical values. This provides the thesis that the initiation rate is slower than the propagation rate so that only a fraction of the used complexes actually initiate the ROP.

With regard to literature values, it has to be taken into account that the DFT calculations were performed in the gas phase. Ling et al.[192] report a value of 30 kcal/mol for their ring-opening transition state and they mention a high dependence of this value for the present state of solvation (+/- 10 kcal/mol between gas phase, THF, other solvents). As charged species play an important role in the reaction, the solvation of these species can facilitate such a reaction and hence lower the activation energy barrier.

At this point in time, this value has to be treated carefully until calculations in an appropriate solvent have been done.

Preliminary calculations of the insertion of the second lactide show that the second insertion proceeds exothermic. This is also supported by the mechanism proposed by Rzepa et al.[37]

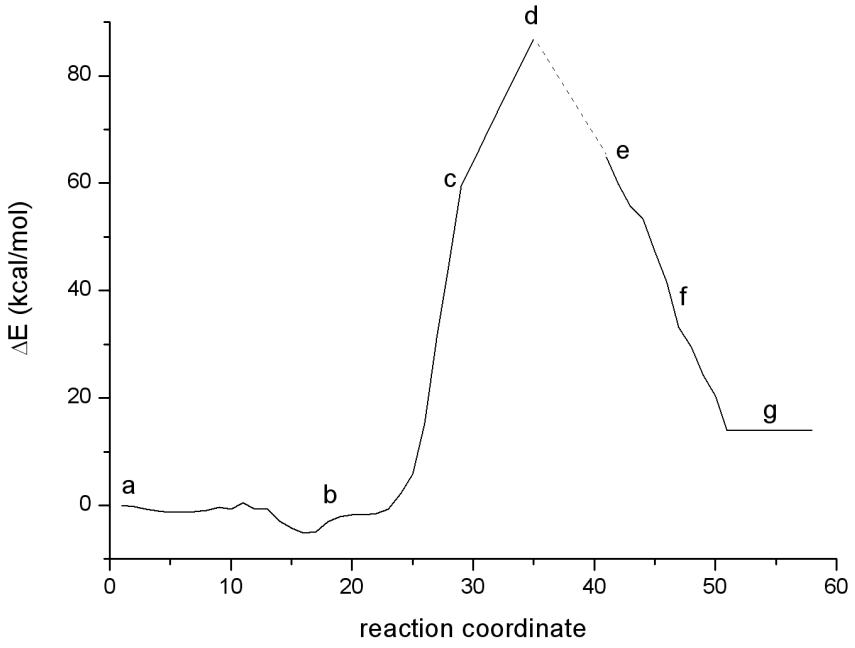

Figure 9.14: Energy profile of the first lactide insertion step with **7c**: a) Lactide and complex **7c** reside at a long distance ($O_{Carbonyl}$-Zn = 6.3 Å); b) Lactide coordinates to the zinc centre (**M1**); c) $C_{Carbonyl}$ atom approaches to the N_{Gua} atom under weakening of the $C_{Carbonyl}$-$O_{Alkoxide}$ bond.; d) Transition state (**M2 TS**); e) $O_{Alkoxide}$ atom binds to the zinc centre (**M3**); f) Unfolding of the opened lactide chain; g) Final state after the first insertion step (**M4**).

9.3 Conclusion

Experimental and theoretical studies were done to gain inside into the mechanism of lactide polymerisation mediated by the guanidine-pyridine zinc complexes $[Zn(DMEGqu)_2(CF_3SO_3)][CF_3SO_3]$ (**6c**) and $[Zn(TMGqu)_2(CF_3SO_3)][CF_3SO_3]$ (**7c**). Kinetic studies demonstrated that the reaction obeys first order kinetics and proceeds in a controlled manner with living character. After EDX investigation proved that the polymer samples do not contain zinc, the UV/Vis and fluorescence measurements indicated that the ligand binds to the polymer and remains as chain end. This together with the absence of racemisation reactions during the polymerisation of pure D- and L-lactide leads to the assumption that the polymerisation proceeds via a coordination-insertion mechanism. The guanidine functions of the coordinated ligand act as nucleophile and support the ring-opening. Hence, they allow the ROP without additional co-catalysts like alcohols or alkoxides. The proposed mechanism was supported by DFT studies. The crucial transition state **M2 TS** was found on the basis of Synchronous Transit-Guided Quasi-Newton calculations and analysed. An energy profile of the first lactide insertion step was provided which demonstrated that this step is with ΔH = +13.8 kcal/mol overall endothermic. But preliminary calculations of the insertion of the second lactide showed that the second insertion proceeds exothermic. These findings are in accordance with previous calculations of Rzepa et al. and the experimental findings.

10 Conclusion and perspective

The main focus of this thesis is the introduction of a new application-oriented catalyst class into the field of the ring-opening polymerisation of cyclic esters. The discovery of influencing variables resulting in a structure-reactivity relationship and the elucidation of the polymerisation mechanism represent the key challenges.

To create zinc complexes providing high robustness combined with high catalytic activity, in this work neutral multidentate chelate ligands with N-donor functions are used.
Aliphatic bisguanidine-stabilised zinc complexes were proven to be active initiators in the ring-opening polymerisation of D,L-lactide. PLAs with molecular masses (M_w) of around 18,000-59,000 g/mol could be obtained. In complexes with the same ligand the activity of the initiator depends on the anionic component of the zinc salt. Complexes with zinc triflate and zinc dichloride seem to be the most auspicious candidates for application in the ROP of lactide. The catalytic activity of complexes including the same anionic component of the zinc salt increases from btmgp via $DMEG_2$e to TMG_2e.
By changing the reaction temperature it was shown that lower temperatures allow side reactions to be avoided. Moreover, the Mark-Houwink correlation demonstrates that the obtained polymers are linear and homogeneous.
The first examples of imidazoline based guanidine zinc complexes **5a** and **5b** were synthesised, completely characterised and investigated for their activity in the solvent-free ROP of lactide. It was shown that these compounds are able to act as efficient initiators. A comparative DFT study on **5a** and **5b** and their guanidine counterparts **1a** and **1b** revealed that the two complex series possess a strikingly similar electronic structure. Although the imidazoline based guanidine is more basic, its zinc complexes have only a slightly higher positive charge on the zinc atom in comparison to the corresponding imidazolidine complexes. Accordingly, their activity in the initiation of the ring-opening polymerisation is increased which is directly related to the Lewis acidity of the zinc atom. Hence, the strategy of using neutral, strongly nucleophilic ligand systems for the stabilisation of catalytically active and environmentally benign zinc complexes has been positively evaluated.
These findings lead to two mechanistic evidences: (a) enhanced Lewis acidity of the zinc centre directly correlates with the enhanced polymerisation activity and (b) by using exclusively neutral N-donor ligands for the stabilisation of the catalysts, it is proven that anionic (co-)ligands

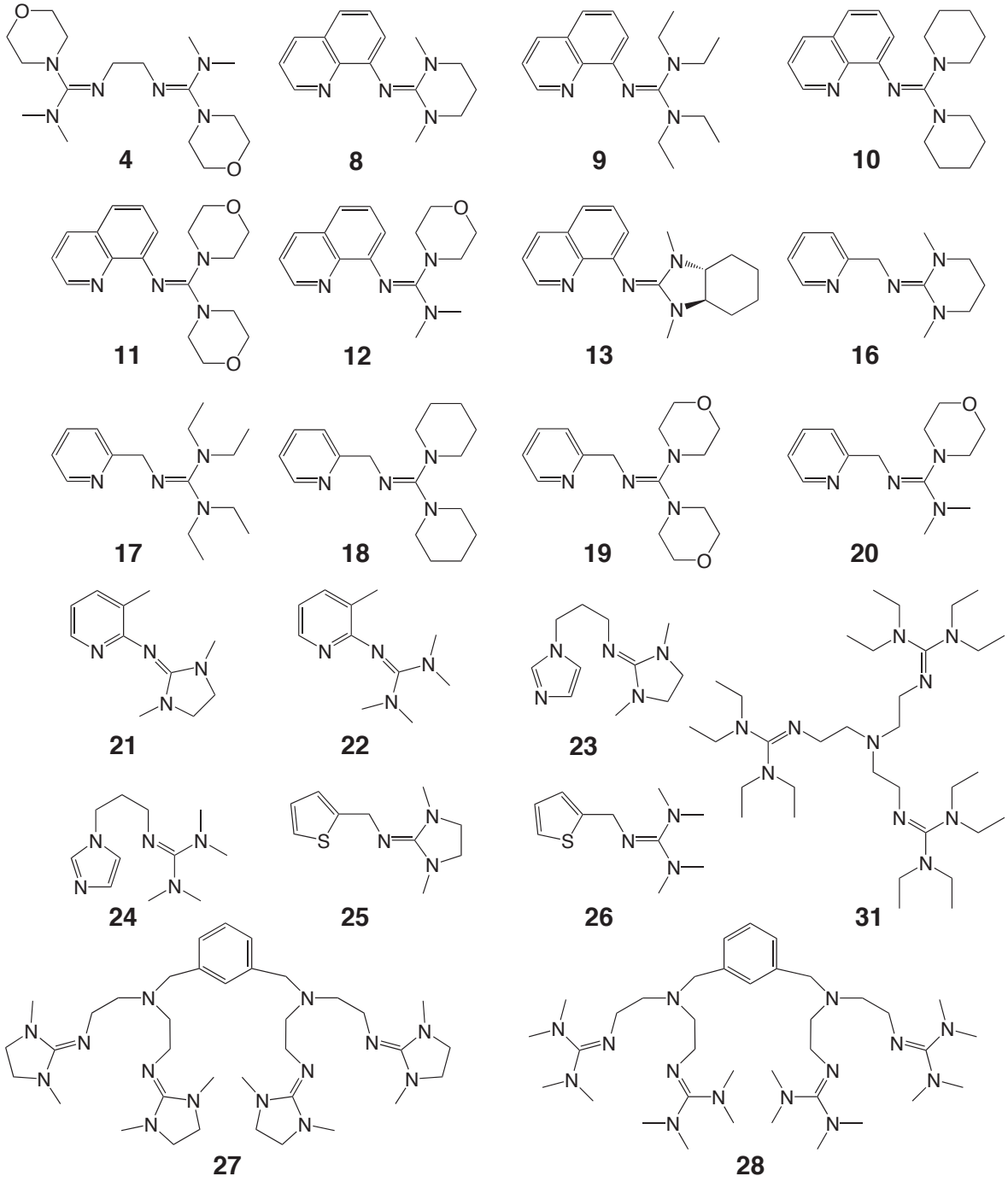

Figure 10.1: Schematic summary of the synthesised guanidine ligands.

are not necessary prerequisites for the nucleophilic lactide-opening step.
A library of zinc complexes stabilised by guanidine-pyridine ligands was developed and the complexes were screened towards their activity. They proved to be active initiators in the polymerisation of lactide with only few exceptions. Polylactides with molecular weights (M_w) up to 176,000 g/mol and in almost quantitative yields could be obtained. These results represent a significant augmentation over bisguanidine zinc complexes and corroborate the strategy of building up N-donor ligands with different donor strengths and substituents with varied sterical demand.
In complexes with the same ligand, the anionic component of the zinc salt has a significant impact on the activity of the corresponding initiator. It defines the molecular structure, the charge distribution and the thermal stability of the complex and therefore its properties. The charge distribution within the complex (especially the positive charge on the zinc atom) influences the attraction towards the substrate lactide and the accessibility to the zinc centre regulates the substrate coordination. Consequently, the reactivity of the complexes is directly correlated to the coordination behaviour of the anionic component and the anion effect plays an important role in context of catalyst design. A clear trend concerning the guanidine impact on the catalytic activity could not be observed under the given conditions. Similarly, the influence of the guanidine moiety on the grade of heterotactic enchainment cannot be clarified due to the very low overall effect.
Guanidine-pyridine zinc complexes including zinc triflate were proven to be excellent catalysts in ROP of lactide. The flexible coordination of one triflate anion to the zinc centre is considered responsible for their outstanding activity. It facilitates pre-coordination of the lactide molecule, while the higher positive charge at the zinc centre in comparison to the tetrahedral complexes offers higher Lewis acidity for the activation of lactide. This argument was supported by studies on the corresponding complexes with zinc mesylate.
In addition, it was demonstrated that the triflate complexes are also suited for the general application in the polymerisation of cyclic esters like D-lactide, L-lactide, glycolide and ε-caprolactone and therefore possess also high potential for the copolymerisation of lactide.
Rather simple aliphatic and aromatic diamines as well as oxabispidines were also found to provide catalytic active zinc complexes. Hence, this ligand class was proven to be well suited to develop initiators for the ROP of lactide. They combine the advantageous properties of a simple assembly, low cost production and high activity. However, the stereogenic information in complexes with the chiral ligands **37**, **38** and **39** is not able to control the tacticity of the resultant PLA under the chosen conditions. It seems that the impact on the polymer microstructure is higher for steric demanding ligands.
Experimental and theoretical studies were performed to gain inside into the mechanism of lactide polymerisation mediated by the guanidine-pyridine zinc triflate complexes **6c** and **7c**. Kinetic studies demonstrated that the reaction obeys first order kinetics and proceeds in a controlled manner with living character. EDX, UV/Vis and fluorescence measurements indicated that the ligand or a part of it binds to the polymer and remains as chain end. This together with

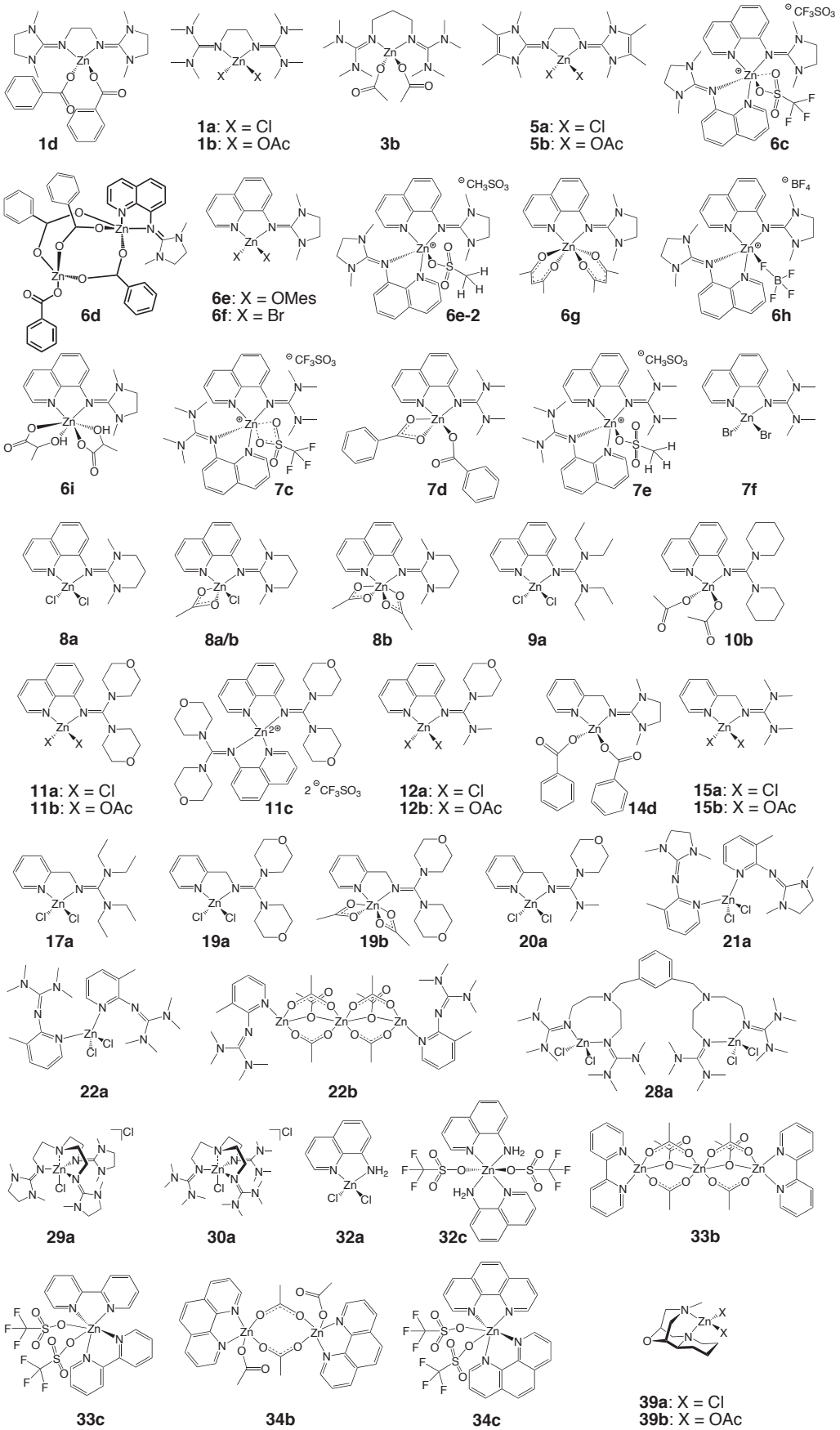

Figure 10.2: Schematic summary of the synthesised zinc complexes.

the absence of racemisation reactions during the polymerisation of pure D- and L-lactide leads to the assumption that the polymerisation proceeds via a coordination-insertion mechanism. The guanidine functions of the coordinated ligand act as nucleophile and support the ring-opening. Hence, they allow the ROP without additional co-catalysts like alcohols or alkoxides. The proposed mechanism was supported by DFT studies. The crucial transition state **M2 TS** was found and analysed and an energy profile of the first lactide insertion step was provided which demonstrated that this step is overall endothermic. Preliminary calculations of the insertion of the second lactide showed that the second insertion proceeds exothermic.

In summary, a library of zinc complexes stabilised by neutral N-donor ligands was generated consisting of 67 complexes prepared of 29 varying ligands and 9 different zinc salts. 49 zinc complexes (Fig. 10.2) and 21 ligands (Fig. 10.1) were prepared and completely characterised for the first time. This complex variety enables the systematic screening of each complex for its catalytic activity in the solvent-free ring-opening polymerisation of lactide.
It was proven that the neutral ligand classes including bisguanidines, guanidine-amine hybrids, imidazolin-2-imines and simple amines are qualified to stabilise highly active zinc complexes. The most auspicious initiators were guanidine-pyridine zinc triflate complexes which combine excellent catalytic activity with high robustness towards air, moisture and small impurities in the monomer as well as thermal stability. They do not need co-catalysts like alkoxides or alcohols to give via a coordination-insertion mechanism PLAs with high molecular masses under industrially attractive conditions. They are also able to polymerise glycolide and ε-caprolactone and thus provide a wide range of application.

A perspective of further investigations is the large-scale application of guanidine-pyridine based zinc catalysts to prove their industrial qualification and the broadening of their application range. Therefore, the screening of the library of zinc complexes towards their catalytic activity in the ring-opening polymerisation of further monomers like 1,5-dioxepan-2-one, propylene oxide, β-butyrolactone and substituted lactides (e.g. hexylglycolide) or in related polymer reactions like the copolymerisation of carbon dioxide and expoxides to obtain polycarbonates is of great importance. Since guanidine-pyridine zinc complexes were proven to initiate the polymerisation of lactide as well as glycolide and ε-caprolactone the copolymerisation of these cyclic esters can be topic of onward studies. A further challenge of great interest is the development of highly stereoselective catalysts for the ring-opening polymerisation of D,L-lactide as well as the preparation of initiator systems based on guanidine-pyridine ligands and different metals like magnesium or aluminum.

Thus, the introduction of three neutral ligand classes into the field of single site metal catalysts for the polymerisation of cyclic esters, that provide active but stable initiators, opens up a new promising area of research.

11 Experimental section

11.1 Material and methods

11.1.1 General remarks

All manipulations were performed under pure dinitrogen (99.996%) or argon (99.996%) dried with P_4O_{10} granulate using Schlenk techniques or a glovebox. Solvents were dried and purified according to literature procedures[195] and also kept under inert gas. Unless otherwise noted, chemicals were purchased at common trade companies and used as purchased. Yields of the synthesised products are given from the pure isolated products. In most instances the reaction conditions as well as the yields were not optimised.

11.1.2 Physical measurements

NMR spectroscopy

The NMR spectra were recorded with the spectrometer Bruker Avance 500. The NMR signals were calibrated to the residual signals of the deuterated solvents (δ_H ($CDCl_3$) = 7.26 ppm, $\delta_H(CD_3CN)$ = 1.94 ppm, $\delta_H((CD_3)_2SO)$ = 2.50 ppm). The allocation of signals of ^{1}H- and ^{13}C-NMR spectra were supported by H,H COSY, DEPT135 and HMQC experiments. The results are implemented in the corresponding data. The chemical drift is given in ppm oriented to the δ-scale. Spin-spin coupling constants (^nJ) are given in hertz (Hz), where n is the bond number between the coupling cores. The multiplicities and signal forms are described with the following abbreviations s = singlet, d = doublet, t = triplet, q = quartet, dd = double doublet, m = multiplet, br = broad signal. The DPFGSE-NOE spectra[196] were recorded with a mixing time of 0.5 s and Gaussian-shaped pulses for selective excitation. The temperature ranged from 0 to -90 °C. Samples for homonuclear decoupling were prepared by dissolving 10 mg of the polymer in 1 ml of $CDCl_3$ and the samples were left for 2 hours to ensure full dissolution.[159] The ^{1}H homonuclear decoupled spectra were recorded on a Bruker Avance 400 MHz spectrometer and referenced to residual solvent peaks. The parameter P_r (probability of heterotactic enchainment) was determined via analysis of the respective integrals of the tetrads, using P_r^2 = 2 [sis]. For the NMR analysis of the respective integrals of the tetrads [sis], see the work of Coates et al.[24]

IR spectroscopy

The infrared spectra were recorded with the FT-IR spectrometer Nicolet P510.

Mass spectroscpy

The EI mass spectra were recorded at a Finnigan MAT 95 mass spectrometer with 70 eV and 200°C source temperature; the CI mass spectra were recorded at Finnigan MAT 8200 spectrometer with isobutane as reaction gas and 100°C source temperature.

Elemental analyses

The elemental analyses were performed with a Perkin-Elmer analysator type 2400 as well as with an elementar vario MICRO cube. Microanalyses of fluorine containing compounds were performed at the Mikroanalytisches Labor, Ilse Beetz, Kronach, Germany or at the Technische Universität Dortmund with the device CHNS-932 from Leco Instruments.

Fluorescence measurements

a) Fluorescence measurements of the ligands were performed on a Hitachi F-2000 (with prescan for the best response). b) The fluorescence measurements of the polymer samples were performed on the following fluorescence setup: the fluorescence light was dispersed with a Horiba Jobin Yvon spectrometer with 140 mm focal length and detected with a standard CCD detector array. Optical excitation of the polymer samples was done by a semiconductor laser source (405 nm wavelength) with a power density of 70 kW/cm^2 and a spot size of 3 μm diameter. The excitation and detection paths were aligned in confocal geometry. The polymer samples were melted at 150°C and prepared between two microscope glass plates with polymer layer thicknesses between 50 and 160 μm. For reference, the integral fluorescence intensity was calibrated as a function of the polymer thickness. For the calibration of the fluorescence measurements, two series of polymer samples with **6c** and **7c** were produced. These samples were applied between glass plates and polymer thicknesses between 40 and 160 μm were achieved by different pressure on the polymer layers between the glass plates. The thickness of the samples was controlled by a film thickness monitor. The dependence between integral fluorescence intensity and layer thickness was measured for both series and found to be linear. Further measurements with samples of different thickness were then normalised by the calibration graphs.

EDX measurements

The energy dispersive X-ray spectroscopy measurements were accomplished on a standard RönTec EDX system in a JEOL JSM-6060 scanning electron microscope. The acceleration voltage was 15 kV.

UV/Vis spectroscopy

The UV/Vis spectra were recorded with a Perkin-Elmer Lambda 45 spectrometer.

Crystal structure analyses

Crystal data for the crystal structures are presented the separate crystallographic appendix. Data were collected on a Bruker-AXS SMART[197] APEX CCD with MoKα radiation (λ = 0.71073 Å) and a graphite monochromator. Data reduction and absorption correction were performed with SAINT and SADABS.[197] The structures were solved by direct and conventional Fourier methods, and all non-hydrogen atoms refined anisotropically by full-matrix least-squares techniques based on F^2 (SHELXTL[197]). Hydrogen atoms were derived from difference Fourier maps and placed at idealised positions, riding on their parent C atoms, with isotropic displacement parameters $U_{iso}(H) = 1.2U_{eq}(C)$ and $1.5U_{eq}(C_{methyl})$. All methyl groups were allowed to rotate but not to tip. The molecular structures of **7c**, **22a** and **28a** exhibit two independent molecules per asymmetric unit each. The crystal structure of **22a** and **28a** contain highly disordered solvent molecules in the asymmetric unit whose atom positions could not be refined properly. However, treatment of data with the SQUEEZE facility of the PLATON[198,199] program resulted in the smooth refinement of the ordered part of the structure. CCDC-numbers are available for all published structures (see the appropriate tables in the appendix). They contain the supplementary crystallographic data which can be obtained free of charge from The Cambridge Crystallographic Data Centre via `www.ccdc.cam.ac.uk/data_request/cif`.

Gel permeation chromatography

To obtain Mark-Houwink constants of the PLA samples prepared by ROP with $SnOct_2$ and the zinc complexes of guanidine-pyridine hybrid ligands, GPC measurements were performed on a Waters GPC 2000 instrument equipped with a precolumn (10 mm) and a combination of three PSS SDV columns (10^6, 10^5, 10^3 Å). The detection system included an integrated refractive index (RI) detector and an integrated viscosity detector H502B (Viscotek). All measurements were performed at 35 °C with THF as eluent. The flow rate was 1 $mLmin^{-1}$. Sample concentrations were 2-3 gL^{-1}. Molecular weight analysis was based on a universal calibration, carried out with polystyrene standards (Polymer Standard Service) in THF at 35 °C. Use of the universal calibration gave absolute values for the molecular weight, which are discussed as weight-average molar mass values M_w and as the polydispersity index ($PD = M_w/M_n$ where M_n is the number-average molar mass) which describes the width of the molecular weight distribution. The data are summarised in Table A.7 (see Appendix). The whole series of polymers was investigated with a different GPC setup: A combination of PSS SDV columns with porosities of 10^5 and 10^3 Å was used together with a HPLC pump (L6200, Merck Hitachi) and a refractive index detector (Smartline RI Detector 2300, Knauer). THF was used as mobile phase at a flow rate of 1 $mLmin^{-1}$. The instrument was calibrated with standard polystyrene samples, for which the following Mark-Houwink constants could be taken from literature (K_{PS} = 0.011 mLg^{-1},

α_{PS} = 0.725).[200] Hence, the obtained values for the molecular weight and molecular weight distribution are polystyrene-analogous. To obtain absolute values for PLA amples, K_{PLA} = 0.053 mLg^{-1}, α_{PLA} = 0.610 were chosen from Table A.7 (see Appendix) as representative Mark-Houwink constants for PLA. Combination of these two sets of data enables equalisation[128] of the hydrodynamically effective volumes of PS and PLA, $V_{h,PS}$ and $V_{h,PLA}$, at any elution volume according to the equation:

$$V_{h,PS} = K_{PS}M^{\alpha(PS)}M = K_{PS}M^{\alpha(PS)+1} = V_{h,PLA} = K_{PLA}M^{\alpha(PLA)+1}$$

The molecular weight and molecular weight distribution of D-PLA and L-PLA samples were determined by a GPC setup using chloroform as mobile phase at a flow rate of 1 mLmin^{-1}. A combination of PSS SDV columns with porosities of 10^6, 10^5 and 10^3 Å was used together with a HPLC pump (880-PU, Jasco) and a refractive index detector (RI Detector 2410, Waters). The instrument was calibrated with standard poly(methyl methacrylate) samples and universal calibration was applied by the application of Mark-Houwink constants taken from literature (K_{PMMA} = 0.005 mLg^{-1}, α_{PMMA} = 0.800; K_{PLA} = 0.022 mLg^{-1}, α_{PLA} = 0.810).[184,200]

11.1.3 Computational details

Density functional theory (DFT) calculations were performed with the program suite Gaussian 03.[142] The geometries of the complexes and ligands were optimised by using the B3LYP[138–140] hybrid DFT functional and the 6-31g(d) and 6-31g+(d) basis sets implemented in Gaussian on all atoms. In special cases (marked in the corresponding chapters), other functionals or basis sets were used. Tight conversion criteria were applied. The starting geometries of complexes were generated from their crystal structures, whereas the starting geometries of ligands were derived from their optimised complexes. Frequency calculations confirmed the stationary points to be minima. Electronic energies for gas-phase optimised structures were computed by using the BLYP functional and a 6-311g(d) basis set on the Zn, O and N atoms and a 6-31g(d) basis set on the remaining atoms. The Mulliken charge of each atom was calculated by a Mulliken population analysis.

11.2 Synthesis of educt compounds

11.2.1 Preparation of zinc compounds

Dehydratation of zinc diacetate

The dehydration of zinc diacetate was done on the basis of the ortho ester method described by van Leeuwen and Groeneveld[201] for Co(II) and Ni(II) compounds. In a Schlenk flask zinc diacetate dihydrate (7.00 g, 32 mmol) and triethyl orthoformate (1,1,1-triethoxy methane, 18.90 g, 22 ml, 128 mmol) were suspended in 20 ml of dry acetonitrile. The reaction mixture was heated to 60°C for 2 hours, while stirring. After the reaction time, the solvent and the volatile

contents were evaporated under vacuum to give a white solid which was dried in vacuo at 60°C while stirring. **$Zn(CH_3COO)_2$** (M = 183.51 g/mol); Yield: 5.52 g = 30.1 mmol = 94%.

Preparation of zinc dimesylate

The preparation of zinc dimesylate was carried out according to a procedure described by Wang et. al.[202] Methanesulfonic acid (5.77 g, 3.9 ml, 60 mmol) was added dropwise to a suspension of zinc oxide (2.60 g, 32 mmol) in 20 ml of bidistilled water with stirring (exothermic reaction). The reaction mixture was heated to 100-120°C for 6 hours. The white suspension was gravitation filtered and the filtration residue was extensively washed with water. The resulting clear solution was concentrated to give a colourless solid which was washed with diethyl ether and dried at 150°C until no water could be determined by elemental analysis. Pestilation of the zinc compound could accelerate the drying process. **$Zn(CH_3SO_3)_2$** (M = 241.89 g/mol); Yield: 6.05 g = 25.0 mmol = 83%.

Preparation of zinc D,L-dilactate

The preparation of zinc D,L-dilactate was carried out according to a procedure described by Vert et. al.[69] D,L-Lactic acid (5.46 g, 4.5 ml, 60 mmol) was added dropwise to a suspension of zinc powder (2.00 g, 31 mmol) in 20 ml of dry acetonitrile with stirring. The reaction mixture was heated to reflux for 72 hours. In the course of time the formation of a white precipitate can be observed. The suspension of remaining zinc powder and zinc lactate was isolated by filtration. To separate the zinc lactate the filtration residue was treated with hot water and the resulting clear solution was concentrated to give a colourless solid which was washed with acetone and dried in vacuo at 50°C. **$Zn(C_3H_5O_3)_2$** (M = 243.53 g/mol); Yield: 4.53 g = 18.6 mmol = 62%.

11.2.2 Synthesis of amines

Synthesis of 2,6-bis{[bis(2-aminoethyl)amino]methyl}benzene

The synthesis of 2,6-bis{[bis(2-aminoethyl)amino]methyl}benzene starts with the protection of the amine functions of 1,5-diamino-3-azapentane as phthalimids according to Miranda et al.[160] In the next step two equivalents of the 1,5-phthalimido-3-azapentane were added to 2,6-bis(bromo-methyl)-benzene to give the protected tetrakisamine 2,6-bis{[bis(2-phthalimidoethyl)amino]methyl}benzene.[161] The removal of the protecting groups occur by simple acescent cleavage[161] and 2,6-bis[bis(2-aminoethyl)amino]methylbenzene was obtained in almost quantitative yields.

Synthesis of (R,R)-N,N'-dimethyl-1,2-cyclohexanediamine

The methylated bisamine can be synthesised from enatiomeric pure R,R-diaminocyclohexane which was separated with the aid of L-tartaric acid. The methylation followed a modified pro-

cedure by Seebach,[203] whereat the diaminocyclohexane was converted with ethyl formate to N,N'-(1,2-phenylene)diformamide. Lithium aluminum hydride was used as reducing agent to provide (R,R)-N,N'-dimethyl-1,2-cyclohexanediamine.

11.2.3 Synthesis of Vilsmeier salts

Caution! Phosgene is a severe toxic agent that can cause pulmonary embolism and in the case of heavy exposition may be lethal. Use only in a well-ventilated fume hood.

The chloroformamidinium chlorides N,N,N',N'-dimethylethylenechloroformamidinium chloride (DMEG, **V1**), N,N,N',N'-tetramethylchloroformamidinium chloride (TMG, **V2**), N,N,N',N'-dimethylpropylenechloroformamidinium chloride (DMPG, **V3**), N,N,N',N'-tetraethylchloroformamidinium chloride (TEG, **V4**), N,N,N',N'-dipiperidylchloroformamidinium chloride (DPipG, **V5**) and N,N,N',N'-dimorpholinochloroformamidinium chloride (DMorphG, **V6**) were prepared according to literature procedures.[99,100]

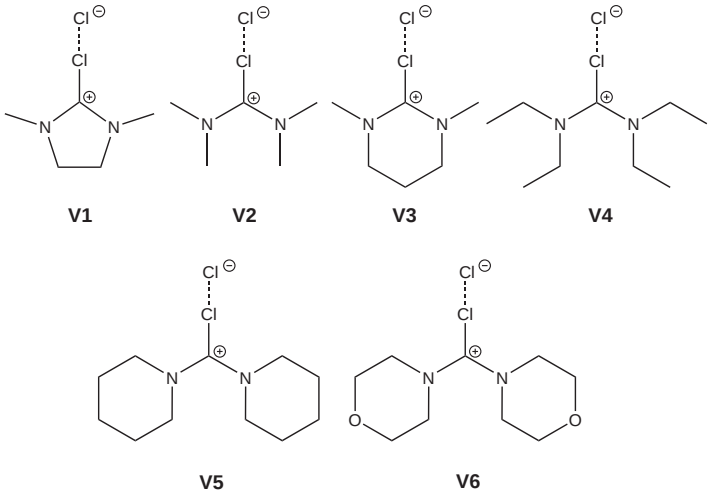

N,N,N',N'-morpholinodimethylchloroformamidinium chloride (MorphDMG, V7)

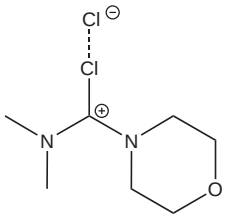

$\mathbf{C_7H_{14}N_2OCl_2}$ (M = 213.12 g/mol): In 400 ml of acetonitrile, dimethyl carbamoyl chloride (300 mmol, 32.26 g) was combined with morpholine (300 mmol, 26.14 g) in the presence of triethylamine (300 mmol, 30.36 g). The reaction started immediately and was highly exothermic. The precipitation of triethylamin hydrochloride was enormous and yielded a vicous yellow slurry. Under vigorous stirring, the reaction mixture was cooled in an ice bath. Then, phosgene (300 mmol) was condensed into this reaction mixture. After addition of phosgene, the mixture was heated for 48 h to 40°C. The product mixture containing the desired chloroformamidinium chloride and triethylamin hydrochloride could not be worked up due to the high sensitivity.

(R,R)-N,N,N',N'-dimethylcyclohexenechloroformamidinium chloride ((R,R)-DMCHG, V8)

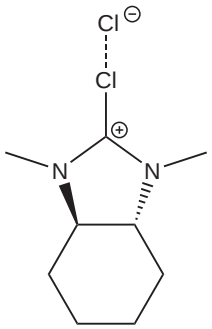

$\mathbf{C_9H_{16}N_2Cl_2}$(M = 223.16 g/mol): The Vilsmeier salt (R,R)-N,N,N',N'-dimethylcyclohexenechloroformamidinium chloride was directly obtained by the conversion of the methylated bisamine (R,R)-N,N'-dimethyl-1,2-cyclohexanediamine with 2 equivalents of phosgene. In 100 ml of toluene, N,N'-dimethylcyclohexanediamine (64 mmol, 9.1 g) was combined with triethylamine (130 mmol, 13.2 g). Under vigorous stirring, the reaction mixture was cooled in an ice bath. Then, phosgene (130 mmol) was condensed into this reaction mixture. After addition of phosgene, the mixture was heated for 48 h to 40°C. The product mixture containing the desired chloroformamidinium chloride and triethylamin hydrochloride could not be worked up due to the high sensitivity.

11.3 Synthesis of product compounds

11.3.1 Synthesis of guanidine ligands

The guanidine ligands N^1,N^2-bis(1,3-dimethylimidazolidin-2-ylidene)ethane-1,2-diamine ($DMEG_2e$, **1**)[119] 1,2-di[2N-(1,1,3,3-tetramethylguanidino)]ethane (TMG_2e, **2**),[111] 1,3-bis(N,N,N',N'-tetramethylguanidino)propanane (btmgp, **3**),[92] N-(1,3-dimethylimidazolidin-2-yliden)quinolin-8-amine (DMEGqu, **6**),[101,121] 1,1,3,3-tetramethyl-2-(quinolin-8-yl)-guanidine (TMGqu, **7**),[101,121,122] N-(1,3-dimethylimidazolidin-2-yliden)pyridin-8-amine (DMEGpy, **14**),[101,121] 1,1,3,3-tetramethyl-2-((pyridin-2-yl)methyl)guanidine (TMGpy, **15**),[101,121,123] 1,1,1-tris{2-[2N-(1,3-dimethylethylenguanidino)]ethyl}amine ($DMEG_3$tren, **29**)[124] and 1,1,1-tris{2-[N^2-(1,1,3,3-tetramethylguanidino)]ethyl}amine (TMG_3tren, **30**)[112] were prepared according to literature procedures.

General synthesis of guanidine ligands with chloroformamidinium chlorides V1-V5

A solution of the chloroformamidinium chloride (for guanidine-amine hybrid: 30 mmol, for bisguanidine: 60 mmol, for trisguanidine: 90 mmol, for tetrakisguanidine: 120 mmol) in dry MeCN was added dropwise under vigorous stirring to an ice-cooled solution of an amine (30 mmol) and triethylamine (equimolar to the amount of chloroformamidinium chloride) in dry MeCN. After 3 - 8h at reflux, an aqueous solution of NaOH (equimolar to the amount of chloroformamidinium chloride) was added. The solvent and NEt_3 were then evaporated under vacuum. In order to deprotonate the guanidine hydrochloride, 50 wt.% KOH (aq., 15 mL) was added and the free base was extracted into the MeCN phase (3 x 30 mL). The organic phase was dried with Na_2SO_4 and after filtration, the solvent was evaporated under reduced pressure.

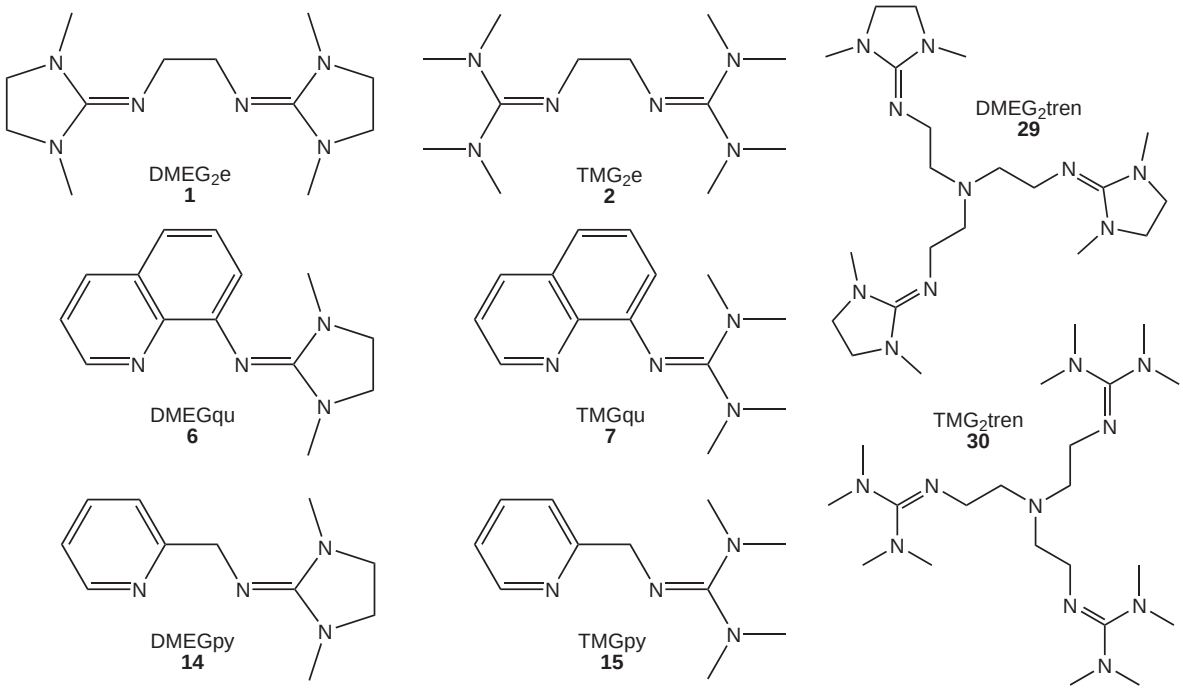

General synthesis of guanidine ligands with chloroformamidinium chlorides V6-V7

The reaction mixture containing the chloroformamidinium chloride (for guanidine-amine hybrid: 30 mmol, for bisguanidine: 60 mmol, for trisguanidine: 90 mmol, for tetrakisguanidine: 120 mmol) in dry MeCN was added dropwise under vigorous stirring to an ice-cooled solution of an amine (30 mmol) and triethylamine (equimolar to the amount of chloroformamidinium chloride) in dry MeCN. After 3 - 8h at reflux, an aqueous solution of NaOH (3 molar to the amount of chloroformamidinium chloride) was added. The solvent and NEt_3 were then evaporated under vacuum. In order to deprotonate the guanidine hydrochloride, 50 wt.% KOH (aq., 25 mL) was added and the free base was extracted into the MeCN phase (3 x 30 mL). The organic phase was dried with Na_2SO_4 and after filtration, the solvent was evaporated under reduced pressure.

N',N"-(ethane-1,2-diyl)bis(N,N-dimethylmorpholine-4-carboximidamide) (MorphDMG$_2$e, 4):

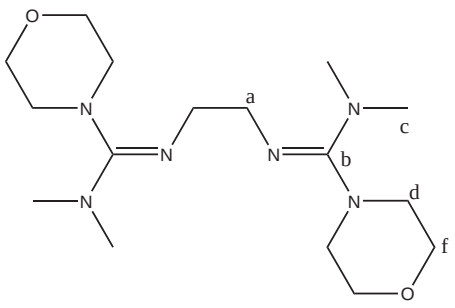

$C_{16}H_{32}N_6O_2$ (M = 340.47 g/mol): Colourless solid, **Yield**: 3.57 g = 10.5 mmol = 35 %, m.p. 130°C. ^{1}**H-NMR** (500 MHz, $CDCl_3$, 25 °C): δ [ppm] = 2.66 (s, 2H, c), 2.67 (s, 2H, c'), 2.78 (s, 6H, c"), 2.79 (s, 2H, c'"), 3.00 (m, 5H, d), 3.16 (m, 3H, d'), 3.28 (s, 2H, a), 3.32 (s, 2H, a), 3.65 (m, 4H, e), 3.70 (m, 4H, e'). ^{13}**C-NMR** (125 MHz, $CDCl_3$, 25 °C): δ [ppm] = 39.1 (CH_3, c), 39.7 (CH_3, c'), 48.2 (CH_2, d), 52.4 (CH_2, a), 67.1 (CH_2, e), 159.5 (C, b).

IR (KBr, $\tilde{\nu}$[cm^{-1}]): 2976 s (ν(C-H$_{aliph.}$)), 2968 s (ν(C-H$_{aliph.}$)), 2956 s (ν(C-H$_{aliph.}$)), 2900 s (ν(C-H$_{aliph.}$)), 2866 s (ν(C-H$_{aliph.}$)), 2848 s (ν(C-H$_{aliph.}$)), 2831 s, 2796 m, 2708 m, 2683 m, 1631 vs (ν(C=N)), 1560 m, 1545 m, 1535 m, 1527 m, 1508 m, 1489 m, 1460 s, 1448 s, 1439 s, 1412 m, 1373 s, 1363 s, 1358 s, 1331 m, 1300 m, 1290 m, 1263 s, 1242 m, 1211 m, 1201 m, 1190 m, 1173 m, 1115 vs, 1092 s, 1068 m ,1036 m, 1022 w, 985 m, 922 m, 895 s, 841 m, 746 w, 725 w, 669 m, 640 vw, 557 w. **EI-MS** (m/z, (%)): 340 (12) [M$^+$], 254 (14) [$C_{12}H_{24}N_5O^+$], 183 (25) [$C_9H_{18}N_3O^+$ -H], 170 (85) [$C_8H_{16}N_3O^+$], 127 (33) [$C_5H_8N_3O^+$ +H], 120 (33), 119 (71), 91 (17), 85 (100) [$C_4H_8NO^+$ -H], 71 (11) [$C_3H_6N_2^+$ +H]. **MS high resolution (molecular isotope distribution)** main isotope calculated: 340.25832; found: 340.25849.

N-(1,3-dimethyltetrahydropyrimidin-2(1H)-ylidene)quinolin-8-amine (DMPGqu, 8):

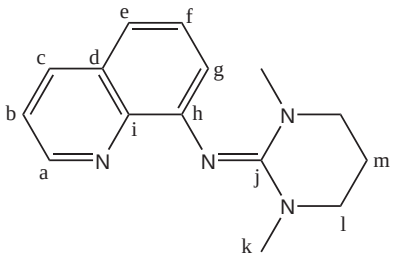

C$_{15}$H$_{18}$N$_4$ (M = 254.33 g/mol): Light yellow solid; **Yield**: 6.71 g = 26.4 mmol = 88 %. ^{1}**H-NMR** (500 MHz, $CDCl_3$, 25 °C): δ [ppm] = 2.17 (q, 2H, m, ^{3}J = 6.2 Hz), 2.95 (s, 6H, k), 3.33 (t, 4H, l, ^{3}J = 6.2 Hz), 7.45 (dd, 1H, b, ^{3}J = 8.3 Hz, ^{3}J = 4.1 Hz), 7.45 (dd, 1H, f, ^{3}J = 8.2 Hz, ^{3}J = 7.4 Hz), 7.51 (dd, 1H, g, ^{3}J = 8.2 Hz, ^{4}J = 1.4 Hz), 7.85 (dd, 1H, e, ^{3}J = 7.4 Hz, ^{4}J = 1.4 Hz), 8.11 (dd, 1H, c, ^{3}J = 8.3 Hz, ^{4}J = 1.7 Hz), 8.66 (dd, 1H, a, ^{3}J = 4.1 Hz, ^{4}J = 1.7 Hz). ^{13}**C-NMR** (125 MHz, $CDCl_3$, 25 °C): δ [ppm] = 22.3 (CH_2, m), 40.3 (CH_3, k), 48.3 (CH_2, l), 121.6 (CH, b+e), 123.6 (CH, g), 127.5 (CH, f), 128.7 (C, d), 136.5 (CH, c), 136.8 (C, i), 140.9 (C, h), 149.0 (CH, a), 157.0 (C, j). **IR** (KBr, $\tilde{\nu}$[cm^{-1}]): 3178 m (ν(C-H$_{arom.}$)), 3039 m (ν(C-H$_{arom.}$)), 2999 m (ν(C-H$_{arom.}$)), 2987 m (ν(C-H$_{aliph.}$)), 2972 m (ν(C-H$_{aliph.}$)), 2954 m (ν(C-H$_{aliph.}$)), 2926 m (ν(C-H$_{aliph.}$)), 2898 m (ν(C-H$_{aliph.}$)), 2870 m (ν(C-H$_{aliph.}$)), 2818 (ν(C-H$_{aliph.}$)), 2777 m (ν(C-H$_{aliph.}$)), 2657 s, 1620 vs (ν(C=N)), 1608 vs (ν(C=N)), 1597 s, 1560 vs (ν(C=N)), 1504 vs, 1470 m, 1460 m, 1443 m 1410 s, 1385 s, 1365 m, 1311 s, 1279 m, 1232 m, 1209 m, 1186 m, 1132 w, 1120 w, 1105 m, 1097 m, 1088 m, 1018 m, 989 w, 945 vw, 912 vw, 881 vw, 872 vw, 829 m, 812 w, 791 s, 764 m, 733 m, 667 w, 640 m, 613 m, 590 vw, 567 w, 527 vw. **EI-MS** (m/z, (%)): 254 (64) [M$^+$], 225 (13), 183 (20), 167 (46), 155 (29) [$C_{10}H_6N_2^+$ +H], 149 (100), 144 (38) [$C_9H_6N_2^+$ +2H], 129 (27) [$C_9H_6N^+$ +H], 120 (27), 91 (51), 83 (27), 71 (55), 69 (45), 57 (78).

1,1,3,3-tetraethyl-2-(quinolin-8-yl)guanidine (TEGqu, 9):

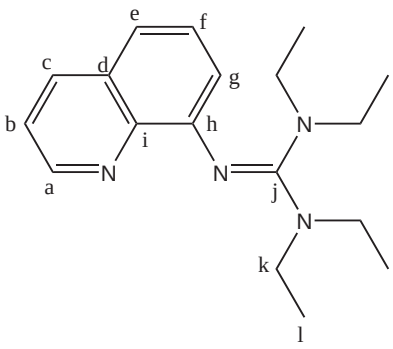

C$_{18}$H$_{26}$N$_4$ (M = 298.43 g/mol): Green oil ; **Yield**: 8.86 g = 29.7 mmol = 99 %. ^{1}**H-NMR** (500 MHz, $CDCl_3$, 25 °C): δ [ppm] = 1.05 (t, 12H, l, ^{3}J = 7.1 Hz), 3.12 (q, 8H, k, ^{3}J = 7.1 Hz), 6.93 (m, 1H, g), 7.28 (m, 2H, b+e), 7.36 (dd, 1H, f, ^{3}J = 7.8 Hz, ^{3}J = 7.7 Hz), 8.04 (dd, 1H, c, ^{3}J = 8.3 Hz, ^{4}J = 1.7 Hz), 8.83 (dd, 1H, a, ^{3}J = 4.1 Hz, ^{4}J = 1.7 Hz). ^{13}**C-NMR** (125 MHz, $CDCl_3$, 25 °C): δ [ppm] = 13.1 (CH_3, l), 42.3 (CH_2, k), 118.7 (CH, g), 120.6 (CH, b+e), 127.1 (CH, f), 129.5 (C, d), 135.8 (CH, c), 142.9 (C, i), 147.5 (C, h), 148.4 (CH, a), 160.3 (C, j). **IR**

(film between NaCl plates, $\tilde{\nu}$[cm^{-1}]): 3043 vw (ν(C-H$_{arom.}$)), 3022 vw (ν(C-H$_{arom.}$)), 2968 m (ν(C-H$_{aliph.}$)), 2931 m (ν(C-H$_{aliph.}$)), 2870 m (ν(C-H$_{aliph.}$)), 1676 w, 1641 m, 1589 m (ν(C=N)), 1579 m (ν(C=N)), 1556 s, 1493 m, 1481 m, 1460 m, 1417 m, 1377 m, 1358 m, 1304 m, 1267 m, 1207 m, 1136 m, 1061 m, 1041 s. **EI-MS** (m/z, (%)): 298 (16) [M$^+$], 226 (10) [M$^+$ - N(CH$_2$CH$_3$)$_2$], 198 (13), 172 (56) [M$^+$ - NC$_9$H$_6$ +2H], 156 (24) [M$^+$ - N$_2$C$_9$H$_6$], 144 (44) [N$_2$C$_9$H$_6^+$ +2H], 117 (13), 100 (74), 72 (100) [N(CH$_2$CH$_3$)$_2^+$], 59 (49), 44 (52).

N-(dipiperidin-1-ylmethylene)quinolin-8-amine (DPipGqu, 10):

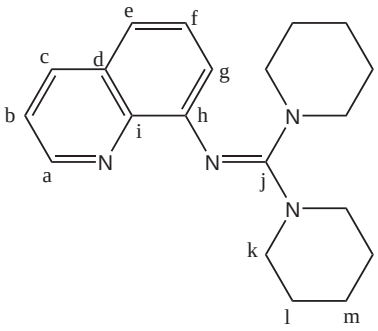

C$_{20}$H$_{26}$N$_4$ (M = 322.45 g/mol): Viscous yellow oil; **Yield**: 7.06 g = 21.9 mmol = 73 %. ^{1}**H-NMR** (500 MHz, CDCl$_3$, 25 °C): δ [ppm] = 1.54 (m, 12H, l + m), 3.16 (t, 8H, k, ^{3}J = 5.7 Hz, ^{3}J = 4.5 Hz), 6.84 (m, 1H, g), 7.27 (m, 2H, b+e), 7.36 (t, 1H, f, ^{3}J = 7.7 Hz, ^{3}J = 7.8 Hz), 8.04 (dd, 1H, c, ^{3}J = 8.2 Hz, ^{4}J = 1.7 Hz), 8.84 (dd, 1H, a, ^{3}J = 4.1 Hz, ^{4}J = 1.7 Hz). ^{13}**C-NMR** (125 MHz, CDCl$_3$, 25 °C): δ [ppm] = 25.8 (CH$_2$, m + l), 47.9 (CH$_2$, k), 119.3 (CH, g), 120.6 (CH, b+e), 127.0 (CH, f), 129.4 (C, d), 135.8 (CH, c), 143.0 (C, i), 147.4 (C, h), 148.7 (CH, a), 161.3 (C, j). **IR** (film between NaCl plates, $\tilde{\nu}$[cm^{-1}]): 3053 vw (ν(C-H$_{arom.}$)), 2987 w (ν(C-H$_{aliph.}$)), 2931 vs (ν(C-H$_{aliph.}$)), 2850 m (ν(C-H$_{aliph.}$)), 1724 m (ν(C=N)), 1643 s (ν(C=N)), 1589 s, 1556 vs, 1493 m, 1450 s, 1417 s, 1371 m, 1334 m, 1308 w, 1249 vs, 1215 m, 1178 m, 1157 m, 1132 m, 1097 m, 1070 m, 1055 m, 1028 s, 1014 s. **EI-MS** (m/z, (%)): 322 (6) [M$^+$], 239 (4) [M$^+$ - C$_5$H$_{10}$N +H], 196 (68) [N=C(C$_5$H$_{10}$N)$_2^+$ +2H], 186 (26), 168 (16), 151 (32), 139 (25), 121 (15), 112 (59) [C(N)(N(CH$_3$)$_2$)$_2^+$ +2H], 85 (43) [C$_5$H$_{10}$N$^+$ +H], 84 (100) [C$_5$H$_{10}$N$^+$], 69 (64).

N-(dimorpholinomethylene)quinolin-8-amine (DMorphGqu, 11):

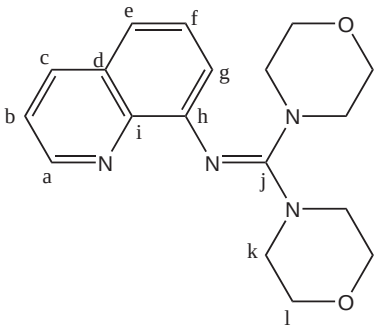

C$_{18}$H$_{22}$N$_4$O$_2$ (M = 326.40 g/mol): Light yellow solid; **Yield**: 7.44 g = 22.8 mmol = 76 %, MP = 152°C. ^{1}**H-NMR** (500 MHz, CDCl$_3$, 25 °C): δ [ppm] = 3.16 (t, 8H, k, ^{3}J = 4.3 Hz), 3.56 (t, 8H, l, ^{3}J = 4.3 Hz), 6.97 (dd, 1H, g, ^{3}J = 7.4 Hz, ^{4}J = 1.3 Hz), 7.31 (dd, 1H, b, ^{3}J = 8.2 Hz, ^{3}J = 4.1 Hz), 7.34 (dd, 1H, e, ^{3}J = 8.1 Hz, ^{4}J = 1.3 Hz), 7.39 (dd, 1H, f, ^{3}J = 8.1 Hz, ^{3}J = 7.4 Hz), 8.07 (dd, 1H, c, ^{3}J = 8.2 Hz, ^{4}J = 1.7 Hz), 8.84 (dd, 1H, a, ^{3}J = 4.1 Hz, ^{4}J = 1.7 Hz). ^{13}**C-NMR** (125 MHz, CDCl$_3$, 25 °C): δ [ppm] = 48.6 (CH$_2$, k), 66.7 (CH$_2$, l), 119.6 (CH, g), 120.0 (CH, e), 120.9 (CH, b), 127.0 (CH, f), 129.4 (C, d), 136.1 (CH, c), 142.5 (C, i), 149.0 (CH, a), 149.9 (C, h), 159.4 (C, j). **IR** (KBr, $\tilde{\nu}$[cm^{-1}]): 3047 w (ν(C-H$_{arom.}$)), 2960 m (ν(C-H$_{aliph.}$)), 2922 m (ν(C-H$_{aliph.}$)), 2897 m (ν(C-H$_{aliph.}$)), 2850 m (ν(C-H$_{aliph.}$)), 2841 m (ν(C-H$_{aliph.}$)), 2675 w (ν(C-H$_{aliph.}$)), 1591 s (ν(C=N)), 1572 s (ν(C=N)), 1549 vs (ν(C=N)), 1493 s, 1473 m, 1458 m, 1437 m, 1417 m, 1387 m, 1362 m, 1340 m, 1302 m, 1281 m, 1263 s, 1236 m, 1207 m, 1173 m, 1113 vs, 1070 m, 1057 m, 1032 m, 982 m, 931 m, 899 m, 877 m, 835 m, 827 m, 804 m, 760 m, 735 w, 677 m, 660 w, 646 w, 613 w,

598 w, 569 w, 555 vw, 527 w. **EI-MS** (m/z, (%)): 326 (100) [M^+], 241 (46) [$C_{14}H_{14}N_3O^+$ +H], 240 (52) [$C_{14}H_{14}N_3O^+$], 213 (28), 183 (17) [$C_9H_{16}N_2O_2^+$ -H], 182 (12), 169 (29) [$C_9H_{16}N_2O^+$ +H], 156 (84), 155 (63), 129 (29) [$C_9H_6N^+$ +H], 128 (26) [$C_9H_6N^+$], 112 (17), 86 (8) [$C_4H_8NO^+$]. **MS high resolution (molecular isotope distribution)** main isotope calculated: 326.17401; found: 326.17413.

N,N-dimethyl-N'-(quinolin-8-yl)morpholine-4-carboximidamide (MorphDMGqu, 12):

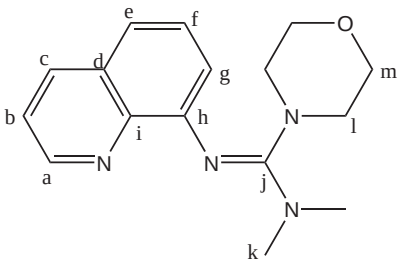

$C_{16}H_{20}N_4O$ (M = 284.36 g/mol): Amber coloured oil; **Yield**: 6.48 g = 22.8 mmol = 76 %. ^{1}**H-NMR** (500 MHz, $CDCl_3$, 25 °C): δ [ppm] = 2.77 (s, 6H, k), 3.05 (t, 4H, l, ^3J = 4.5 Hz), 3.53 (t, 4H, m, ^3J = 4.5 Hz), 6.93 (d, 1H, g, ^3J = 7.2 Hz), 7.29 (m, 2H, b+e), 7.37 (dd, 1H, f, ^3J = 7.9 Hz, ^3J = 7.5 Hz), 8.04 (dd, 1H, c, ^3J = 8.2 Hz, ^4J = 1.7 Hz), 8.82 (dd, 1H, a, ^3J = 4.1 Hz,^4J = 1.7 Hz). ^{13}**C-NMR** (125 MHz, $CDCl_3$, 25 °C): δ [ppm] = 39.6 (CH_3, k), 48.6 (CH_2, l), 66.7 (CH_2, m), 119.6 (CH, g+e), 120.8 (CH, b), 127.1 (CH, f), 129.4 (C, d), 136.0 (CH, c), 142.7 (C, i), 148.8 (CH, a), 149.3 (C, h), 160.4 (C, j). **IR** (film between NaCl plates, $\tilde{\nu}$[cm^{-1}]): 3043 m (ν(C-$H_{arom.}$)), 3022 m (ν(C-$H_{arom.}$)), 2956 m (ν(C-$H_{aliph.}$)), 2918 s (ν(C-$H_{aliph.}$)), 2893 s (ν(C-$H_{aliph.}$)), 2852 s (ν(C-$H_{aliph.}$)), 2800 m (ν(C-$H_{aliph.}$)), 2679 w (ν(C-$H_{aliph.}$)), 1648 vs (ν(C=N)), 1593 vs (ν(C=N)), 1556 vs (ν(C=N)), 1493 vs, 1458 vs, 1441 vs, 1389 vs, 1362 vs, 1338 s, 1306 m, 1263 s, 1215 s, 1201 s, 1182 s, 1165 m, 1140 m, 1115 vs, 1097 s, 1065 vs, 1018 s. **EI-MS** (m/z, (%)): 284 (3) [M^+], 154 (15) [$C_{10}H_6N_2^+$], 144 (79) [$C_9H_6N_2^+$ +2H, $C_7H_{14}N_2O^+$ +2H], 127 (31) [$C_9H_6N^+$ -H], 117 (22), 115 (11), 101 (15) [$C_7H_3N^+$], 86 (15) [$C_4H_8NO^+$], 72 (100) [$C_4H_8O^+$], 70 (16). **MS high resolution (molecular isotope distribution)** main isotope calculated: 284.16358; found: 284.16354.

N-((3aR,7aR)-1,3-dimethyl-1H-benzo[d]imidazol-2(3H,3aH,4H,5H,6H,7H,7aH)-ylidene)quinolin-8-amine ((R,R)-DMCHGqu, 13):

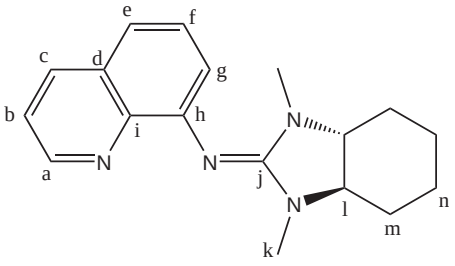

$C_{18}H_{22}N_4$ (M = 294.40 g/mol) Amber coloured oil; **Yield**: 8.13 g = 27.6 mmol = 92 %. ^{1}**H-NMR** (500 MHz, $CDCl_3$, 25 °C): δ [ppm] = 1.28-1.39 (m, 4H, m+n), 1.86 (m, 2H, n'), 2.00 (m, 2H, m'), 2.55 (m, 2H, l), 2.69 (s, 6H, k), 7.45 (m, 2H, b+e), 7.56 (dd, 1H, f, ^3J = 8.1 Hz, ^3J = 7.8 Hz), 8.16 (dd, 1H, c, ^3J = 8.2 Hz, ^4J = 1.7 Hz), 8.69 (dd, 1H, g, ^3J = 7.8 Hz, ^4J = 1.2 Hz), 8.82 (dd, 1H, a, ^3J = 4.2 Hz, ^4J = 1.7 Hz). ^{13}**C-NMR** (125 MHz, $CDCl_3$, 25 °C): δ [ppm] = 24.3 (CH_2, n), 28.2 (CH_2, m), 29.6 (CH_3, k), 63.9 (CH, l), 115.1 (CH, g), 120.1 (CH, e), 121.5 (CH, b), 127.6 (CH, f), 129.4 (C, d), 136.4 (CH, c), 143.4 (C, i), 147.8 (CH, a), 152.0 (C, h), 164.8 (C, j). **IR** (film between NaCl plates, $\tilde{\nu}$[cm^{-1}]): 3045 m (ν(C-$H_{arom.}$)), 2937 s (ν(C-$H_{aliph.}$)), 2864 m (ν(C-$H_{aliph.}$)), 2715 w (ν(C-$H_{aliph.}$)), 1705 s (ν(C=N)), 1597 m, 1562 m, 1525

s, 1487 s, 1462 s, 1433 s, 1412 m, 1373 s, 1321 s, 1290 m, 1257 s, 1227 m, 1205 m, 1188 s, 1132 m, 1072 s, 1051 s, 1022 s. **EI-MS** (m/z, (%)): 294 (26) [M^+], 293 (13), 210 (18), 171 (24), 169 (41), 168 (98), 167 (100) [$C_9H_{16}N_3^+$ +H], 144 (93) [$C_9H_6N_2^+$ +2H], 139(23), 126 (82), 125 (98), 117 (60), 113 (34), 112 (59) [$C_7H_{13}N^+$ +H], 110 (47) [$C_5H_8N_3^+$], 100 (27), 90 (15), 89 (18), 83 (19), 82 (23) [$C_6H_{10}^+$], 81 (23), 79 (25), 72 (27), 70 (15), 68 (37), 56 (24) [$C_4H_8^+$]. **MS high resolution (molecular isotope distribution)** main isotope calculated: 294.18457; found: 294.18470.

N-(1,3-dimethyltetrahydropyrimidin-2(1H)-ylidene)-1-(pyridin-2-yl)methanamine (DMPGpy, 16):

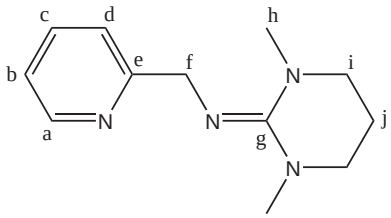

$C_{12}H_{18}N_4$ (M = 218.30 g/mol): Yellow oil; **Yield**: 6.22 g = 28.5 mmol = 95 %. ^{1}**H-NMR** (500 MHz, $CDCl_3$, 25 °C): δ [ppm] = 1.94 (m, 2H, j), 3.02 (s, 6H, h), 3.17 (m, 4H, i), 4.59 (s, 2H, f), 7.10 (m, 1H, b), 7.66 (m, 2H, c + d), 8.46 (m, 1H, a). ^{13}**C-NMR** (125 MHz, $CDCl_3$, 25 °C): δ [ppm] = 21.2 (CH_2, j), 39.6 (CH_3, h), 48.5 (CH_2, i), 52.4 (CH_2, f), 121.6 (CH, b), 121.7 (CH, d), 136.7 (CH, c), 148.6 (CH, a), 158.4 (C, e), 161.2 (C, g). **IR** (film between NaCl plates, $\tilde{\nu}$[cm^{-1}]): 3055 w (ν(C-$H_{arom.}$)), 3003 w (ν(C-$H_{arom.}$)), 2941 m (ν(C-$H_{aliph.}$)), 2873 m (ν(C-$H_{aliph.}$)), 1612 vs (ν(C=N)), 1585 vs (ν(C=N)), 1531 w, 1500 m, 1471 m, 1435 m, 1421 m, 1398 m, 1363 m, 1346 m, 1321 m, 1304 m, 1273 m, 1230 m, 1163 m, 1111 m, 1045 s, 1016 vs. **EI-MS** (m/z, (%)): 218 (82) [M^+], 140 (46) [M^+ - NC_5H_4], 128 (100) [$N_3C_6H_{12}^+$ +2H], 127 (38) [$N_3C_6H_{12}^+$ +H], 126 (68) [$N_3C_6H_{12}^+$], 113 (27) [$N_2C_6H_{12}^+$ +H], 112 (26) [$N_2C_6H_{12}^+$], 111 (32) [$N_2C_6H_{12}^+$ -H], 108 (19) [M^+ - $N_2C_6H_{12}$ +2H], 107 (14) [M^+ - $N_2C_6H_{12}$ +H], 99 (24), 93 (26) [$NC_6H_6^+$ +H], 92 (23) [$NC_6H_6^+$], 85 (20), 84 (22), 80 (23), 79 (24), 70 (46), 69 (27), 65 (14), 58 (20), 57 (26), 55 (18), 44 (51), 43 (40), 42 (59).

1,1,3,3-tetraethyl-2-(pyridin-2-ylmethyl)guanidine (TEGpy, 17):

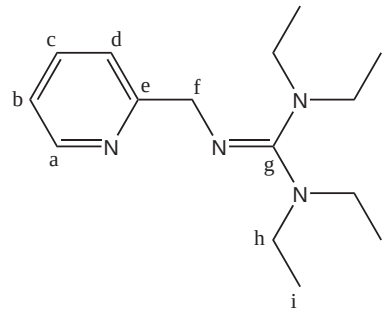

$C_{15}H_{26}N_4$ (M = 262.40 g/mol): Light yellow oil; **Yield**: 7.16 g = 27.3 mmol = 91 %. ^{1}**H-NMR** (500 MHz, $CDCl_3$, 25 °C): δ [ppm] = 1.04 (m, 5H, i), 1.09 (m, 7H, i'), 3.14 (m, 3H, h), 3.27 (m, 5H, h'), 4.52 (s, 2H, f), 7.08 (m, 1H, b), 7.65 (m, 2H, c + d), 8.47 (m, 1H, a). ^{13}**C-NMR** (125 MHz, $CDCl_3$, 25 °C): δ [ppm] = 13.0 (CH_3, i'), 13.6 (CH_3, i), 42.3 (CH_2, h'), 42.9 (CH_2, h), 54.7 (CH_2, f), 121.2 (CH, b), 121.5 (CH, d), 136.4 (CH, c), 148.5 (CH, a), 160.0 (C, e), 162.0 (C, g). **IR** (KBr, $\tilde{\nu}$[cm^{-1}]): 3060 vw (ν(C-$H_{arom.}$)), 2968 m (ν(C-$H_{aliph.}$)), 2929 m (ν(C-$H_{aliph.}$)), 2870 m (ν(C-$H_{aliph.}$)), 1608 s (ν(C=N)), 1587 vs (ν(C=N)), 1471 m, 1435 m, 1408 m, 1375 m, 1358 m, 1338 m, 1302 m, 1263 s, 1221 m, 1205 m, 1134 m, 1070 m, 1045 m, 1036 m, 1009 m, 993 m, 939 w, 889 vw, 858 vw, 823 w, 756 m, 712 w, 669 vw, 631 w, 611 w, 584 w, 550 vw, 519 vw. **EI-MS** (m/z, (%)): 262 (59) [M^+], 233 (6) [M^+ - CH_2CH_3], 191 (23) [M^+ - $N(CH_2CH_3)_2$ +H], 190 (82) [M^+ - $N(CH_2CH_3)_2$], 162 (12) [M^+ - $N(CH_2CH_3)_2$ - CH_2CH_3 +H], 161 (12) [M^+ - $N(CH_2CH_3)_2$ - CH_2CH_3], 160 (17) [M^+

- $N(CH_2CH_3)_2$ - CH_2CH_3 -H], 120 (8) [M^+ - 2 $N(CH_2CH_3)_2$ +2H], 93 (100) [$C_6H_6N^+$ +H], 92 (90) [$C_6H_6N^+$], 72 (23) [$N(CH_2CH_3)_2^+$], 65 (20).

N-(dipiperidin-1-ylmethylene)-1-(pyridin-2-yl)methanamine (DPipGpy, 18):

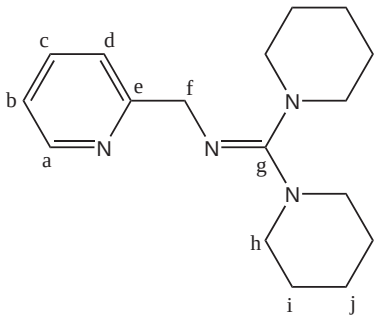

$C_{17}H_{26}N_4$ (M = 286.42 g/mol): Amber coloured oil; **Yield**: 7.22 g = 25.2 mmol = 84 %. ^{1}**H-NMR** (500 MHz, $CDCl_3$, 25 °C): δ [ppm] = 1.56 (s, 12H, i+j), 3.14 (t, 8H, h, 3J = 5.1 Hz, 3J = 4.2 Hz), 4.55 (s, 2H, f), 7.07 (m, 1H, b), 7.62 (m, 2H, c+d), 8.46 (m, 1H, a). ^{13}**C-NMR** (125 MHz, $CDCl_3$, 25 °C): δ [ppm] = 25.8 (CH_2, i + j), 47.9 (CH_2, h), 54.6 (CH_2, f), 121.1 (CH, b), 121.4 (CH, d), 136.4 (CH, c), 148.5 (CH, a), 161.2 (C, e), 162.8 (C, g). **IR** (film between NaCl plates, $\tilde{\nu}$[cm^{-1}]): 3055 w (ν(C-$H_{arom.}$)), 2976 m (ν(C-$H_{aliph.}$)), 2931 vs (ν(C-$H_{aliph.}$)), 2850 m (ν(C-$H_{aliph.}$)), 1643 s (ν(C=N)), 1614 s (ν(C=N)), 1587 s (ν(C=N)), 1517 m, 1469 m, 1450 m, 1435 m, 1415 s, 1369 m, 1347 m, 1286 m, 1248 vs, 1213 m, 1157 m, 1132 s. **EI-MS** (m/z, (%)): 286 (84) [M^+], 203 (63) [M^+ - NC_5H_{10} +H], 202 (80) [M^+ - NC_5H_{10}], 196 (74) [$NC(NC_5H_{10})_2^+$ +2H], 120 (31) [M+ - 2 NC_5H_{10} +2H], 112 (41), 93 (100) [$(NC_5H_4)CH_2^+$ +H], 92 (61) [$(NC_5H_4)CH_2^+$], 85 (20) [$NC_5H_{10}^+$ +H], 84 (100) [$NC_5H_{10}^+$], 69 (18).

N-(dimorpholinomethylene)-1-(pyridin-2-yl)methanamine (DMorphGpy, 19):

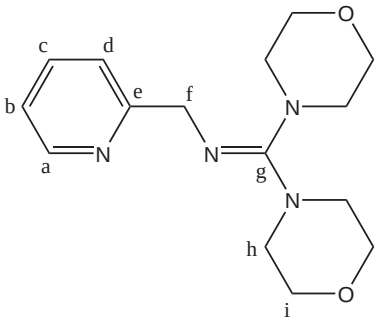

$C_{15}H_{22}N_4O_2$ (M = 290.36 g/mol): Amber coloured oil; **Yield**: 6.48 g = 22.3 mmol = 74 %. ^{1}**H-NMR** (500 MHz, $CDCl_3$, 25 °C): δ [ppm] = 3.16 (t, 4H, h, ^{3}J = 4.7 Hz), 3.20 (t, 4H, h', ^{3}J = 4.7 Hz), 3.70 (m, 8H, i), 4.58 (s, 2H, f), 7.09 (m, 1H, b), 7.56 (m, 1H, d), 7.64 (m, 1H, c), 8.48 (m, 1H, a). ^{13}**C-NMR** (125 MHz, $CDCl_3$, 25 °C): δ [ppm] = 48.3 (CH_2, h), 48.4 (CH_2, h'), 54.9 (CH_2, f), 66.8 (CH_2, i), 67.1 (CH_2, i'), 121.2 (CH, d), 121.3 (CH, b), 136.5 (CH, c), 148.7 (CH, a), 157.2 (C, e), 158.7 (C, g). **IR** (film between NaCl plates, $\tilde{\nu}$[cm^{-1}]): 3059 w (ν(C-$H_{arom.}$)), 2962 s (ν(C-$H_{aliph.}$)), 2912 m (ν(C-$H_{aliph.}$)), 2891 m (ν(C-$H_{aliph.}$)), 2850 s (ν(C-$H_{aliph.}$)), 2754 w (ν(C-$H_{aliph.}$)), 2681 w (ν(C-$H_{aliph.}$)), 1620 s (ν(C=N)), 1589 s (ν(C=N)), 1570 m, 1539 m, 1452 s, 1435 s, 1419 s, 1402 s, 1362 s, 1342 m, 1300 m, 1263 s, 1232 s, 1176 m, 1149 m, 1115 s, 1068 s, 1047 s, 1030 s, 995 s. **EI-MS** (m/z, (%)): 290 (7) [M^+], 204 (10) [$C_{11}H_{14}N_3O^+$], 170 (17) [$C_9H_{16}N_2O^+$ +2H], 169 (66) [$C_9H_{16}N_2O^+$ +H], 143 (25), 114 (100), 93 (24) [$C_6H_6N^+$ +H], 92 (24) [$C_6H_6N^+$], 86 (54) [$C_4H_8NO^+$], 70 (97) [$C_4H_8N^+$], 57 (14), 56 (23). **MS high resolution (molecular isotope distribution)** main isotope calculated: 290.1741; found: 290.17408.

N,N-dimethyl-N'-(pyridin-2-ylmethyl)morpholine-4-carboximidamide (MorphDMGpy, 20):

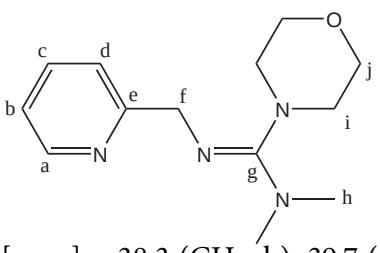

$C_{13}H_{20}N_4O$ (M = 248.33 g/mol): Yellow oil; **Yield**: 5.81 g = 23.4 mmol = 78 %. ^{1}**H-NMR** (500 MHz, $CDCl_3$, 25 °C): δ [ppm] = 2.72 (s, 3H, h), 2.74 (s, 3H, h'), 3.04 (t, 2H, i, ^3J = 4.7 Hz), 3.09 (t, 2H, i', ^3J = 4.7 Hz), 3.61 (t, 4H, j, ^3J = 4.7 Hz), 4.45 (s, 1H, f), 4.49 (s, 1H, f'), 6.99 (m, 1H, b), 7.51 (m, 1H, d), 7.55 (m, 1H, c), 8.39 (m, 1H, a). ^{13}**C-NMR** (125 MHz, $CDCl_3$, 25 °C): δ [ppm] = 38.3 (CH_3, h), 39.7 (CH_3, h'), 47.2 (CH_2, i), 48.2 (CH_2, i'), 55.1 (CH_2, f), 55.2 (CH_2, f'), 66.9 (CH_2, j), 121.1 (CH, b), 121.1 (CH, d), 136.4 (CH, c), 148.5 (CH, a), 160.2 (C, e), 163.1 (C, g). **IR** (film between NaCl plates, $\tilde{\nu}$[cm^{-1}]): 3060 w (ν(C-$H_{arom.}$)), 2960 m (ν(C-$H_{aliph.}$)), 2893 m (ν(C-$H_{aliph.}$)), 2852 m (ν(C-$H_{aliph.}$)), 1620 s (ν(C=N)), 1589 s, 1570 m, 1537 m, 1495 m, 1471 m, 1454 m, 1437 m, 1421 m, 1387 m, 1363 m, 1344 m, 1298 m, 1265 m, 1246 m, 1211 m, 1201 m, 1180 m, 1144 m, 1115 s, 1082 m, 1067 m, 1047 m. **EI-MS** (m/z, (%)): 248 (26) [M^+], 162 (15) [$C_9H_{12}N_3^+$], 127 (31), 101 (14), 93 (50) [$C_6H_6N^+$ +H], 92 (58) [$C_6H_6N^+$], 86 (17) [$C_4H_8NO^+$], 72 (100) [$C_4H_8O^+$], 70 (16), 65 (29). **MS high resolution (molecular isotope distribution)** main isotope calculated: 248.16369; found: 284.16373.

N-(1,3-dimethylimidazolidin-2-ylidene)-3-methylpyridin-2-amine (DMEGpico, 21):

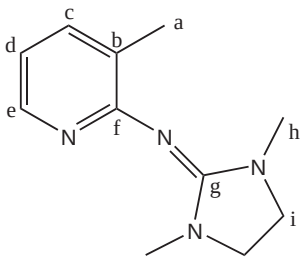

$C_{11}H_{16}N_4$ (M = 204.27 g/mol): Dark red solid; **Yield**: 3.86 g = 18.9 mmol = 63 %. ^{1}**H-NMR** (500 MHz, $CDCl_3$, 25 °C): δ [ppm] = 2.18 (s, 3H, a), 2.65 (s, 6H, h), 3.35 (s, 4H, i), 6.62 (m, 1H, d), 7.29 (m, 1H, c), 8.09 (m, 1H, e). ^{13}**C-NMR** (125 MHz, $CDCl_3$, 25 °C): δ [ppm] = 18.5 (CH_3, a), 34.6 (CH_3, h), 48.3 (CH_2, i), 115.3 (CH, d), 125.2 (C, b), 137.1 (CH, c), 145.5 (CH, e), 156.8 (C, f), 160.9 (C, g). **IR** (KBr, $\tilde{\nu}$[cm^{-1}]): 3059 vw (ν(C-$H_{arom.}$)), 3032 vw (ν(C-$H_{arom.}$)), 2993 w (ν(C-$H_{aliph.}$)), 2972 w (ν(C-$H_{aliph.}$)), 2927 w (ν(C-$H_{aliph.}$)), 2873 w (ν(C-$H_{aliph.}$)), 1620 s (ν(C=N)), 1577 vs (ν(C=N)), 1508 m, 1489 m, 1462 m, 1437 s, 1394 m, 1375 m, 1290 m, 1269 w, 1241 m, 1201 w, 1103 w, 1080 w, 1036 m, 974 m, 928 vw, 891 vw, 798 w, 787 w, 766 m, 735 w, 690 w, 654 w, 602 vw, 565 w, 534 vw. **EI-MS** (m/z, (%)): 204 (34) [M^+], 189 (100) [M^+ - CH_3], 119 (8) [M^+ - $(CH_3)_2NCH_2CH_2N(CH_3)_2$ +H], 114 (10) [M^+ - C_6H_6N +2H], 108 (94), 106 (22), 92 (13) [$C_6H_6N^+$], 81 (14), 80 (43), 65 (9), 42 (8).

1,1,3,3-tetramethyl-2-(3-methylpyridin-2-yl)guanidine (TMGpico, 22):

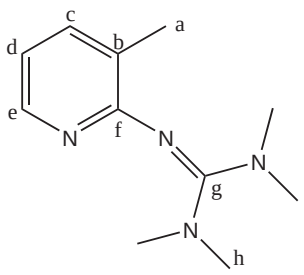

$C_{11}H_{18}N_4$ (M = 206.29 g/mol): Orange coloured oil; **Yield**: 4.64 g = 22.5 mmol = 75 %. ^{1}**H-NMR** (500 MHz, $CDCl_3$, 25 °C): δ [ppm] = 2.16 (s, 3H, a), 2.71 (s, 12H, h), 6.62 (m, 1H, d), 7.30 (m, 1H, c), 8.07 (m, 1H, e). ^{13}**C-NMR** (125 MHz, $CDCl_3$, 25 °C): δ [ppm] = 18.5 (CH_3, a), 39.5 (CH_3, h), 115.2 (CH, d), 124.4 (C, b), 137.4 (CH, c), 145.9 (CH, e), 161.6 (C, f), 162.7 (C, g). **IR** (film between NaCl plates, $\tilde{\nu}$[cm^{-1}]): 3059 vw (ν(C-$H_{arom.}$)), 3001 w (ν(C-$H_{arom.}$)), 2931 m (ν(C-$H_{aliph.}$)),

2885 m (ν(C-$H_{aliph.}$)), 2812 vw (ν(C-$H_{aliph.}$)), 2792 vw (ν(C-$H_{aliph.}$)), 1601 m (ν(C=N)), 1564 vs (ν(C=N)), 1512 m, 1460 m, 1441 m, 1417 s, 1381 s, 1286 w, 1269 w, 1227 m, 1178 m, 1146 m, 1105 m, 1059 m, 1022 s. **EI-MS** (m/z, (%)): 206 (66) [M^+], 191 (92) [M^+ - CH_3], 162 (69) [M^+ - $N(CH_3)_2$], 148 (62), 119 (100) [M^+ - 2 $N(CH_3)_2$ +H], 107 (16), 93 (17) [$C_6H_6N^+$ +H], 92 (85) [$C_6H_6N^+$], 85 (12), 65 (34), 44 (16) [$N(CH_3)_2^+$], 42 (22).

N-(1,3-dimethylimidazolidin-2-ylidene)-3-(1H-imidazol-1-yl)propan-1-amine (DMEGimi, 23):

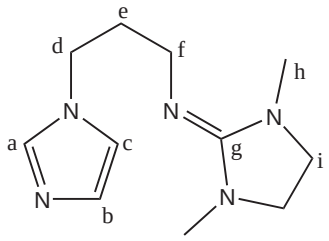

$\mathbf{C_{11}H_{19}N_5}$ (M = 221.30 g/mol): Yellow oil; **Yield**: 6.31 g = 28.5 mmol = 95 %. ^{1}**H-NMR** (500 MHz, $CDCl_3$, 25 °C): δ [ppm] = 1.93 (q, 2H, e, ^3J = 6.7 Hz, ^3J = 6.1 Hz), 2.75 (m, 6H, h), 3.13 (s, 4H, i), 3.31 (t, 2H, f, ^3J = 6.1 Hz), 4.09 (t, 2H, d, ^3J = 6.7 Hz), 6.89 (d, 1H, c, ^3J = 1.0 Hz), 7.01 (d, 1H, b, ^3J = 1.0 Hz), 7.42 (s, 1H, a). ^{13}**C-NMR** (125 MHz, $CDCl_3$, 25 °C): δ [ppm] = 31.5 (CH_3, h), 34.1 (CH_2, e), 43.5 (CH_2, f), 44.5 (CH_2, d), 49.9 (CH_2, i), 119.0 (CH, c), 129.1 (CH, b), 137.4 (CH, a), 157.6 (C, g). **IR** (film between NaCl plates, $\tilde{\nu}$[cm^{-1}]): 3103 w (ν(C-$H_{arom.}$)), 2933 m (ν(C-$H_{aliph.}$)), 2839 m (ν(C-$H_{aliph.}$)), 1658 vs (ν(C=N)), 1506 m, 1483 m, 1446 m, 1414 m, 1383 m, 1279 m, 1265 m, 1228 m, 1200 m, 1109 m, 1076 m. **EI-MS** (m/z, (%)): 221 (20) [M^+], 153 (20) [M^+ - $C_3H_3N_2$ -H], 140 (75) [M^+ - $CH_3NCH_2CH_2NCH_3$ +H], 127 (52) [M^+ - $C_5H_{10}N_2$ +2H], 126 (100) [M^+ - $C_5H_{10}N_2$ +H], 124 (28) [M^+ - $C_5H_{10}N_2$ -H], 98 (30) [$C_5H_{10}N_2^+$ +2H], 82 (16) [$CH_3NCH_2CH_2NCH_3^+$], 69 (22) [$C_3H_3N_2^+$ +2H], 56 (33), 42 (31).

2-(3-(1H-imidazol-1-yl)propyl)-1,1,3,3-tetramethylguanidine (TMGimi, 24):

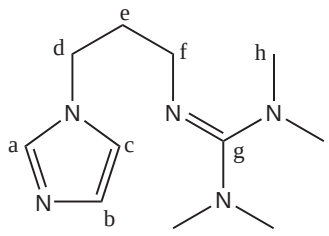

$\mathbf{C_{11}H_{21}N_5}$ (M = 223.32 g/mol): Yellow oil; **Yield**: 6.30 g = 28.2 mmol = 94 %. ^{1}**H-NMR** (500 MHz, $CDCl_3$, 25 °C): δ [ppm] = 2.01 (m, 2H, e), 2.71 (s, 6H, h), 2.73 (s, 1H, h'), 2.74 (s, 5H, h"), 3.06 (t, 2H, f, ^3J = 6.3 Hz), 4.06 (t, 2H, d, ^3J = 6.8 Hz), 6.86 (s, 1H, c), 7.02 (s, 1H, b), 7.38 (s, 1H, a). ^{13}**C-NMR** (125 MHz, $CDCl_3$, 25 °C): δ [ppm] = 32.8 (CH_2, e), 39.3 (CH_3, h+h'), 39.6 (CH_3, h), 44.6 (CH_2, d), 44.8 (CH_2, f), 118.9 (CH, c), 129.3 (CH, b), 137.2 (CH, a), 161.0 (C, g). **IR** (film between NaCl plates, $\tilde{\nu}$[cm^{-1}]): 3105 w (ν(C-$H_{arom.}$)), 2995 w (ν(C-$H_{arom.}$)), 2931 m (ν(C-$H_{aliph.}$)), 2875 m (ν(C-$H_{aliph.}$)), 2804 w (ν(C-$H_{aliph.}$)), 1612 vs (ν(C=N)), 1504 m, 1452 m, 1404 w, 1371 s, 1315 w, 1281 w, 1230 m, 1136 m, 1109 m. **EI-MS** (m/z, (%)): 223 (6) [M^+], 179 (14) [M^+ - $N(CH_3)_2$], 142 (20) [$CH_2CH_2N{=}C(N(CH_3)_2)_2^+$], 116 (83) [$N{=}C(N(CH_3)_2)_2^+$ +2H], 114 (30) [$N{=}C(N(CH_3)_2)_2^+$], 109 (34) [M^+ - $N{=}C(N(CH_3)_2)_2$], 85 (30) [$C(NCH_3)N(CH_3)_2^+$], 72 (100) [$N{=}CN(CH_3)_2^+$ +2H], 71 (67) [$N{=}CN(CH_3)_2^+$ +H], 57 (18) [$CN(CH_3)_2^+$ +H], 44 (78) [$N(CH_3)_2^+$].

N-(1,3-dimethylimidazolidin-2-ylidene)-1-(thiophen-2-yl)methanamine (DMEGthio, 25):

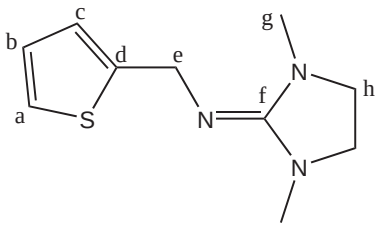

$C_{10}H_{15}N_3S$ (M = 209.50 g/mol): Yellow oil, **Yield**: 5.59 g = 26.7 mmol = 89 %. ^{1}**H-NMR** (500 MHz, $CDCl_3$, 25 °C): δ [ppm] = 2.84 (s, 6H, g), 3.16 (s, 6H, h), 4.80 (s, 2H, e), 6.88 (m, 1H, c), 6.92 (m, 1H, b), 7.11 (m, 1H, a). ^{13}**C-NMR** (125 MHz, $CDCl_3$, 25 °C): δ [ppm] = 36.2 (CH_3, g), 46.7 (CH_2, e), 49.4 (CH_2, h), 121.6 (CH, c), 123.0 (CH, a), 126.4 (CH, b), 149.4 (C, d), 158.0 (C, f). **IR** (film between NaCl plates, $\tilde{\nu}$[cm^{-1}]): 3099 w (ν(C-$H_{arom.}$)), 3064 w (ν(C-$H_{arom.}$)), 3041 w (ν(C-$H_{arom.}$)), 2935 m (ν(C-$H_{aliph.}$)), 2846 m (ν(C-$H_{aliph.}$)), 1655 s (ν(C=N)), 1647 s (ν(C=N)), 1560 w, 1535 w, 1483 m, 1439 m, 1414 m, 1387 m, 1321 m, 1281 s, 1267 s, 1230 m, 1200 m, 1167 m, 1140 m, 1119 m, 1066 s, 1018 s. **EI-MS** (m/z, (%)): 210 (34) [M^+: $C_9{}^{13}CH_{15}N_3S$], 209 (100) [M^+: $C_{10}H_{15}N_3S$], 208 (92), 176 (18), 126 (36) [$C_6H_{12}N_3^+$], 125 (81), 124 (22) [$C_6H_5NS^+$ +H], 113 (28), 112 (46) [$C_5H_{10}N_3^+$], 98 (69) [$C_5H_{10}N_2^+$], 97 (92) [$C_5H_5S^+$], 70 (72), 69 (26), 57 (22) [$C_3H_7N^+$], 56 (34), 55 (34).

1,1,3,3-tetramethyl-2-(thiophen-2-ylmethyl)guanidine (TMGthio, 26):

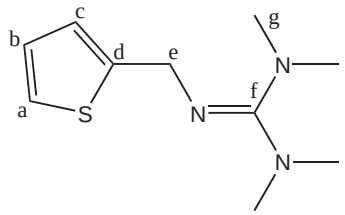

$C_{10}H_{17}N_3S$ (M = 211.52 g/mol): Yellow oil; **Yield**: 6.03 g = 28.5 mmol = 95 %. ^{1}**H-NMR** (500 MHz, $CDCl_3$, 25 °C): δ [ppm] = 2.73 (s, 6H, g), 2.76 (s, 6H, g'), 4.53 (s, 2H, e), 6.86 (m, 1H, c), 6.91 (m, 1H, b), 7.10 (m, 1H, a). ^{13}**C-NMR** (125 MHz, $CDCl_3$, 25 °C): δ [ppm] = 38.9 (CH_3, g), 39.6 (CH_3, g'), 48.7 (CH_2, e), 121.6 (CH, c), 122.9 (CH, a), 126.4 (CH, b), 149.2 (C, d), 161.0 (C, f). **IR** (KBr, $\tilde{\nu}$[cm^{-1}]): 3064 vw (ν(C-$H_{arom.}$)), 2997 vw (ν(C-$H_{aliph.}$)), 2918 w (ν(C-$H_{aliph.}$)), 2871 w (ν(C-$H_{aliph.}$)), 2841 w (ν(C-$H_{aliph.}$)), 2806 w (ν(C-$H_{aliph.}$)), 1614 vs (ν((ν(C=N)), 1498 m, 1452 m, 1437 m, 1404 m, 1369 s, 1308 m, 1236 m, 1134 s, 1109 w, 1063 m, 1039 w, 1003 m, 968 m, 912 m, 897 vw, 852 m, 897 vw, 852 m, 816 w, 766 w, 692 s, 615 vw, 598 vw, 561 w. **EI-MS** (m/z, (%)): 211 (84) [M^+], 196 (31) [M^+ - CH_3], 167 (72) [M^+ - $N(CH_3)_2$], 166 (91) [M^+ - $N(CH_3)_2$ -H], 151 (83) [M^+ - $N(CH_3)_2$ - CH_3 -H], 124 (62) [M^+ - 2 $N(CH_3)_2$ +H], 100 (55) [$C(N(CH_3)_2)_2^+$], 99 (54), 98 (74), 97 (100) [$C_5H_5S^+$ +2H], 85 (80) [$C_4H_3S^+$ +2H, $C(NCH_3)N(CH_3)_2^+$], 71 (81) [$N{=}CN(CH_3)_2^+$ +H], 53 (59), 44 (65) [$N(CH_3)_2^+$].

2,6-bis[bis(2-Aminoethyl)1,3-dimethylimidazolidin-2-ylidene]methylbenzol ($DMEG_4(baem)_2b$, 27):

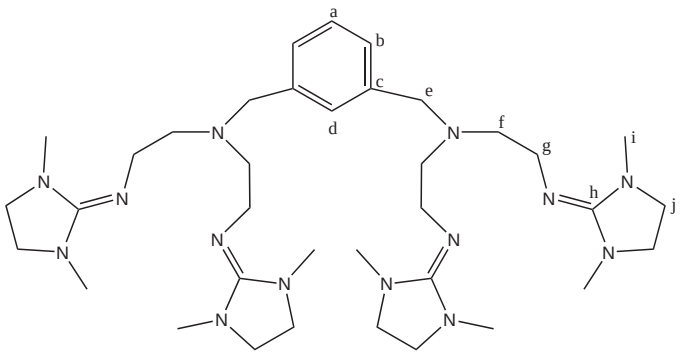

$C_{36}H_{64}N_{14}$ (M = 692.99 g/mol): Yellow oil; **Yield**: 18.92 g = 27.3 mmol = 91 %. ^{1}**H-NMR** (500 MHz, $CDCl_3$, 25 °C): δ [ppm] = 2.72 (m, 24+8H, i+f), 3.11 (m, 16H, j), 3.49 (m, 8H, g), 3.70 (m, 4H, e), 7.20 (m, 4H, a+b+d). ^{13}**C-NMR** (125 MHz, $CDCl_3$, 25 °C): δ [ppm] = 39.9 (CH_3, i), 49.4 (CH_2, j), 46.4 (CH_2, g), 58.1 (CH_2, f), 60.1 (CH_2, e), 127.0 (CH, b), 128.1 (CH, a), 129.2 (CH, d), 140.5 (C, c), 157.4 (C, h). **IR** (film between NaCl plates, $\tilde{\nu}$[cm^{-1}]): 3352 m (ν(C-$H_{arom.}$)), 3294 m (ν(C-$H_{arom.}$)), 2933 s (ν(C-H aliph.)), 2835 s (ν(C-$H_{aliph.}$)), 1662 vs (ν(C=N)), 1483 m, 1441 m, 1414 m, 1383 m, 1265 s, 1198 m, 1138 m, 1120 m, 1066 m, 1018 s. **EI-MS** (m/z, (%)): 693 (9) [M^+], 596 (24) [M^+ - $C_5H_{10}N_2$ +H], 566 (38) [M^+ - $C_6H_{12}N_3^+$ -H], 500 (22) , 483 (55) [M^+ - $C_5H_{10}N_2$ - $C_5H_{10}N_3$], 471 (70) , 470 (91) [M^+ - 2 $C_5H_{10}N_3$ +H], 466 (26), 456 (20), 453 (16), 440 (10) [M^+ - 2 $C_6H_{12}N_3^+$ -H], 427 (29), 397 (9), 387 (13), 374 (79), 360 (10), 357 (27), 331 (12), 301 (22), 286 (6), 272 (12), 198 (8), 182 (6), 169 (25), 167 (10), 149 (88), 127 (51) [$C_6H_{12}N_3^+$ +H], 126 (100) [$C_6H_{12}N_3^+$], 114 (17) [$C_5H_{10}N_3^+$ +2H], 105 (18), 98 (10) [$C_5H_{10}N_2^+$], 70 (10) [$CH_2CH_2NCH_2CH_2^+$], 56 (30).

2,6-bis[bis(2-Aminoethyl)tetramethyl-guanidino]methylbenzol ($TMG_4(baem)_2b$, 28):

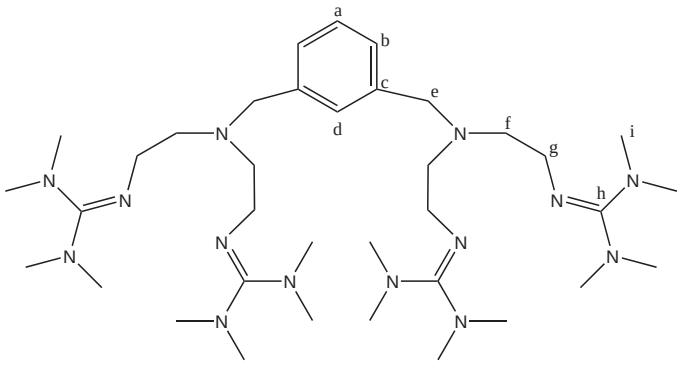

$C_{36}H_{72}N_{14}$ (M = 701,06 g/mol): Orange coloured oil; **Yield**: 18.30 g = 26.1 mmol = 87 %. ^{1}**H-NMR** (500 MHz, $CDCl_3$, 25 °C): δ [ppm] = 2.62 (m, 48+8H, i+f), 3.17 (m, 8H, g), 3.57 (s, 4H, e), 7.11 (m, 4H, a+b+d). ^{13}**C-NMR** (125 MHz, $CDCl_3$, 25 °C): δ [ppm] = 38.5 (CH_3, i), 38.9 (CH_3, i'), 39.2 (CH_3, i"), 39.6 (CH_3, i'"), 47.9 (CH_2, g), 57.3 (CH_2, f), 59.8 (CH_2, e), 127.0 (CH, b), 128.1 (CH, a), 129.1 (CH, d), 140.3 (C, c), 160.3 (C, h). **IR** (KBr, $\tilde{\nu}$[cm^{-1}]): 2997 m (ν(C-$H_{arom.}$)), 2929 m (ν(C-$H_{aliph.}$)), 2891 m (ν(C-$H_{aliph.}$)), 2841 m (ν(C-$H_{aliph.}$)), 2802 m (ν(C-$H_{aliph.}$)), 1616 vs (ν(C=N)), 1496 m, 1452 m, 1404 m, 1369 m, 1313 w, 1236 w, 1132 m, 1063 w, 993 w, 912 w, 796 vw, 746 w, 704 w, 669 vw, 592 w. **EI-MS** (m/z, (%)): 702 (21) [M^+], 701 (52) [M^+], 586 (9) [M^+ - $HN(C(N(CH_3)_2)_2)$], 573 (70) [M^+ - $CH_2N(C(N(CH_3)_2)_2)$], 572 (100) [M^+ - $CH_3N(C(N(CH_3)_2)_2)$], 558 (16), 470 (19), 457 (49), 432 (15), 401 (15) [M^+ - 3 $C(N(CH_3)_2)$], 274 (16), 142 (77), 128 (54) [$CH_2N(C(N(CH_3)_2)_2)^+$], 85 (96), 77 (23) [$C_6H_5^+$], 58 (30) [$C(N(CH_3)_2^+$ +2H].

2',2',2"-(2,2',2"-nitrilotris(ethane-2,1-diyl))tris(1,1,3,3-tetraethylguanidine) (TEG_3tren, 31):

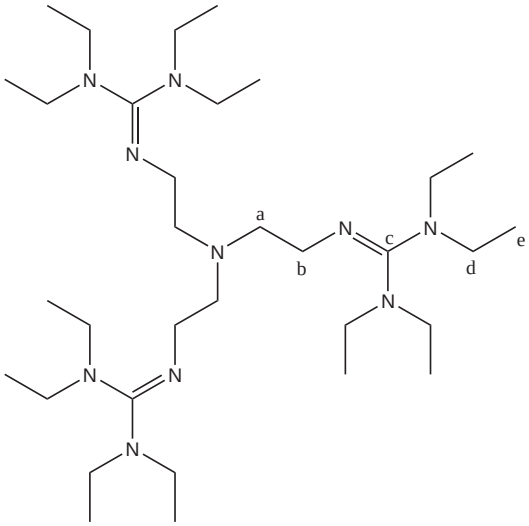

$\mathbf{C_{33}H_{72}N_{10}}$ (M = 609.00 g/mol): Yellow oil; **Yield**: 11.69 g = 19.2 mmol = 64 %. ^{1}**H-NMR** (500 MHz, $CDCl_3$, 25 °C): δ [ppm] = 1.00 (6, t, 36H, e, ^3J = 7.1 Hz), 2.72 (m, 6H, a), 3.02 (6, q, 12H, d, ^3J = 7.1 Hz), 3.10 (6, q, 12H, d', ^3J = 7.1 Hz), 3.25 (m, 6H, b). ^{13}**C-NMR** (125 MHz, $CDCl_3$, 25 °C): δ [ppm] = 13.0 (CH_3, e), 13.8 (CH_3, e'), 41.6 (CH_2, d'), 42.6 (CH_2, d), 48.6 (CH_2, b), 58.2 (CH_2, a), 158.4 (C, c). **IR** (film between NaCl plates, $\tilde{\nu}$[cm^{-1}]): 2966 s (ν(C-$H_{aliph.}$)), 2929 m (ν(C-$H_{aliph.}$)), 2868 m (ν(C-$H_{aliph.}$)), 1612 vs (ν(C=N)), 1460 m, 1402 m, 1375 m, 1358 m, 1338 m, 1302 m, 1261 s, 1219 m, 1205 m, 1130 m, 1068 s. **EI-MS** (m/z, (%)): 610 (4) [M^+], 438 (10) [M^+ - $C_9H_{20}N_3$ - H], 424 (97) [M^+ - $C_{10}H_{22}N_3$ - H], 266 (97), 253 (10), 240 (13), 198 (48) [$C_{11}H_{24}N_3^+$], 184 (72) [$C_{10}H_{22}N_3^+$], 168 (33), 156 (29) [$C_9H_{20}N_2^+$], 154 (11), 127 (24), 113 (100), 100 (13) [$N(CH_2CH_2)_3^+$ +2H], 99 (13) [$N(CH_2CH_2)_3^+$ +H], 86 (22), 72 (18) [$C_4H_{10}N^+$], 57 (11).

11.3.2 Synthesis of zinc(II) complexes

The zinc (II) complexes [Zn(DMEG$_2$e)Cl$_2$] (**1a**),[101,204] [Zn(DMEG$_2$e)(CH$_3$COO)$_2$] (**1b**),[101,204] [Zn(DMEG$_2$e)$_2$][CF$_3$SO$_3$]$_2$ (**1c**),[101,204] [Zn(btmgp)Cl$_2$] (**2a**),[107] [Zn(DMEGqu)Cl$_2$] (**6a**),[101,205] [Zn(DMEGqu)(CH$_3$COO)$_2$] (**6b**),[101,205] [Zn(TMGqu)Cl$_2$] (**7a**),[101,205] [Zn(TMGqu)(CH$_3$COO)$_2$] (**7b**),[101,205] [Zn(DMEGpy)Cl$_2$] (**14a**),[101,205] [Zn(DMEGpy)(CH$_3$COO)$_2$] (**14b**),[101,205] [Zn(bipy)Cl$_2$] (**33a**)[149] and [Zn(phen)Cl$_2$] (**34a**)[150] were prepared according to literature procedures.

General synthesis of zinc complexes with guanidine ligands:

A solution of the ligand (1.1 mmol) in dry MeCN or THF was added to a suspension of the zinc compound (1 mmol, 0.5 mmol or less, depending on the molar ratio given in the complex) in a dry aprotic solvent (MeCN, THF) with stirring. The resulting reaction mixture was stirred for 20 min or longer. In the case of a clear solution, single crystals could be obtained by diffusion of diethyl ether, diisopropyl ether or pentane. When the complex precipitated, the reaction mixture was slowly heated under reflux to give a clear solution. Single crystals could be obtained by slowly cooling to room temperature.

[Zn(DMEG$_2$e)(C$_6$H$_5$COO)$_2$] (1d):

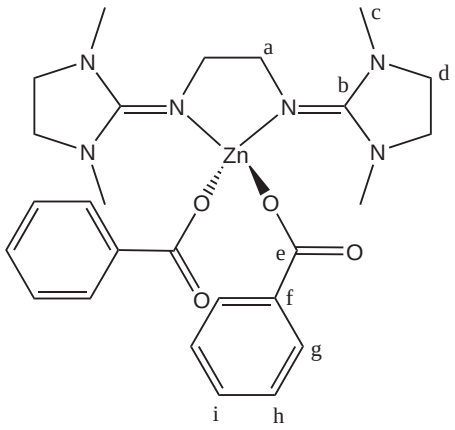

C$_{26}$H$_{34}$N$_6$O$_4$Zn (M = 559.98 g/mol): Colourless crystals; **Yield**: 0.190 g = 0.34 mmol = 34 %; **m.p.** 138°C. ^{1}**H-NMR** (500 MHz, CD_3CN, 25 °C): δ [ppm] = 2.96 (s, 12H, c), 3.24 (s, 8H, d), 3.57 (s, 4H, a), 7.40 (m, 4H, h), 7.46 (m, 2H, i), 8.00 (m, 4H, g). ^{13}**C-NMR** (125 MHz, CD_3CN, 25 °C): δ [ppm] = 35.5 (CH_3, c), 49.4 (CH_2, d), 49.7 (CH_2, a), 127.7 (CH, h), 129.3 (CH, g), 130.2 (CH, i), 137.2 (C, f), 164.3 (C, b), 170.8 (C, e). **IR** (KBr, $\tilde{\nu}$[cm^{-1}]): 3076 w (ν(C-H$_{arom.}$)), 3058 w (ν(C-H$_{arom.}$)), 3032 w (ν(C-H$_{arom.}$)), 2937 m (ν(C-H$_{aliph.}$)), 2866 m (ν(C-H$_{aliph.}$)), 1631 vs (ν(C=N)), 1585 s (ν(C=N)), 1506 m, 1489 m, 1448 m, 1423 m, 1402 m, 1354 vs, 1292 m, 1236 m, 1173 w, 1130 w, 1093 w, 1066 w, 1053 w, 1024 w, 982 vw, 943 vw, 918 m, 864 vw, 837 w, 793 vw, 766 w, 733 m, 725 m, 696 vw, 679 m, 650 vw, 606 w, 571 vw. **EI-MS** (m/z, (%)): 437 (68) [M$^+$ - $C_7H_5O_2$], 351 (8), 315 (12) [M$^+$ - 2 $C_7H_5O_2$ -H], 298 (6), 251 (18) [M$^+$ - Zn($C_7H_5O_2$) -H], 140 (19) [$C_7H_{14}N_3^+$], 139 (26) [$C_7H_{14}N_3^+$ -H], 127 (70) [$C_6H_{12}N_3^+$ +H], 126 (100) [$C_6H_{12}N_3^+$], 124 (26), 122 (30) [$C_7H_5O_2^+$ +H], 105 (46), 98 (13) [$C_5H_{10}N_2^+$], 77 (27), 70 (14) [$CCH_2CH_2N^+$ +2H], 69 (14) [$CCH_2CH_2N^+$ +H], 56 (45) [$NCH_2CH_2N^+$]. **CHN analysis**: calculated: C 55.72, H 6.07, N 15.00; found: C 55.08, H 5.92, N 14.92.

[Zn(TMG$_2$e)Cl$_2$] (2a):

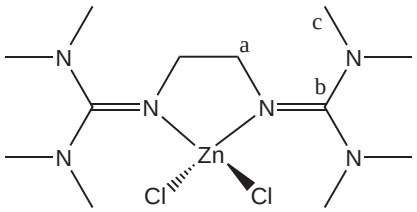

C$_{12}$H$_2$8N$_6$Cl$_2$Zn (M = 392.70 g/mol): Colourless crystals; **Yield**: 0.380 g = 0.97 mmol = 97 %; **m.p.** 284°C. ^{1}**H-NMR** (500 MHz, $CDCl_3$, 25° C) δ [ppm] = 2.82 (s, 12H, c), 2.94 (s, 12H, c'), 3.22 (s, 4H, a). ^{13}**C-NMR** (125 MHz, $CDCl_3$, 25° C) δ [ppm] = 39.8 (CH_3, c), 39.9 (CH_3, c'), 49.8 (CH_2, a), 165.0 (C, b). **IR** (KBr, $\tilde{\nu}$[cm^{-1}]): 3005 w (ν(C-H$_{aliph.}$)), 2981 w (ν(C-H$_{aliph.}$)), 2947 m (ν(C-H$_{aliph.}$)), 2900 m (ν(C-H$_{aliph.}$)), 2852 m (ν(C-H$_{aliph.}$)), 2823 w (ν(C-H$_{aliph.}$)), 2804 w (ν(C-H$_{aliph.}$)),1568 vs (ν(C=N)), 1525 s (ν(C-H)), 1477 m, 1463 m, 1442 m, 1427 m, 1392 s (ν(C-H)), 1344 m, 1327 m, 1242 m, 1211 w, 1157 m, 1122 m, 1082 m, 1068 m, 1045 m, 1018 m, 964 vw, 916 w, 895 m, 806 w, 779 w, 768 m, 737 w, 594 w, 579 vw, 552 vw. **EI-MS** (m/z, (%)): 392 (6) [M$^+$], 357 (9) [M$^+$ -^{35}Cl], 355 (19) [M$^+$ -^{37}Cl], 243 (66), 165 (26), 142 (24), 128 (100) [$CH_2N{=}CN_2(CH_3)_4^+$ -2H], 85 (92) [$CN_3(CH_3)_2^+$ +H]. **CHN analysis**: calculated: C 36.67, H 7.13, N 21.39; found: C 36.63, H 7.17, N 21.36.

[Zn(TMG$_2$e)(CH$_3$COO)$_2$] (2b):

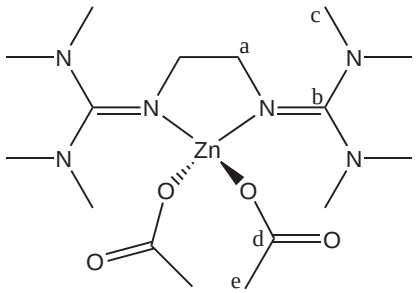

C$_{16}$H$_{34}$N$_6$O$_4$Zn (M = 439.87 g/mol): Colourless crystals; **Yield**: 0.230 g = 0.52 mmol = 52 %; **m.p.** 139°C. ^{1}**H-NMR** (500 MHz, CD$_3$CN, 25° C) δ [ppm] = 1.76 (s, 6H, e), 2.84 (s, 24H, c), 3.22 (s, 4H, a). ^{13}**C-NMR** (125 MHz, CD$_3$CN, 25° C) δ [ppm] = 22.8 (CH$_3$, e), 38.2 (CH$_3$, c), 38.7 (CH$_3$, c'), 49.9 (CH$_2$, a), 164.6 (C, b), 175.3 (C, d). **IR** (KBr, $\tilde{\nu}$[cm^{-1}]): 3001 m (ν(C-H$_{aliph.}$)), 2954 m (ν(C-H$_{aliph.}$)), 2816 w (ν(C-H$_{aliph.}$)), 1628 vs (ν(C=N)), 1581 vs, 1518 m, 1475 m, 1460 m, 1431 s, 1408 vs, 1338 m, 1317 m, 1254 w, 1236 m, 1226 m, 1169 m, 1120 vw, 1107 vw, 1068 w, 1045 m, 1011 m, 957 vw, 922 w, 906 m, 895 w, 881 vw, 864 vw, 768 m, 717 m, 669 m, 648 m, 617 m, 521 w. **EI-MS** (m/z, (%)): 379 (41) [M$^+$ - CH$_3$COO], 319 (8) [M$^+$ - 2 CH$_3$COO], 266 (12), 264 (22), 142 (16) [C$_7$H$_{16}$N$_3^+$], 128 (65) [C$_6$H$_{14}$N$_3^+$], 85 (100) [CN$_3$(CH$_3$)$_2^+$ +H], 84 (14) [CN$_3$(CH$_3$)$_2^+$], 71 (15). **CHN analysis**: calculated: C 43.65, H 7.73, N 19.10; found: C 42.96, H 7.51, N 18.99.

[Zn(btmgp)(CH$_3$COO)$_2$] (3b):

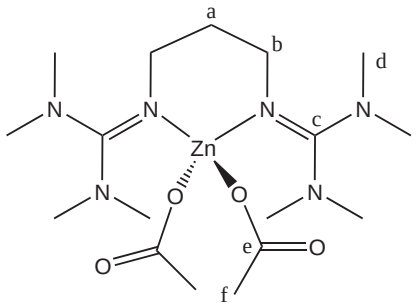

C$_{17}$H$_3$6N$_6$O$_4$Zn (M = 453.89 g/mol): Colourless crystals; **Yield**: 0.580 g = 0.89 mmol = 89 %. ^{1}**H-NMR** (500 MHz, CD$_3$CN, 25 °C): δ [ppm] = 1.78 (s, 6H, f), 1.94 (m, 2H, a), 2.79 (s, 12H, d), 2.81 (s, 12H, d'), 3.38 (t, 4H, b, ^{3}J = 5.2 Hz). ^{13}**C-NMR** (125 MHz, CD$_3$CN, 25 °C): δ [ppm] = 23.3 (CH$_3$, f), 31.9 (CH$_2$, a), 38.3 (CH$_3$, d), 39.0 (CH$_3$, d'), 50.9 (CH$_2$, b), 165.7 (C, c), 174.9 (C, e). **IR** (KBr, $\tilde{\nu}$[cm^{-1}]): 2364 w (ν(C-H$_{aliph.}$)), 2345 w (ν(C-H$_{aliph.}$)), 1620 vs (ν(C=N)), 1585 vs (ν(C=N)), 1508 w, 1473 m, 1458 m, 1431 m, 1404 s, 1340 w, 1238 vw, 1213 vw, 1173 vw, 1151 vw, 1117 vw, 1068 vw, 1016 vw, 899 vw, 852 vw, 669 w, 650 w, 619 vw. MI-MS (m/z, (%)): 393 (11) [M$^+$ -CH$_3$COO], 270 (44) [M$^+$ -Zn(CH$_3$COO)$_2$], 226 (14) [M$^+$ -Zn(CH$_3$COO)$_2$ - N(CH$_3$)$_2$], 156 (35) [CH$_2$CH$_2$CH$_2$N=C(N(CH$_3$)$_2$)$_2$)$^+$], 142 (44) [CH$_2$CH$_2$N=C(N(CH$_3$)$_2$)$_2$)$^+$], 139 (32) [M$^+$ -Zn(CH$_3$COO)$_2$ - 3 N(CH$_3$)$_2$ +H], 111 (46), 100 (20) [C(N(CH$_3$)$_2$)$_2$)$^+$], 85 (51) [C(N(CH$_3$)$_2$)$_2$)$^+$ -CH$_3$], 71 (44). **CHN analysis**: calculated: C 44.94, H 7.93, N 18.51; found: C 42.45, H 8.31, N 17.97.

[Zn(8MeBL)Cl$_2$] (5a):

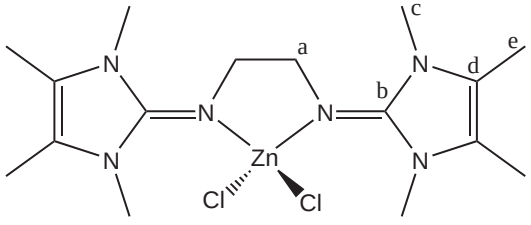

C$_{16}$H$_{28}$Cl$_2$N$_6$Zn (M = 440.74 g/mol): Colourless crystals; **Yield**: 0.405 g = 0.92 mmol = 92 %; **m.p.** 261°C. ^{1}**H-NMR** (500 MHz, CD$_3$CN, 25 °C): δ [ppm] = 2.03 (s, 12H, e), 3.45 (s, 12H, c), 3.62 (s, 4H, a). ^{13}**C-NMR** (125 MHz, CD$_3$CN, 25 °C): δ [ppm] = 8.0 (CH$_3$, e), 31.0 (CH$_3$, c), 50.7 (CH$_2$, a), 153.3 (C, d), 155.1 (C, b). **IR** (KBr, $\tilde{\nu}$[cm^{-1}]):

2981 w (ν(C-$H_{aliph.}$)), 2937 m (ν(C-$H_{aliph.}$)), 2916 m (ν(C-$H_{aliph.}$)), 2848 m (ν(C-$H_{aliph.}$)), 1577 vs (ν(C=N)), 1477 m, 1444 m, 1425 m, 1402 m, 1363 m, 1350 m, 1333 m, 1261 w, 1213 w, 1124 m, 1084 w, 1028 w, 987 vw, 949 w, 883 w, 846 vw, 822 vw, 717 w, 690 w, 669 w, 611 w, 602 w, 563 w. **EI-MS** (m/z, (%)): 442 (11) [M^+: $C_{16}H_{28}{}^{35}Cl_2N_6{}^{64}Zn$], 440 (17) [$M^+$: $C_{16}H_{28}{}^{35}Cl_2N_6{}^{66}Zn$, $C_{16}H_{28}{}^{35}Cl^{37}ClN_6{}^{64}Zn$], 438 (14) [$M^+$: $C_{16}H_{28}{}^{35}Cl^{37}ClN_6{}^{66}Zn$, $C_{16}H_{28}{}^{37}Cl_2N_6{}^{64}Zn$, $C_{16}H_{28}{}^{35}Cl_2N_6{}^{68}Zn$], 407 (11) [$M^+$ -Cl], 405 (19) [M^+ -Cl], 403 (17) [M^+ -Cl], 303 (17) [$C_{16}H_{28}N_6{}^+$ -H], 165 (11) [$C_9H_{16}N_3{}^+$ -H], 153 (69) [$C_8H_{14}N_3{}^+$ +H], 152 (100) [$C_8H_{14}N_3{}^+$], 124 (27) [$C_7H_{12}N_2{}^+$], 56 (24) [$NCH_2CH_2N^+$]. **CHN analysis**: calculated: C 43.56, H 6.35, N 19.06; found: C 43.58, H 6.37, N 18.92.

[Zn(8MeBL)(CH_3COO)$_2$] (5b):

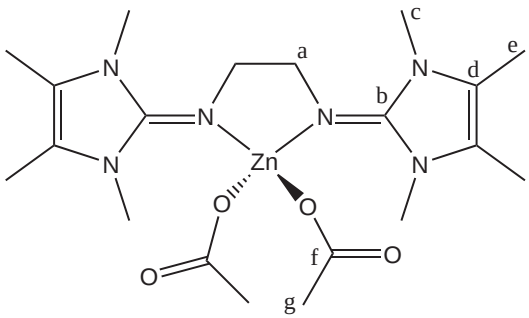

$C_{20}H_{34}N_6O_4Zn$ (M = 487.91 g/mol): Colourless crystals; **Yield**: 0.449 g = 0.92 mmol = 92 %; **m.p.** 162°C. ^{1}**H-NMR** (500 MHz, CD_3CN, 25 °C): δ [ppm] = 1.73 (s, 6H, g), 2.01 (s, 12H, e), 3.36 (s, 12H, c), 3.59 (s, 4H, a). ^{13}**C-NMR** (125 MHz, CD_3CN, 25 °C): δ [ppm] = 8.0 (CH_3, e), 22.8 (CH_3, g), 30.1 (CH_3, c), 50.9 (CH_2, a), 153.7 (C, d), 175.4 (C, b), 199.9 (C, f). **IR** (KBr, $\tilde{\nu}$[cm^{-1}]): 3138 m, 3053 m, 2999 m, 2978 m, 2949 m, 1599 vs (ν(C=N)), 1581 vs (ν(C=N)), 1491 m, 1444 m, 1446 m, 1421 m, 1404 m, 1267 m, 1246 m, 1223 w, 1128 w, 1113 w, 1072 m, 1020 w, 991 w, 955 vw, 918 w, 897 w, 847 w, 766 m, 735 m, 725 m, 706 m, 648 m, 619 m, 596 m, 561 m. **EI-MS** (m/z, (%)): 486 (2) [M^+], 425 (45) [M^+ - CH_3COO -2H], 266 (17), 198 (7) [$C_8H_{18}N_6{}^+$], 184 (7) [$C_7H_{16}N_6{}^+$], 165 (8) [$C_9H_{16}N_3{}^+$ -H], 153 (10) [$C_8H_{14}N_3{}^+$ +H], 152 (100) [$C_8H_{14}N_3{}^+$], 124 (6) [$C_7H_{12}N_2{}^+$], 113 (15) [$C_6H_{13}N_2{}^+$]. **CHN analysis**: calculated: C 49.19, H 6.97, N 17.22; found: C 48.63, H 7.03, N 16.94.

[Zn(DMEGqu)$_2$(CF_3SO_3)][CF_3SO_3] (6c):

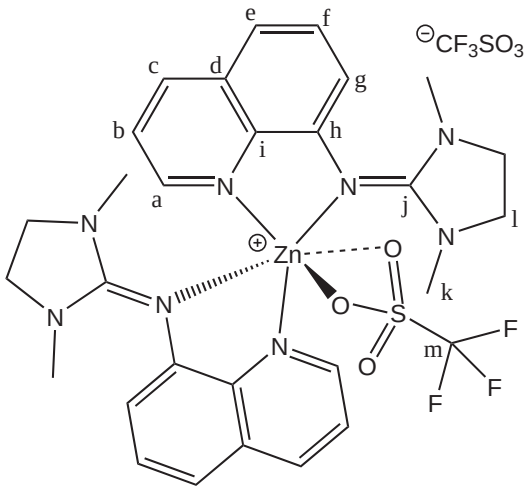

$C_{30}H_{32}N_8O_6F_6S_2Zn$ (M = 845.48 g/mol): Yellow crystals; **Yield**: 0.310 g = 0.37 mmol = 73 %; **m.p.** 234°C. ^{1}**H-NMR** (500 MHz, CD_3CN, 25 °C): δ [ppm] = 2.56 (s, 12H, k), 3.48 (s, 4H, l), 3.72 (s, 4H, l'), 7.16 (dd, 2H, g, ^3J = 7.7 Hz, ^4J = 1.1 Hz), 7.60 (dd, 2H, e, ^3J = 8.2 Hz, ^4J = 1.1 Hz), 7.68 (dd, 2H, f, ^3J = 8.2 Hz, ^3J = 7.7 Hz), 7.85 (dd, 2H, b, ^3J = 8.3 Hz, ^3J = 4.7 Hz), 8.69 (dd, 2H, c, ^3J = 8.3 Hz, ^4J = 1.5 Hz), 8.78 (dd, 2H, a, ^3J = 4.7 Hz, ^4J = 1.5 Hz). ^{13}**C-NMR** (125 MHz, CD_3CN, 25 °C): δ [ppm] = 33.9 (CH_3, k), 47.5 (CH_2, l), 116.2 (CH, g), 118.2 (CH, e), 122.2 (C, m), 122.4 (CH, b), 128.9 (CH, f), 129.7 (C, d), 137.7 (C, i), 141.0 (CH, c), 142.1 (C, h), 148.1

(CH, a), 164.4 (C, j). **IR** (KBr, $\tilde{\nu}$[cm^{-1}]): 3057 vw (ν(C-H$_{arom.}$)), 2960 vw (ν(C-H$_{aliph.}$)), 2935 vw (ν(C-H$_{aliph.}$)), 2889 w (ν(C-H$_{aliph.}$)), 1597 m (ν(C=N)), 1558 s (ν(C=N)), 1504 m, 1468 m, 1419 m, 1396 m, 1327 m, 1302 m, 1267 vs, 1232 m, 1225 m, 1174 m, 1155 m, 1103 w, 1032 s, 1024 s, 976 w, 912 vw, 827 m, 806 w, 789 m, 771 w, 756 w, 692 w, 636 m, 582 w, 573 w, 536 vw, 517 w. **EI-MS** (m/z, (%)): 693 (1) [M$^+$ - CF_3SO_3], 602 (6), 453 (27) [M$^+$ -CF_3SO_3 -$C_{14}H_{16}N_4$], 240 (100) [$C_{14}H_{16}N_4^+$], 183 (20) [$C_{14}H_{16}N_4^+$ -$CH_3NCH_2CH_2$], 169 (18), 155 (63) [$C_{10}H_6N_2^+$ +H], 142 (19) [$C_{14}H_{16}N_4^+$ -$C_5H_{10}N_2$], 129 (33) [$C_9H_6N_2^+$ +H], 98 (75) [$C_5H_{10}N_2^+$]. **CHN analysis**: calculated: C 42.58, H 3.78, N 13.25; found: C 42.66, H 3.89, N 13.17.

[Zn(DMEGqu)(μ-C_6H_5COO)$_3$)Zn(C_6H_5COO)] (6d):

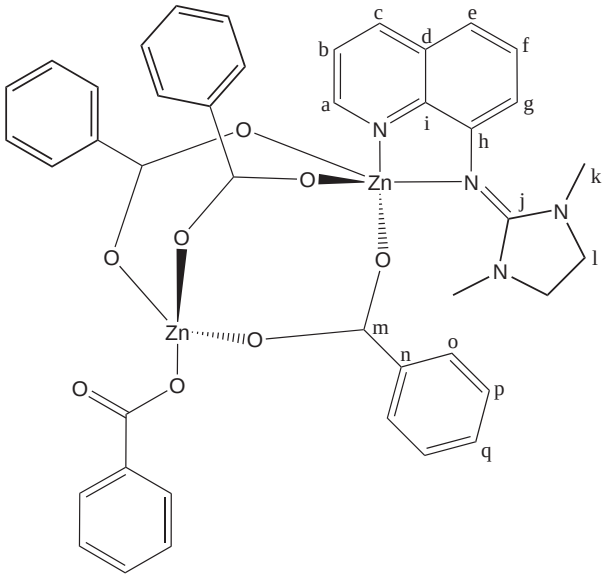

$C_{42}H_{36}N_4O_8Zn_2$ (M = 855.54 g/mol): Yellow crystals; **Yield**: 0.740 g = 0.86 mmol = 86 %; **m.p.** 183°C. ^{1}**H-NMR** (500 MHz, CD_3CN, 25 °C): δ [ppm] = 2.86 (s, 6H, k), 3.30 (s, 2H, l), 3.67 (s, 2H, l'), 7.04 (d, 1H, g, ^{3}J = 7.7 Hz), 7.40 (t, 8H, p, ^{3}J = 7.6 Hz), 7.46 (d, 1H, e, ^{3}J = 8.1 Hz), 7.52 (t, 4H, q, ^{3}J = 7.6 Hz), 7.58 (dd, 1H, f, ^{3}J = 8.1 Hz, 3J = 7.7 Hz), 7.72 (dd, 1H, b, ^{3}J = 8.2 Hz, 3J = 4.0 Hz), 8.02 (d, 8H, o, ^{3}J = 7.6 Hz), 8.53 (d, 1H, c, ^{3}J = 8.2 Hz), 9.18 (d, 1H, a, ^{3}J = 4.0 Hz). ^{13}**C-NMR** (125 MHz, CD_3CN, 25 °C): δ [ppm] = 34.1 (CH_3, k), 47.8 (CH_2, l), 115.8 (CH, g), 117.3 (CH, e), 122.3 (CH, b), 128.1 (CH, p) 128.5 (CH, f), 129.6 (C, d), 129.8 (CH, o) 131.7 (CH, q), 133.9 (C, n), 138.2 (C, i), 139.9 (CH, c), 143.8 (C, h), 148.2 (CH, a), 165.2 (C, j), 173.1 (C, n). **IR** (KBr, $\tilde{\nu}$[cm^{-1}]): 3087 vw (ν(C-H$_{arom.}$)), 3066 w (ν(C-H$_{arom.}$)), 3026 vw (ν(C-H$_{arom.}$)), 2929 w (ν(C-H$_{aliph.}$)), 2891 w (ν(C-H$_{aliph.}$)), 1630 vs (ν(C=N)), 1573 s (ν(C=N)), 1504 m, 1481 m, 1466 m, 1448 m, 1410 vs, 1369 s, 1325 m, 1302 m, 1288 w, 1238 w, 1238 w, 1207 vw, 1171 w, 1157 vw, 1136 vw, 1105 w, 1068 w, 1045 vw, 1026 m, 978 vw, 937 vw, 912 vw, 850 w, 829 w, 814 w, 783 w, 754 vw, 717 s, 688 m, 677 w, 640 vw, 580 vw, 534 vw. **EI-MS** (m/z, (%)): 425 (5) [$C_{21}H_{21}N_4O_2Zn^+$], 240 (100) [$C_{14}H_{16}N_4^+$], 183 (17) [$C_{14}H_{16}N_4^+$ -C_3H_7N], 169 (13), 155 (45) [$C_{14}H_{16}N_4^+$ -$CH_3NCH_2CH_2NCH_3$ +H], 142 (15) [$C_9H_6N_2^+$], 129 (23) [$C_9H_6N^+$ +H], 105 (10), 98 (61) [$C_5H_{10}N_2^+$], 77 (10). **CHN analysis**: calculated: C 58.91, H 4.21, N 6.55; found: C 58.45, H 4.16, N 6.65.

[Zn(DMEGqu)(CH_3SO_3)$_2$] (6e-1):

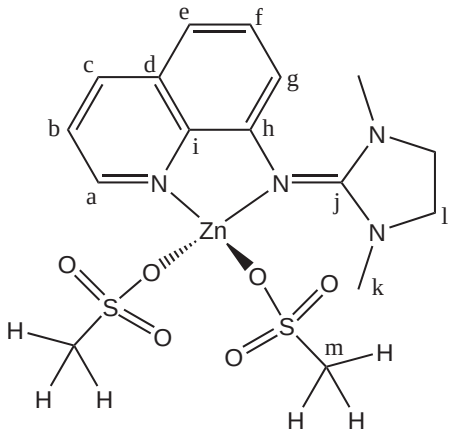

$C_{16}H_{22}N_4O_6S_2Zn$ (M = 496.70 g/mol): Yellow crystals; **Yield**: 0.496 g = 0.99 mmol = 99 %; **m.p.** 185°C. **^{1}H-NMR** (500 MHz, CD_3CN, 25 °C): δ [ppm] = 2.76 (s, 6H, k), 2.88 (s, 6H, m), 3.75 (m, 4H, l), 7.14 (d, 1H, g, ^3J = 7.6 Hz), 7.52 (d, 1H, e, ^3J = 8.1 Hz), 7.61 (dd, 1H, f, ^3J = 8.1 Hz, ^3J = 7.6 Hz), 7.78 (dd, 1H, b, ^3J = 8.3 Hz, ^3J = 4.7 Hz), 8.59 (dd, 1H, c, ^3J = 8.3 Hz, ^4J = 1.3 Hz), 9.00 (dd, 1H, a, ^3J = 4.7 Hz, ^4J = 1.3 Hz). **^{13}C-NMR** (125 MHz, CD_3CN, 25 °C): δ [ppm] = 34.4 (CH_3, m), 38.7 (CH_3, k), 48.1 (CH_2, l), 116.7 (CH, g), 118.2 (CH, e), 122.4 (CH, b), 128.6 (CH, f), 129.4 (C, d), 137.9 (C, i), 140.9 (CH, c), 142.2 (C, h), 148.9 (CH, a), 164.5 (C, j). **IR** (KBr, $\tilde{\nu}$[cm^{-1}]): 3016 vw (ν(C-$H_{arom.}$)), 2933 vw (ν(C-$H_{aliph.}$)), 2889 vw (ν(C-$H_{aliph.}$)), 1595 m (ν(C=N)), 1560 m (ν(C=N)), 1502 m, 1468 m, 1417 m, 1392 m, 1327 m, 1298 w, 1273 w, 1240 m, 1207 s, 1194 vs, 1157 m, 1103 w, 1059 m, 1026 m, 978 vw, 912 vw, 827 w, 806 w, 785 m, 773 m, 696 vw, 669 vw, 638 w, 611 vw, 582 w, 563 m, 536 m, 526 m. **EI-MS** (m/z, (%)): 494 (2) [M^+], 399 (8) [M^+ -CH_3SO_3], 241 (27), 240 (100) [M^+ -Zn(CH_3SO_3)$_2$], 239 (70), 183 (11) [$C_{11}H_9N_3^+$], 155 (27) [$C_{10}H_6N_2^+$ +H], 142 (10) [$C_9H_6N_2^+$], 129 (14) [$C_9H_6N^+$ +H], 98 (42) [$C_5H_{10}N_2^+$]. **CHN analysis**: calculated: C 38.67, H 4.43, N 11.27; found: C 38.84, H 4.56, N 11.33.

[Zn(DMEGqu)$_2$(CH_3SO_3)][CH_3SO_3] (6e-2):

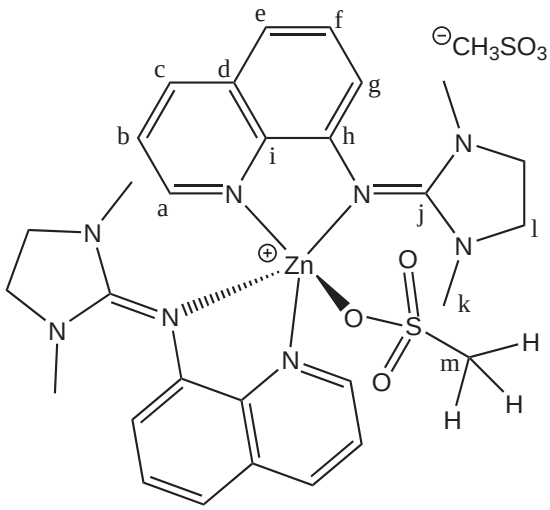

$C_{30}H_{38}N_8O_6S_2Zn$ (M = 737.37 g/mol): Yellow crystals; **Yield**: 0.361 g = 0.49 mmol = 98 %; **m.p.** 268°C. **^{1}H-NMR** (500 MHz, CD_3CN, 25 °C): δ [ppm] = 2.32 (s, 6H, m), 2.47 (b, 12H, k), 3.56 (b, 8H, l), 7.00 (dd, 2H, g, ^3J = 7.6 Hz, ^4J = 1.0 Hz), 7.49 (dd, 2H, e, ^3J = 8.2 Hz, ^4J = 1.0 Hz), 7.60 (dd, 2H, f, ^3J = 8.2 Hz, ^3J = 7.6 Hz), 7.82 (dd, 2H, b, ^3J = 8.3 Hz, ^3J = 4.6 Hz), 8.60 (dd, 2H, c, ^3J = 8.3 Hz, ^4J = 1.5 Hz), 8.89 (dd, 2H, a, ^3J = 4.6 Hz, ^4J = 1.5 Hz). **^{13}C-NMR** (125 MHz, CD_3CN, 25 °C): δ [ppm] = 38.9 (CH_3, m), 47.3 (CH_2, l), 114.8 (CH, g), 117.0 (CH, e), 122.0 (CH, b), 128.7 (CH, f), 129.6 (C, d), 137.8 (C, i), 139.9 (CH, c), 143.2 (C, h), 147.7 (CH, a), 165.1 (C, j). **IR** (KBr, $\tilde{\nu}$[cm^{-1}]): 3109 w (ν(C-$H_{arom.}$)), 3070 w (ν(C-$H_{arom.}$)), 3045 w (ν(C-$H_{arom.}$)), 3008 w (ν(C-$H_{arom.}$)), 2997 w (ν(C-$H_{aliph.}$)), 2962 w (ν(C-$H_{aliph.}$)), 2927 w (ν(C-$H_{aliph.}$)), 2877 w (ν(C-$H_{aliph.}$)), 1558 s (ν(C=N)), 1502 s, 1483 m, 1468 s, 1423 m, 1392 s, 1327 m, 1300 m, 1248 s, 1207 s, 1196 s, 1161 s, 1107 m, 1059 w, 1039 s, 1026 m, 974 w, 910 vw, 829 m, 806 w, 793 m, 773 m ,762

m, 748 m, 694 w, 662 vw, 640 w, 609 vw, 582 w, 550 m, 536 w, 521 m. **EI-MS** (m/z, (%)): 448 (13) [M^+- 2 CH_3SO_3 -$C_5H_{10}N_2$ +2H], 422 (12), 240 (10) [M^+ -$Zn(CH_3SO_3)_2$], 204 (15), 189 (44) [$C_{11}H_{13}N_3^+$ +2H], 174 (13), 146 (98), 145 (59), 131 (42), 123 (100) [$C_6H_{11}N_3^+$ -H], 119 (45), 117 (62) [$C_8H_6N^+$ +H], 115 (31), 105 (18) [$C_7H_4N^+$ +3H], 103 (22) [$C_7H_4N^+$ +H], 91 (35) [$C_6H_3N^+$ +2H], 77 (23) [$C_5H_3N^+$], 57 (16) [$C_3H_7N^+$]. **CHN analysis**: calculated: C 48.82, H 5.15, N 15.19; found: C 48.87, H 5.08, N 15.16.

[Zn(DMEGqu)Br_2] (6f):

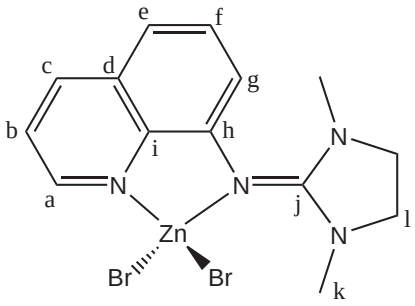

$C_{14}H_{16}N_4ZnBr_2$ (M = 465.51 g/mol): Yellow crystals; **Yield**: 0.430 g = 0.92 mmol = 92 %; **m.p.** 262°C. ^{1}**H-NMR** (500 MHz, CD_3CN, 25 °C): δ [ppm] = 2.91 (s, 6H, k), 3.75 (m, 4H, l), 7.17 (d, 1H, g, ^3J = 7.7 Hz), 7.53 (d, 1H, e, ^3J = 8.1 Hz), 7.63 (dd, 1H, f, ^3J = 8.1 Hz, ^3J = 7.7 Hz), 7.76 (dd, 1H, b, ^3J = 8.3 Hz, ^3J = 4.5 Hz), 8.57 (d, 1H, c, ^3J = 8.3 Hz), 8.81 (dd, 1H, a, ^3J = 4.5 Hz, ^4J = 1.0 Hz). ^{13}**C-NMR** (125 MHz, CD_3CN, 25 °C): δ [ppm] = 35.1 (CH_3, k), 48.2 (CH_2, l), 117.8 (CH, g), 118.5 (CH, e), 122.6 (CH, b), 128.7 (CH, f), 129.6 (C, d), 138.2 (C, i), 140.4 (CH, c), 142.8 (C, h), 147.7 (CH, a), 164.8 (C, j). **IR** (KBr, $\tilde{\nu}$[cm^{-1}]): 3037 m (ν(C-$H_{arom.}$)), 2943 m (ν(C-$H_{aliph.}$)), 2922 m (ν(C-$H_{aliph.}$)), 2879 m (ν(C-$H_{aliph.}$)), 2794 m (ν(C-$H_{aliph.}$)), 1593 m (ν(C=N)), 1552 s (ν(C=N)), 1500 s, 1470 s, 1410 m, 1392 s, 1325 m, 1294 m, 1244 m, 1201 m, 1167 m, 1138 m, 1103 m, 1078 m, 1045 w, 1026 m, 978 m, 943 w, 912 w, 897 vw, 856 w, 827 m, 816 m, 808 m, 779 m, 766 m, 696 m, 665 w, 636 m, 611 w, 579 m, 534 w. **EI-MS** (m/z, (%)): 466 (1) [M^+: $C_{14}H_{16}N_4{}^{79}Br^{81}Br^{66}Zn$, $C_{14}H_{16}N_4{}^{79}Br_2{}^{68}Zn$, $C_{14}H_{16}N_4{}^{81}Br_2{}^{64}Zn$], 464 (1) [$M^+$: $C_{14}H_{16}N_4{}^{79}Br^{81}Br^{64}Zn$, $C_{14}H_{16}N_4{}^{79}Br_2{}^{66}Zn$], 387 (12) [$M^+$ -Br], 385 (21) [M^+ -Br], 383 (13) [M^+ -Br], 241 (22) [M^+ - $ZnBr_2$ +H], 240 (100) [M^+ - $ZnBr_2$], 239 (38) [M^+ -$ZnBr_2$ -H], 193 (4), 183 (6) [M^+ -C_3H_7N -$ZnBr_2$], 169 (5) [$C_{10}H_6N_3^+$ +H], 155 (18) [M^+ -$CH_3NCH_2CH_2NCH_3$ -$ZnBr_2$ +H], 142 (7) [$C_9H_6N_2^+$], 129 (9) [$C_9H_6N^+$ +H], 98 (24) [$C_5H_{10}N_2^+$]. **CHN analysis**: calculated: C 36.10, H 3.44, N 12.03; found: C 36.00, H 3.44, N 12.05.

[Zn(DMEGqu)($C_4H_7O_2$)$_2$)] (6g):

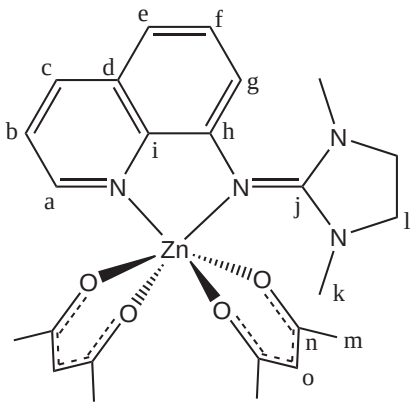

$C_{24}H_{30}N_4O_4Zn$ (M = 503.91 g/mol): Yellow crystals; **Yield**: 0.500 g = 0.99 mmol = 99 %; **m.p.** 199°C. ^{1}**H-NMR** (500 MHz, CD_3CN, 25 °C): δ [ppm] = 1.76 (s, 12H, m), 2.82 (s, 6H, k), 3.47 (s, 2H, l), 3.65 (s, 2H, l'), 5.18 (s, 2H, o), 6.86 (dd, 1H, g, ^3J = 7.8 Hz, ^4J = 1.0 Hz), 7.25 (dd, 1H, e, ^3J = 7.8 Hz, ^4J = 1.0 Hz), 7.45 (t, 1H, f, ^3J = 7.8 Hz, ^3J = 7.8 Hz), 7.54 (dd, 1H, b, ^3J = 8.3 Hz, ^3J = 3.9 Hz), 8.31 (dd, 1H, c, ^3J = 8.3 Hz, ^4J = 1.4 Hz), 8.57 (dd, 1H, a, ^3J = 3.9 Hz, ^4J = 1.4 Hz). ^{13}**C-NMR** (125 MHz, CD_3CN, 25 °C): δ [ppm] = 27.4 (CH_3, m), 34.4 (CH_3, k), 48.0 (CH_2, l), 97.3 (CH, o), 115.0 (CH, g), 115.3 (CH, e), 121.5 (CH, b), 128.0 (CH, f), 129.7 (C, d), 137.9 (CH, c), 138.3 (C, i), 145.3 (C, h), 146.4 (CH, a), 164.6 (C, j), 189.8 (C, n). **IR** (KBr, $\tilde{\nu}$[cm^{-1}]): 3060 w (ν(C-H$_{arom.}$)), 2981 w (ν(C-H$_{aliph.}$)), 2918 m (ν(C-H$_{aliph.}$)), 2873 m (ν(C-H$_{aliph.}$)), 2798 w (ν(C-H$_{aliph.}$)), 1618 vs (ν(C=N)), 1603 vs (ν(C=N)), 1562 vs (ν(C=N)), 1510 vs, 1473 vs, 1415 vs, 1404 s, 1358 m, 1321 m, 1298 m, 1286 m, 1250 m, 1238 m, 1190 m, 1142 w, 1103 w, 1084 w, 1045 w, 1030 m, 1011 m, 976 w, 953 vw, 916 m, 827 m, 812 m, 800 w, 783 w, 750 m, 694 w, 661 w, 652 w, 638 w, 607 vw, 580 w, 546 m. **CI-MS** (m/z, (%)): 483 (16), 481 (43), 403 (11) [M$^+$ - $C_5H_7O_2$], 298 (17), 273 (16), 270 (15), 242 (23) [M$^+$ - Zn($C_5H_7O_2$)$_2$ +2H], 241 (100) [M$^+$ -Zn($C_5H_7O_2$)$_2$ +H], 240 (34) [M$^+$ -Zn($C_5H_7O_2$)$_2$], 201 (11), 157 (8), 101 (58) [$C_5H_7O_2^+$ +2H], 57 (94). **CHN analysis**: calculated: C 57.15, H 5.95, N 11.13; found: C 56.69, H 5.70, N 11.03.

[Zn(DMEGqu)$_2$(BF_4)][BF_4] (6h):

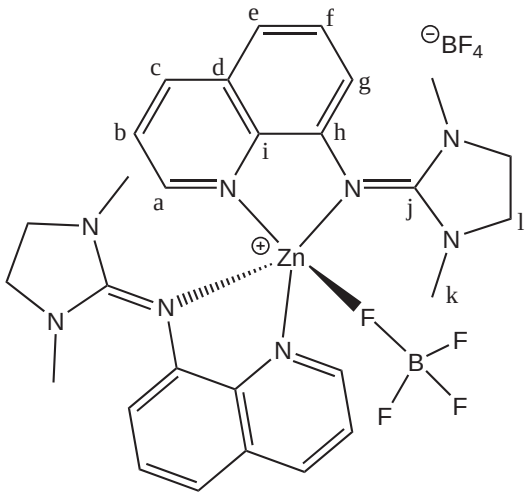

$C_{28}H_{32}N_8F_8B_2Zn$ (M = 719.63 g/mol): Yellow crystals; **Yield**: 0.345 g = 0.48 mmol = 96 %; **m.p.** 278°C. ^{1}**H-NMR** (500 MHz, CD_3CN, 25 °C): δ [ppm] = 2.63 (s, 12H, k), 3.55 (s, 4H, l), 3.72 (s, 4H, l'), 7.19 (dd, 2H, g, ^3J = 7.7 Hz, ^4J = 1.1 Hz), 7.63 (dd, 2H, e, ^3J = 8.2 Hz, ^4J = 1.1 Hz), 7.71 (dd, 2H, f, ^3J = 8.2 Hz, ^3J = 7.7 Hz), 7.85 (dd, 2H, b, ^3J = 8.4 Hz, ^3J = 4.7 Hz), 8.72 (dd, 2H, c, ^3J = 8.4 Hz, ^4J = 1.5 Hz), 8.78 (dd, 2H, a, ^3J = 4.7 Hz, ^4J = 1.5 Hz). ^{13}**C-NMR** (125 MHz, CD_3CN, 25 °C): δ [ppm] = 34.1 (CH_3, k), 47.6 (CH_2, l), 116.7 (CH, g), 118.6 (CH, e), 122.6 (CH, b), 128.9 (CH, f), 129.7 (C, d), 137.8 (C, i), 141.2 (C, h), 141.8 (CH, c), 148.2 (CH, a), 164.3 (C, j). **IR** (KBr, $\tilde{\nu}$[cm^{-1}]): 3066 w (ν(C-H$_{arom.}$)), 3043 w (ν(C-H$_{arom.}$)), 2931 w (ν(C-H$_{aliph.}$)), 2895 w (ν(C-H$_{aliph.}$)), 1567 m (ν(C=N)), 1560 vs (ν(C=N)), 1500 s, 1485 m, 1467 s, 1419 m, 1394 s, 1325 m, 1300 m, 1242 m, 1211 w, 1171 w,1105 s, 1084 s,1065 s, 1038 s, 976 m, 910 vw, 833 m, 806 w, 791 m, 771 m, 762 w, 696 w, 669 vw, 640 w, 584 w, 534 w, 520 w. **EI-MS** (m/z, (%)): 460 (13)

[M^+ -2 BF_4 -$C_4H_{10}N_2$ +2H], 240 (100) [$C_{14}H_{16}N_4^+$], 239 (83), 210 (14), 183 (16) [$C_{11}H_9N_3^+$], 178 (15), 169 (14) [$C_{10}H_6N_3^+$ +H], 165 (22), 155 (48) [$C_{10}H_6N_2^+$ +H], 142 (16) [$C_9H_6N_2^+$], 129 (26) [$C_9H_6N^+$ +H], 98 (56) [$C_5H_{10}N_2^+$]. **CHN analysis**: calculated: C 46.69, H 4.45, N 15.56; found: C 46.4, H 4.5, N 15.2.

[Zn(DMEGqu)(D,L-$C_3H_5O_3$)$_2$)] (6i):

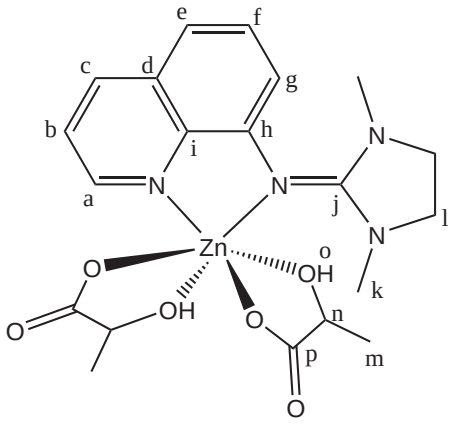

$C_{20}H_{26}N_4O_6Zn$ (M = 483.84 g/mol): Yellow solid; **Yield**: 0.460 g = 0.95 mmol = 95 %; **m.p.** 60°C with decomposition. ^{1}**H-NMR** (500 MHz, CD_3CN, 25 °C): δ [ppm] = 1.23 (d, 6H, m, ^3J = 6.8 Hz), 2.09-2.94 (br, 6H, k), 3.50-3.81 (br, 4H, l), 3.95 (q, 2H, n, ^3J = 6.8 Hz), 4.23-5.71 (br, 2H, o), 7.01 (d, 1H, g, ^3J = 7.5 Hz), 7.43 (d, 1H, e, ^3J = 7.5 Hz), 7.55 (t, 1H, f, ^3J = 7.5 Hz), 7.69 (s, 1H, b), 8.49 (s, 1H, c), 8.81 (m, 1H, a). ^{13}**C-NMR** (125 MHz, CD_3CN, 25 °C): δ [ppm] = 20.6 (CH_3, m), 34.0 (CH_3, k), 47.8 (CH_2, l), 67.3 (CH, n), 117.2 (CH, g), 117.3 (CH, e), 122.1 (CH, b), 128.4 (CH, f), 129.5 (C, d), 138.3 (C, i), 139.6 (CH, c), 144.2 (C, h), 148.3 (CH, a), 165.1 (C, j), 180.2 (C, p). **IR** (KBr, $\tilde{\nu}$[cm^{-1}]): 2970 m (ν(C-$H_{aliph.}$)), 2929 m (ν(C-$H_{aliph.}$)), 2887 m (ν(C-$H_{aliph.}$)), 1653 m, 1595 s (ν(C=N)), 1560 vs (ν(C=N)), 1502 s, 1483 m, 1466 s, 1416 m, 1392 s, 1325 m, 1298 m, 1238 m, 1209 w, 1171 w, 1119 m, 1103 m, 1026 m, 976 w, 926 vw, 910 vw, 856 w, 833 m, 804 w, 789 m, 770 m, 690 m, 667 w, 661 w, 642 m, 606 w, 582 m, 532 w. **EI-MS** (m/z, (%)): 482 (1) [M^+], 471 (2), 440 (3), 254 (15), 240 (100) [$C_{14}H_{16}N_4^+$], 239 (48), 183 (13) [$C_{10}H_6N_4^+$ +H], 170 (14) [$C_{10}H_6N_3^+$ +2H], 155 (27) [$C_{10}H_6N_2^+$ +H], 142 (11) [$C_9H_6N_2^+$], 129 (18) [$C_9H_6N^+$ +H], 120 (40), 119 (79), 98 (37) [$C_5H_{10}N_2^+$], 91 (18) [$C_6H_3N^+$ +2H], 85 (23) [$C_4H_{10}N_2^+$ -H], 77 (12) [$C_5H_3N^+$], 57 (12). **CHN analysis**: calculated: C 49.60, H 5.37, N 11.57; found: C 50.06, H 6.01, N 12.24.

[Zn(TMGqu)$_2$(CF_3SO_3)][CF_3SO_3] (7c):

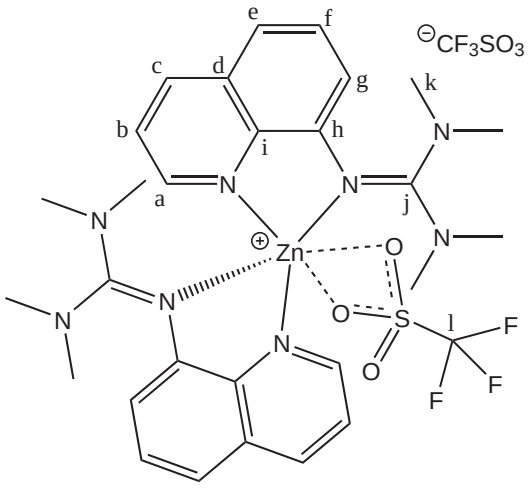

$C_{30}H_{36}N_8O_6F_6S_2Zn$ (M = 849.52 g/mol): Yellow crystals; **Yield**: 0.421 g = 0.49 mmol = 99 %; **m.p.** 225°C. ^{1}**H-NMR** (500 MHz, CD_3CN, 25 °C): δ [ppm] = 2.47 (s, 12H, k), 2.76 (s, 6H, k'), 3.07 (s, 6H, k"), 7.02 (dd, 2H, g, ^3J = 7.5 Hz, ^4J = 1.3 Hz), 7.71 (dd, 2H, e, ^3J = 8.2 Hz, ^4J = 1.3 Hz), 7.75 (dd, 2H, f, ^3J = 8.2 Hz, ^3J = 7.5 Hz), 7.87 (dd, 2H, b, ^3J = 8.4 Hz, ^3J = 4.7 Hz), 8.72 (dd, 2H, c, ^3J = 8.4 Hz, ^4J = 1.5 Hz), 8.75 (dd, 2H, a, ^3J = 4.7 Hz, ^4J = 1.5 Hz). ^{13}**C-NMR** (125 MHz, CD_3CN, 25 °C): δ [ppm] = 39.3 (CH_3, k), 39.7 (CH_3, k'), 40.8 CH_3, k"), 116.8 (CH, g), 119.6 (CH, e), 122.2 (C, l), 122.7 (CH, b), 129.2 (CH, f), 129.6 (C, d), 137.8 (C, i), 140.9 (CH,

c), 142.3 (C, h), 148.7 (CH, a), 165.3 (C, j). **IR** (KBr, $\tilde{\nu}$[cm^{-1}]): 3086 w (ν(C-H$_{arom.}$)), 3057 w (ν(C-H$_{arom.}$)), 3012 w (ν(C-H$_{arom.}$)), 2941 m (ν(C-H$_{aliph.}$)), 2875 m (ν(C-H$_{aliph.}$)), 2808 w (ν(C-H$_{aliph.}$)), 1574 s (ν(C=N)), 1523 vs (ν(C=N)), 1502 s, 1468 s, 1425 s, 1406 s, 1387 s, 1333 s, 1275 vs, 1261 vs, 1161 s, 1103 m, 1061 m, 1030 vs, 920 w, 901 w, 839 m, 806 m, 793 m, 760 m, 702 m, 638 s, 573 m, 542 m, 517 m. **EI-MS** (m/z, (%)): 847 (1) [M$^+$], 697 (1) [M$^+$ -CF_3SO_3], 604 (8), 455 (34) [M$^+$ -CF_3SO_3 -$C_{14}H_{18}N_4$], 329 (2), 325 (6), 266 (3), 242 (100) [M$^+$ -Zn$(CF_3SO_3)_2$], 198 (70) [M$^+$ -Zn$(CF_3SO_3)_2$ -N$(CH_3)_2$], 184 (19), 171 (48), 155 (53), 142 (11) [M$^+$ -Zn$(CF_3SO_3)_2$ -C$(N(CH_3)_2)_2$], 128 (14) [M$^+$ -Zn$(CF_3SO_3)_2$ -C(N)$(N(CH_3)_2)_2$], 100 (43) [C$(N(CH_3)_2)_2^+$], 42 (9). **CHN analysis**: calculated: C 42.38, H 4.24, N 13.18; found: C 42.41, H 4.54, N 13.14.

[Zn(TMGqu)$(C_6H_5COO)_2$] (7d):

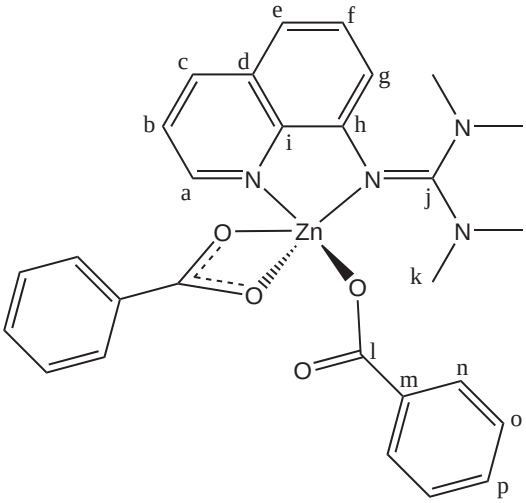

$C_{28}H_{28}N_4O_4Zn$ (M = 549.94 g/mol): Yellow crystals; **Yield**: 0.540 g = 0.99 mmol = 98 %; **m.p.** 180°C. ^{1}**H-NMR** (500 MHz, $CDCl_3$, 25 °C): δ [ppm] = 2.92 (s, 6H, k), 2.99 (s, 6H, k'), 6.74 (dd, 1H, g, ^3J = 7.7 Hz, ^4J = 1.1 Hz), 7.31 (m, 4H, o), 7.39 (m, 2+1H, p+e), 7.48 (dd, 1H, f, ^3J = 7.7 Hz, ^3J = 7.9 Hz), 7.59 (dd, 1H, b, ^3J = 8.4 Hz, ^3J = 4.6 Hz), 8.11 (m, 4H, n), 8.29 (dd, 1H, c, ^3J = 8.4 Hz, ^4J = 1.6 Hz), 9.26 (dd, 1H, a, ^3J = 4.6 Hz, ^4J = 1.6 Hz). ^{13}**C-NMR** (125 MHz, $CDCl_3$, 25 °C): δ [ppm] = 39.7 (CH_3, k), 40.1 (CH_3, k'), 116.0 (CH, g), 118.9 (CH, e), 122.4 (CH, b), 127.5 (CH, o), 128.0 (CH, f), 129.4 (C, d), 130.2 (CH, n), 130.7 (CH, p), 134.6 (CH, m), 138.9 (CH, c), 139.2 (C, i), 144.1 (C, h), 149.2 (CH, a), 165.7 (C, j), 174.3 (C, m). **IR** (KBr, $\tilde{\nu}$[cm^{-1}]): 3062 w (ν(C-H$_{arom.}$)), 3016 w (ν(C-H$_{arom.}$)), 2943 m (ν(C-H$_{aliph.}$)), 2897 w (ν(C-H$_{aliph.}$)), 2868 w (ν(C-H$_{aliph.}$)), 2798 w, 1614 m, 1566 s, 1525 s, 1500 m, 1466 m, 1446 m, 1408 s, 1388 s, 1377 s, 1336 m, 1275 w, 1238 w, 1163 m, 1138 w, 1103 w, 1066 m, 1043 w, 1020 m, 982 vw, 926 w, 903 vw, 854 w, 843 w, 833 m, 818 m, 808 w, 787 m, 754 w, 721 s, 685 m, 656 w, 634 w, 584 w, 540 w. **EI-MS** (m/z, (%)): 427 (6) [M$^+$ -$C_7H_5O_2$], 242 (100) [M$^+$ -Zn$(C_7H_5O_2)_2$], 198 (79) [M$^+$ -Zn$(C_7H_5O_2)_2$ -N$(CH_3)_2$], 184 (36), 183 (18), 182 (20), 171 (39), 157 (34), 155 (85), 143 (18) [M$^+$ -Zn$(C_7H_5O_2)_2$ -C$(N(CH_3)_2)_2$ +H], 142 (17) [M$^+$ -Zn$(C_7H_5O_2)_2$ -C$(N(CH_3)_2)_2$], 129 (28) [M$^+$ -Zn$(C_7H_5O_2)_2$ -N=C$(N(CH_3)_2)_2$ +H], 100 (33) [C$(N(CH_3)_2)_2^+$], 77 (10). **CHN analysis**: calculated: C 61.10, H 5.09, N 10.18; found: C 60.60, H 4.97, N 10.13.

[Zn(TMGqu)$_2$(CH$_3$SO$_3$)][CH$_3$SO$_3$] (7e):

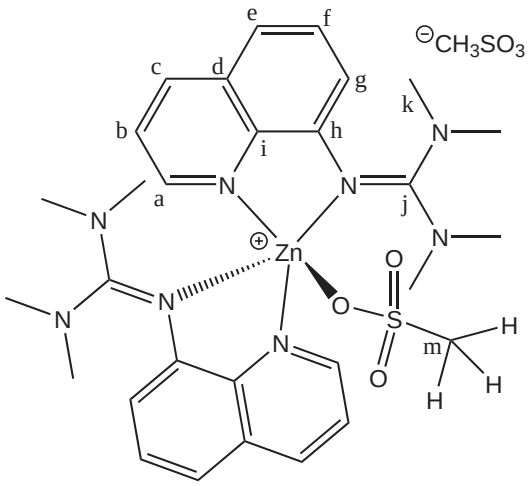

C$_{30}$H$_{42}$N$_8$O$_6$S$_2$Zn (M = 741.41 g/mol): Yellow crystals; **Yield**: 0.360 g = 0.48 mmol = 96 %; **m.p.** 264°C. ^{1}**H-NMR** (500 MHz, CD$_3$CN, 25 °C): δ [ppm] = 2.32 (s, 6H, l), 2.37 (m, 12H, k), 2.79 (s, 6H, k'), 3.03 (s, 6H, k"), 6.85 (dd, 2H, g, ^{3}J = 7.6 Hz, ^{4}J = 1.2 Hz), 7.61 (dd, 2H, e, ^{3}J = 8.2 Hz, ^{4}J = 1.2 Hz), 7.68 (dd, 2H, f, ^{3}J = 8.2 Hz, ^{3}J = 7.6 Hz), 7.82 (dd, 2H, b, ^{3}J = 8.4 Hz, ^{3}J = 4.6 Hz), 8.62 (dd, 2H, c, ^{3}J = 8.4 Hz, ^{4}J = 1.6 Hz), 8.92 (dd, 2H, a, ^{3}J = 4.6 Hz, ^{4}J = 1.6 Hz). ^{13}**C-NMR** (125 MHz, CD$_3$CN, 25 °C): δ [ppm] = 38.9 (CH$_3$, k+l), 39.4 (CH$_3$, k'), 41.0 (CH$_3$, k"), 115.7 (CH, g), 118.6 (CH, e), 122.3 (CH, b), 129.0 (CH, f), 129.5 (C, d), 137.9 (C, i), 139.9 (CH, c), 143.6 (C, h), 148.5 (CH, a), 165.9 (C, j). **IR** (KBr, $\tilde{\nu}$[cm^{-1}]): 3103 w (ν(C-H$_{arom.}$)), 3037 w (ν(C-H$_{arom.}$)), 3001 w (ν(C-H$_{arom.}$)), 2929 w (ν(C-H$_{aliph.}$)), 2877 w (ν(C-H$_{aliph.}$)), 2806 w (ν(C-H$_{aliph.}$)), 1576 m (ν(C=N)), 1525 s (ν(C=N)), 1502 m, 1468 s, 1421 m, 1400 s, 1388 m, 1379 m, 1331 m, 1277 w, 1248 m, 1205 s, 1194 vs, 1165 m, 1159 s, 1103 m, 1059 w, 1038 m, 1032 m, 962 vw, 924 vw, 903 vw, 881 vw, 849 m, 833 m, 823 w, 806 m, 796 w, 783 w, 775 w, 764 m, 750 m, 702 w, 669 vw, 652 vw, 633 w, 586 w, 550 m, 538 m, 526 m. **EI-MS** (m/z, (%)): 643 (4) [M$^+$ -CH$_3$SO$_3$], 242 (100) [M$^+$ -Zn(CH$_3$SO$_3$)$_2$], 199 (18) [M$^+$ -Zn(CH$_3$SO$_3$)$_2$ - N(CH$_3$)$_2$ +H], 198 (74) [M$^+$ -Zn(CH$_3$SO$_3$)$_2$ -N(CH$_3$)$_2$], 184 (74) [M$^+$ -Zn(CH$_3$SO$_3$)$_2$ -N(CH$_3$)$_2$ -CH$_3$ +H], 183 (18) [M$^+$ -Zn(CH$_3$SO$_3$)$_2$ -N(CH$_3$)$_2$ -CH$_3$], 182 (17) [M$^+$ -Zn(CH$_3$SO$_3$)$_2$ -N(CH$_3$)$_2$ -CH$_3$ -H], 171 (44), 157 (35) [C$_{10}$H$_6$N$_2^+$ +H], 156 (25) [C$_{10}$H$_6$N$_2^+$], 155 (69), 143 (17) [M$^+$ -Zn(CH$_3$SO$_3$)$_2$ -C(N(CH$_3$)$_2$)$_2$ +H], 142 (18) [M$^+$ -Zn(CH$_3$SO$_3$)$_2$ -C(N(CH$_3$)$_2$)$_2$], 129 (24) [M$^+$ -Zn(CH$_3$SO$_3$)$_2$ -C(N)(N(CH$_3$)$_2$)$_2$ +H], 128 (13) [M$^+$ -Zn(CH$_3$SO$_3$)$_2$ -C(N)(N(CH$_3$)$_2$)$_2$], 100 (36) [C(N(CH$_3$)$_2$)$_2^+$]. **CHN analysis**: calculated: C 48.56, H 5.66, N 15.11; found: C 48.60, H 5.76, N 15.14.

[Zn(TMGqu)Br$_2$] (7f):

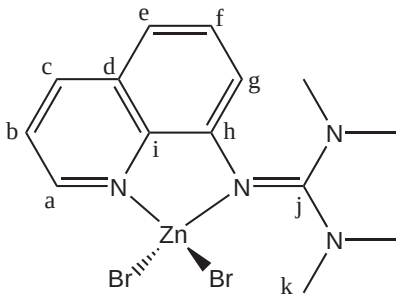

C$_{14}$H$_{18}$N$_4$ZnBr$_2$ (M = 467.52 g/mol): Yellow crystals; **Yield**: 0.440 g = 0.94 mmol = 94 %; **m.p.** >300°C. ^{1}**H-NMR** (500 MHz, DMSO-d$_6$, 25 °C): δ [ppm] = 2.76 (s, 6H, k), 3.02 (s, 6H, k'), 6.99 (dd, 1H, g, ^{3}J = 7.3 Hz, ^{4}J = 1.2 Hz), 7.65 (m, 2H, e+f), 7.84 (dd, 1H, b, ^{3}J = 8.3 Hz, ^{3}J = 4.6 Hz), 8.71 (dd, 1H, c, ^{3}J = 8.3 Hz, ^{4}J = 1.3 Hz), 8.86 (dd, 1H, a, ^{3}J = 4.6 Hz, ^{4}J = 1.3 Hz). ^{13}**C-NMR** (125 MHz, DMSO-d$_6$, 25 °C): δ [ppm] = 40.4 (CH$_3$, k), 118.0 (CH, g), 119.8 (CH, e), 123.3 (CH, b), 129.4 (CH, f), 129.4 (C, d), 138.3 (C, i), 140.9 (CH, c), 143.3 (C, h), 148.9 (CH, a), 165.3 (C, j). **IR** (KBr, $\tilde{\nu}$[cm^{-1}]): 3107 w (ν(C-H$_{arom.}$)), 3080 w (ν(C-H$_{arom.}$)), 3060 w (ν(C-H$_{arom.}$)), 3039 m (ν(C-

$H_{arom.}$)), 3014 w (ν(C-$H_{arom.}$)), 2949 m (ν(C-$H_{aliph.}$)), 2933 m (ν(C-$H_{aliph.}$)), 2893 m (ν(C-$H_{aliph.}$)), 2868 m (ν(C-$H_{aliph.}$)), 2798 w, 1562 s (ν(C=N)), 1525 s (ν(C=N)), 1500 s (ν(C=N)), 1466 s, 1433 m,1417 s, 1402 m, 1334 m, 1387 s, 1377 m, 1336 m, 1315 m, 1273 w, 1236 m, 1209 w, 1163 m, 1140 m, 1103 m, 1065 m, 1018 m, 982 vw, 964 vw, 947 vw, 956 w, 903 vw, 893 vw, 876 vw, 833 m, 816 m, 806 m, 785 m, 756 m, 702 m, 656 w, 631 w, 582 w, 542 w, 528 vw. **EI-MS** (m/z, (%)): 468 (2) [M^+: $C_{14}H_{18}N_4{}^{79}Br^{81}Br^{66}Zn$, $C_{14}H_{18}N_4{}^{79}Br_2{}^{68}Zn$, $C_{14}H_{18}N_4{}^{81}Br_2{}^{64}Zn$], 466 (2) [$M^+$: $C_{14}H_{18}N_4{}^{79}Br^{81}Br^{64}Zn$, $C_{14}H_{18}N_4{}^{79}Br_2{}^{66}Zn$], 391 (12) [$M^+$ -Br], 389 (28) [M^+ -Br], 387 (46) [M^+ -Br], 385 (30) [M^+ -Br], 243 (23) [M^+ -$ZnBr_2$ +H], 242 (100) [M^+ -$ZnBr_2$], 198 (48) [M^+ -$N(CH_3)_2$ -$ZnBr_2$], 184 (12) [$C_{11}H_9N_3{}^+$ +H], 182 (12) [$C_{11}H_9N_3{}^+$ -H], 171 (35), 157 (21), 155 (43) [$C_{10}H_6N_2{}^+$ +H], 143 (10) [$C_9H_6N_2{}^+$ +H], 142 (12) [$C_9H_6N_2{}^+$], 129 (12) [$C_9H_6N^+$ +H], 100 (36) [$C(N(CH_3)_2)_2{}^+$]. **CHN analysis**: calculated: C 35.93, H 3.85, N 11.98; found: C 35.98, H 3.82, N 12.02.

[Zn(DMPGqu)Cl_2] (8a):

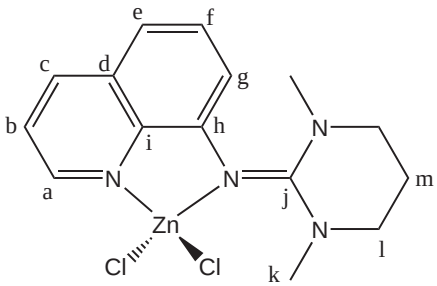

$C_{15}H_{18}N_4ZnCl_2$ (M = 390.99 g/mol): Green-yellow crystals; **Yield**: 0.368 g = 0.94 mmol = 94 %; **m.p.** 248°C with decomposition. ^{1}**H-NMR** (500 MHz, CD_3CN, 25 °C): δ [ppm] = 2.13 (m, 2H, m), 3.02 (s, 6H, k), 3.48 (m, 4H, l), 6.92 (dd, 1H, g, ^3J = 7.7 Hz, ^4J = 0.8 Hz), 7.39 (dd, 1H, e, ^3J = 8.2 Hz, ^4J = 0.8 Hz), 7.55 (dd, 1H, f, ^3J = 8.2 Hz, ^3J = 7.7 Hz), 7.71 (dd, 1H, b, ^3J = 8.4 Hz, ^3J = 4.6 Hz), 8.52 (dd, 1H, c, ^3J = 8.4 Hz, 4J = 1.5 Hz), 8.72 (dd, 1H, a, ^3J = 4.6 Hz, ^4J = 1.5 Hz). ^{13}**C-NMR** (125 MHz, CD_3CN, 25 °C): δ [ppm] = 21.6 (CH_2, m), 39.6 (CH_3, k), 48.6 (CH_2, l), 114.2 (CH, g), 116.5 (CH, e), 122.4 (CH, b), 129.1 (CH, f), 129.8 (C, d), 137.9 (C, i), 140.0 (CH, c), 144.4 (C, h), 147.2 (CH, a), 161.1 (C, j). **IR** (KBr, $\tilde{\nu}$[cm^{-1}]): 3217 m (ν(C-$H_{arom.}$)), 3176 m (ν(C-$H_{arom.}$)), 3111 m (ν(C-$H_{arom.}$)), 2943 m (ν(C-$H_{aliph.}$)), 2868 m (ν(C-$H_{aliph.}$)), 1572 s (ν(C=N)), 1524 s (ν(C=N)), 1502 s (ν(C=N)), 1466 s, 1458 s, 1417 s, 1387 s, 1323 s, 1286 m, 1259 m, 1234 m, 1213 m, 1190 m, 1173 m, 1144 w, 1124 w, 1117 m, 1105 m, 1090 m, 1076 m, 1057 m, 1039 m, 1030 m, 987 w, 947 w, 914 vw, 899 w, 879 vw, 831 m, 820 m, 806 m, 787 m, 766 m, 756 m, 743 m, 721 w, 698 w, 669 vw, 627 w, 582 m, 544 vw, 527 vw, 509 vw. **EI-MS** (m/z, (%)): 392 (0.4) [M^+: $C_{15}H_{18}N_4{}^{68}Zn^{35}Cl_2$, $C_{15}H_{18}N_4{}^{64}Zn^{37}Cl_2$, $C_{15}H_{18}N_4{}^{66}Zn^{35}Cl^{37}Cl$], 390 (0.6) [$M^+$: $C_{15}H_{18}N_4{}^{66}Zn^{35}Cl_2$, $C_{15}H_{18}N_4{}^{64}Zn^{35}Cl^{37}Cl$], 388 (0.5) [$M^+$: $C_{15}H_{18}N_4{}^{64}Zn^{35}Cl_2$], 357 (3) [$M^+$ -Cl: $C_{15}H_{18}N_4{}^{68}Zn^{35}Cl$, $C_{15}H_{18}N_4{}^{66}Zn^{37}Cl$], 355 (4) [$M^+$ -Cl: $C_{15}H_{18}N_4{}^{66}Zn^{35}Cl$, $C_{15}H_{18}N_4{}^{64}Zn^{37}Cl$], 353 (5) [$M^+$ -Cl: $C_{15}H_{18}N_4{}^{64}Zn^{35}Cl$], 326 (10), 254 (68) [$C_{15}H_{18}N_4{}^+$], 253 (15), 155 (10), 145 (77), 144 (100) [$C_9H_6N_2{}^+$ +2H], 143 (59) [$C_9H_6N_2{}^+$ +H], 118 (30), 117 (99), 116 (72), 90 (74), 89 (76), 72 (40), 63 (37), 59 (36). **CHN analysis**: calculated: C 46.04, H 4.60, N 14.32; found: C 45.87, H 4.28, N 14.07.

[Zn(DMPGqu)(CH_3COO)Cl] (8a/b):

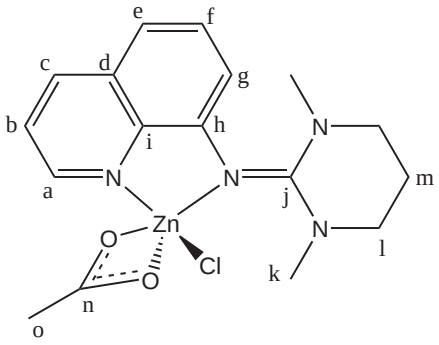

$C_{15}H_{18}N_4$ (M = 414.23 g/mol): Yellow crystals; **Yield**: 0.350 g = 0.84 mmol = 84 %; **m.p.** 222°C. ^{1}**H-NMR** (500 MHz, CD_3CN, 25 °C): δ [ppm] = 1.88 (s, 3H, o), 2.12 (m, 2H, m), 2.99 (s, 6H, k), 3.47 (m, 4H, l), 6.88 (d, 1H, g, ^3J = 7.9 Hz), 7.35 (d, 1H, e, ^3J = 7.9 Hz), 7.52 (dd, 1H, f, ^3J = 7.9 Hz, ^3J = 7.9 Hz), 7.68 (dd, 1H, b, ^3J = 8.3 Hz, ^3J = 3.9 Hz), 8.48 (dd, 1H, c, ^3J = 8.3 Hz, ^4J = 1.0 Hz), 8.82 (d, 1H, a, ^3J = 3.9 Hz). ^{13}**C-NMR** (125 MHz, CD_3CN, 25 °C): δ [ppm] = 21.3 (CH_3, o), 21.35 (CH_2, m), 39.2 (CH_3, k), 48.5 (CH_2, l), 115.9 (CH, g), 117.3 (CH, e), 122.3 (CH, b), 128.9 (CH, f), 129.7 (C, d), 137.9 (C, i), 139.6 (CH, c), 144.8 (C, h), 147.4 (CH, a), 161.4 (C, j), 178.4 (C, n). **IR** (KBr, $\tilde{\nu}$[cm^{-1}]): 3059 w (ν(C-$H_{arom.}$)), 2979 w (ν(C-$H_{aliph.}$)), 2933 m (ν(C-$H_{aliph.}$)), 2864 m (ν(C-$H_{aliph.}$)), 1577 vs (ν(C=N)), 1522 s (ν(C=N)), 1502 vs, 1466 s, 1444 m, 1414 s, 1402 vs, 1394 vs, 1336 m, 1321 m, 1292 m, 1257 w, 1238 m, 1215 w, 1192 w, 1173 w, 1105 m, 1057 m, 1038 w, 1028 w, 1009 w, 949 w, 931 w, 924 w, 899 vw, 872 vw, 835 m, 819 m, 808 m, 791 m, 750 m, 681 m, 648 w, 617 w, 582 w, 548 w, 511 w. **EI-MS** (m/z, (%)): 414 (2) [M^+], 412 (3) [M^+], 381 (35), 379 (56) [M^+ - Cl^{35}], 377 (79) [M^+ - Cl^{37}], 357 (57), 355 (76) [M^+ -CH_3COO], 353 (79) [M^+ -CH_3COO], 282 (10), 255 (88), 254 (100) [M^+ -Zn(CH_3COO)Cl], 253 (99), 239 (10) [M^+ -Zn(CH_3COO)Cl -CH_3], 225 (80) [M^+ -Zn(CH_3COO)Cl - 2 CH_3 +H], 211 (14) [$C_{13}H_{13}N_3^+$], 196 (19) [$C_{12}H_{10}N_3^+$], 184 (71), 183 (88) [$C_{11}H_9N_3^+$], 182 (55), 170 (33), 169 (60) [$C_{10}H_6N_3^+$ +H], 157 (82), 155 (89) [$C_{10}H_6N_2^+$ +H], 143 (68) [$C_9H_6N_2^+$ +H], 142 (59) [$C_9H_6N_2^+$], 129 (83) [$C_9H_6N^+$ +H], 128 (48) [$C_9H_6N^+$], 116 (30), 112 (92) [$C_6H_{12}N_2^+$], 101 (18), 99 (16), 98 (17), 70 (29). **CHN analysis**: calculated: C 49.25, H 5.07, N 13.52; found: C 49.49, H 5.10, N 13.57.

[Zn(DMPGqu)($CH_3COO)_2$] (8b):

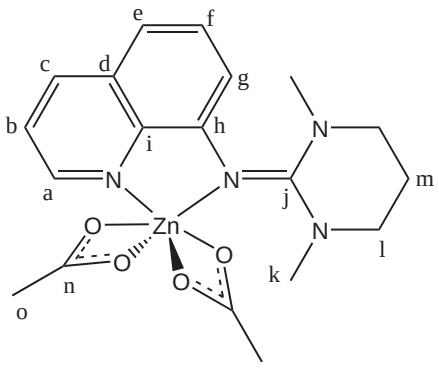

$C_{19}H_24N_4O_4Zn$ (M = 437.81 g/mol): Yellow crystals; **Yield**: 0.420 g = 0.96 mmol = 96 %; **m.p.** 188°C. ^{1}**H-NMR** (500 MHz, CD_3CN, 25 °C): δ [ppm] = 1.86 (s, 6H, o), 2.11 (m, 2H, m), 2.95 (s, 6H, k), 3.45 (m, 4H, l), 6.83 (dd, 1H, g, ^3J = 7.7 Hz, ^4J = 0.9 Hz), 7.30 (dd, 1H, e, ^3J = 8.2 Hz, ^4J = 0.9 Hz), 7.49 (dd, 1H, f, ^3J = 8.2 Hz, ^3J = 7.7 Hz), 7.65 (dd, 1H, b, ^3J = 8.3 Hz, ^3J = 4.6 Hz), 8.44 (dd, 1H, c, ^3J = 8.3 Hz, ^4J = 1.6 Hz), 8.92 (dd, 1H, a, ^3J = 4.6 Hz, ^4J = 1.6 Hz). ^{13}**C-NMR** (125 MHz, CD_3CN, 25 °C): δ [ppm] = 21.4 (CH_2, m), 21.5 (CH_3, o), 38.7 (CH_3, k), 48.4 (CH_2, l), 112.9 (CH, g), 115.4 (CH, e), 122.0 (CH, b), 128.7 (CH, f), 129.6 (C, d), 138.0 (C, i), 139.3 (CH, c), 145.1 (C, h), 147.9 (CH, a), 161.4 (C, j), 177.9 (C, n). **IR** (KBr, $\tilde{\nu}$[cm^{-1}]): 3066 w (ν(C-$H_{arom.}$)), 3043 w (ν(C-$H_{arom.}$)), 2985 m (ν(C-$H_{aliph.}$)), 2926 m (ν(C-$H_{aliph.}$)), 2870 m (ν(C-$H_{aliph.}$)), 2804 w (ν(C-$H_{aliph.}$)), 1578 vs (ν(C=N)), 1523 s, 1500 vs , 1468 s, 1450 s, 1414 s, 1390 vs, 1381

vs, 1333 s, 1290 m, 1259 m, 1242 m, 1233 m, 1211 m, 1190 m, 1178 m, 1136 w, 1105 m, 1078 w, 1055 m, 1036 m, 1024 m, 1012 m, 947 w, 930 w, 879 vw, 835 m, 824 m, 806 m, 785 m, 767 w, 741 w, 681 m, 675 m, 648 w, 621 m, 584 m, 544 w, 507 w. **EI-MS** (m/z, (%)): 381 (20) [M^+ - CH_3COO: $C_{17}H_{21}N_4O_4{}^{68}Zn$], 379 (31) [$M^+$ - CH_3COO: $C_{17}H_{21}N_4O_4{}^{66}Zn$], 377 (58) [$M^+$ - CH_3COO: $C_{17}H_{21}N_4O_4{}^{64}Zn$], 326 (11), 285 (21), 255 (73), 254 (100) [$C_{15}H_{18}N_4{}^+$], 253 (96), 225 (56), 196 (15), 183 (74), 169 (33), 157 (64), 155 (82) [$C_{10}H_6N_2{}^+$ +H], 143 (38) [$C_9H_6N_2{}^+$ +H], 142 (30) [$C_9H_6N_2{}^+$], 129 (62) [$C_9H_6N^+$ +H], 112 (80), 70 (15). **CHN analysis**: calculated: C 52.08, H 5.48, N 12.79; found: C 51.39, H 5.51, N 12.62.

[Zn(TEGqu)Cl_2] (9a):

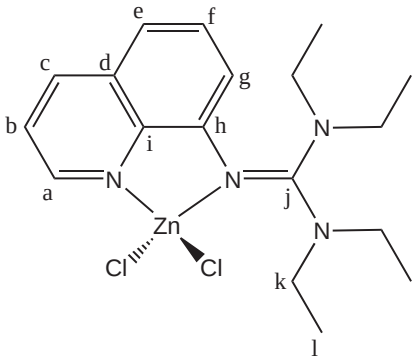

$C_{18}H_{26}N_4Cl_2Zn$ (M = 434.74 g/mol): Yellow crystals; **Yield**: 0.420 g = 0.97 mmol = 97 %; **m.p.** 237°C. ^{1}**H-NMR** (500 MHz, $CDCl_3$, 25 °C): δ [ppm] = 1.12 (m, 6H, l), 1.35 (m, 6H, l'), 3.18 (m, 3H, k), 3.39 (m, 5H, k'), 7.06 (d, 1H, g, ^{3}J = 7.9 Hz), 7.43 (d, 1H, e, ^{3}J = 7.9 Hz), 7.52 (dd, 1H, f, ^{3}J = 7.9 Hz, ^{3}J = 7.9 Hz), 7.62 (dd, 1H, b, ^{3}J = 8.3 Hz, ^{4}J = 4.6 Hz), 8.36 (dd, 1H, c, ^{3}J = 8.3 Hz, ^{4}J = 1.3 Hz), 8.85 (dd, 1H, a, ^{3}J = 4.6 Hz, ^{4}J = 1.3 Hz). ^{13}**C-NMR** (125 MHz, $CDCl_3$, 25 °C): δ [ppm] = 12.3 (CH_3, l'), 13.4 (CH_3, l), 43.1 (CH_2, k), 44.7 (CH_2, k'), 116.5 (CH, g), 119.5 (CH, e), 122.4 (CH, b), 128.4 (CH, f), 129.5 (C, d), 139.1 (C, i), 139.6 (CH, c), 143.8 (C, h), 148.2 (CH, a), 165.3 (C, j). **IR** (KBr, $\tilde{\nu}$[cm^{-1}]): 3205 w (ν(C-$H_{arom.}$)), 3120 w (ν(C-$H_{arom.}$)), 3076 w (ν(C-$H_{arom.}$)), 3045 w (ν(C-$H_{arom.}$)), 2976 m (ν(C-$H_{aliph.}$)), 2937 m (ν(C-$H_{aliph.}$)), 2891 m (ν(C-$H_{aliph.}$)), 2873 m (ν(C-$H_{aliph.}$)), 2004 vw, 1973 vw, 1938 vw, 1579 m (ν(C=N)), 1529 s (ν(C=N)), 1489 vs (δ(C-H)), 1464 s (δ(C-H)), 1439 vs (δ(C-H)), 1375 m, 1348 s, 1336 m, 1294 m, 1240 w, 1232 w, 1203 m, 1147 m, 1111 m, 1090 m, 1078 m, 1066 m, 1055 m, 1036 m, 1005 w, 976 w, 941 vw, 904 vw, 887 vw, 860 vw, 835 m, 804 w, 791 m, 768 m, 733 m, 692 m, 648 w, 631 w, 588 w, 548 w, 530 w, 507 vw. **EI-MS** (m/z, (%)): 438 (2) [M^+: $C_{18}H_{26}N_4{}^{68}Zn^{35}Cl^{37}Cl$], 437 (1) [$M^+$: $C_{17}{}^{13}CH_{26}N_4{}^{68}Zn^{35}Cl_2$, $C_{17}{}^{13}CH_{26}N_4{}^{66}Zn^{35}Cl^{37}Cl$, $C_{18}H_{26}N_4{}^{67}Zn^{35}Cl^{37}Cl$], 436 (4) [$M^+$: $C_{18}H_{26}N_4{}^{68}Zn^{35}Cl_2$, $C_{18}H_{26}N_4{}^{64}Zn^{37}Cl_2$, $C_{18}H_{26}N_4{}^{66}Zn^{35}Cl^{37}Cl$], 435 (2) [$M^+$: $C_{17}{}^{13}CH_{26}N_4{}^{64}Zn^{35}Cl^{37}Cl$, $C_{17}{}^{13}CH_{26}N_4{}^{66}Zn^{35}Cl_2$], 434 (5) [$M^+$: $C_{18}H_{26}N_4{}^{66}Zn^{35}Cl_2$, $C_{18}H_{26}N_4{}^{64}Zn^{35}Cl^{37}Cl$], 433 (1) [$M^+$: $C_{17}{}^{13}CH_{26}N_4{}^{64}Zn^{35}Cl_2$], 432 (4) [$M^+$: $C_{18}H_{26}N_4{}^{64}Zn^{35}Cl_2$], 399 (70) [$M^+$ -^{35}Cl], 397 (93) [M^+ -^{37}Cl], 299 (88) [M^+ -$ZnCl_2$ +H], 298 (92) [M^+ -$ZnCl_2$], 227 (89) [M^+ -$ZnCl_2$ -$N(CH_2CH_3)_2$ +H], 226 (85) [M^+ -$ZnCl_2$ -$N(CH_2CH_3)_2$], 198 (92), 182 (77), 170 (100) [$N{=}C(N(CH_2CH_3)_2)^+$], 156 (96) [$C(N(CH_2CH_3)_2)^+$], 142 (56) [M^+ -$ZnCl_2$ -$C(N(CH_2CH_3)_2)$], 129 (36) [M^+ -$ZnCl_2$ -$N{=}C(N(CH_2CH_3)_2)$ +H], 116 (26), 72 (24) [$N(CH_2CH_3)_2{}^+$]. **CHN analysis**: calculated: C 49.68, H 5.98, N 12.88; found: C 49.57, H 6.04, N 12.89.

[Zn(DPipGqu)($CH_3COO)_2$] (10b):

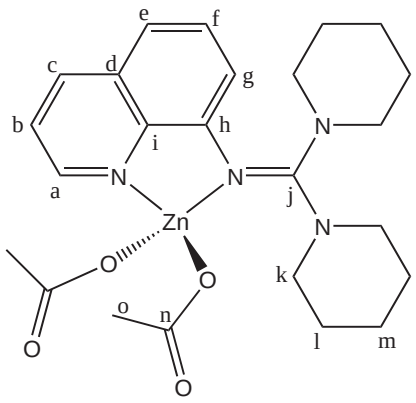

$C_{24}H_{32}N_4O_4Zn$ (M = 505.93 g/mol): Yellow crystals; **Yield**: 0.240 g = 0.47 mmol = 47 %; **m.p.**262°C. ^{1}**H-NMR** (500 MHz, CD_3CN, 70 °C): δ [ppm] = 1.66 (m, 12H, l + m), 1.87 (s, 6H, o), 3.29 (m, 8H, k), 6.89 (d, 1H, g, ^3J = 8.1 Hz), 7.68 (d, 1H, e, ^3J = 8.1 Hz), 7.36 (t, 1H, f, ^3J = 8.1 Hz, ^3J = 8.1 Hz), 7.68 (dd, 1H, b, ^3J = 8.3 Hz, ^4J = 4.6 Hz), 8.49 (dd, 1H, c, ^3J = 8.3 Hz, ^4J = 1.4 Hz), 8.95 (dd, 1H, a, ^3J = 4.6 Hz, ^4J = 1.6 Hz). ^{13}**C-NMR** (125 MHz, CD_3CN, 70 °C): δ [ppm] = 21.4 (CH_3, o), 24.0 (CH_2, m), 24.8 (CH_2, l), 49.0 (CH_2, k), 117.1 (CH, g), 118.8 (CH, e), 122.2 (CH, b), 128.4 (CH, f), 129.2 (C, d), 138.7 (C, i), 139.4 (CH, c), 144.3 (C, h), 148.6 (CH, a), 165.3 (C, j), 177.9 (C, n). **IR** (KBr, $\tilde{\nu}$[cm^{-1}]): 3060 vw (ν(C-$H_{arom.}$)), 3010 w (ν(C-$H_{arom.}$)), 2943 m (ν(C-$H_{aliph.}$)), 2933 m (ν(C-$H_{aliph.}$)), 2858 m (ν(C-$H_{aliph.}$)), 1616 s (ν(C=N)), 1593 s (ν(C=N)), 1537 s, 1500 vs, 1485 s, 1466 s, 1448 s, 1388 s, 1375 s, 1325 s, 1279 m, 1252 m, 1223 w, 1192 w, 1161 w, 1134 m, 1109 w, 1082 w, 1061 m, 1028 m, 1016 m, 982 w, 957 vw, 914 w, 881 vw, 852 m, 823 m, 810 w, 798 w, 785 m, 750 m, 737 vw, 694 m, 675 m, 654 vw, 633 w, 617 w, 590 vw, 582 w, 534 w, 525 vw. **EI-MS** (m/z, (%)): 504 (3) [M^+], 445 (53) [M^+ -CH_3COO], 322 (100) [M^+ -$Zn(CH_3COO)_2$], 239 (36) [M^+ -$Zn(CH_3COO)_2$ -$C_5H_{10}N$ +H], 211 (16), 156 (40) [M^+ - $Zn(CH_3COO)_2$ -2 $C_5H_{10}N$ +2H], 128 (10) [$C_9H_6N_2^+$], 84 (11) [$C_5H_{10}N^+$]. **CHN analysis**: calculated: C 56.92, H 6.32, N 11.07; found: C 54.00, H 5.62, N 10.97.

[Zn(DMorphGqu)Cl_2] (11a):

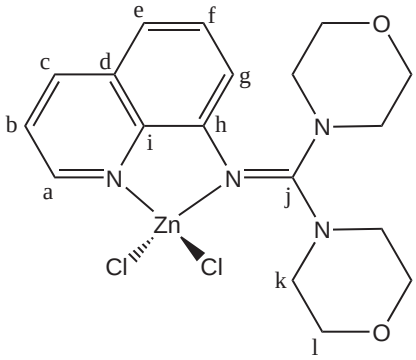

$C_{18}H_{22}N_4O_2ZnCl_2$ (M = 462.70 g/mol): Yellow crystals; **Yield**: 0.444 g = 0.96 mmol = 96 %; **m.p.** >300°C. ^{1}**H-NMR** (500 MHz, DMSO-d_6, 25 °C): δ [ppm] = 3.40 (m, 4H, k), 3.60 (m, 4H, k'), 3.79 (m, 8, l), 7.17 (t, 1H, g, ^3J = 4.3 Hz), 7.72 (m, 2H, e+f), 7.85 (dd, 1H, b, ^3J = 8.3 Hz, ^3J = 4.5 Hz), 8.74 (dd, 1H, c, ^3J = 8.3 Hz), 8.90 (d, 1H, a, ^3J = 4.5 Hz). ^{13}**C-NMR** (125 MHz, DMSO-d_6, 25 °C): δ [ppm] = 48.5 (CH_2, k), 50.2 (CH_2, k'), 65.6 (CH_2, l), 119.3 (CH, g), 120.9 (CH, e), 123.5 (CH, b), 129.2 (CH, f), 129.4 (C, d), 138.6 (C, i), 141.0 (CH, c), 143.0 (C, h), 149.3 (CH, a), 164.2 (C, j). **IR** (KBr, $\tilde{\nu}$[cm^{-1}]): 3099 m (ν(C-$H_{arom.}$)), 3074 m (ν(C-$H_{arom.}$)), 3049 m (ν(C-$H_{arom.}$)), 3024 m (ν(C-$H_{arom.}$)), 2991 m (ν(C-$H_{aliph.}$)), 2968 m (ν(C-$H_{aliph.}$)), 2943 m (ν(C-$H_{aliph.}$)), 2908 m (ν(C-$H_{aliph.}$)), 2852 m (ν(C-$H_{aliph.}$)), 2767 w, 2713 w, 2692 w, 1957 w, 1583 m, 1533 vs (ν(C=N)), 1495 vs (ν(C=N)), 1471 vs, 1443 vs, 1431 vs, 1396 s, 1375 s, 1363 s, 1336 vs, 1304 m, 1275 s, 1254 s, 1221 m, 1186 m, 1159 w, 1140 vw, 1113 vs, 1076 m, 1066 m, 1049 w, 1034 s, 991 s, 935 w, 912 w, 883 m, 843 m ,827 m, 806 m, 783 s, 760 m, 743 m, 687 m, 661 w, 638 m, 631 w, 613 m ,584 m, 552 w, 538 m. **EI-MS** (m/z, (%)): 425 (5) [M^+ -Cl], 357 (9) [M^+ -Cl -C_4H_8NO], 326 (100) [M^+ -$ZnCl_2$], 242 (32),

241 (41) [$C_{14}H_{14}N_3O^+$ +H], 240 (47) [$C_{14}H_{14}N_3O^+$], 213 (24), 198 (17) [$C_9H_{16}N_3O_2^+$], 183 (18) [$C_9H_{16}N_2O_2^+$ -H], 169 (29) [$C_9H_{16}N_2O^+$ +H], 156 (88) [$C_{10}H_6N_2^+$ +2H], 155 (74) [$C_{10}H_6N_2^+$ +H], 144 (38) [$C_9H_6N_2^+$ +2H], 129 (38) [$C_9H_6N^+$ +H], 128 (46) [$C_9H_6N^+$], 119 (18), 115 (16), 85 (41), 71 (21) [$C_4H_8N^+$ +H], 69 (21). **CHN analysis**: calculated: C 46.68, H 4.75, N 12.10; found: C 46.66, H 4.65, N 12.08.

[Zn(DMorphGqu)(CH_3COO)$_2$] (11b):

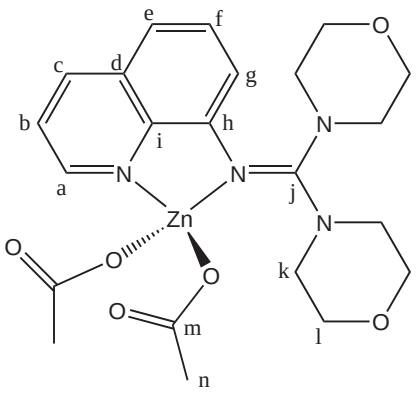

$C_{22}H_{28}N_4O_6Zn$ (M = 509.87 g/mol): Yellow crystals; **Yield**: 0.500 g = 0.98 mmol = 98 %; **m.p.** 220°C. ^{1}**H-NMR** (500 MHz, CD_3CN, 25 °C): δ [ppm] = 1.87 (s, 6H, n), 3.61 (bs, 8H, k), 3.82 (bs, 8H, l), 6.99 (dd, 1H, g, ^3J = 7.5 Hz, ^4J = 1.0 Hz), 7.59 (dd, 1H, e, ^3J = 8.2 Hz, ^4J = 1.0 Hz), 7.65 (dd, 1H, f, ^3J = 8.2 Hz, ^3J = 7.5 Hz), 7.71 (dd, 1H, b, ^3J = 8.3 Hz, ^3J = 4.6 Hz), 8.53 (dd, 1H, c, ^3J = 8.3 Hz, ^4J = 1.6 Hz), 8.93 (dd, 1H, a, ^3J = 4.6 Hz, ^4J = 1.6 Hz). ^{13}**C-NMR** (125 MHz, CD_3CN, 25 °C): δ [ppm] = 21.3 (CH_3, n), 48.4 (CH_2, k), 65.5 (CH_2, l), 117.7 (CH, g), 119.7 (CH, e), 122.4 (CH, b), 128.4 (CH, f), 129.2 (C, d), 138.7 (C, i), 139.6 (CH, c), 143.6 (C, h), 148.8 (CH, a), 164.8 (C, j), 178.1 (C, m). **IR** (KBr, $\tilde{\nu}$[cm^{-1}]): 3062 w (ν(C-$H_{arom.}$)), 2962 m (ν(C-$H_{arom.}$)), 2908 m (ν(C-$H_{aliph.}$)), 2883 w (ν(C-$H_{aliph.}$)), 2848 m (ν(C-$H_{aliph.}$)), 1616 s (ν(C=N)), 1589 s (ν(C=N)), 1543 s(ν(C=N)), 1493 vs (ν(C=N)), 1462 s, 1444 s, 1433 s, 1396 s, 1375 s, 1360 m, 1333 s, 1308 m ,1298 m 1286 m 1257 m, 1271 m, 1216 w, 1184 w, 1157 w, 1136 w, 1113 s, 1086 m, 1068 m, 1036 m, 1022 m, 989 m, 930 m, 908 w, 887 m, 854 w, 843 m, 835 m, 810 m, 795 m, 756 m 741 w, 675 m, 656 w, 638 m, 631 w, 611 m, 586 w, 552 w, 536 m. **EI-MS** (m/z, (%)): 511 (8) [M^+], 357 (63), 326 (30) [M^+ -Zn(CH_3COO)$_2$], 298 (19), 226 (15) [$C_{14}H_{14}N_3^+$ +2H], 198 (22) [$C_9H_{16}N_3O_2^+$], 183 (21) [$C_9H_{16}N_2O_2^+$ -H], 156 (50) [$C_{10}H_6N_2^+$ +2H], 155 (24) [$C_{10}H_6N_2^+$ +H], 120 (17), 119 (100), 105 (12), 91 (18), 77 (10) [$C_5H_3N^+$]. **CHN analysis**: calculated: C 51.78, H 5.49, N 10.98; found: C 51.83, H 5.27, N 11.01.

[Zn(DMorphGqu)$_2$][CF$_3$SO$_3$]2 *H$_2$O (11c):

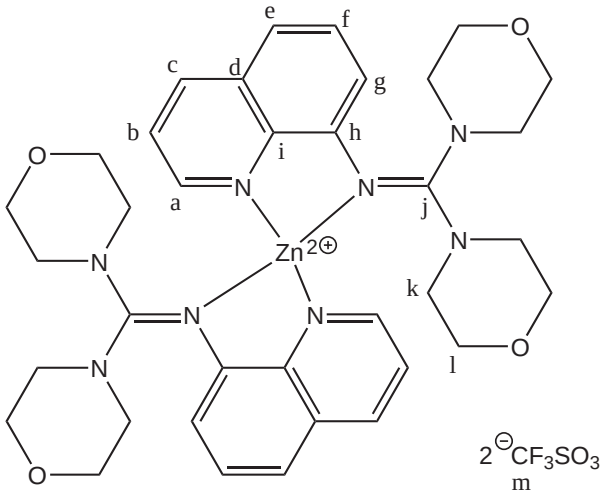

$C_{38}H_{44}N_8O_{10}F_6S_2Zn$*$H_2O$ (M = 1035.95 g/mol): Light yellow crystals; **Yield**: 0.240 g = 0.24 mmol = 47 %; **m.p.** 262°C with decomposition. ^{1}**H-NMR** (500 MHz, CD_3CN, 25 °C): δ [ppm] = 2.64-3.76 (m, 16H, k), 3.53-3.94 (m, 16H, l), 7.31 (dd, 2H, g, ^3J = 5.5 Hz, ^4J = 3.3 Hz), 7.86 (m, 4H, e+f), 7.99 (dd, 2H, b, ^3J = 8.3 Hz, ^3J = 4.8 Hz), 8.82 (m, 4H, a+c). ^{13}**C-NMR** (125 MHz, CD_3CN, 25 °C): δ [ppm] = 49.1 (CH_2, k), 51.2 (CH_2, k'), 64.9 (CH_2, l), 65.2 (CH_2, l'), 65.6 (CH_2, l''), 119.3 (CH, g), 121.4 (CH, e), 122.2 (C, m), 123.5 (CH, b), 129.4 (CH, f), 129.7 (C, d), 138.0 (C, i), 141.6 (C, h), 141.9 (CH, c), 149.3 (CH, a), 164.5 (C, j). **IR** (KBr, $\tilde{\nu}$[cm^{-1}]): 3111 w (ν(C-H$_{arom.}$)), 3074 w (ν(C-H$_{arom.}$)), 3053 w (ν(C-H$_{arom.}$)), 3014 w (ν(C-H$_{arom.}$)), 2966 m (ν(C-H$_{aliph.}$)), 2910 m (ν(C-H$_{aliph.}$)), 2862 m (ν(C-H$_{aliph.}$)), 2771 vw (ν(C-H$_{aliph.}$)), 1635 w, 1595 m, 1583 m, 1533 vs (ν(C=N)), 1502 vs (ν(C=N)), 1469 s, 1444 vs, 1389 s, 1356 s, 1333 vs, 1286 vs, 1271 vs, 1252 vs, 1223 s, 1163 s, 1151 s, 1117 vs, 1084 m, 1068 s, 1030 vs, 989 s, 928 w, 908 w, 883 m, 852 m, 839 m, 829 m, 810 m, 787 m, 756 m, 741 w, 692 m, 638 vs, 623 m, 609 m,582 m, 573 m, 552 m, 538 m, 517 m. **EI-MS** (m/z, (%)): 357 (6) [M^{++}], 326 (9) [$C_{18}H_{22}N_4O_2^+$], 279 (13), 240 (7) [$C_{14}H_{14}N_3O^+$], 210 (7) [$C_{10}H_{16}N_3O_2^+$], 183 (30) [$C_9H_{16}N_2O_2^+$ -H], 170 (81), 167 (33) [$C_9H_{16}N_3^+$ +H], 149 (41), 144 (82) [$C_9H_6N_2^+$ +2H], 142 (43) [$C_9H_6N_2^+$], 129 (29) [$C_9H_6N^+$ +H], 120 (100), 117 (39), 115 (44), 111 (25) [$C_5H_8N_3^+$ +H], 105 (46), 97 (35), 91 (40), 85 (47), 83 (35), 77 (31) [$C_5H_3N^+$], 73 (49), 71 (58), 69 (52), 58 (78). **CHN analysis**: calculated: C 44.02, H 4.44, N 10.81; found: C 43.6, H 4.6, N 10.7.

[Zn(MorphDMGqu)Cl$_2$] (12a):

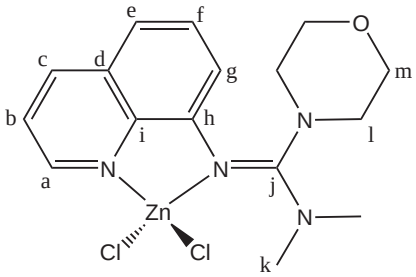

$C_{16}H_{20}N_4OZnCl_2$ (M = 420.67 g/mol): Yellow crystals; **Yield**: 0.280 g = 0.67 mmol = 67 %; **m.p.** 279°C. ^{1}**H-NMR** (500 MHz, CD_3CN, 25 °C): δ [ppm] = 2.65 (s, 3H, k), 3.07 (s, 3H, k'), 3.53 (m, 4H, l), 3.74 (m, 4H, m), 7.07 (dd, 1H, g, ^3J = 7.4 Hz, ^4J = 1.3 Hz), 7.64 (dd, 1H, e, ^3J = 8.2 Hz, ^4J = 1.3 Hz), 7.68 (dd, 1H, f, ^3J = 7.4 Hz, ^3J = 8.2 Hz), 7.76 (dd, 1H, b, ^3J = 8.4 Hz, ^3J = 4.6 Hz), 8.59 (dd, 1H, c, ^3J = 8.4 Hz, ^4J = 1.5 Hz), 8.83 (dd, 1H, a, ^3J = 4.6 Hz, ^4J = 1.75 Hz). ^{13}**C-NMR** (125 MHz, CD_3CN, 25 °C): δ [ppm] = 39.4 (CH_3, k), 40.7 (CH_3, k'), 48.8 (CH_2, l), 66.5 (CH_2, m), 118.4 (CH, g), 120.2 (CH, e), 122.7 (CH, b), 128.9 (CH, f), 129.5 (C, d), 138.8 (C, i), 140.3 (CH, c), 143.0 (C, h), 148.3 (CH, a), 164.9 (C, j). **IR** (KBr, $\tilde{\nu}$[cm^{-1}]): 3051 m (ν(C-H$_{arom.}$)), 3010 m (ν(C-H$_{arom.}$)), 2991 m (ν(C-H$_{aliph.}$)), 2970 m (ν(C-H$_{aliph.}$)), 2907 m (ν(C-H$_{aliph.}$)), 2850 m

(ν(C-$H_{aliph.}$)), 1583 m (ν(C=N)), 1560 s (ν(C=N)), 1510 s (ν(C=N)), 1493 vs (ν(C=N)), 1468 s, 1450 m, 1433 m, 1427 m, 1411 s, 1389 s, 1381 s, 1329 s, 1282 m, 1263 m, 1240 m, 1228 m, 1196 m, 1169 m, 1149 w, 1113 s, 1065 m, 1016 m, 1003 m, 993 w, 918 w, 895 m, 843 m, 829 m, 818 m, 806 m, 783 m, 758 m, 748 m, 696 m, 658 w, 636 m, 619 w, 582 m, 561 w, 540 m. **EI-MS** (m/z, (%)): 422 (1) [M^+: $C_{16}H_{20}N_4O^{68}Zn^{35}Cl_2$, $C_{16}H_{20}N_4O^{64}Zn^{37}Cl_2$, $C_{16}H_{20}N_4O^{66}Zn^{35}Cl^{37}Cl$], 420 (1.4) [$M^+$: $C_{16}H_{20}N_4O^{66}Zn^{35}Cl_2$, $C_{16}H_{20}N_4O^{64}Zn^{35}Cl^{37}Cl$], 418 (1.2) [$M^+$: $C_{16}H_{20}N_4O^{64}Zn^{35}Cl_2$], 387 (11) [$M^+$ -Cl: $C_{16}H_{20}N_4O^{66}Zn^{35}Cl$, $C_{16}H_{20}N_4O^{64}Zn^{37}Cl$], 385 (18) [$M^+$ -Cl: $C_{16}H_{20}N_4O^{68}Zn^{35}Cl$, $C_{16}H_{20}N_4O^{66}Zn^{37}Cl$], 383 (21) [$M^+$ -Cl: $C_{16}H_{20}N_4O^{64}Zn^{35}Cl$], 285 (64), 284 (100) [$C_{16}H_{20}N_4O^+$], 240 (29) [$C_{14}H_{14}N_3O^+$], 213 (32) [$C_{12}H_{12}N_4O^+$ +H], 199 (64), 198 (72) [$C_{12}H_{12}N_3O^+$], 186 (22), 184 (56), 183 (21) [$C_{11}H_9N_3^+$], 182 (24) [$C_{10}H_6N_4^+$], 171 (20), 169 (22) [$C_8H_{14}N_3O^+$ +H], 157 (24), 156 (71) [$C_7H_{14}N_3O^+$], 155 (79), 143 (26), 142 (24) [$C_9H_6N_2^+$, $C_7H_{14}N_2O^+$], 129 (36), 128 (27) [$C_9H_6N^+$], 116 (11), 101 (10) [$C_7H_3N^+$], 70 (12). **CHN analysis**: calculated: C 45.64, H 4.75, N 13.31; found: C 45.35, H 4.68, N 13.28.

[Zn(MorphDMGqu)(CH_3COO)$_2$] (12b):

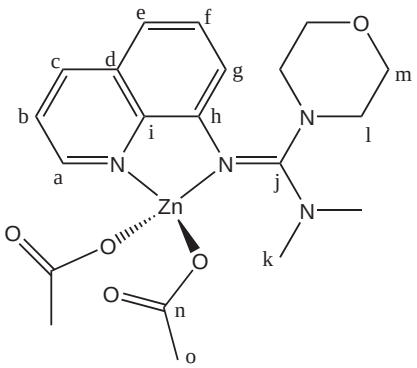

$C_{20}H_{26}N_4O_5Zn$ (M = 467.84 g/mol): Yellow crystals; **Yield**: 0.350 g = 0.75 mmol = 75 %; **m.p.** 181°C. ^{1}**H-NMR** (500 MHz, CD_3CN, 25 °C): δ [ppm] = 1.86 (s, 6H, o), 2.74 (s, 3H, k), 3.07 (s, 3H, k'), 3.32 (m, 4H, l), 3.72 (m, 4H, m), 6.93 (d, 1H, g, ^{3}J = 7.6 Hz), 7.55 (dd, 1H, e, ^{3}J = 8.1 Hz, ^{4}J = 0.8 Hz), 7.62 (dd, 1H, f, ^{3}J = 7.6 Hz, ^{3}J = 8.1 Hz), 7.70 (dd, 1H, b, ^{3}J = 8.3 Hz, ^{3}J = 4.6 Hz), 8.50 (dd, 1H, c, ^{3}J = 8.3 Hz, ^{4}J = 1.5 Hz), 8.94 (dd, 1H, a, ^{3}J = 4.6 Hz, ^{4}J = 1.75 Hz). ^{13}**C-NMR** (125 MHz, CD_3CN, 25 °C): δ [ppm] = 21.3 (CH_3, o), 39.0 (CH_3, k), 40.9 (CH_3, k'), 48.9 (CH_2, l), 65.7 (CH_2, m), 117.1 (CH, g), 119.1 (CH, e), 122.3 (CH, b), 128.5 (CH, f), 129.2 (C, d), 138.7 (C, i), 139.5 (CH, c), 143.8 (C, h), 148.7 (CH, a), 165.2 (C, j), 178.1 (C, n). **IR** (KBr, $\tilde{\nu}$[cm^{-1}]): 3059 m (ν(C-$H_{arom.}$)), 2970 m (ν(C-$H_{aliph.}$)), 2945 m (ν(C-$H_{aliph.}$)), 2927 m (ν(C-$H_{aliph.}$)), 2899 m (ν(C-$H_{aliph.}$)), 2856 m (ν(C-$H_{aliph.}$)), 1618 m (ν(C=N)), 1578 s (ν(C=N)), 1560 s (ν(C=N)), 1498 vs (ν(C=N)), 1466 s, 1404 s, 1389 s, 1330 s, 1265 m, 1240 m, 1227 m, 1213 w, 1169 w, 1138 vw, 1113 m, 1080 w, 1063 m, 1036 vw, 1018 w, 1001 m, 931 vw, 914 vw, 893 vw, 854 w, 831 m, 816 w, 806 w, 789 m ,760 m, 677 m, 654 w, 636 w, 619 m, 586 w, 559 vw, 538 w. **EI-MS** (m/z, (%)): 466 (2) [M^+], 407 (25) [M^+ -CH_3COO], 389 (16), 285 (45), 284 (98) [$C_{16}H_{20}N_4O^+$], 240 (53), 213 (51) [$C_{12}H_{12}N_4O^+$ +H], 199 (83), 198 (92) [$C_{12}H_{12}N_3O^+$], 184 (93), 183 (35) [$C_{11}H_9N_3^+$], 182 (34) [$C_{10}H_6N_4^+$], 171 (34), 169 (41), 157 (49), 156 (96) [$C_7H_{14}N_3O^+$], 155 (100), 143 (49), 142 (37) [$C_7H_{14}N_2O^+$, $C_9H_6N_2^+$], 129 (73), 128 (48) [$C_9H_6N^+$], 101 (18) [$C_7H_3N^+$], 70 (25). **CHN analysis**: calculated: C 51.30, H 5.56, N 11.97; found: C 50.97, H 5.45, N 11.91.

[Zn(DMEGpy)($C_6H_5COO)_2$] (14d):

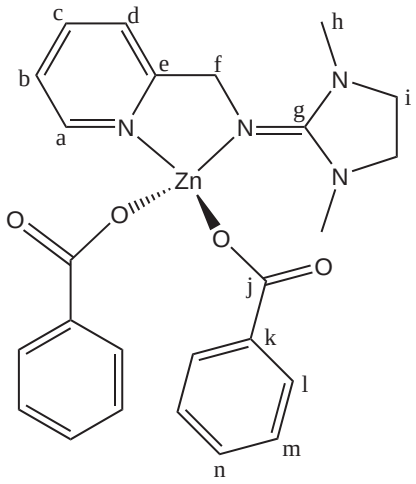

$C_{25}H_{26}N_4O_4Zn$ (M = 511.89 g/mol): Colourless crystals; **Yield**: 0.456 g = 0.89 mmol = 89 %; **m.p.** 131°C. ^{1}**H-NMR** (500 MHz, $CDCl_3$, 25 °C): δ [ppm] = 3.08 (s, 6H, h), 3.39 (s, 4H, i), 4.91 (s, 2H, f), 7.31 (m, 1H, d), 7.32 (m, 4H, m), 7.37 (m, 1H, b), 7.39 (m, 2H, n), 7.81 (m, 1H, c), 8.12 (m, 4H, l), 9.04 (m, 1H, a). ^{13}**C-NMR** (125 MHz, $CDCl_3$, 25 °C): δ [ppm] = 36.6 (CH_3, h), 49.7 (CH_2, i), 51.7 (CH_2, f), 121.7 (CH, d), 123.4 (CH, b), 127.5 (CH, m), 130.1 (CH, l), 130.5 (CH, n), 135.4 (C, k), 139.2 (CH, c), 148.9 (CH, a), 157.9 (C, e), 164.9 (C, g), 173.4 (C, j). **IR** (KBr, $\tilde{\nu}$[cm^{-1}]): 3062 m (ν(C-$H_{arom.}$)), 3053 m (ν(C-$H_{arom.}$)), 3022 w (ν(C-$H_{arom.}$)), 2954 m (ν(C-$H_{aliph.}$)), 2893 m (ν(C-$H_{aliph.}$)), 1624 vs, 1614 vs, 1597 vs (ν(C=N)), 1572 vs, 1508 m, 1489 m, 1444 m, 1421 m, 1406 m, 1375 vs, 1361 vs, 1300 m, 1286 m, 1234 m,1221 w, 1196 w, 1169 m, 1134 w, 1066 m, 1053 m, 1026 m, 970 w, 941 vw, 931 vw, 901 vw, 841 m, 818 w, 791 m, 769 m, 715 s, 687 m, 650 m, 627 w, 582 m, 565 w. **CI-MS** (m/z, (%)): 513 (2) [M^+], 409 (14), 318 (6), 262 (3), 247 (4), 206 (29) [M^+ -Zn($C_6H_5COO)_2$ +2H], 205 (100) [M^+ -Zn($C_6H_5COO)_2$ +H], 204 (8) [M^+ -Zn($C_6H_5COO)_2$], 124 (9), 114 (19) [$N_3C_5H_{10}^+$ +2H], 57 (41) [$CH_3NCH_2CH_2^+$]. **CHN analysis**: calculated: C 58.61, H 5.08, N 10.94; found: C 58.16, H 4.97, N 10.85.

[Zn(TMGpy)Cl_2] (15a):

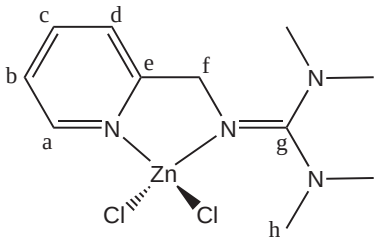

$C_{11}H_{18}N_4ZnCl_2$ (M = 342.60 g/mol): Colourless crystals; **Yield**: 0.220 g = 0.64 mmol = 64 %; **m.p.** 190°C. ^{1}**H-NMR** (500 MHz, CD_3CN, 25 °C): δ [ppm] = 2.77 (s, 6H, h), 2.98 (s, 6H, h'), 4.59 (s, 2H, f), 7.54 (m, 2H, b+d), 8.03 (m, 1H, c), 8.50 (m, 1H, a). ^{13}**C-NMR** (125 MHz, CD_3CN, 25 °C): δ [ppm] = 39.1 (CH_3, h), 51.8 (CH_2, f), 122.8 (CH, d), 123.9 (CH, b), 140.1 (CH, c), 147.0 (CH, a), 158.6 (C, e), 166.1 (C, g). **IR** (KBr, $\tilde{\nu}$[cm^{-1}]): 3302 vw (ν(C-$H_{arom.}$)), 3122 vw (ν(C-$H_{arom.}$)), 2993 vw (ν(C-$H_{aliph.}$)), 2945 w (ν(C-$H_{aliph.}$)), 2891 w (ν(C-$H_{aliph.}$)), 2844 vw (ν(C-$H_{aliph.}$)), 2796 vw (ν(C-$H_{aliph.}$)), 1608 m (ν(C=N)), 1574 s (ν(C=N)), 1558 vs (ν(C=N)), 1537 s (ν(C=N)), 1483 m, 1473 m, 1441 m, 1425 m, 1410 m, 1396 m, 1356 m, 1286 m, 1238 m, 1221 w, 1163 m, 1140 m, 1105 w, 1078 w, 1063 w, 1053 w, 1026 m, 978 vw, 906 m, 839 w, 773 m, 760 m, 715 w, 650 w, 623 w, 594 w, 553 vw. **EI-MS** (m/z, (%)): 342 (4) [M^+], 307 (2) [M^+ -^{35}Cl], 305 (4) [M^+ -^{37}Cl], 249 (73), 224 (80), 206 (35) [M^+ -$ZnCl_2$], 162 (23) [M^+ -$ZnCl_2$ -N($CH_3)_2$], 147 (15) [M^+ -$ZnCl_2$ -N($CH_3)_2$ -CH_3], 126 (73) [$CH_2NC(N(CH_3)_2)_2^+$ -2H], 121 (36), 119 (100) [M^+ -$ZnCl_2$ -2 N($CH_3)_2$ +H], 108 (95) [M^+ -$ZnCl_2$ -C(N($CH_3)_2)_2$ +2H], 107 (89) [M^+ -$ZnCl_2$ -C(N($CH_3)_2)_2$ +H], 92 (53) [M^+ -$ZnCl_2$ -NC(N($CH_3)_2)_2$], 87 (51), 85 (39) [$CH_2NC(N(CH_3)_2)^+$ +H], 80 (96) [$C_5NH_4^+$ +2H], 79 (90) [$C_5NH_4^+$ +H], 71 (38) [$NCN(CH_3)_2^+$ +H], 58 (78) [$C(N(CH_3)_2)^+$ +2H], 52 (71), 44 (26)

[$N(CH_3)_2^+$]. **CHN analysis**: calculated: C 38.53, H 5.25, N 16.35; found: C 38.77, H 5.20, N 15.90.

[Zn(TMGpy)(CH_3COO)$_2$] (15b):

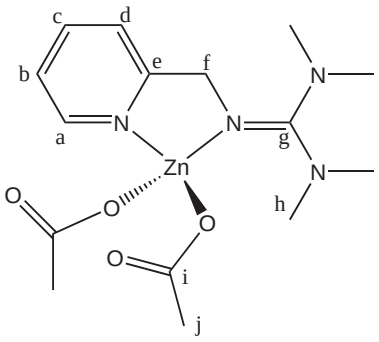

$C_{15}H_{24}N_4O_4Zn$ (M = 389.77 g/mol): Colourless crystals; **Yield**: 0.300 g = 0.76 mmol = 76 %; **m.p.** 160°C. ^{1}**H-NMR** (500 MHz, $CDCl_3$, 25 °C): δ [ppm] = 1.99 (s, 6H, j), 2.79 (s, 6H, h), 2.94 (s, 6H, h'), 4.56 (s, 2H, f), 7.29 (m, 1H, d), 7.34 (t, 1H, b, ^{3}J = 5.6 Hz, ^{3}J = 6.3 Hz), 7.79 (t, 1H, c, ^{3}J = 7.0 Hz, ^{3}J = 7.5 Hz), 8.78 (m, 1H, a). ^{13}**C-NMR** (125 MHz, $CDCl_3$, 25 °C): δ [ppm] = 22.7 (CH_3, j), 39.3 (CH_3, h'), 39.8 (CH_3, h), 52.5 (CH_2, f), 122.6 (CH, d), 123.2 (CH, b), 138.9 (CH, c), 148.6 (CH, a), 158.1 (C, e), 165.8 (C, g), 178.9 (C, i). **IR** (KBr, $\tilde{\nu}$[cm^{-1}]): 3068 w (ν(C-$H_{arom.}$)), 3024 w (ν(C-$H_{arom.}$)), 2995 w (ν(C-$H_{aliph.}$)), 2941 w (ν(C-$H_{aliph.}$)), 2902 w (ν(C-$H_{aliph.}$)), 2893 w (ν(C-$H_{aliph.}$)), 2862 w (ν(C-$H_{aliph.}$)), 2833 w (ν(C-$H_{aliph.}$)), 1618 s, 1608 s, 1593 m, 1574 s, 1560 vs (ν(C=N)), 1541 m, 1489 m, 1473 m, 1441 m, 1427 m, 1396 s, 1354 m, 1327 m, 1296 m, 1254 w, 1236 w, 1165 w, 1147 w, 1109 vw, 1078 w, 1057 w, 1026 w, 987 vw, 918 vw, 908 w, 833 vw, 779 w, 769 vw, 742 vw, 717 vw, 675 m, 650 w, 617 w, 594 w. **EI-MS** (m/z, (%)): 388 (36) [M^+], 329 (9) [M^+ -CH_3COO], 206 (81) [M^+ -$Zn(CH_3COO)_2$], 162 (88) [M^+ -$Zn(CH_3COO)_2$ -$N(CH_3)_2$], 147 (69) [M^+ -$Zn(CH_3COO)_2$ -$N(CH_3)_2$ -CH_3], 93 (90) [M^+ -$Zn(CH_3COO)_2$ -$NC(N(CH_3)_2)_2$ +H], 92 (100) [M^+ -$Zn(CH_3COO)_2$ -$NC(N(CH_3)_2)_2$], 85 (86) [$CH_2NC(N(CH_3)_2)^+$ +2H], 65 (77). **CHN analysis**: calculated: C 46.18, H 6.16, N 14.37; found: C 46.23, H 6.25, N 14.30.

[Zn(TEGpy)Cl_2] (17a):

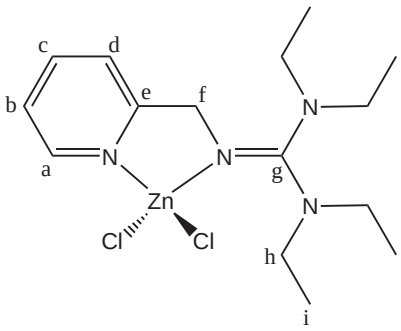

$C_{15}H_{26}N_4Cl_2Zn$ (M = 398.70 g/mol): Colourless crystals; **Yield**: 0.370 g = 0.93 mmol = 93 %; **m.p.** 148°C. ^{1}**H-NMR** (500 MHz, CD_3CN, 25 °C): δ [ppm] = 1.11 (q, 6H, i, ^{3}J = 7.1 Hz), 1.18 (q, 6H, i', ^{3}J = 7.1 Hz), 3.11 (q, 4H, h, ^{3}J = 7.1 Hz), 3.45 (q, 4H, h', ^{3}J = 7.1 Hz), 4.57 (s, 2H, f), 7.54 (dd, 1H, b, ^{3}J = 5.4 Hz, ^{3}J = 7.2 Hz), 7.58 (d, 1H, d, ^{3}J = 7.9 Hz), 8.03 (m, 1H, c), 8.51 (d, 1H, a, ^{3}J = 5.4 Hz). ^{13}**C-NMR** (125 MHz, CD_3CN, 25 °C): δ [ppm] = 12.5 (CH_3, i'), 12.7 (CH_3, i), 42.9 (CH_2, h'), 43.1 (CH_2, h), 52.4 (CH_2, f), 122.9 (CH, d), 124.0 (CH, b), 140.1 (CH, c), 146.8 (CH, a), 158.4 (C, e), 165.4 (C, g). **IR** (KBr, $\tilde{\nu}$[cm^{-1}]): 3086 w (ν(C-$H_{arom.}$)), 3061 w (ν(C-$H_{arom.}$)), 2970 s (ν(C-$H_{aliph.}$)), 2933 m (ν(C-$H_{aliph.}$)), 2872 m (ν(C-$H_{aliph.}$)), 2827 w (ν(C-$H_{aliph.}$)), 1608 s (ν(C=N)), 1574 s (ν(C=N)), 1541 vs (ν(C=N)), 1498 s, 1477 s, 1456 s, 1439 s, 1425 s, 1383 m, 1369 m, 1336 m, 1348 m, 1282 s, 1240 m, 1203 m, 1149 m, 1107 m, 1080 m, 1073 m, 1057 m, 1038 m, 1024 m, 1005 m, 976 w, 957 w, 947 w, 937 w, 899 vw, 866 w, 831 vw, 791 m, 775 s, 754 m, 741 w, 717 m, 650 m, 625 w, 594 w, 563 vw.

EI-MS (m/z, (%)): 365 (16) [M^+ -Cl: $C_{15}H_{26}N_4{}^{68}Zn^{35}Cl$, $C_{15}H_{26}N_4{}^{66}Zn^{37}Cl$], 363 (29) [$M^+$ -Cl: $C_{15}H_{26}N_4{}^{66}Zn^{35}Cl$, $C_{15}H_{26}N_4{}^{64}Zn^{37}Cl$], 361 (30) [$M^+$ -Cl: $C_{15}H_{26}N_4{}^{64}Zn^{35}Cl$], 262 (82) [$C_{15}H_{26}N_4{}^+$], 233 (13) [$C_{13}H_{21}N_4{}^+$], 191 (65), 190 (91) [$C_{11}H_{16}N_3{}^+$], 189 (25), 162 (27) [$C_9H_{12}N_3{}^+$ +H], 161 (34) [$C_9H_{12}N_3{}^+$], 160 (44), 132 (13), 120 (21) [$C_7H_6N_2{}^+$ +2H], 113 (11), 94 (20), 93 (100) [$C_6H_6N^+$ +H], 92 (93) [$C_6H_6N^+$], 72 (45) [$C_4H_{10}N^+$], 65 (51), 56 (12). **CHN analysis**: calculated: C 45.15, H 6.52, N 14.05; found: C 45.25, H 6.46, N 14.05.

[Zn(DMorphGpy)Cl_2] (19a):

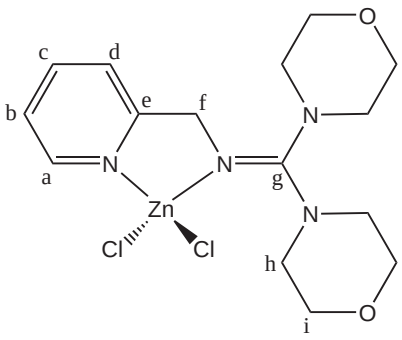

$C_{15}H_{22}N_4O_2ZnCl_2$ (M = 426.67 g/mol): Colourless crystals; **Yield**: 0.226 g = 0.53 mmol = 53 %; **m.p.** 264°C with decomposition. ^{1}**H-NMR** (500 MHz, CD_3CN, 25 °C): δ [ppm] = 3.17 (t, 4H, h, ^3J = 4.7 Hz), 3.50 (t, 4H, h', ^3J = 4.7 Hz), 3.71 (t, 4H, i, ^3J = 4.7 Hz), 3.77 (t, 4H, i', ^3J = 4.7 Hz), 4.67 (s, 2H, f), 7.57 (m, 2H, b+d), 8.05 (m, 1H, c), 8.52 (d, 1H, a, ^3J = 5.1 Hz). ^{13}**C-NMR** (125 MHz, CD_3CN, 25 °C): δ [ppm] = 48.6 (CH_2, h), 52.3 (CH_2, f), 65.9 (CH_2, i), 66.1 (CH_2, i'), 122.8 (CH, d), 124.2 (CH, b), 140.4 (CH, c), 147.0 (CH, a), 158.0 (C, e), 164.9 (C, g). **IR** (KBr, $\tilde{\nu}$[cm^{-1}]): 3115 w (ν(C-$H_{aliph.}$)), 3089 w (ν(C-$H_{aliph.}$)), 3062 w (ν(C-$H_{aliph.}$)), 3030 m (ν(C-$H_{aliph.}$)), 2970 m (ν(C-$H_{aliph.}$)), 2924 m (ν(C-$H_{aliph.}$)), 2904 m (ν(C-$H_{aliph.}$)), 2856 m (ν(C-$H_{aliph.}$)), 1612 m, 1576 s, 1549 vs (ν(C=N)), 1506 s (ν(C=N)), 1441 s, 1385 m, 1350 m, 1298 m, 1269 s, 1250 s, 1228 m, 1219 m, 1198 m, 1186 w, 1159 m, 1107 s, 1068 m, 1051 m, 1026 m, 1001 m, 986 w, 968 w, 930 w, 883 s, 845 m, 766 m, 758 m, 731 w, 708 w, 669 vw, 650 w, 642 m, 598 m, 563 m, 538 w. **EI-MS** (m/z, (%)): 380 (15) [M^+ -C_2H_4O], 349 (6) [M^+ -C_2H_4O -Cl], 326 (10), 248 (65) [$C_{13}H_{18}N_4O^+$ +2H], 240 (15), 204 (17) [$C_{11}H_{14}N_3{}^+$], 183 (14) [$C_9H_{16}N_2O_2{}^+$ -H], 162 (28), 120 (37), 119 (77), 108 (91), 107 (58) [$C_6H_6N_2{}^+$ +H], 93 (59), 92 (66) [$C_6H_6N^+$], 91 (56), 86 (27) [$C_4H_8NO^+$], 85 (27), 80 (100), 79 (75) [$C_5H_4N^+$ +H], 72 (69), 71 (58). **CHN analysis**: calculated: C 42.19, H 5.16, N 13.12; found: C 42.16, H 5.10, N 13.19.

[Zn(DMorphGpy)($CH_3COO)_2$] (19b):

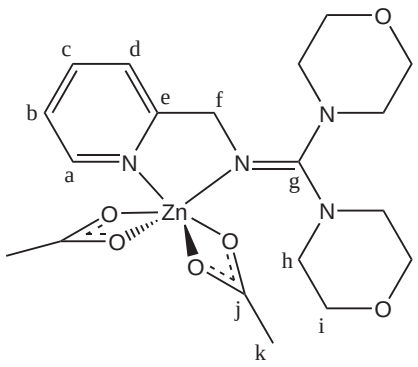

$C_{19}H_{28}N_4O_6Zn$ (M = 473.84 g/mol): Colourless crystals; **Yield**: 0.402 g = 0.85 mmol = 85 %; **m.p.** 192°C. ^{1}**H-NMR** (500 MHz, CD_3CN, 25 °C): δ [ppm] = 1.86 (s, 6H, k), 3.20 (t, 4H, h, ^3J = 4.7 Hz), 3.40 (t, 4H, h', ^3J = 4.7 Hz), 3.71 (dd, 8H, i, ^3J = 4.7 Hz), 4.64 (s, 2H, f), 7.47 (t, 1H, b, ^3J = 6.4 Hz), 7.50 (d, 1H, d, ^3J = 7.9 Hz), 7.97 (m, 1H, c), 8.69 (d, 1H, a, ^3J = 5.0 Hz). ^{13}**C-NMR** (125 MHz, CD_3CN, 25 °C): δ [ppm] = 21.7 (CH_3, k), 48.5 (CH_2, h), 52.2 (CH_2, f), 66.1 (CH_2, i), 122.3 (CH, d), 123.3 (CH, b), 139.7 (CH, c), 148.0 (CH, a), 158.4 (C, e), 164.9 (C, g), 177.5 (C, j). **IR** (KBr, $\tilde{\nu}$[cm^{-1}]): 3111 m (ν(C-$H_{arom.}$)), 3076 m (ν(C-$H_{arom.}$)), 3053 m (ν(C-$H_{arom.}$)), 3034 m (ν(C-

$H_{arom.}$)), 3003 m (ν(C-$H_{arom.}$)), 2972 m (ν(C-$H_{aliph.}$)), 2902 m (ν(C-$H_{aliph.}$)), 2864 m (ν(C-$H_{aliph.}$)), 2771 w (ν(C-$H_{aliph.}$)), 2744 w (ν(C-$H_{aliph.}$)), 2686 w (ν(C-$H_{aliph.}$)), 1606 s (ν(C=N)), 1591 vs (ν(C=N)), 1543 vs (ν(C=N)), 1491 s, 1460 s, 1446 s, 1437 s, 1428 s, 1411 s, 1394 s, 1356 m, 1340 m, 1292 m, 1265 m, 1261 s, 1242 s, 1228 m, 1215 m, 1207 m, 1159 m, 1109 vs, 1072 m, 1063 m, 1049 m, 1032 m, 1022 m, 999 m, 978 w, 962 w, 930 m, 878 s, 852 w, 841 m, 829 w, 775 m, 762 m, 748 m, 731 w, 714 w, 677 m, 638 m, 623 m, 604 m, 559 m. **EI-MS** (m/z, (%)): 472 (6) [M^+], 290 (66) [M^+ - $Zn(CH_3COO)_2$], 257 (12), 256 (13), 245 (49), 205 (22) [$C_{11}H_{14}N_3O^+$ +H], 204 (77) [$C_{11}H_{14}N_3O^+$], 127 (14), 117 (10), 93 (100) [$C_6H_6N^+$ +H], 92 (96) [$C_6H_6N^+$], 86 (16) [$C_4H_8NO^+$], 78 (11) [$C_5H_4N^+$], 65 (36), 56 (14). **CHN analysis**: calculated: C 48.12, H 5.91, N 11.82; found: C 48.04, H 5.77, N 11.79.

[Zn(MorphDMGpy)Cl_2] (20a):

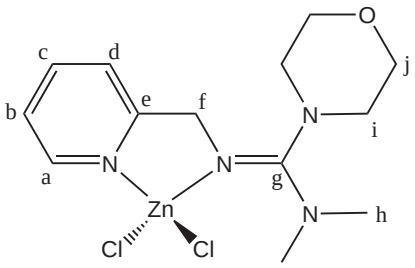

$C_{13}H_{20}N_4OZnCl_2$ (M = 384.63 g/mol): Colourless crystals; **Yield**: 0.212 g = 0.55 mmol = 55 %; **m.p.** 218°C. ^{1}**H-NMR** (500 MHz, CD_3CN, 25 °C): δ [ppm] = 2.80 (s, 4H, h), 3.02 (s, 2H, h'), 3.14 (t, 2H, i, ^3J = 4.6 Hz), 3.45 (t, 2H, i', ^3J = 4.6 Hz), 3.71 (t, 2H, j, ^3J = 4.6 Hz), 3.77 (t, 2H, j', ^3J = 4.6 Hz), 4.61 (s, 1H, f'), 4.66 (s, 1H, f), 7.56 (m, 2H, b+d), 8.04 (t, 1H, c, ^3J = 7.6 Hz), 8.53 (d, 1H, a, ^3J = 4.7 Hz). ^{13}**C-NMR** (125 MHz, CD_3CN, 25 °C): δ [ppm] = 39.4 (CH_3, h), 48.3 (CH_2, i), 52.0 (CH_2, f), 66.1 (CH_2, j), 122.8 (CH, b), 124.0 (CH, d), 140.3 (CH, c), 147.0 (CH, a), 158.3 (C, e), 166.1 (C, g). **IR** (KBr, $\tilde{\nu}$[cm^{-1}]): 3095 vw (ν(C-$H_{arom.}$)), 3059 vw (ν(C-$H_{arom.}$)), 2979 w (ν(C-$H_{aliph.}$)), 2954 m (ν(C-$H_{aliph.}$)), 2893 m (ν(C-$H_{aliph.}$)), 2862 m (ν(C-$H_{aliph.}$)), 2796 vw (ν(C-$H_{aliph.}$)), 1610 s (ν(C=N)), 1587 vs (ν(C=N)), 1566 s (ν(C=N)), 1516 vs, 1471 m, 1448 m, 1410 s, 1375 w, 1358 m, 1340 m, 1302 w, 1286 m ,1271 m, 1252 m, 1228 m, 1209 m, 1151 w, 1113 s, 1097 m, 1068 m, 1051 w, 1036 w, 1026 m, 1014 w, 978 vw, 930 vw, 891 m, 843 w, 775 m, 762 w, 743 vw, 721 w, 658 w, 646 m, 621 w, 565 w, 542 vw. **EI-MS** (m/z, (%)): 382 (42) [M^+], 370 (17), 352 (12), 326 (11), 279 (16), 248 (21) [M^+ -$ZnCl_2$], 167 (31), 162 (17) [$C_9H_{12}N_3^+$], 149 (100) [$C_8H_9N_3^+$ +2H], 127 (10) [$C_7H_{14}N_2^+$ +H], 113 (12), 93 (49) [$C_6H_6N^+$ +H], 92 (50) [$C_6H_6N^+$], 85 (19), 71 (23) [$C_4H_8N^+$ +H, $C_3H_6N_2^+$ +H], 70 (14) [$C_4H_8N^+$, $C_3H_6N_2^+$], 69 (15), 64 (13), 57 (52) [$C_3H_6N^+$ +H], 55 (18). **CHN analysis**: calculated: C 40.56, H 5.20, N 14.56; found: C 40.63, H 5.10, N 14.51.

[(DMEGpico)$_2$ZnCl$_2$] (21a):

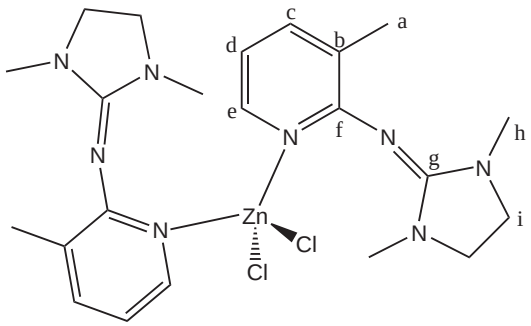

C$_{22}$H$_{32}$N$_8$ZnCl$_2$ (M = 544.86 g/mol): Colourless crystals; **Yield**: 0.264 g = 0.49 mmol = 97 %; **m.p.** 206°C. ^{1}**H-NMR** (500 MHz, CD_3CN, 25 °C): δ [ppm] = 2.02 (s, 6H, a), 2.41 (s, 12H, h), 3.20 (s, 8H, i), 7.30 (dd, 2H, d, ^3J = 5.7 Hz, ^3J = 7.2 Hz), 7.83 (d, 2H, c, ^3J = 7.2 Hz,), 8.44 (m, 2H, e). ^{13}**C-NMR** (125 MHz, CD_3CN, 25 °C): δ [ppm] = 16.8 (CH_3, a), 33.2 (CH_3, h), 47.7 (CH_2, i), 115.5 (CH, d), 126.2 (C, b), 139.7 (CH, c), 144.4 (CH, e), 154.5 (C, f), 160.9 (C, g). **IR** (KBr, $\tilde{\nu}$[cm^{-1}]): 3070 w (ν(C-H$_{arom.}$)), 3053 w (ν(C-H$_{arom.}$)), 2939 m (ν(C-H$_{aliph.}$)), 2860 m (ν(C-H$_{aliph.}$)), 1651 vs (ν(C=N)), 1599 s (ν(C=N)), 1562 s (ν(C=N)), 1506 s, 1471 s, 1446 s, 1433 s, 1404 s, 1381 m, 1333 m, 1284 s, 1240 m, 1188 m, 1122 m, 1080 m, 1034 s, 995 m, 970 m, 899 w, 849 vw, 810 w, 787 m, 715 m, 708 m, 698 m, 654 w, 607 w, 592 vw, 532 vw. **EI-MS** (m/z, (%)): 307 (3) [$C_{11}H_{16}N_4ZnCl^+$], 305 (4) [$C_{11}H_{16}N_4ZnCl^+$], 303 (5) [$C_{11}H_{16}N_4ZnCl^+$], 204 (92) [$C_{11}H_{16}N_4^+$], 189 (100) [$C_{11}H_{16}N_4^+$ -CH_3], 148 (9), 119 (10) [$C_7H_6N_2^+$ +H], 98 (15) [$C_5H_{10}N_2^+$], 92 (19) [$C_6H_6N^+$], 65 (10). **CI-MS** (m/z, (%)): 511 (0.1) [M^+ -Cl], 509 (0.4) [M^+ -Cl], 507 (0.2) [M^+ -Cl], 410 (2), 409 (6) [M^+ -Cl -$C_5H_{10}N_2$], 307 (0.5) [$C_{11}H_{16}N_4ZnCl^+$], 305 (1) [$C_{11}H_{16}N_4ZnCl^+$], 303 (0.8) [$C_{11}H_{16}N_4ZnCl^+$], 205 (100) [$C_{11}H_{16}N_4^+$ +H], 204 (39) [$C_{11}H_{16}N_4^+$], 57 (100). **CHN analysis**: calculated: C 48.45, H 5.87, N 20.56; found: C 48.83, H 5.99, N 20.50.

[(TMGpico)$_2$ZnCl$_2$] (22a):

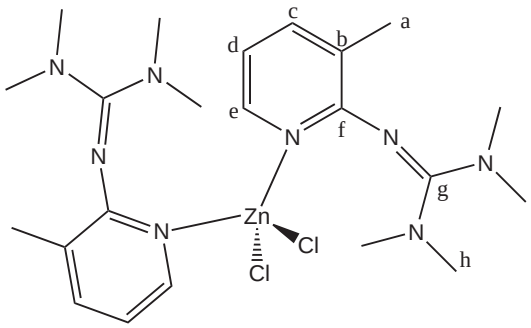

C$_{22}$H$_{36}$N$_8$ZnCl$_2$ (M = 548.89 g/mol): Colourless crystals; **Yield**: 0.270 g = 0.49 mmol = 98 %; **m.p.** 232°C. ^{1}**H-NMR** (500 MHz, CD_3CN, 25 °C): δ [ppm] = 2.24 (s, 6H, a), 2.99 (s, 24H, h), 7.30 (m, 2H, d), 7.83 (m, 2H, c), 8.45 (m, 2H, e). ^{13}**C-NMR** (125 MHz, CD_3CN, 25 °C): δ [ppm] = 16.3 (CH_3, a), 39.8 (CH_3, h), 121.3 (CH, d), 126.0 (C, b), 141.9 (CH, c), 146.2 (CH, e), 159.0 (C, f), 166.2 (C, g). **IR** (KBr, $\tilde{\nu}$[cm^{-1}]): 3199 m (ν(C-H$_{arom.}$)), 3161 m (ν(C-H$_{arom.}$)), 3124 m (ν(C-H$_{arom.}$)), 3101 m (ν(C-H$_{arom.}$)), 3057 m (ν(C-H$_{arom.}$)), 3022 m (ν(C-H$_{arom.}$)), 2974 m (ν(C-H$_{aliph.}$)), 2947 m (ν(C-H$_{aliph.}$)), 2914 m (ν(C-H$_{aliph.}$)), 2806 m, 1633 vs (ν(C=N)), 1603 s (ν(C=N)), 1585 m (ν(C=N)), 1562 vs (ν(C=N)), 1508 w, 1458 s, 1442 s, 1419 m, 1410 s, 1396 s, 1311 m, 1284 m, 1267 w, 1228 m, 1190 m, 1169 m, 1151 m, 1122 m, 1068 m, 1039 m, 1001 m, 926 m, 879 m, 810 m, 789 m, 733 m, 700 m, 687 m, 650 m, 592 w, 552 w. **EI-MS** (m/z, (%)): 305 (21) [$ZnCl^{37}C_{11}H_{18}N_4^+$], 303 (30) [$ZnCl^{35}C_{11}H_{18}N_4^+$], 206 (93) [$C_{11}H_{18}N_4^+$], 191 (100) [$C_{11}H_{18}N_4^+$ -CH_3], 190 (26), 162 (84) [$C_{11}H_{18}N_4^+$ -$N(CH_3)_2$], 148 (41), 119 (89) [$C_{11}H_{18}N_4^+$ -$2N(CH_3)_2$ +H], 107 (14), 92 (17) [$C_6H_6N^+$], 65 (32). **CHN analysis**: calculated: C 48.10, H 6.56, N 20.40; found: C 48.05, H 6.54, N 20.21.

[(TMGpico)$_2$Zn$_3$(CH$_3$COO)$_6$] (22b):

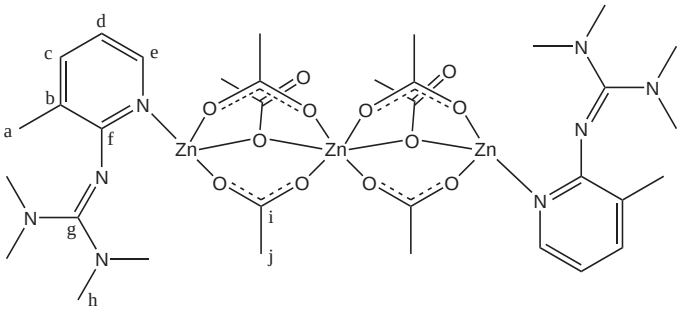

C$_{34}$H$_{54}$N$_8$Zn$_3$O$_{12}$ (M = 963.01 g/mol): Colourless crystals; **Yield**: 0.968 g = 1.01 mmol = 67 %; **m.p.** 88°C. ^{1}**H-NMR** (500 MHz, CD$_3$CN, 25 °C): δ [ppm] = 1.96 (s, 18H, j), 2.08 (s, 6H, a), 2.79 (s, 24H, h), 6.91 (dd, 2H, d, ^{3}J = 7.4 Hz, ^{3}J = 5.1 Hz), 7.60 (dd, 2H, c, ^{3}J = 7.4 Hz, ^{4}J = 0.9 Hz), 8.07 (dd, 2H, e, ^{3}J = 5.1 Hz, ^{4}J = 0.9 Hz). ^{13}**C-NMR** (125 MHz, CD$_3$CN, 25 °C): δ [ppm] = 16.6 (CH$_3$, a), 22.1 (CH$_3$, j), 39.0 (CH$_3$, h), 116.9 (CH, d), 124.4 (C, b), 140.4 (CH, c), 144.26 (CH, e), 159.4 (C, f), 168.3 (C, g), 179.2 (C, i). **IR** (KBr, $\tilde{\nu}$[cm^{-1}]): 3005 m (ν(C-H$_{arom.}$)), 2931 m (ν(C-H$_{aliph.}$)), 2802 w (ν(C-H$_{aliph.}$)), 1589 vs (ν(C=N)), 1552 s, 1427 s, 1390 s, 1335 m, 1273 vw, 1234 w, 1221 w, 1186 w, 1153 w, 1065 vw, 1029 m, 995 vw, 926 vw, 887 vw, 798 w, 741 vw, 673 m, 617 w, 561 vw, 538 vw. **EI-MS** (m/z, (%)): 206 (56) [C$_{11}$H$_{18}$N$_4^+$], 191 (97) [C$_{11}$H$_{18}$N$_4^+$ -CH$_3$], 162 (65) [C$_{11}$H$_{18}$N$_4^+$ -N(CH$_3$)$_2$], 148 (51), 119 (100) [C$_{11}$H$_{18}$N$_4^+$ -2 N(CH$_3$)$_2$ +H], 107 (16), 93 (17) [C$_6$H$_6$N$^+$ +H], 92 (82) [C$_6$H$_6$N$^+$], 65 (31). **CHN analysis**: calculated: C 42.37, H 5.61, N 11.63; found: C 42.04, H 5.47, N 11.52.

[TMG$_4$(beam)$_2$b(ZnCl$_2$)$_2$] (28a):

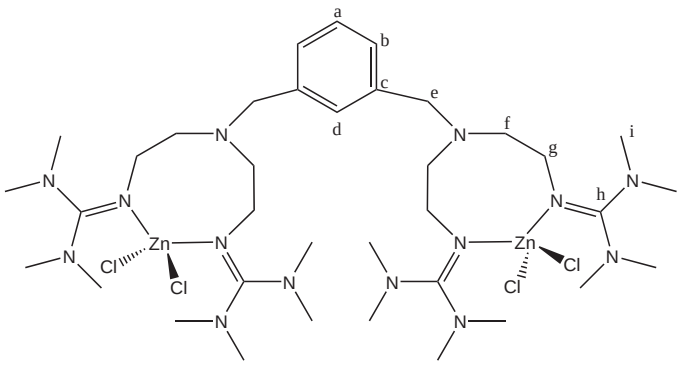

C$_{36}$H$_{72}$N$_{14}$Zn$_2$Cl$_4$ (M = 973.67 g/mol): Colourless crystals; **Yield**: 1.499 g = 1.54 mmol = 77 %; **m.p.** 158°C. ^{1}**H-NMR** (500 MHz, CD$_3$CN, 25 °C): δ [ppm] = 2.61 (m, 8H, f), 2.81 (m, 24H, i), 2.87 (m, 24H, i'), 3.18 (m, 8H, g), 4.03 (s, 4H, e), 7.35 (m, 3H, a+b), 7.59 (s, 1H, d). ^{13}**C-NMR** (125 MHz, CD$_3$CN, 25 °C): δ [ppm] = 38.9 (CH$_3$, i), 39.2 (CH$_3$, i'), 46.5 (CH$_2$, g), 53.8 (CH$_2$, f), 59.2 (CH$_2$, e), 127.9 (CH, b), 130.2 (CH, a), 133.9 (CH, d), 135.6 (C, c), 166.6 (C, h). **IR** (KBr, $\tilde{\nu}$[cm^{-1}]): 3003 w (ν(C-H$_{arom.}$)), 2931 m (ν(C-H$_{aliph.}$)), 2898 m (ν(C-H$_{aliph.}$)), 2854 m (ν(C-H$_{aliph.}$)), 1618 s (ν(C=N)), 1577 vs (ν(C=N)), 1533 m, 1458 m, 1425 m, 1400 m, 1394 m, 1361 w, 1346 w, 1261 vw, 1238 w, 1159 m, 1147 m, 115 vw, 1066 w, 1049 w, 1022 vw, 987 vw, 893 w, 808 vw, 768 w, 742 vw, 719 w, 669 w, 617 w, 586 w. **EI-MS** (m/z, (%)): 701 (44) [M$^+$ - 2 ZnCl$_2$], 586 (8) [M$^+$ -HN(C(N(CH$_3$)$_2$)$_2$) -2 ZnCl$_2$], 572 (100) [M$^+$ -CH$_3$N(C(N(CH$_3$)$_2$)$_2$) -2 ZnCl$_2$], 558 (13), 470 (17), 457 (42), 432 (9), 401 (14) [M$^+$ -3 C(N(CH$_3$)$_2$) -2 ZnCl$_2$], 274 (15), 180 (26), 142 (73), 128 (36) [CH$_2$N(C(N(CH$_3$)$_2$)$_2$)$^+$], 85 (89), 72 (22), 58 (25) [C(N(CH$_3$)$_2^+$ + 2H]. **CHN analysis**: calculated: C 44.37, H 7.39, N 20.13; found: C 44.18, H 7.47, N 18.35.

[Zn(DMEG$_3$tren)Cl][Cl] (29a):

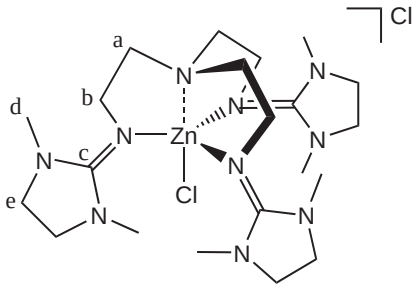

$C_{21}H_{42}N_{10}ZnCl_2$ (M = 570.94 g/mol): Colourless crystals; **Yield**: 0.347 g = 0.61 mmol = 61 % ; **m.p.** 230°C. ^{1}**H-NMR** (500 MHz, CD_3CN, 25 °C): δ [ppm] = 2.61 (s, 6H, a), 2.82 (s, 18H, d), 3.32 (br, 6H, b), 3.43 (s, 12H, e). ^{13}**C-NMR** (125 MHz, CD_3CN, 25 °C): δ [ppm] = 35.8 (CH_3, d), 46.3 (CH_2, b), 48.8 (CH_2, e), 56.0 (CH_2, a), 166.8 (C, c). **IR** (KBr, $\tilde{\nu}$[cm^{-1}]): 2945 s (ν(C-H$_{aliph.}$)), 2858 s (ν(C-H$_{aliph.}$)), 1653 vs (ν(C=N)), 1645 vs (ν(C=N)), 1635 vs (ν(C=N)), 1616 vs (ν(C=N)), 1597 vs (ν(C=N)), 1560 s, 1543 m, 1508 s, 1491 s, 1458 s, 1421 s, 1406 s, 1383 m, 1342 m, 1298 s, 1271 s, 1232 m, 1167 m, 1138 m, 1124 m, 1078 m, 1053 m, 1020 m, 976 m, 939 w, 910 m, 895 w, 851 vw, 770 m, 725 m, 702 m, 648 m, 604 m, 554 m, 525 m. **EI-MS** (m/z, (%)): 537 (1) [M$^+$: $C_{21}H_{42}N_{10}{}^{66}Zn^{37}Cl$, $C_{21}H_{42}N_{10}{}^{68}Zn^{35}Cl$], 535 (2) [M$^+$: $C_{21}H_{42}N_{10}{}^{66}Zn^{35}Cl$, $C_{21}H_{42}N_{10}{}^{64}Zn^{37}Cl$], 533 (2) [M$^+$: $C_{21}H_{42}N_{10}{}^{64}Zn^{35}Cl$], 435 (2) [M$^+$ -ZnCl], 308 (41) [M$^+$ - ZnCl - $N_3C_6H_{10}{}^+$ -H], 208 (19), 195 (38) [$N_4C_{10}H_{20}{}^+$ -H], 169 (14) [$N_4C_8H_{16}{}^+$ +H], 140 (34) [$N_3C_7H_{14}{}^+$], 126 (100) [$N_3C_6H_{10}{}^+$], 98 (11) [$N_2C_5H_{10}{}^+$]. **CHN analysis**: calculated: C 44.14, H 7.36, N 24.52; found: C 43.38, H 7.34, N 24.02.

[Zn(TMG$_3$tren)Cl][Cl] (30a):

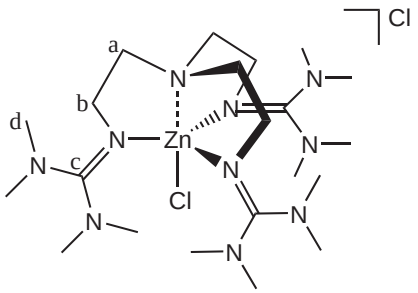

$C_{21}H_{48}N_{10}ZnCl_2$ (M = 576.98 g/mol): Colourless crystals; **Yield**: 0.207 g = 0.36 mmol = 36 %; **m.p.** 180°C. ^{1}**H-NMR** (500 MHz, CD_3CN, 25 °C): δ [ppm] = 2.63 (m, 6H, a), 2.67 (s, 8H, d), 2.75 (s, 9H, d'), 2.82 (s, 10H, d"), 2.85 (m, 3H, b), 2.92 (s, 9H, d'"), 3.40 (m, 3H, b'). ^{13}**C-NMR** (125 MHz, CD_3CN, 25 °C): δ [ppm] = 37.9 (CH_3, d), 38.6 (CH_3, d'), 39.2 (CH_3, d"), 39.4 (CH_3, d'"), 46.2 (CH_2, b), 54.2 (CH_2, a), 166.0 (C, c). **IR** (KBr, $\tilde{\nu}$[cm^{-1}]): 2991 m (ν(C-H$_{aliph.}$)), 2945 s (ν(C-H$_{aliph.}$)), 2887 s (ν(C-H$_{aliph.}$)), 2854 m (ν(C-H$_{aliph.}$)), 1556 vs (ν(C=N)), 1468 s, 1444 m, 1425 s, 1394 vs, 1344 s, 1282 m, 1257 m, 1248 m, 1232 m, 1165 s, 1149 s, 1119 w, 1080 m, 1066 m, 1051 m, 1026 w, 1011 m, 985 m, 908 m, 893 m, 766 m, 743 w, 721 w, 590 w, 559 w, 532 w. **EI-MS** (m/z, (%)): 543 (1) [M$^+$: $C_{21}H_{48}N_{10}{}^{66}Zn^{37}Cl$, $C_{21}H_{48}N_{10}{}^{68}Zn^{35}Cl$], 541 (1) [M$^+$: $C_{21}H_{48}N_{10}{}^{66}Zn^{35}Cl$, $C_{21}H_{48}N_{10}{}^{64}Zn^{37}Cl$], 539 (2) [M$^+$: $C_{21}H_{48}N_{10}{}^{64}Zn^{35}Cl$], 439 (1) [M$^+$ -ZnCl -H], 396 (2) [$N_9C_{19}H_{42}{}^+$], 313 (31), 312 (95) [$N_7C_{15}H_{34}{}^+$], 255 (20), 222 (15), 210 (93), 197 (20), 171 (20), 142 (83) [$N_3C_7H_{16}{}^+$], 128 (91) [$N_3C_6H_{14}{}^+$], 126 (45), 111 (21), 100 (20) [$N_2C_5H_{12}{}^+$], 97 (22), 85 (100). **CHN analysis**: calculated: C 43.68, H 8.32, N 24.26; found: C 43.46, H 8.08, N 23.67.

[Zn(qu)Cl_2] (32a):

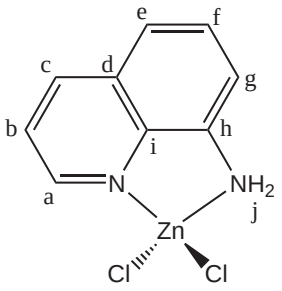

$C_9H_8N_2ZnCl_2$ (M = 280.48 g/mol): Colourless crystals; **Yield**: 0.275 g = 0.98 mmol = 98 %; **m.p.** 280°C with decomposition. ^{1}**H-NMR** (500 MHz, DMSO-d_6, 25 °C): δ [ppm] = 5.89 (s, 2H, j), 6.88 (dd, 1H, g, ^3J = 7.8 Hz, ^4J = 1.2 Hz), 7.07 (dd, 1H, e, ^3J = 7.8 Hz, ^4J = 1.2 Hz), 7.30 (t, 1H, f, ^3J = 7.8 Hz), 7.46 (dd, 1H, b, ^3J = 8.3 Hz, ^3J = 4.1 Hz), 8.18 (dd, 1H, c, ^3J = 8.3 Hz, ^4J = 1.7 Hz), 8.73 (dd, 1H, a, ^3J = 4.1 Hz, ^4J = 1.7 Hz). ^{13}**C-NMR** (125 MHz, DMSO-d_6, 25 °C): δ [ppm] = 109.3 (CH, g), 114.3 (CH, e), 121.9 (CH, b), 128.0 (CH, f), 129.0 (C, d), 136.3 (CH, c), 137.9 (C, i), 145.6 (C, h), 147.4 (CH, a). **IR** (KBr, $\tilde{\nu}$[cm^{-1}]): 3205 vs (ν(N-H)), 3120 s (ν(C-$H_{arom.}$)), 3072 m (ν(C-$H_{arom.}$)), 1628 m, 1593 m, 1572 s, 1527 w, 1504 vs, 1471 m, 1425 w, 1389 m, 1375 m, 1321 m, 1259 w, 1217 m, 1201 w, 1171 w, 1134 w, 1120 m, 1078 s, 1059 m, 1032 m, 991 vw, 960 vw, 901 m, 829 s, 808 vw, 783 m, 771 m, 721 m, 627 m, 590 m, 532 w, 511 m. **EI-MS** (m/z, (%)): 279 (17) [M^+], 175 (14), 173 (21), 167 (33), 149 (100), 144 (83) [M^+ - $ZnCl_2$], 127 (17), 117 (34), 106 (16), 97 (12), 83 (17), 71 (26), 69 (18), 57 (39), 55 (25). **CHN analysis**: calculated: C 38.51, H 2.85, N 9.98; found: C 38.61, H 3.01, N 9.94.

[Zn(qu)$_2$(CF_3SO_3)$_2$] (32c):

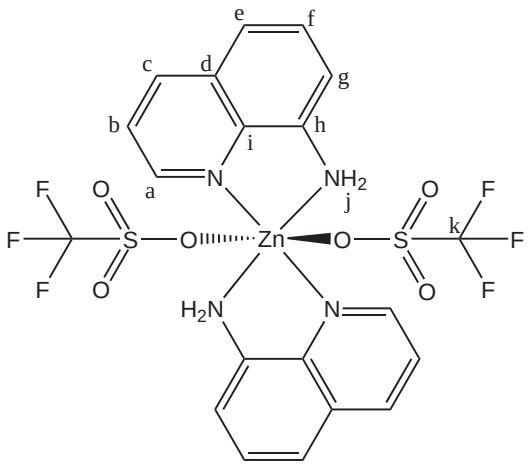

$C_{20}H_{16}N_4O_6F_6S_2Zn$ (M = 652.93 g/mol): Colourless crystals; **Yield**: 0.274 g = 0.42 mmol = 84 %; **m.p.** 299°C with decomposition. ^{1}**H-NMR** (500 MHz, DMSO-d_6, 25 °C): δ [ppm] = 5.88 (s, 4H, k), 6.90 (dd, 2H, g, ^3J = 7.8 Hz, ^4J = 1.2 Hz), 7.08 (dd, 2H, e, ^3J = 7.8 Hz, ^4J = 1.2 Hz), 7.31 (t, 2H, f, ^3J = 7.8 Hz, ^3J = 7.8 Hz), 7.46 (dd, 2H, b, ^3J = 8.3 Hz, ^3J = 4.1 Hz), 8.19 (dd, 2H, c, ^3J = 8.3 Hz, ^4J = 1.7 Hz), 8.73 (dd, 2H, a, ^3J = 4.1 Hz, ^4J = 1.7 Hz). ^{13}**C-NMR** (125 MHz, DMSO-d_6, 25 °C): δ [ppm] = 109.6 (CH, g), 114.5 (CH, e), 121.9 (CH, b), 122.5 (C, k), 128.0 (CH, f), 129.0 (C, d), 136.4 (CH, c), 138.0 (C, i), 145.4 (C, h), 147.5 (CH, a). **IR** (KBr, $\tilde{\nu}$[cm^{-1}]): 3275 m (ν(C-$H_{arom.}$)), 3234 m (ν(C-$H_{arom.}$)), 3147 m (ν(C-$H_{arom.}$)), 1632 w, 1593 w, 1585 w, 1506 m, 1475 w, 1427 vw, 1408 w, 1381 w, 1323 m, 1302 s, 1236 vs, 1226 s, 1207 m,1176 m, 1161 s, 1136 m, 1117 m, 1078 m, 1065 m, 1034 vs, 980 vw, 912 vw, 901 w, 829 m, 812 vw, 791 m, 773 m, 761 w, 719 w, 644 s, 636 s, 590 w, 577 m, 519 m. **CI-MS** (m/z, (%)): 651 (1) [M^+ +H], 289 (24), 201 (17), 187 (19), 183 (12), 145 (100) [M^+ -Zn(CF_3SO_3)$_2$ +H], 144 (78) [M^+ -Zn(CF_3SO_3)$_2$ +H], 57 (96). **CHN analysis**: calculated: C 36.8, H 2.5, N 8.6; found: C 36.8, H 2.6, N 8.7.

[Zn_3(bipy)$_2$(CH_3COO)$_6$] (33b):

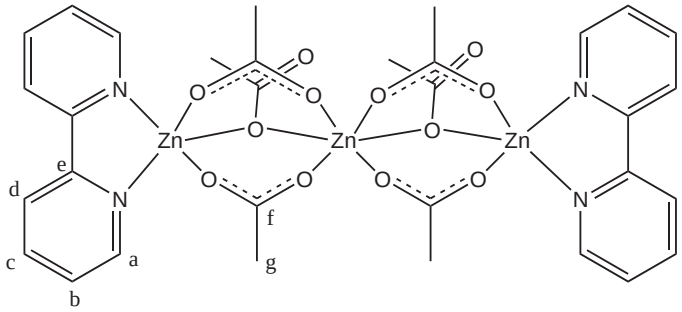

$C_{32}H_{34}N_4O_{12}Zn_3$ (M = 862.80 g/mol): Colourless crystals; **Yield**: 1.255 g = 1.46 mmol = 97 %; **m.p.** 168°C. ^{1}**H-NMR** (500 MHz, CD_3CN, 25 °C): δ [ppm] = 1.95 (s, 18H, g), 7.75 (m, 4H, b), 8.24 (m, 4H, c), 8.43 (m, 4H, d), 8.85 (m, 4H, a). ^{13}**C-NMR** (125 MHz, CD_3CN, 25 °C): δ [ppm] = 21.6 (CH_3, g), 122.0 (CH, d), 126.9 (CH, b), 141.3 (CH, c), 148.9 (C, e), 149.2 (CH, a), 179.4 (C, f). **IR** (KBr, $\tilde{\nu}$[cm^{-1}]): 3103 m (ν(C-$H_{arom.}$)), 3089 m (ν(C-$H_{arom.}$)), 3066 m (ν(C-$H_{arom.}$)), 3033 m (ν(C-$H_{arom.}$)), 3008 m (ν(C-$H_{arom.}$)), 2927 w (ν(C-$H_{aliph.}$)), 2852 w (ν(C-$H_{aliph.}$)), 1599 vs (ν(C-O)), 1577 s (ν(C-O)), 1493 m, 1473 m, 1446 s, 1425 m, 1338 m, 1313 m, 1286 w, 1254 w, 1223 vw, 1161 w, 1109 w, 1061 m, 1028 m, 1018 m, 972 vw, 941 w, 904 vw, 773 m, 735 m, 692 m, 677 m, 658 m, 634 m, 649 m. **EI-MS** (m/z, (%)): 571 (70), 469 (4), 389 (18), 256 (6), 156 (100) [$C_{10}H_8N_2^+$], 128 (18), 78 (14), 51 (12). **CHN analysis**: calculated: C 44.51, H 3.94, N 6.49; found: C 44.53, H 4.00, N 6.50.

[Zn(bipy)$_2$(CF_3SO_3)$_2$] (33c):

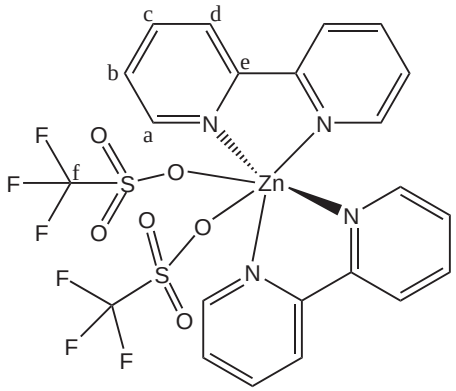

$C_{22}H_{16}F_6N_4O_6S_2Zn$ (M = 676.99 g/mol): Colourless crystals; **Yield**: 0.300 g = 0.44 mmol = 88 %; **m.p.** 291°C. ^{1}**H-NMR** (500 MHz, CD_3CN, 25 °C): δ [ppm] = 7.74 (m, 4H, b), 8.32 (m, 4H, c), 8.46 (m, 4H, a), 8.57 (m, 4H, d). ^{13}**C-NMR** (125 MHz, CD_3CN, 25 °C): δ [ppm] = 122.1 (C, f), 122.9 (CH, d), 127.3 (CH, b), 141.8 (CH, c), 148.1 (CH, a), 148.9 (C, e). **IR** (KBr, $\tilde{\nu}$[cm^{-1}]): 3114 w (ν(C-$H_{arom.}$)), 3097 w (ν(C-$H_{arom.}$)), 3086 w (ν(C-$H_{arom.}$)), 3074 w (ν(C-$H_{arom.}$)), 1610 m, 1601 m, 1579 m, 1568 w, 1493 m, 1477 m, 1446 m, 1306 vs, 1246 s, 1234 vs, 1219 s, 1176 m, 1161 s, 1120 w, 1107 w, 1063 w, 1026 vs, 980 vw, 904 vw, 895 vw, 818 vw, 771 s, 739 m, 654 m, 636 s, 580 w, 573 w, 517 m. **EI-MS** (m/z, (%)): 376 (2) [M^+ -2 CF_3SO_3], 373 (29), 371 (44), 369 (69), 348 (14), 346 (13), 243 (19), 241 (30), 239 (53), 157 (15), 156 (100) [$C_{10}H_8N_2^+$], 155 (66), 130 (12), 129 (29), 128 (37), 78 (36) [$C_5H_4N^+$], 52 (15), 51 (31), 50 (15). **CHN analysis**: calculated: C 39.0, H 2.4, N 8.3; found: C 39.0, H 2.6, N 8.2.

[Zn(phen)(CH_3COO)(μ-CH_3COO)$_2$Zn(phen)(CH_3COO)] (34b):

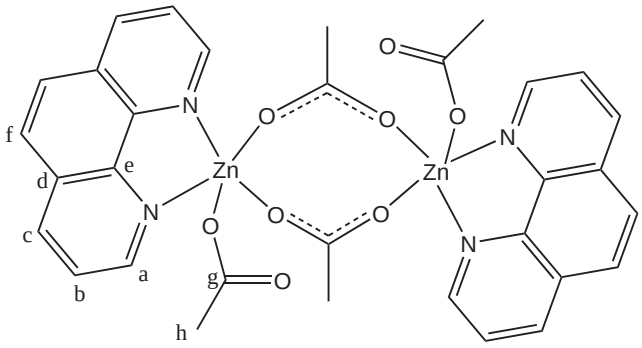

$C_{32}H_{28}N_4O_8Zn_2$ (M = 727.37 g/mol): Colourless crystals; **Yield**: 0.713 g = 0.98 mmol = 98 %; **m.p.** 248°C. ^{1}**H-NMR** (500 MHz, $CDCl_3$, 25 °C): δ [ppm] = 2.05 (s, 12H, h), 7.90 (dd, 4H, b, ^3J = 4.7 Hz, ^3J = 8.2 Hz), 7.97 (s, 4H, f), 8.52 (dd, 4H, c, ^3J = 8.2 Hz, ^4J = 1.5 Hz), 9.31 (dd, 4H, a, ^3J = 4.7 Hz, ^4J = 1.5 Hz). ^{13}**C-NMR** (125 MHz, $CDCl_3$, 25 °C): δ [ppm] = 21.7 (CH_3, h), 125.4 (CH, b), 126.8 (CH, f), 128.7 (C, d), 139.0 (CH, c), 141.1 (C, e), 150.4 (CH, a), 181.3 (C, g). **IR** (KBr, $\tilde{\nu}$[cm^{-1}]): 3064 w (ν(C-$H_{arom.}$)), 3014 w (ν(C-$H_{arom.}$)), 2927 w (ν(C-$H_{aliph.}$)), 1599 s (ν(C-O)), 1585 s (ν(C-O)), 1516 m, 1495 w, 1425 m, 1387 m, 1333 m, 1257 vw, 1217 vw, 1140 m, 1101 w, 1049 vw, 1016 w, 937 vw, 924 vw, 868 w, 854 m, 783 vw, 729 m, 679 w, 667 w, 640 w, 623 vw. **EI-MS** (m/z, (%)): 577 (37), 575 (70), 573 (84), 571 (88), 569 (54), 393 (27), 391 (52), 389 (72), 387 (62), 385 (33), 197 (16), 194 (71), 183 (39), 180 (100) [$C_{12}H_8N_2^+$], 179 (51), 154 (27). **CHN analysis**: calculated: C 52.79, H 3.85, N 7.70; found: C 52.62, H 3.83, N 7.72.

[Zn(phen)$_2$(CF_3SO_3)$_2$] (34c):

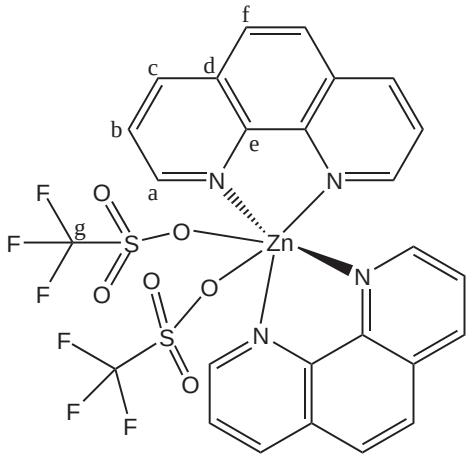

$C_{26}H_{16}F_6N_4O_6S_2Zn$ (M = 725.11 g/mol): Colourless crystals; **Yield**: 0.355 g = 0.49 mmol = 98 %; **m.p.** >300°C. ^{1}**H-NMR** (500 MHz, CD_3CN, 25 °C): δ [ppm] = 8.01 (dd, 4H, b, ^3J = 4.7 Hz, ^3J = 8.2 Hz), 8.27 (s, 4H, f), 8.79 (dd, 4H, a, ^3J = 4.7 Hz, ^4J = 1.3 Hz), 8.85 (dd, 4H, c, ^3J = 8.3 Hz, ^4J = 1.3 Hz). ^{13}**C-NMR** (125 MHz, CD_3CN, 25 °C): δ [ppm] = 122.1 (C, g), 125.8 (CH, b), 127.5 (CH, f), 129.7 (C, d), 140.4 (C, e), 140.5 (CH, c), 148.8 (CH, a). **IR** (KBr, $\tilde{\nu}$[cm^{-1}]): 3084 w (ν(C-$H_{arom.}$)), 3068 w (ν(C-$H_{arom.}$)), 1628 w, 1608 w, 1585 w, 1522 m, 1496 w, 1431 m, 1346 w, 1300 s, 1284 m, 1259 m, 1246 m, 1343 m, 1221 m, 1213 m, 1178 m, 1165 m, 1107 w, 1024 m, 999 w, 968 vw, 870 w, 850 m, 787 w, 758 vw, 729 m, 636 m, 580 w, 573 w, 516 m. **EI-MS** (m/z, (%)): 577 (6) [M^+ -CF_3SO_3], 496 (6), 467 (10), 439 (19), 410 (12), 386 (16), 368 (10), 344 (22), 331 (26), 312 (16), 293 (26), 264 (13), 257 (17), 248 (18), 239 (21), 215 (25), 183 (33) [$N_2C_{12}H_8^+$ +2H], 125 (22), 111 (36), 107 (36), 97 (57), 96 (43), 85 (42), 83 (58), 81 (44), 71 (59), 69 (68), 57 (100), 55 (77). **CHN analysis**: calculated: C 43.0, H 2.2, N 7.7; found: C 42.6, H 2.3, N 7.7.

[(9-oxa)$ZnCl_2$] (39a):

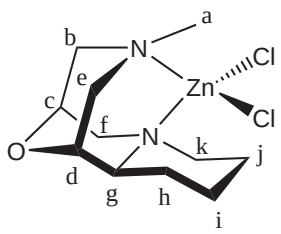

$C_{11}H_{20}N_2OZnCl_2$ (M = 332.60 g/mol): Colourless crystals; **Yield**: 0.276 g = 0.83 mmol = 83 %, MP 260°C. ^{1}**H-NMR** (500 MHz, CD_3CN, 25 °C): δ [ppm] = 1.54 (m, 1+1H, j+h), 1.73 (m, 1H, i), 1.92 (m, 1H, h), 2.21 (m, 1+1H, i+k), 2.33 (m, 1H, j), 2.45 (s, 3H, a), 2.69 (m, 1H, f), 2.77 (m, 1+1H, e+b), 2.92 (m, 1H, c), 3.17 (m, 1H, k), 3.37 (m, 1H, f), 3.42 (m, 1H, e), 3.59 (m, 1H, b), 3.79 (m, 1H, d), 4.08 (m, 1H, g). ^{13}**C-NMR** (125 MHz, CD_3CN, 25 °C): δ [ppm] = 23.2 (CH_2, h), 23.4 (CH_2, i), 24.9 (CH_2, j), 46.5 (CH_3, a), 54.1 (CH_2, f), 57.6 (CH_2, k), 58.0 (CH_2, e), 58.7 (CH_2, b), 66.8 (CH, g), 67.5 (CH, c), 70.1 (CH, d). **IR** (KBr, $\tilde{\nu}$[cm^{-1}]): 2993 m (ν(C-$H_{aliph.}$)), 2947 s (ν(C-$H_{aliph.}$)), 2937 m (ν(C-$H_{aliph.}$)), 2861 m (ν(C-$H_{aliph.}$)), 2793 m (ν(C-$H_{aliph.}$)), 1635 vw, 1466 s, 1458 m, 1402 w, 1387 w, 1369 m, 1361 m, 1334 w, 1300 m, 1284 m, 1277 m, 1250 m, 1228 m, 1219 w, 1203 w, 1188 vw, 1159 w, 1128 m, 1113 m, 1095 vs, 1061 m, 1051 s, 1034 s, 1018 m, 989 m, 980 m, 941 w, 928 w, 916 m, 885 m, 862 w, 850 m, 822 m, 812 m, 787 m, 758 m, 723 m, 607 m, 548 w, 526 w. **EI-MS** (m/z, (%)): 332 (8) [M^+], 279 (25), 245 (27), 196 (27) [M^+ -$ZnCl_2$], 167 (43), 149 (100), 124 (19), 122 (34), 119 (29), 113 (14), 105 (37), 84 (25), 77 (22), 71 (19), 57 (26). **CHN analysis**: calculated: C 39.69, H 6.01, N 8.42; found: C 39.68, H 6.13, N 8.56.

[(9-oxa)$Zn(CH_3COO)_2$] (39b):

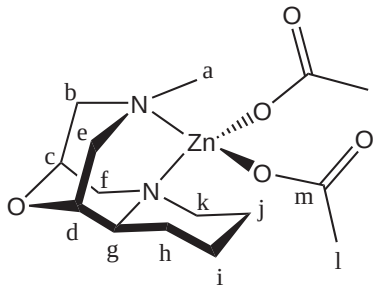

$C_{15}H_{26}N_2O_5Zn$ (M = 379.77 g/mol): Colourless crystals; **Yield**: 0.304 g = 0.80 mmol = 80 %; **m.p.** 176°C. ^{1}**H-NMR** (500 MHz, CD_3CN, 25 °C): δ [ppm] = 1.46 (m, 1H, i), 1.52 (m, 1H, j), 1.62 (m, 1H, h), 1.82 (m, 1H, i), 1.92 (m, 6+1H, l+j), 2.06 (m, 1+1H, k+h), 2.49 (s, 3H, a), 2.58 (m, 1H, f), 2.64 (m, 1H, b), 2.70 (m, 1H, e), 2.76 (m, 1H, c), 3.29 (m, 1+1H, k+b), 3.36 (m, 1H, e), 3.68 (m, 1H, f), 3.72 (m, 1H, d), 4.01 (m, 1H, g). ^{13}**C-NMR** (125 MHz, CD_3CN, 25 °C): δ [ppm] = 21.5 (CH_3, l), 23.1 (CH_2, h), 23.3 (CH_2, i), 25.3 (CH_2, j), 47.1 (CH_3, a), 54.5 (CH_2, f), 58.0 (CH_2, k), 58.6 (CH_2, e), 58.7 (CH_2, b), 67.1 (CH, g), 67.5 (CH, c), 70.3 (CH, d), 178.6 (C, m). **IR** (KBr, $\tilde{\nu}$[cm^{-1}]): 2949 m (ν(C-$H_{aliph.}$)), 2866 m (ν(C-$H_{aliph.}$)), 1624 vs (ν(C-O)), 1589 vs (ν(C-O)), 1406 s, 1421 s, 1385 vs, 1329 s, 1302 m, 1286 m, 1277 m, 1252 w, 1232 w, 1219 w, 1205 vw, 1192 w, 1163 w, 1147 w, 1130 m, 117 m, 1095 s, 1063 m, 1051 m, 1034 m, 1020 m, 993 w, 982 m, 958 vw, 941 w, 918 m, 887 m, 864 w, 850 m, 823 w, 812 m, 789 m, 758 m, 725 m, 677 m, 619 m, 611 m, 548 w, 530 w. **EI-MS** (m/z, (%)): 323 (30) [M^+ -CH_3COO], 321 (45) [M^+ -CH_3COO], 319 (74) [M^+ -CH_3COO], 196 (100) [M^+ -$Zn(CH_3COO)_2$], 195 (43) [M^+ -$Zn(CH_3COO)_2$ -H], 153 (16), 124 (81), 122 (28), 98 (68), 97 (35), 96 (30), 84 (87), 82 (32), 70 (13), 58 (19), 55 (14). **CHN analysis**: calculated: C 47.40, H 6.85, N 7.37; found: C 47.12, H 6.80, N 7.37.

11.4 Ring-opening polymerisation of lactide initiated by zinc(II) complexes

11.4.1 General procedure for the melt polymerisation of D,L-lactide

D,L-Lactide (3,6-dimethyl-1,4-dioxane-2,5-dione, 3.603 g, 25 mmol, used as purchased) and the initiator (I/M ratio 1/500, calculated relative to the zinc centres) were weighed into a 50 mL flask, which was flushed with argon and closed with a glass stopper. The reaction vessel was then heated at 150 °C. After the reaction time the polymer melt was allowed to cool to room temperature and then was dissolved in 25 mL of dichloromethane. The PLA was precipitated in 350 mL of ice-cooled ethanol and dried in vacuo at 50 °C.

11.4.2 Procedure for kinetic measurements of the melt polymerisation of D,L-lactide

D,L-Lactide (3,6-dimethyl-1,4-dioxane-2,5-dione, 3.603 g, 25 mmol, for each time-entry) and the initiator (I/M ratio 1/500, calculated relative to the zinc centres) were weighed into a glass beaker, mixed and homogenised by means of mortar. Then for each entry the appropriate amount of the reaction mixture was weighed into a 50 mL flask, which was flushed with argon and closed with a glass stopper. The reaction vessels were then heated at 150 °C. The reaction time starts at the moment the lactide was molten. After their respective reaction times the polymer melts were cooled in an ice-water bath to room temperature and then were dissolved in 25 mL of dichloromethane. From this solution samples 1 ml was taken, dried in vacuo and used for the determination of conversion via NMR spectroscopy and of the molecular weight distribution by GPC. The PLA of the residual solution was precipitated in 350 mL of ice-cooled ethanol and dried in vacuo at 50 °C.

11.5 Ring-opening polymerisation of glycolide initiated by zinc(II) complexes

Glycolide (1,4-dioxane-2,5-dione, 1.0000 g, 8.6 mmol) and the initiator (I/M ratio 1/500, calculated relative to the zinc centres) were weighed into a 50 mL flask, which was flushed with argon and closed with a glass stopper. The reaction vessel was then heated at 150 °C. After the reaction time the polymer was allowed to cool to room temperature and then was dissolved in 8 mL of hexafluoroisopropanol. The polyglycolide was precipitated in 200 mL of ice-cooled ethanol and dried in vacuo at 50 °C.

11.6 Ring-opening polymerisation of ε-caprolactone initiated by zinc(II) complexes

The initiator (I/M ratio 1/500, calculated relative to the zinc centres) was weighed into a 50 mL flask, which was flushed with argon and closed with a glass stopper after the injection of ε-caprolactone (6-hexanolactone, 2.8525 g, 2.77 ml, 25 mmol). The reaction vessel was then heated at 150 °C. After the reaction time the polymer melt was allowed to cool to room temperature and then was dissolved in 25 mL of dichloromethane. From this solution a sample of 0.5 ml was taken, dried in vacuo and used for the determination of conversion via NMR spectroscopy. The polycaprolactone of the residual solution was precipitated in 350 mL of ice-cooled ethanol, isolated by centrifugation and dried in vacuo.

Bibliography

[1] *Biopolymers - Polyesters II Properties and Chemical Synthesis* (Eds.: Y. Doi, A. Steinbüchel), Wiley-VCH, Weinheim, **2002**.

[2] *Biopolymers - Polyesters III Application and Commercial Products* (Eds.: Y. Doi, A. Steinbüchel), Wiley-VCH, Weinheim, **2002**.

[3] S. Jacobsen, P. Degée, H. Fritz, P. Dubois, R. Jérôme, *Polym. Eng. Sci.* **1999**, *39*, 1311–1319.

[4] M. Vert, *Biomacromolecules* **2005**, *6*, 538–546.

[5] O. Dechy-Cabaret, B. Martin-Vaca, D. Bourissou, *Chem. Rev.* **2004**, *104*, 6147–6176.

[6] O. Wolf, M. Crank, M. Patel, F. Marscheider-Weidemann, J. Schleich, B. Hüsing, G. Angerer, Techno-economic Feasibility of Large-scale Production of Bio-based Polymers in Europe, tech. rep. EUR 22103 EN, European Commission, **2005**.

[7] *bioplastics magazine* (Ed.: M. Thielen), **2006**, 26–27.

[8] B. Nagel, H. Dellweg, L. M. Gierasch, *Pure Appl. Chem.* **1992**, *64*, 143–168.

[9] Packaging - Requirements for packaging recoverable through composting and biodegradation - Test scheme and evaluation criteria for the final acceptance of packaging, EN 13432:2000, European Union.

[10] Plastics - Evaluation of compostability - Test scheme and specifications, EN 14995, European Union.

[11] S. Mecking, *Angew. Chem. Int. Ed.* **2004**, *43*, 1078–1085.

[12] C. Gahle, M. Carus, M. Geuder, *Marktanalyse Biokunststoffe: Verfügbarkeit, Akteure, Märkte, Trends*, nova-Institut GmbH, Hürth, **2007**.

[13] H. Kricheldorf, *Chemosphere* **2001**, *43*, 49–54.

[14] P. T. Anastas, J. C. Warner, *Green Chemistry: Theory and Practice*, Oxford University Press, New York, USA, **1998**.

[15] P. Anastas, J. Zimmerman, *Environmental science & technology* **2003**, *37*, 94–101.

[16] *Natural Fibres, Biopolymers, and Biocomposites* (Eds.: A. Mohanty, M. Misra, L. Drzal), CRC Press, Taylor & Francis Group, New York, **2005**.

[17] A. Gupta, V. Kumar, *Europ. Polym. J.* **2007**, *43*, 4053–4074.

[18] R. Mehta, V. Kumar, H. Bhunia, S. Upadhyay, *J. Macromol. Sci.-Pol. R.* **2005**, *C45*, 325–349.

[19] D. Garlotta, *J. Polym. Environ.* **2001**, *9*, 63–84.

[20] R. Platel, L. Hodgson, C. Williams, *Polym. Rev.* **2008**, *48*, 11–63.

[21] A. J. Chmura, D. M. Cousins, M. G. Davidson, M. D. Jones, M. D. Lunn, M. F. Mahon, *Dalton Trans.* **2008**, 1437–1443.

[22] E. Vink, K. Rabago, D. Glassner, B. Springs, R. O´Connor, J. Kolstad, P. Gruber, *Macromol. Biosci.* **2004**, *4*, 551–564.

[23] K. Sakai, M. Taniguchi, S. Miura, H. Ohara, T. Masumoto, Y. Shirai, *J. Indust. Ecology* **2004**, *7*, 63–74.

[24] B. M. Chamberlain, M. Cheng, D. R. Moore, T. M. Ovitt, E. B. Lobkovsky, G. W. Coates, *J. Am. Chem. Soc.* **2001**, *123*, 3229–3238.

[25] R. Drumwright, P. Gruber, D. Henton, *Adv. Mat.* **2000**, *12*, 1841–1846.

[26] H. Tsuji, *Macromol. Biosci.* **2005**, *5*, 569–597.

[27] *Biopolymers from Renewable Resources* (Ed.: D. Kaplan), Springer, Berlin, Heidelberg, **1998**.

[28] W. H. Carothers, G. L. Dorough, F. J. v. Natta, *J. Am. Chem. Soc.* **1932**, *54*, 761–772.

[29] N. E. Kamber, W. Jeong, R. M. Waymouth, R. C. Pratt, B. G. G. Lohmeijer, J. L. Hedrick, *Chem. Rev.* **2007**, *107*, 5813–5840.

[30] H. R. Kricheldorf, J. M. Jonté, R. Dunsing, *Makromol. Chemie* **1986**, *187*, 771–785.

[31] H. R. Kricheldorf, R. Dunsing, *Makromol. Chemie* **1986**, *187*, 1611–1625.

[32] H. R. Kricheldorf, R. Dunsing, A. Serra, *Macromolecules* **1987**, *20*, 2050–2057.

[33] H. R. Kricheldorf, I. Kreiser, *Makromol. Chemie* **1987**, *188*, 1861–1873.

[34] P. Dubois, C. Jacobs, R. Jérôme, P. Teyssié, *Macromolecules* **1991**, *24*, 2266–2270.

[35] H. R. Kricheldorf, M. Berl, N. Scharnagl, *Macromolecules* **1988**, *21*, 286–293.

[36] J. L. Eguiburu, M. J. Fernandez-Berridi, F. P. Cossio, J. S. Roman, *Macromolecules* **1999**, *32*, 8252–8258.

[37] E. L. Marshall, V. C. Gibson, H. S. Rzepa, *J. Am. Chem. Soc.* **2005**, *127*, 6048–6051.

[38] M. Ryner, K. Stridsberg, A.-C. Albertsson, H. von Schenck, M. Svensson, *Macromolecules* **2001**, *34*, 3877–3881.

[39] A. Kowalski, A. Duda, S. Penczek, *Macromolecules* **2000**, *33*, 7359–7370.

[40] B. G. G. Lohmeijer, R. C. Pratt, F. Leibfarth, J. W. Logan, D. A. Long, A. P. Dove, F. Nederberg, J. Choi, C. Wade, R. M. Waymouth, J. L. Hedrick, *Macromolecules* **2006**, *39*, 8574–8583.

[41] R. Pratt, B. Lohmeijer, D. Long, R. Waymouth, J. Hedrick, *J. Am. Chem. Soc.* **2006**, *128*, 4556–4557.

[42] A. Chuma, H. Horn, W. Swope, R. Pratt, L. Zhang, B. Lohmeijer, C. Wade, R. Waymouth, J. Hedrick, J. Rice, *J. Am. Chem. Soc.* **2008**, *130*, 6749–6754.

[43] E. F. Connor, G. W. Nyce, M. Myers, A. Mock, J. L. Hedrick, *J. Am. Chem. Soc.* **2002**, *124*, 914–915.

[44] B. O'Keefe, M. Hillmyer, W. Tolman, *J. Chem. Soc. Dalton. Trans.* **2001**, 2215–2224.

[45] M. Lechner, K. Gerke, E. Nordmeier, *Makromolekulare Chemie*, Birkhäuser Verlag, Basel, Boston, Berlin, 2nd ed., **1996**.

[46] C. Wheaton, P. Hayes, B. Ireland, *Dalton Trans.* **2009**, 4832–4846.

[47] J. Wu, T. Yu, C. Chen, C. Lin, *Coord. Chem. Rev.* **2006**, *250*, 602–626.

[48] *Biopolymers - Polyesters I Biological Systems and Biotechnological Production* (Eds.: Y. Doi, A. Steinbüchel), Wiley-VCH, Weinheim, **2002**.

[49] M. Chisholm, J. Gallucci, K. Phomphrai, *Chem. Commun.* **2003**, 48–49.

[50] M. Chisholm, N. Eilerts, J. Huffman, S. Iyer, M. Pacold, K. Phomphrai, *J. Am. Chem. Soc.* **2000**, *122*, 11845–11854.

[51] M. Chisholm, J. Gallucci, K. Phomphrai, *Inorg. Chem.* **2004**, *43*, 6717–6725.

[52] M. Cheng, A. B. Attygalle, E. B. Lobkovsky, G. W. Coates, *J. Am. Chem. Soc.* **1999**, *121*, 11583–11584.

[53] N. Ajellal, D. Lyubov, M. Sinenkov, G. Fukin, A. Cherkasov, C. Thomas, J.-F. Carpentier, A. Trifonov, *Chem. - Eur. J.* **2008**, *14*, 5440–5448.

[54] M. Coles, *Dalton Trans.* **2006**, 985–1001.

[55] M. Coles, P. Hitchcock, *Eur. J. Inorg. Chem.* **2004**, 2662–2672.

[56] M. Chisholm, J. Gallucci, K. Phomphrai, *Inorg. Chem.* **2002**, *41*, 2785–2794.

[57] V. C. Gibson, E. L. Marshall, D. Navarro-Llobet, A. J. P. White, D. J. Williams, *J. Chem. Soc. Dalton Trans.* **2002**, 4321–4322.

[58] A. P. Dove, V. C. Gibson, E. L. Marshall, H. S. Rzepa, A. J. P. White, D. J. Williams, *J. Am. Chem. Soc.* **2006**, *128*, 9834–9843.

[59] A. J. Chmura, M. G. Davidson, C. J. Frankis, M. D. Jones, M. D. Lunn, *Chem. Commun.* **2008**, 1293–1295.

[60] M. Frediani, D. Sémeril, A. Mariotti, L. Rosi, P. Frediani, L. Rosi, D. Matt, L. Toupet, *Macromol. Rapid Commun.* **2008**, *29*, 1554–1560.

[61] C. Williams, L. Breyfogle, S. Choi, W. Nam, V. Young, M. Hillmyer, W. Tolman, *J. Am. Chem. Soc.* **2003**, *125*, 11350–11359.

[62] J. Ejfler, S. Szafert, K. Mierzwicki, L. B. Jerzykiewicz, P. Sobota, *Dalton Trans.* **2008**, 6556–6562.

[63] J. Wu, B. Huang, M. Hsueh, S. Lai, C. Lin, *Polymer* **2005**, *46*, 9784–9792.

[64] H. Ma, T. Spaniol, J. Okuda, *Inorg. Chem.* **2008**, *47*, 3328–3339.

[65] H. Ma, T. P. Spaniol, J. Okuda, *Angew. Chem. Int. Ed.* **2006**, *45*, 7818–7821.

[66] J. Leenslag, S. Gogolewski, A. Pennings, *J. Appl. Polym. Sci.* **1984**, *29*, 2829–2842.

[67] H. Korhonen, A. Helminen, J. Seppala, *Polymer* **2001**, *42*, 7541–7549.

[68] A. Duda, S. Penczek, A. Kowalski, J. Libiszowski, *Macromol. Symp.* **2000**, *153*, 41–53.

[69] G. Schwach, J. Coudane, R. Engel, M. Vert, *Polym. Bull.* **1996**, *37*, 771–776.

[70] J. E. Kasperczyk, *Macromolecules* **1995**, *28*, 3937–3939.

[71] P. Degée, P. Dubois, R. Jérôme, *Macromol. Chem. Phys.* **1997**, *198*, 1973–1984.

[72] Z. Zhong, P. J. Dijkstra, J. Feijen, *Angew. Chem. Int. Ed.* **2002**, *41*, 4510–4513.

[73] T. Jensen, C. Schaller, M. Hillmyer, W. Tolman, *J. Organomet. Chem.* **2005**, *690*, 5881–5891.

[74] F. Nederberg, E. F. Connor, M. Möller, T. Glauser, J. L. Hedrick, *Angew. Chem. Int. Ed.* **2001**, *40*, 2712–2715.

[75] M. Myers, E. F. Connor, T. Glauser, A. Möck, G. Nyce, J. L. Hedrick, *J. Polym. Sci. Part A: Polym. Chem.* **2002**, *40*, 844–851.

[76] A. Dove, H. Li, R. Pratt, B. Lohmeijer, D. Culkin, R. Waymouth, J. Hedrick, *Chem. Commun.* **2006**, *2006*, 2881–2883.

[77] A. Dove, R. Pratt, B. Lohmeijer, R. Waymouth, J. Hedrick, *J. Am. Chem. Soc.* **2005**, *127*, 13798–13799.

[78] J. H. Jeong, Y. H. An, Y. K. Kang, Q. T. Nguyen, H. Lee, B. M. Novak, *Polyhedron* **2008**, *27*, 319–324.

[79] C. A. Wheaton, B. J. Ireland, P. G. Hayes, *Organometallics* **2009**, *28*, 1282–1285.

[80] N. Nomura, R. Ishii, Y. Yamamoto, T. Kondo, *Chem.-Eur. J.* **2007**, *13*, 4433–4451.

[81] T. Ishikawa, T. Isobe, *Chem.-Eur. J.* **2002**, *8*, 553–557.

[82] S. Patai, *The Chemistry of amidines and imidates*, Wiley, London, New York, **1991**.

[83] R. Schwesinger, *Nachr. Chem. Tech. Lab.* **1990**, *38*, 1214–1226.

[84] G. Wieland, G. Simchen, *Liebigs Ann. Chem.* **1985**, 2178–2193.

[85] A. V. Santoro, G. Mickevicius, *J. Org. Chem.* **1979**, *44*, 117–120.

[86] P. Pruszynski, *Can. J. Chem.* **1986**, *65*, 626–629.

[87] K. T. Leffek, P. Pruszynski, K. Thanapaalasingham, *Can. J. Chem.* **1989**, *67*, 590–595.

[88] P. Pruszynski, K. T. Leffek, *Can. J. Chem.* **1991**, *69*, 205–210.

[89] T. Kolev, T. Todorov, R. Petrova, *Acta Crystallogr. E* **2002**, *58*, o111–o113.

[90] C. Morimoto, E. Lingafelter, *Acta Crystallogr. B* **1970**, *26*, 335–341.

[91] P. J. Bailey, S. Pace, *Coord. Chem. Rev.* **2001**, *214*, 91–141.

[92] S. Pohl, M. Harmjanz, J. Schneider, W. Saak, G. Henkel, *J. Chem. Soc. Dalton. Trans.* **2000**, 3473–3479.

[93] H. Kessler, D. Leibfritz, *Tetrahedron* **1970**, *26*, 1805–1820.

[94] H. Bredereck, K. Bredereck, *Chem. Ber.* **1961**, *94*, 2278–2295.

[95] W. Kantlehner, E. Haug, W. Mergen, P. Speh, T. Maier, J. Kapassakalidis, H.-J. Bräuner, H. Hagen, *Liebigs Ann. Chem.* **1984**, *1*, 108–125.

[96] H. Eilingsfeld, G. Neubauer, M. Seefelder, H. Weidinger, *Chem. Ber.* **1964**, *97*, 1232–1245.

[97] H. Eilingsfeld, M. Seefelder, H. Weidinger, *Angew. Chem. Int. Ed. Engl.* **1960**, *72*, 48–58.

[98] H. Beyer, W. Walter, *Lehrbuch der organischen Chemie*, Hirzel Verlag, Stuttgart, **1998**.

[99] S. Herres-Pawlis, A. Neuba, O. Seewald, T. Seshadri, H. Egold, U. Flörke, G. Henkel, *Eur. J. Org. Chem.* **2005**, 4879–4890.

[100] S. Herres-Pawlis, PhD thesis, Universität Paderborn, **2005**.

[101] J. Börner, MA thesis, Universität Paderborn, **2006**.

[102] R. Haase, MA thesis, Universität Paderborn, **2006**.

[103] T. L. Cleland, S. D. Bunge, *Polyhedron* **2007**, *26*, 5506–5512.

[104] S. D. Bunge, J. M. Lance, J. A. Bertke, *Organometallics* **2007**, *26*, 6320–6328.

[105] S. Aoki, K. Iwaida, N. Hanamoto, M. Shiro, E. Kimura, *J. Am. Chem. Soc.* **2002**, *124*, 5256–5257.

[106] U. Köhn, M. Schulz, H. Görls, E. Anders, *Tetrahedron: Asymmetry* **2005**, *16*, 2125–2131.

[107] A. Neuba, S. Herres-Pawlis, O. Seewald, J. Börner, A. J. Heuwing, U. Flörke, G. Henkel, in preparation.

[108] T. Ishikawa, M. Kawahata, *pat.*, EP 1752451A1, **2007**.

[109] D. Domide, C. Neuhäuser, E. Kaifer, H. Wadepohl, H.-J. Himmel, *Eur. J. Inorg. Chem.* **2009**, *2009*, 2170–0178.

[110] C. Neuhäuser, D. Domide, J. Mautz, E. Kaifer, *Dalton Trans.* **2008**, 1821–1824.

[111] H. Wittmann, A. Schorm, J. Sundermeyer, *Z. Anorg. Allg. Chem.* **2000**, *626*, 1583–1590.

[112] H. Wittmann, V. Raab, A. Schorm, J. Plackmeyer, J. Sundermeyer, *Eur. J. Inorg. Chem.* **2001**, 1937–1948.

[113] H. Li, S. Zhang, J. Jiao, Z. Jiao, L. Kong, J. Xu, J. Li, J. Zuo, X. Zhao, *Biomacromolecules* **2009**, *10*, 1311–1314.

[114] J. D. Monegan, S. D. Bunge, *Inorg. Chem.* **2009**, *48*, 3248–3256.

[115] G. G. Skvortsov, M. V. Yakovenko, P. M. Castro, G. K. Fukin, A. V. Cherkasov, J.-F. Carpentier, A. A. Trifonov, *Eur. J. Inorg. Chem.* **2007**, *2007*, 3260–3267.

[116] G. Giesbrecht, G. Whitener, J. Arnold, *J. Chem. Soc. Dalton Trans.* **2001**, *2001*, 923–927.

[117] S. Birch, S. Boss, S. Cole, M. Coles, R. Haigh, P. Hitchcock, A. Wheatley, *Dalton Trans.* **2004**, *2004*, 3568–3574.

[118] S. Oakley, D. Soria, M. Coles, P. Hitchcock, *Polyhedron* **2006**, *25*, 1247–1255.

[119] S. Herres-Pawlis, R. Haase, E. Akin, U. Flörke, G. Henkel, *Z. Anorg. Allg. Chem.* **2008**, *634*, 295–298.

[120] M. Tamm, D. Petrovic, S. Randoll, S. Beer, T. Bannenberg, P. G. Jones, J. Grunenberg, *Org. Biomol. Chem.* **2007**, *5*, 523–530.

[121] A. Hoffmann, J. Börner, U. Flörke, S. Herres-Pawlis, *Inorg. Chim. Acta* **2009**, *362*, 1185–1193.

[122] N. Foroughifar, K. Leffek, Y. Lee, *Can. J. Chem.* **1993**, *71*, 164–166.

[123] H. Wittmann, PhD thesis, Universität Marburg, **2000**.

[124] E. V. Gauchenova, PhD thesis, Universität Marburg, **2006**.

[125] H. Kricheldorf, D.-O. Damrau, *Macromol. Chem. Phys.* **1997**, *198*, 1753–1766.

[126] M. Chisholm, J. Gallucci, H. Yin, *Proc. Natl. Acad. Sci. USA* **2006**, *103*, 15315–15320.

[127] G. Schwach, J. Coudane, R. Engel, M. Vert, *Polym. Bull.* **1994**, *32*, 617–623.

[128] M. Rubinstein, R. H. Colby, *Polymer Physics*, Oxford University Press, Oxford, **2003**, chapter 1.

[129] G. Rafler, J. Dahlmann, K. Wiener, *Acta Polym.* **1990**, *41*, 328–333.

[130] A. Schindler, D. Harper, *J. Polym. Sci. Part A: Polym. Chem.* **1979**, *17*, 2593–2599.

[131] N. Kuhn, M. Grathwohl, M. Steimann, G. Henkel, *Z. Naturforsch.* **1998**, *53b*, 997–1003.

[132] D. Petrovic, T. Glöge, T. Bannenberg, C. G. Hrib, S. Randoll, P. G. Jones, M. Tamm, *Eur. J. Inorg.Chem.* **2007**, *2007*, 3472–3475.

[133] D. Petrovic, T. Bannenberg, S. Randoll, P. G. Jones, M. Tamm, *Dalton Trans.* **2007**, 2812 –2822.

[134] T. Glöge, D. Petrovic, C. Hrib, P. G. Jones, M. Tamm, *Eur. J. Inorg. Chem.* **2009**, 4538–4546.

[135] D. Petrovic, L. M. R. Hill, P. G. Jones, W. B. Tolman, M. Tamm, *Dalton Trans.* **2008**, 887 –894.

[136] D. Petrovic, C. G. Hrib, S. Randoll, P. G. Jones, M. Tamm, *Organometallics* **2008**, *27*, 778–783.

[137] T. K. Panda, C. G. Hrib, P. G. Jones, J. Jenter, P. W. Roesky, M. Tamm, *Eur. J. Inorg. Chem.* **2008**, *2008*, 4270–4279.

[138] A. D. Becke, *J. Chem. Phys.* **1993**, *98*, 5648–5652.

[139] C. Lee, W. Yang, R. G. Parr, *Phys. Rev. B* **1988**, *37*, 785–789.

[140] B. Miehlich, A. Savin, H. Stoll, H. Preuss, *Chem. Phys. Lett.* **1989**, *157*, 200–206.

[141] Y. Zhao, N. Schultz, D. Truhlar, *J. Chem. Theory Comput.* **2006**, *2*, 364–382.

[142] M. J. Frisch, G. W. Trucks, H. B. Schlegel, G. E. Scuseria, M. A. Robb, J. R. Cheeseman, J. J. A. Montgomery, T. Vreven, K. N. Kudin, J. C. Burant, J. M. Millam, S. S. Iyengar, J. Tomasi, V. Barone, B. Mennucci, M. Cossi, G. Scalmani, N. Rega, G. A. Petersson, H. Nakatsuji, M. Hada, M. Ehara, K. Toyota, R. Fukuda, J. Hasegawa, M. Ishida, T. Nakajima, Y. Honda, O. Kitao, H. Nakai, M. Klene, X. Li, J. E. Knox, H. P. Hratchian, J. B. Cross, C. Adamo, J. Jaramillo, R. Gomperts, R. E. Stratmann, O. Yazyev, A. J. Austin, R. Cammi, C. Pomelli, J. W. Ochterski, P. Y. Ayala, K. Morokuma, G. A. Voth, P. Salvador, J. J. Dannenberg, V. G. Zakrzewski, S. Dapprich, A. D. Daniels, M. C. Strain, O. Farkas, D. K. Malick, A. D. Rabuck, K. Raghavachari, J. B. Foresman, J. V. Ortiz, Q. Cui, A. G. Baboul, S. Clifford, J. Cioslowski, B. B. Stefanov, G. Liu, A. Liashenko, P. Piskorz, I. Komaromi, R. L. Martin, D. J. Fox, T. Keith, M. A. Al-Laham, C. Y. Peng, A. Nanayakkara, M. Challacombe, P. M. W. Gill, B. Johnson, W. Chen, M. W. Wong, C. Gonzalez, J. A. Pople, *Gaussian 03, Revision E.01*, Gaussian, Inc., Wallingford CT, **2004**.

[143] G. Frison, G. Ohanessian, *J. Comput. Chem.* **2007**, *29*, 416–433.

[144] S. Wörl, D. Hellwinkel, H. Pritzkow, M. Hofmann, R. Krämer, *Dalton Trans.* **2004**, 2750–2758.

[145] J. Foster, F. Weinhold, *J. Am. Chem. Soc.* **1980**, *102*, 7211–7218.

[146] A. Reed, L. Curtis, F. Weinhold, *Chem. Rev.* **1988**, *88*, 899–926.

[147] C. J. Cramer, *Essentials of Computational Chemistry*, Wiley, Chichester, 2nd ed., **2004**.

[148] H.-J. Endres, A. Siebert-Raths, *Technische Biopolymere*, Polymedia Publisher GmbH, Kierspe, **2009**.

[149] M. Khan, D. Tuck, *Acta Crystallogr. C* **1984**, *40*, 60–62.

[150] C. Reimann, S. Block, A. Perloff, *Inorg. Chem.* **1966**, *5*, 1185–1189.

[151] P. Steel, C. Sumby, *Dalton Trans.* **2003**, 4505–4515.

[152] S. Herres-Pawlis, U. Flörke, G. Henkel, *Eur. J. Inorg. Chem.* **2005**, 3815–3824.

[153] A. Neuba, R. Haase, M. Bernard, U. Flörke, S. Herres-Pawlis, *Z. Anorg. Allg. Chem.* **2008**, *634*, 2511–2517.

[154] V. Raab, PhD thesis, Universität Marburg, **2001**.

[155] S. Herres, U. Flörke, G. Henkel, *Acta Crystallogr. C* **2004**, *60*, o358–o360.

[156] V. Raab, J. Kipke, R. M. Gschwind, J. Sundermeyer, *Chem. - Eur. J.* **2002**, *8*, 1682–1693.

[157] J. Dorgan, J Janzen, D. Knauss, S. Hait, B. Limoges, M. Hutchinson, *J. Polym. Sci. Pol. Phys.* **2005**, *43*, 3100–3111.

[158] M. Hakkarainen, *Adv. Polym. Sci.* **2002**, *157*, 113–138.

[159] M. Zell, B. Padden, A. Paterick, K. Thakur, R. Kean, M. Hillmyer, E. Munson, *Macromolecules* **2002**, *35*, 7700–7707.

[160] C. Miranda, F. Escarti, L. Lamarque, M. Yunta, P. Navarro, E. Garcia-Espana, M. Jimeno, *J. Am. Chem. Soc.* **2004**, *126*, 823–833.

[161] M. Formica, L. Giorgi, V. Fusi, M. Micheloni, R. Pontellini, *Polyhedron* **2002**, *21*, 1351–1356.

[162] J. Sundermeyer, V. Raab, E. Gaoutchenova, U. Garrelts, N. Abacilar, K. Harms in *Activating Unreactive Substrates* (Eds.: C. Bolm, F. Ekkehardt-Hahn), Wiley-VCH, Weinheim, **2009**, Chapter 2, 17–38.

[163] E. Wissing, M. Kaupp, J. Boersma, A. L. Spek, G. van Koten, *Organometallics* **1994**, *13*, 2349–2356.

[164] B. Rodrigues, *Acta Crystallogr. E* **2004**, *60*, m1169–m1171.

[165] F. Cao, Y. Shen, Z. Kan, *Acta Crystallogr. E* **2006**, *62*, m2955–m2956.

[166] X. Chen, R. Wang, X. Yu, *Acta Crystallogr. C* **1995**, *51*, 1545–1547.

[167] X. Chen, Z. Xu, X. Yu, T. Mak, *Polyhedron* **1994**, *13*, 2079–2083.

[168] B. Covelo, R. Carballo, E. Vazquez-Lopez, E. Garcia-Martinez, A. Castineiras, S. Balboa, J. Niclos, *Cryst. Eng. Comm.* **2006**, *8*, 167–177.

[169] H. Erras-Hanauer, Z. Mao, G. Liehr, T. Clark, R. van Eldik, *Eur. J. Inorg. Chem.* **2003**, 1562–1569.

[170] Y. Zhu, K. Zhong, W. Lu, *Acta Crystallogr. E* **2006**, *62*, m2725–m2726.

[171] B. Rodrigues, *Acta Crystallogr. E* **2004**, *60*, m1166–m1168.

[172] X. Fu, M. Li, C. Wang, X. Wang, *Acta Crystallogr. C* **2006**, *62*, m13–m15.

[173] X. Fu, X. Wang, M. Li, C. Wang, *Acta Crystallogr. E* **2006**, *62*, m773–m775.

[174] W. Fitzgerald, B. Hathaway, C. J. Simmons, *J. Chem. Soc. Dalton Trans.* **1985**, 141 –149.

[175] C.-H. Yu, R.-C. Zhang, *Acta Crystallogr. E* **2006**, *62*, m1758–m1759.

[176] V. H. Gessner, C. Strohmann, *J. Am. Chem. Soc.* **2008**, *130*, 14412–14413.

[177] S. P. Green, C. Jones, A. Stasch, *Chem. Commun.* **2008**, 6285–6287.

[178] C. Strohmann, V. H. Gessner, A. Damme, *Chem. Commun.* **2008**, 3381–3383.

[179] E. Hevia, D. J. Gallagher, A. R. Kennedy, R. E. Mulvey, C. T. O'Hara, C. Talmard, *Chem. Commun.* **2004**, 2422–2423.

[180] A. S. Perucha, J. Heilmann-Brohl, M. Bolte, H.-W. Lerner, M. Wagner, *Organometallics* **2008**, *27*, 6170–6177.

[181] D. B. Collum, *Acc. Chem. Res.* **1992**, *25*, 448–454.

[182] G. Crassous, M. Abadie, F. Schue, *Eur. Polym. J.* **1979**, *15*, 747–755.

[183] H. Citeau, O. Conrad, D. M. Giolando, *Acta Crystallogr. E* **2001**, *57*, m5–m6.

[184] I. Bechthold, PhD thesis, Technische Universität Berlin, **2003**.

[185] M. Breuning, M. Steiner, C. Mehler, A. Paasche, D. Hein, *J. Org. Chem.* **2009**, *74*, 1407–1410.

[186] M. Breuning, M. Steiner, *Tetrahedron-Asymmetry* **2008**, *19*, 1978–1983.

[187] M. Breuning, M. Steiner, *Synthesis* **2007**, 1702–1706.

[188] M. Breuning, M. Steiner, *Synthesis* **2008**, 2841–2867.

[189] S. Penczek, T. Biela, A. Duda, *Macromol. Rapid. Comm.* **2000**, *21*, 1276–1276.

[190] S. Penczek, P. Kubisa, R. Szymanski, *Makromol. Chem. Rapid Commun.* **1991**, *12*, 77–80.

[191] I. dos Santos Vieira, MA thesis, Universität Paderborn, **2009**.

[192] J. Ling, J. Shen, T. E. Hogen-Esch, *Polymer* **2009**, *50*, 3575–3581.

[193] H. von Schenck, M. Ryner, A.-C. Albertsson, M. Svensson, *Macromolecules* **2002**, *35*, 1556–1562.

[194] G. J. van Hummel, S. Harkema, F. E. Kohn, J. Feijen, *Acta Crystallogr. B* **1982**, *38*, 1679–1681.

[195] J. Leonard, B. Lygo, G. Procter, *Praxis der Organischen Chemie*, VCH Weinheim, **1996**.

[196] K. Stott, J. Keeler, Q. N. Van, A. J. Shaka, *J. Magn. Reson.* **1997**, *125*, 302–324.

[197] Bruker, SMART (Version 5.62), SAINT (Version 6.02), SHELXTL (Version 6.10) and SADABS (Version 2.03). Bruker AXS Inc., Madison, Wisconsin, 2002.

[198] A. L. Spek, *J. Appl. Cryst.* **2003**, *36*, 7–13.

[199] A. L. Spek (2005) PLATON, A Multipurpose Crystallographic Tool, Utrecht University, Utrecht, The Netherlands.

[200] *Polymer Data Handbook* (Ed.: J. E. Mark), Oxford University Press, Oxford, **1999**.

[201] P. W. N. M. van Leeuwen, W. L. Groeneveld, *Inorg. Nucl. Chem. Lett.* **1967**, *3*, 145–146.

[202] M. Wang, H. Jiang, Z. Wang, *J. Therm. Anal. Calorim.* **2006**, *85*, 751–754.

[203] J. C. Antilla, A. Klapars, S. L. Buchwald, *ChemInform* **2003**, *34*, 1522–2667.

[204] J. Börner, S. Herres-Pawlis, U. Flöke, K. Huber, *Eur. J. Inorg. Chem.* **2007**, 5645–5651.

[205] J. Börner, U. Flörke, K. Huber, A. Döring, D. Kuckling, S. Herres-Pawlis, *Chem.-Eur. J.* **2009**, *15*, 2362–2376.

List of publications

Publications

1. **[Bis(guanidine)]zinc Complexes and Their Application in Lactide Polymerisation**
   J. Börner, S. Herres-Pawlis, U. Flörke, K. Huber
   Eur. J. Inorg. Chem. **2007**, 5645 - 5651

2. **Synthesis and properties of guanidine-pyridine hybridligands and structural characterisation of their mono- and bis(chelated) cobalt complexes**
   A. Hoffmann, **J. Börner**, U. Flörke, S. Herres-Pawlis
   Inorg. Chim. Acta **2009**, *362*, 1185 - 1193

3. **Lactide Polymerisation with Air-Stable and Highly Active Zinc Complexes with Guanidine-Pyridine Hybridligands**
   J. Börner, U. Flörke, K. Huber, A. Döring, D. Kuckling, S. Herres-Pawlis
   Chem.-Eur. J. **2009**, *15*, 2362 - 2376

4. **New Challenge for Classics: Neutral Zinc Complexes Stabilised by 2,2'-bipyridine and 1,10-phenanthroline and Their Application in the Ring-Opening Polymerisation of Lactide**
   J. Börner, U. Flörke, A. Döring, D. Kuckling, M. D. Jones, S. Herres-Pawlis
   Sustainability, **2009**, *1*, 1226 - 1239

5. **New insights into the lactide polymerisation with neutral N donor stabilised zinc complexes: Comparison of imidazolin-2-imine vs. guanidine complexes**
   J. Börner, U. Flörke, T. Glöge, T. Bannenberg, M. Tamm, M. D. Jones, A. Döring, D. Kuckling, S. Herres-Pawlis
   J. Mol. Cat. A: Chemical, **2010**, *316*, 139 - 145

6. **Unexpected activity of novel 9-oxabispidine zinc complexes in lactide polymerization**
   J. Börner, U. Flörke, A. Döring, D. Kuckling, M. D. Jones, M. Steiner, M. Breuning, S. Herres-Pawlis
   Inorg. Chem. Commun., accepted **2010**

7. **Tracking the Structure-Reactivity Relationship of Zinc Guanidine-Pyridine Hybrid Complexes Initiating Lactide Polymerisation**
   J. Börner, U. Flörke, A. Döring, D. Kuckling, S. Herres-Pawlis
   submitted

Patents

1. **Diamin-Zink-Katalysatorkomplexe**
   C. Strohmann, S. Herres-Pawlis, **J. Börner**, V. H. Gessner, P. Eckert
   submitted to the German Patent and Trademark Office, **Jul. 2009**

2. **Polynukleare Aminoethanolat-Zink-Katalysatorkomplexe**
   K. Jurkschat, S. Herres-Pawlis, **J. Börner**, G. Bradtmöller, M. Schürmann, M. Gock
   submitted to the German Patent and Trademark Office, **Aug. 2009**

Appendix

Table A.1: Summary of key geometric parameters from the calculated structures of **6a** and **7a** (bond lengths in Å and angles in °).

	[Zn(DMEGqu)Cl_2] **6a**		[Zn(TMGqu)Cl_2] **7a**	
	6-31G(d)	6-31+G(d)	6-31G(d)	6-31+G(d)
Zn-N_{py}	2.067	2.116	2.07	2.123
Zn-N_{gua}	2.078	2.147	2.071	2.131
Zn-Cl	2.223	2.25	2.257	2.223
	2.257	2.221	2.224	2.251
C_{gua}-N_{gua}	1.326	1.329	1.333	1.334
C_{gua}-N	1.365	1.363	1.367	1.359
	1.354	1.357	1.359	1.369
N-Zn-N	81.06	79.01	81.09	79.10
∠($ZnCl_2$, ZnN_2)	77.06	80.18	79.28	81.51
∠($C_{gua}N_3$, ZnN_2)	55.56	59.68	54.51	54.80
∠($C_{gua}N_3$, NC_3) (av.)	10.61	9.48	32.31	31.97
Structural parameter ρ	0.98	0.98	0.98	0.98

Table A.2: Summary of key geometric parameters from the calculated structures of **14a** and **15a** (bond lengths in Å and angles in °).

	[Zn(DMEGpy)Cl_2] **14a**		[Zn(TMGpy)Cl_2] **15a**	
	6-31G(d)	6-31+G(d)	6-31G(d)	6-31+G(d)
Zn-N_{py}	2.078	2.137	2.102	2.159
Zn-N_{gua}	2.065	2.129	2.04	2.097
Zn-Cl	2.224	2.253	2.246	2.225
	2.258	2.223	2.227	2.244
C_{gua}-N_{gua}	1.312	1.312	1.315	1.315
C_{gua}-N	1.361	1.364	1.384	1.385
	1.381	1.381	1.365	1.366
N-Zn-N	80.8	78.76	80.89	79.16
∠($ZnCl_2$, ZnN_2)	77.90	80.21	85.19	85.68
∠($C_{gua}N_3$, ZnN_2)	58.68	60.33	38.94	41.08
∠($C_{gua}N_3$, NC_3) (av.)	14.09	13.67	36.01	35.77
Structural parameter ρ	0.96	0.96	0.96	0.96

Table A.3: Summary of key geometric parameters from the calculated structures of **6b** and **7b** (bond lengths in Å and angles in °).

	[Zn(DMEGqu)$(CH_3COO)_2$] **6b**		[Zn(TMGqu)$(CH_3COO)_2$] **7b**	
	6-31G(d)	6-31G(d)	6-31+G(d)	6-31+G(d)
Zn-N_{py}	2.079	2.085	2.098	2.094
Zn-N_{gua}	2.141	2.128	2.131	2.145
Zn-O	2.001	1.939	1.958	1.949
	1.931	1.992	1.965	1.978
C_{gua}-N_{gua}	1.334	1.339	1.341	1.335
C_{gua}-N	1.371	1.366	1.355	1.345
	1.343	1.354	1.366	1.369
N-Zn-N	78.79	78.92	79.24	79.01
∠(ZnO_2, ZnN_2)	82.45	79.57	83.11	85.41
∠($C_{gua}N_3$, ZnN_2)	61.36	60.84	58.12	59.42
∠($C_{gua}N_3$, NC_3) (av.)	11.25	31.04	30.42	10.86
Structural parameter ρ	0.98	0.99	0.99	0.98

Table A.4: Summary of key geometric parameters from the calculated structures of **14b** and **15b** (bond lengths in Å and angles in °)

	[Zn(DMEGpy)$(OAc)_2$] **14b-1**		[Zn(DMEGpy)$(OAc)_2$] **14b-2**		[Zn(TMGpy)$(OAc)_2$] **15b**	
	6-31G(d)	6-31+G(d)	6-31G(d)	6-31+G(d)	6-31G(d)	6-31+G(d)
Zn-N_{py}	2.097	2.108	2.071	2.092	2.088	2.100
Zn-N_{gua}	2.107	2.116	2.136	2.138	2.107	2.116
Zn-O	1.931	2.004	1.922	1.941	2.025	1.993
	2.057, 2.264	1.943	1.988	1.963	1.950	1.953
C_{gua}-N_{gua}	1.303	1.306	1.307	1.309	1.313	1.316
C_{gua}-N	1.364	1.365	1.382	1.383	1.383	1.369
	1.391	1.39	1.386	1.386	1.371	1.383
N-Zn-N	79.46	79.80	80.22	80.16	80.11	80.41
∠(ZnO_2, ZnN_2)	85.80	85.16	86.19	88.51	83.21	85.90
∠($C_{gua}N_3$, ZnN_2)	37.01	39.38	49.18	47.61	45.43	42.42
∠($C_{gua}N_3$, NC_3) (av.)	13.54	13.43	14.63	14.58	36.63	35.74
Structural parameter ρ	0.95	0.95	0.94	0.95	0.95	0.96

Table A.5: Summary of key geometric parameters from the calculated structures of **6c** and **7c** (bond lengths in Å and angles in °).

	$[Zn(DMEGqu)_2(CF_3SO_3)][CF_3SO_3]$ **6c**		$[Zn(TMGqu)_2(CF_3SO_3)][CF_3SO_3]$ **7c**	
	6-31g(d)	6-31g+(d)	6-31g(d)	6-31g+(d)
Zn-N_{py}	2.104	2.110	2.083	2.076
	2.114	2.131	2.129	2.110
Zn-N_{gua}	2.077	2.071	2.111	2.123
	2.101	2.132	2.067	2.143
Zn-O	2.423	2.316	2.150	2.514
	2.652	2.690	3.054	2.489
C_{gua}-N_{gua}	1.348	1.346	1.333	1.335
	1.340	1.333	1.355	1.347
C_{gua}-N	1.349, 1.355	1.348, 1.354	1.369, 1.365	1.369, 1.370
	1.358, 1.353	1.361, 1.354	1.369, 1.343	1.358, 1.367
N-Zn-N	81.03	80.83	80.27	81.22
	79.97	78.82	80.65	79.39
N_{py}-Zn-N_{py}	169.52	169.11	167.82	169.61
N_{gua}-Zn-N_{gua}	121.62	115.77	119.35	117.33
$\angle(ZnN_2, ZnN_2)$	62.32	68.61	65.05	66.74
$\angle(C_{gua}N_3, ZnN_2)$	55.55	54.29	49.29	53.78
	61.99	63.33	60.2	60.2
$\angle(C_{gua}N_3, NC_3)$ (av.)	9.17	8.27	30.37	30.44
Structural parameter ρ	0.99	0.99	0.99	0.98

Table A.6: Summary of key geometric parameters from the calculated structures of **6**, **7**, **14**, **15** and the model ligand HGqu (bond lengths in Å and angles in °).

	DMEGqu **6**	TMGqu **7**	DMEGpy **14**	TMGpy **15**	HGqu
	6-31G(d)	6-31G(d)	6-31G(d)	6-31G(d)	6-31G(d)
C_{gua}-N_{gua}	1.285	1.29	1.279	1.287	1.292
C_{gua}-N	1.392	1.395	1.412	1.403	1.375
	1.392	1.394	1.401	1.404	1.395
$\angle(C_{gua}N_3, MN_2)$	66.24	80.31	18.58	58.87(P)	50.34
$\angle(C_{gua}N_3, NC_3)$ (av.)	12.58	33.55	16.41	38.36	n.def.
Structural parameter ρ	0.92	0.93	0.91	0.92	0.91

Table A.7: Mark-Houwink constants of selected complexes at 35°C in THF.

Complex	MH-α	MH-K
14a	0.5710	0.0892
	0.5850	0.0747
15a	0.6172	0.0572
	0.6211	0.0559
14b	0.5929	0.0670
	0.5828	0.0687
15b	0.5961	0.0671
	0.5836	0.0738
6b	0.5567	0.0903
	0.5671	0.0743
6c	0.6001	0.0691
	0.6172	0.0487
	0.6229	0.0503
	0.6138	0.0555
7c	0.6540	0.0387
	0.6097	0.0525
geometrical average	0.5881	0.0674
$SnOct_2$	0.6385	0.0441

Table A.8: Crystal data and structure refinement for **6**

	6
Identification code	b1848
Empirical formula	$C_{14}H_{16}N_4$
Formula weight / g mol^{-1}	240.31
Temperature / K	120(2)
Wavelength / Å	0.71073
Crystal system	Orthorhombic
Space group	$Pna2_1$
Unit cell dimensions:	
a / Å	24.018(4)
b / Å	7.7930(12)
c / Å	6.7135(10)
Volume / Å^3	1256.6(3)
Z	4
D_{calc} / Mg cm^{-3}	1.270
μ / mm^{-1}	0.079
F(000)	512
Crystal size / mm	0.46 x 0.35 x 0.31
Θ_{max} / °	27.88
Index ranges	-31≤h≤31, -10≤k≤9, -8≤l≤8
Reflections collected	10617
Independent reflections	1630 [R(int) = 0.0336]
Absorption correction	Semi-empirical from equivalents
Transmission (max. and min.)	0.9758 and 0.9644
Refinement method	Full-matrix least-squares on F^2
Data / restraints / parameters	1630 / 1 / 165
Goodness-of-fit on F^2	1.020
R1 [I > 2σ(I)]	0.0378
wR2 (all data)	0.1017
Largest diff. peak, hole / e Å^{-3}	0.267, -0.183
Absolute structure parameter	-1(3)

Table A.9: Crystal data and structure refinement for **1d** and **2a**

	1d	**2a**
Identification code	b1729	b1585
Empirical formula	$C_{26}H_{34}N_6O_4Zn$	$C_{12}H_{28}Cl_2N_6Zn$
Formula weight / g mol^{-1}	559.96	392.67
Temperature / K	120(2)	120(2)
Wavelength / Å	0.71073	0.71073
Crystal system	Monoclinic	Monoclinic
Space group	C2/c	C2/c
Unit cell dimensions:		
a / Å	20.651(2)	18.081(4)
b / Å	8.5320(10)	7.3230(18)
c / Å	14.6112(16)	13.989(3)
β /°	100.197(3)	102.114(4)
Volume / Å^3	2533.7(5)	1811.0(8)
Z	4	4
D_{calc} / Mg cm^{-3}	1.468	1.440
μ / mm^{-1}	1.015	1.654
F(000)	1176	824
Crystal size / mm	0.28 x 0.25 x 0.17	0.42 x 0.37 x 0.28
Θ_{max} / °	27.88	27.87
Index ranges	-27≤h≤27, -11≤k≤10, -15≤l≤19	-23≤h≤22, -9≤k≤9, -17≤l≤18
Reflections collected	10820	7579
Independent reflections	3021 [R(int) = 0.0497]	2159 [R(int) = 0.0222]
Absorption correction	Semi-empirical from equivalents	Semi-empirical from equivalents
Transmission (max. and min.)	0.8464 and 0.7643	0.6545 and 0.5434
Refinement method	Full-matrix least-squares on F^2	Full-matrix least-squares on F^2
Data / restraints / parameters	3021 / 0 / 170	2159 / 0 / 96
Goodness-of-fit on F^2	1.035	1.147
R1 [I > 2σ(I)]	0.0392	0.0252
wR2 (all data)	0.0908	0.0778
Largest diff. peak, hole / e Å^{-3}	0.499, -0.256	0.424, -0.373

Table A.10: Crystal data and structure refinement for **2b** and **3b**

	2b	**3b**
Identification code	b1880	b1584
Empirical formula	$C_{16}H_{34}N_6O_4Zn$	$C_{17}H_{36}N_6O_4Zn$
Formula weight / g mol^{-1}	439.86	453.89
Temperature / K	120(2)	120(2)
Wavelength / Å	0.71073	0.71073
Crystal system	Monoclinic	Monoclinic
Space group	$P2_1/n$	$P2_1/c$
Unit cell dimensions:		
a / Å	10.651(6)	8.0972(12)
b / Å	16.051(9)	11.2207(16)
c / Å	12.795(8)	25.177(4)
β /°	98.567(11)	92.455(4)
Volume / Å^3	2163(2)	2285.4(6)
Z	4	4
D_{calc} / Mg cm^{-3}	1.351	1.319
μ / mm^{-1}	1.167	1.107
F(000)	936	968
Crystal size / mm	0.48 x 0.47 x 0.38	0.38 x 0.22 x 0.16
Θ_{max} / °	27.87	27.88
Index ranges	-14≤h≤14, -21≤k≤20, -16≤l≤16	-10≤h≤9, -13≤k≤14, -32≤l≤33
Reflections collected	18089	18867
Independent reflections	5144 [R(int) = 0.0308]	5458 [R(int) = 0.0706]
Absorption correction	Semi-empirical from equivalents	Semi-empirical from equivalents
Transmission (max. and min.)	0.6653 and 0.6042	0.8428 and 0.6784
Refinement method	Full-matrix least-squares on F^2	Full-matrix least-squares on F^2
Data / restraints / parameters	5144 / 0 / 254	5458 / 0 / 261
Goodness-of-fit on F^2	1.071	0.985
R1 [I > 2σ(I)]	0.0366	0.0463
wR2 (all data)	0.1117	0.1040
Largest diff. peak, hole / e Å^{-3}	0.785, -0.311	0.696, -0.423

Table A.11: Crystal data and structure refinement for **5a** and **5b**

	5a	**5b**
Identification code	b1766 (CCDC-739147)	b1835 (CCDC-739148)
Empirical formula	$C_{16}H_{28}Cl_2N_6Zn$	$C_{20}H_{34}N_6O_4Zn$
Formula weight / g mol^{-1}	440.71	487.90
Temperature / K	120(2)	120(2)
Wavelength / Å	0.71073	0.71073
Crystal system	Monoclinic	Monoclinic
Space group	$P2_1/c$	$P2_1/c$
Unit cell dimensions:		
a / Å	8.0823(11)	9.3327(17)
b / Å	8.4648(12)	14.683(3)
c / Å	29.116(4)	16.554(3)
β /°	92.187(3)	92.010(4)
Volume / Å^3	1990.5(5)	2267.0(7)
Z	4	4
D_{calc} / Mg cm^{-3}	1.471	1.429
μ / mm^{-1}	1.514	1.122
F(000)	920	1032
Crystal size / mm	0.43 x 0.36 x 0.31	0.48 x 0.45 x 0.39
Θ_{max} / °	27.88	27.88
Index ranges	-10≤h≤10, -11≤k≤10, -33≤l≤38	-11≤h≤12, -19≤k≤19, -21≤l≤21
Reflections collected	16787	19542
Independent reflections	4747 [R(int) = 0.0215]	5409 [R(int) = 0.0198]
Absorption correction	Semi-empirical from equivalents	Semi-empirical from equivalents
Transmission (max. and min.)	0.6511 and 0.5621	0.6687 and 0.6150
Refinement method	Full-matrix least-squares on F^2	Full-matrix least-squares on F^2
Data / restraints / parameters	4747 / 0 / 234	5409 / 0 / 290
Goodness-of-fit on F^2	1.047	1.031
R1 [I > 2σ(I)]	0.0252	0.0242
wR2 (all data)	0.0635	0.0706
Largest diff. peak, hole / e Å^{-3}	0.381, -0.215	0.318, -0.308

Table A.12: Crystal data and structure refinement for **6c** and **6d**

	6c	**6d**
Identification code	b1694 (CCDC-699078)	b1653
Empirical formula	$C_{30}H_{32}F_6N_8O_6S_2Zn$	$C_{42}H_{36}N_4O_8Zn_2$
Formula weight / g mol^{-1}	844.13	855.49
Temperature / K	120(2)	120(2)
Wavelength / Å	0.71073	0.71073
Crystal system	Monoclinic	Monoclinic
Space group	$P2_1/n$	$P2_1/n$
Unit cell dimensions:		
a / Å	15.4611(19)	14.943(2)
b / Å	13.7377(17)	10.2334(16)
c / Å	16.910(2)	25.194(4)
β /°	98.624(3)	105.166(4)
Volume / Å^3	3551.1(8)	3718.6(10)
Z	4	4
D_{calc} / Mg cm^{-3}	1.579	1.528
μ / mm^{-1}	0.895	1.351
F(000)	1728	1760
Crystal size / mm	0.42 x 0.41 x 0.09	0.46 x 0.19 x 0.10
Θ_{max} / °	27.88	27.88
Index ranges	-18≤h≤20, -17≤k≤18, -22≤l≤22	-16≤h≤19, -13≤k≤13, -33≤l≤33
Reflections collected	30999	30317
Independent reflections	8471 [R(int) = 0.0836]	8862 [R(int) = 0.1144]
Absorption correction	Semi-empirical from equivalents	Semi-empirical from equivalents
Transmission (max. and min.)	0.9237 and 0.7048	0.8767 and 0.5753
Refinement method	Full-matrix least-squares on F^2	Full-matrix least-squares on F^2
Data / restraints / parameters	8471 / 0 / 482	8862 / 0 / 507
Goodness-of-fit on F^2	0.939	0.803
R1 [I > 2σ(I)]	0.0622	0.0501
wR2 (all data)	0.1712	0.0936
Largest diff. peak, hole / e Å^{-3}	1.197, -1.079	0.597, -0.751

Table A.13: Crystal data and structure refinement for **6e-1** and **6e-2**

	6e-1	**6e-2**
Identification code	b1854	b1914
Empirical formula	$C_{16}H_{22}N_4O_6S_2Zn$	$C_{30}H_{38}N_8O_6S_2Zn$
Formula weight / g mol^{-1}	495.87	736.17
Temperature / K	120(2)	120(2)
Wavelength / Å	0.71073	0.71073
Crystal system	Monoclinic	Monoclinic
Space group	$P2_1/c$	$P2_1/c$
Unit cell dimensions:		
a / Å	14.6607(18)	16.599(4)
b / Å	15.4456(18)	9.020(3)
c / Å	8.7244(10)	22.821(6)
β /°	93.843(2)	106.919(6)
Volume / Å^3	1971.1(4)	3268.9(16)
Z	4	4
D_{calc} / Mg cm^{-3}	1.671	1.496
μ / mm^{-1}	1.501	0.935
F(000)	1024	1536
Crystal size / mm	0.48 x 0.20 x 0.13	0.23 x 0.21 x 0.20
Θ_{max} / °	27.88	27.88
Index ranges	-19≤h≤19, -18≤k≤20, -11≤l≤11	-21≤h≤21, -11≤k≤11, -26≤l≤30
Reflections collected	17140	27345
Independent reflections	4684 [R(int) = 0.0279]	7786 [R(int) = 0.1071]
Absorption correction	Semi-empirical from equivalents	Semi-empirical from equivalents
Transmission (max. and min.)	0.8288 and 0.5328	0.8350 and 0.8136
Refinement method	Full-matrix least-squares on F^2	Full-matrix least-squares on F^2
Data / restraints / parameters	4684 / 0 / 266	7786 / 0 / 423
Goodness-of-fit on F^2	1.044	0.945
R1 [I > 2σ(I)]	0.0275	0.0620
wR2 (all data)	0.0726	0.1690
Largest diff. peak, hole / e Å^{-3}	0.465, -0.292	0.915, -0.765

Table A.14: Crystal data and structure refinement for **6f** and **6g**

	6f	**6g**
Identification code	b1896	b1730
Empirical formula	$C_{14}H_{16}Br_2N_4Zn$	$C_{24}H_{30}N_4O_4Zn$
Formula weight / g mol^{-1}	465.50	503.89
Temperature / K	120(2)	293(2)
Wavelength / Å	0.71073	0.71073
Crystal system	Triclinic	Monoclinic
Space group	$P\bar{1}$	$P2_1/n$
Unit cell dimensions:		
a / Å	7.6210(9)	8.626(2)
b / Å	8.1377(10)	14.134(4)
c / Å	13.2064(15)	19.255(5)
α /°	92.007(2)	
β /°	90.954(2)	99.593(5)
γ /°	100.949(2)	
Volume / Å^3	803.40(16)	2314.8(10)
Z	2	4
D_{calc} / Mg cm^{-3}	1.924	1.446
μ / mm^{-1}	6.500	1.100
F(000)	456	1056
Crystal size / mm	0.34 x 0.29 x 0.25	0.36 x 0.33 x 0.25
Θ_{max} / °	27.88	27.88
Index ranges	-10≤h≤9, -10≤k≤10, -17≤l≤16	-11≤h≤11, -18≤k≤16, -25≤l≤25
Reflections collected	6983	20287
Independent reflections	3778 [R(int) = 0.0201]	5524 [R(int) = 0.1149]
Absorption correction	Semi-empirical from equivalents	Semi-empirical from equivalents
Transmission (max. and min.)	0.2934 and 0.2160	0.7706 and 0.6930
Refinement method	Full-matrix least-squares on F^2	Full-matrix least-squares on F^2
Data / restraints / parameters	3778 / 0 / 192	5524 / 0 / 304
Goodness-of-fit on F^2	1.025	0.817
R1 [I > 2σ(I)]	0.0240	0.0455
wR2 (all data)	0.0620	0.0700
Largest diff. peak, hole / e Å^{-3}	0.769, -0.358	0.373, -0.554

Table A.15: Crystal data and structure refinement for **6h**·H_2O and **7c**

	6h·H_2O	**7c**
Identification code	b1762	b1712 (CCDC-699079)
Empirical formula	$C_{28}H_{34}B_2F_8N_8OZn$	$C_{34}H_{44}F_6N_8O_7S_2Zn$
Formula weight / g mol^{-1}	737.62	920.26
Temperature / K	120(2)	120(2)
Wavelength / Å	0.71073	0.71073
Crystal system	Monoclinic	Orthorhombic
Space group	$P2_1/c$	$Pca2_1$
Unit cell dimensions:		
a / Å	16.727(2)	18.2063(17)
b / Å	8.4544(14)	14.7468(13)
c / Å	23.208(3)	29.956(3)
β /°	108.709(3)	
Volume / Å^3	3108.6(8)	8042.7(13)
Z	4	8
D_{calc} / Mg cm^{-3}	1.576	1.520
μ / mm^{-1}	0.877	0.799
F(000)	1512	3808
Crystal size / mm	0.28 x 0.21 x 0.18	0.40 x 0.33 x 0.32
Θ_{max} / °	27.88	27.88
Index ranges	-20≤h≤22, -10≤k≤11, -30≤l≤30	-23≤h≤23, -19≤k≤19, -34≤l≤39
Reflections collected	26573	69596
Independent reflections	7405 [R(int) = 0.1465]	18098 [R(int) = 0.0654]
Absorption correction	Semi-empirical from equivalents	Semi-empirical from equivalents
Transmission (max. and min.)	0.8581 and 0.7913	0.7840 and 0.7404
Refinement method	Full-matrix least-squares on F^2	Full-matrix least-squares on F^2
Data / restraints / parameters	7405 / 0 / 437	18098 / 27 / 1062
Goodness-of-fit on F^2	0.872	1.017
R1 [I > 2σ(I)]	0.0664	0.0471
wR2 (all data)	0.1521	0.1126
Largest diff. peak, hole / e Å^{-3}	0.921, -0.752	0.535, -0.390
Absolute structure parameter		0.488(9)

Table A.16: Crystal data and structure refinement for **7d** and **7e**

	7d	**7e**
Identification code	b1663	b1834
Empirical formula	$C_{28}H_{28}N_4O_4Zn$	$C_{30}H_{42}N_8O_6S_2Zn$
Formula weight / g mol^{-1}	549.91	740.21
Temperature / K	153(2)	120(2)
Wavelength / Å	0.71073	0.71073
Crystal system	Triclinic	Monoclinic
Space group	$P\bar{1}$	$P2_1/c$
Unit cell dimensions:		
a / Å	9.3799(12)	16.961(2)
b / Å	11.9853(17)	9.1946(12)
c / Å	13.4526(18)	22.674(3)
α /°	65.079(3)	
β /°	85.137(3)	107.600(3)
γ /°	71.324(3)	
Volume / Å^3	1297.1(3)	3370.4(8)
Z	2	4
D_{calc} / Mg cm^{-3}	1.408	1.459
μ / mm^{-1}	0.988	0.908
F(000)	572	1552
Crystal size / mm	0.47 x 0.38 x 0.10	0.47 x 0.41 x 0.11
Θ_{max} / °	27.10	27.87
Index ranges	-12≤h≤11, -15≤k≤15, -17≤l≤17	-22≤h≤22, -12≤k≤12, -28≤l≤29
Reflections collected	10722	28944
Independent reflections	5666 [R(int) = 0.0221]	8024 [R(int) = 0.0342]
Absorption correction	Semi-empirical from equivalents	Semi-empirical from equivalents
Transmission (max. and min.)	0.9077 and 0.6538	0.9068 and 0.6750
Refinement method	Full-matrix least-squares on F^2	Full-matrix least-squares on F^2
Data / restraints / parameters	5666 / 0 / 338	8024 / 0 / 434
Goodness-of-fit on F^2	1.047	1.023
R1 [I > 2σ(I)]	0.0342	0.0323
wR2 (all data)	0.0842	0.0851
Largest diff. peak, hole / e Å^{-3}	0.445, -0.270	0.502, -0.270

Table A.17: Crystal data and structure refinement for **7f** and **8a**

	7f	**8a**
Identification code	b1895	b1944
Empirical formula	$C_{14}H_{18}Br_2N_4Zn$	$C_{15}H_{18}Cl_2N_4Zn$
Formula weight / g mol^{-1}	467.51	390.60
Temperature / K	120(2)	120(2)
Wavelength / Å	0.71073	0.71073
Crystal system	Monoclinic	Monoclinic
Space group	$P2_1/c$	$P2_1/n$
Unit cell dimensions:		
a / Å	8.1385(10)	11.0454(15)
b / Å	14.7701(18)	9.9117(13)
c / Å	14.2071(17)	14.8241(19)
β /°	101.057(2)	94.355(3)
Volume / Å^3	1676.1(4)	1618.2(4)
Z	4	4
D_{calc} / Mg cm^{-3}	1.853	1.603
μ / mm^{-1}	6.231	1.848
F(000)	920	800
Crystal size / mm	0.43 x 0.40 x 0.33	0.47 x 0.40 x 0.19
Θ_{max} / °	27.88	27.88
Index ranges	-10≤h≤10, -18≤k≤19, -18≤l≤18	-14≤h≤14, -12≤k≤13, -14≤l≤19
Reflections collected	14483	12827
Independent reflections	4001 [R(int) = 0.0266]	3862 [R(int) = 0.0252]
Absorption correction	Semi-empirical from equivalents	Semi-empirical from equivalents
Transmission (max. and min.)	0.2329 and 0.1747	0.7202 and 0.4770
Refinement method	Full-matrix least-squares on F^2	Full-matrix least-squares on F^2
Data / restraints / parameters	4001 / 0 / 194	3862 / 0 / 201
Goodness-of-fit on F^2	1.049	1.058
R1 [I > 2σ(I)]	0.0219	0.0291
wR2 (all data)	0.0558	0.0760
Largest diff. peak, hole / e Å^{-3}	0.453, -0.437	0.724, -0.233

Table A.18: Crystal data and structure refinement for **8a/b** and **8b**·0.13 H_2O

	8a/b	**8b**·0.13 H_2O
Identification code	b1783	b1919
Empirical formula	$C_{17}H_{21}ClN_4O_2Zn$	$C_{19}H_{24.26}N_4O_{4.13}Zn$
Formula weight / g mol^{-1}	414.20	440.13
Temperature / K	120(2)	120(2)
Wavelength / Å	0.71073	0.71073
Crystal system	Monoclinic	Monoclinic
Space group	$P2_1/n$	$P2_1/n$
Unit cell dimensions:		
a / Å	7.5495(14)	7.9880(8)
b / Å	29.000(5)	17.4877(18)
c / Å	8.0159(14)	14.1965(15)
β /°	91.131(4)	100.523(2)
Volume / $Å^3$	1754.6(5)	1949.8(3)
Z	4	4
D_{calc} / Mg cm^{-3}	1.568	1.499
μ / mm^{-1}	1.571	1.294
F(000)	856	917
Crystal size / mm	0.32 x 0.21 x 0.18	0.44 x 0.26 x 0.20
Θ_{max} / °	27.88.	27.87.
Index ranges	-9≤h≤9, -38≤k≤38, -10≤l≤9	-9≤h≤10, -23≤k≤23, -18≤l≤17
Reflections collected	15193	16925
Independent reflections	4189 [R(int) = 0.0459]	4650 [R(int) = 0.0271]
Absorption correction	Semi-empirical from equivalents	Semi-empirical from equivalents
Transmission (max. and min.)	0.7652 and 0.6334	0.7819 and 0.5999
Refinement method	Full-matrix least-squares on F^2	Full-matrix least-squares on F^2
Data / restraints / parameters	4189 / 0 / 229	4650 / 0 / 267
Goodness-of-fit on F^2	1.081	1.069
R1 [I > 2σ(I)]	0.0419	0.0354
wR2 (all data)	0.1059	0.1001
Largest diff. peak, hole / e $Å^{-3}$	0.993, -0.504	0.851, -0.303

Table A.19: Crystal data and structure refinement for **9a** and **10b**

	9a	**10b**
Identification code	b1631	b1629
Empirical formula	$C_{18}H_{26}Cl_2N_4Zn$	$C_{24}H_{32}N_4O_4Zn$
Formula weight / g mol^{-1}	434.70	505.91
Temperature / K	120(2)	120(2)
Wavelength / Å	0.71073	0.71073
Crystal system	Orthorhombic	Monoclinic
Space group	$P2_12_12_1$	C2/c
Unit cell dimensions:		
a / Å	9.9775(12)	31.868(5)
b / Å	11.8290(15)	9.2468(14)
c / Å	17.077(2)	15.887(3)
β /°		92.956(3)
Volume / Å^3	2015.5(4)	4675.4(12)
Z	4	8
D_{calc} / Mg cm^{-3}	1.433	1.437
μ / mm^{-1}	1.492	1.089
F(000)	904	2128
Crystal size / mm	0.49 x 0.41 x 0.39	0.37 x 0.30 x 0.24
Θ_{max} / °	27.88	27.88
Index ranges	-12≤h≤13, -15≤k≤15, -22≤l≤22	-41≤h≤41, -12≤k≤11, -20≤l≤20
Reflections collected	16540	20016
Independent reflections	4799 [R(int) = 0.0224]	5568 [R(int) = 0.0365]
Absorption correction	Semi-empirical from equivalents	Semi-empirical from equivalents
Transmission (max. and min.)	0.5938 and 0.5285	0.7801 and 0.6887
Refinement method	Full-matrix least-squares on F^2	Full-matrix least-squares on F^2
Data / restraints / parameters	4799 / 0 / 230	5568 / 0 / 300
Goodness-of-fit on F^2	1.035	1.055
R1 [I > 2σ(I)]	0.0205	0.0362
wR2 (all data)	0.0540	0.0940
Largest diff. peak, hole / e Å^{-3}	0.372, -0.229	0.541, -0.256
Absolute structure parameter	0.014(7)	

Table A.20: Crystal data and structure refinement for **11a** and **11b**

	11a	**11b**
Identification code	b1897	b1917
Empirical formula	$C_{18}H_{22}Cl_2N_4O_2Zn$	$C_{22}H_{28}N_4O_6Zn$
Formula weight / g mol^{-1}	462.67	509.85
Temperature / K	120(2)	293(2)
Wavelength / Å	0.71073	0.71073
Crystal system	Monoclinic	Monoclinic
Space group	$P2_1/c$	$P2_1/n$
Unit cell dimensions:		
a / Å	8.822(3)	12.196(11)
b / Å	14.920(5)	15.530(15)
c / Å	14.810(5)	12.341(11)
β /°	99.911(7)	97.78(2)
Volume / Å^3	1920.3(11)	2316(4)
Z	4	4
D_{calc} / Mg cm^{-3}	1.600	1.462
μ / mm^{-1}	1.579	1.106
F(000)	952	1064
Crystal size / mm	0.30 x 0.25 x 0.21	0.42 x 0.39 x 0.32
Θ_{max} / °	27.87	27.88
Index ranges	-11≤h≤11, -16≤k≤19, -19≤l≤19	-16≤h≤15, -20≤k≤20, -14≤l≤16
Reflections collected	15528	20219
Independent reflections	4540 [R(int) = 0.0408]	5509 [R(int) = 0.1390]
Absorption correction	Semi-empirical from equivalents	Semi-empirical from equivalents
Transmission (max. and min.)	0.7327 and 0.6488	0.7185 and 0.6537
Refinement method	Full-matrix least-squares on F^2	Full-matrix least-squares on F^2
Data / restraints / parameters	4540 / 0 / 244	5509 / 0 / 300
Goodness-of-fit on F^2	1.057	0.911
R1 [I > 2σ(I)]	0.0345	0.0672
wR2 (all data)	0.1070	0.1678
Largest diff. peak, hole / e Å^{-3}	0.529, -0.426	0.923, -0.925

Table A.21: Crystal data and structure refinement for **11c**·0.44 H_2O and **12b**·0.27 H_2O

	11c·0.44 H_2O	**12b**·0.27 H_2O
Identification code	b1921	b1923
Empirical formula	$C_{38}H_{44.88}F_6N_8O_{10.44}S_2Zn$	$C_{20}H_{26.54}N_4O_{5.27}Zn$
Formula weight / g mol^{-1}	1024.23	472.68
Temperature / K	120(2)	120(2)
Wavelength / Å	0.71073	0.71073
Crystal system	Monoclinic	Monoclinic
Space group	$P2_1/c$	$P2_1/n$
Unit cell dimensions:		
a / Å	13.313(5)	11.8067(18)
b / Å	21.016(8)	15.002(2)
c / Å	15.591(6)	12.2981(18)
β /°	101.160(9)	97.157(4)
Volume / $Å^3$	4279(3)	2161.3(6)
Z	4	4
D_{calc} / Mg cm^{-3}	1.590	1.493
μ / mm^{-1}	0.766	1.176
F(000)	2114	987
Crystal size / mm	0.42 x 0.29 x 0.22	0.39 x 0.32 x 0.20
Θ_{max} / °	27.88	27.88
Index ranges	-17≤h≤17, -25≤k≤27, -19≤l≤20	-15≤h≤13, -19≤k≤19, -16≤l≤16
Reflections collected	38067	17477
Independent reflections	10228 [R(int) = 0.1159]	5156 [R(int) = 0.0745]
Absorption correction	Semi-empirical from equivalents	Semi-empirical from equivalents
Transmission (max. and min.)	0.8496 and 0.7392	0.7988 and 0.6569
Refinement method	Full-matrix least-squares on F^2	Full-matrix least-squares on F^2
Data / restraints / parameters	10228 / 0 / 596	5156 / 0 / 280
Goodness-of-fit on F^2	0.899	0.935
R1 [I > 2σ(I)]	0.0597	0.0657
wR2 (all data)	0.1421	0.1953
Largest diff. peak, hole / e $Å^{-3}$	0.867, -0.433	0.951, -0.574

Table A.22: Crystal data and structure refinement for **14d** and **17a**

	14d	**17a**
Identification code	b1664	b1942
Empirical formula	$C_{25}H_{26}N_4O_4Zn$	$C_{15}H_{26}Cl_2N_4Zn$
Formula weight / g mol^{-1}	511.87	398.67
Temperature / K	153(2)	120(2)
Wavelength / Å	0.71073	0.71073
Crystal system	Monoclinic	Orthorhombic
Space group	C2/c	$P2_12_12_1$
Unit cell dimensions:		
a / Å	13.2490(19)	9.4282(14)
b / Å	20.075(3)	13.349(2)
c / Å	17.875(3)	15.240(2)
β /°	91.508(3)	
Volume / Å^3	4752.6(12)	1918.2(5)
Z	8	4
D_{calc} / Mg cm^{-3}	1.431	1.380
μ / mm^{-1}	1.073	1.560
F(000)	2128	832
Crystal size / mm	0.47 x 0.28 x 0.20	0.49 x 0.12 x 0.11
Θ_{max} / °	27.87	27.88
Index ranges	-15≤h≤17, -26≤k≤26, -23≤l≤23	-12≤h≤12, -17≤k≤17, -17≤l≤19
Reflections collected	20493	15746
Independent reflections	5669 [R(int) = 0.0348]	4558 [R(int) = 0.0360]
Absorption correction	Semi-empirical from equivalents	Semi-empirical from equivalents
Transmission (max. and min.)	0.8141 and 0.6326	0.8471 and 0.5152
Refinement method	Full-matrix least-squares on F^2	Full-matrix least-squares on F^2
Data / restraints / parameters	5669 / 0 / 309	4558 / 0 / 199
Goodness-of-fit on F^2	1.040	1.045
R1 [I > 2σ(I)]	0.0361	0.0320
wR2 (all data)	0.0921	0.0702
Largest diff. peak, hole / e Å^{-3}	0.477, -0.248	0.547, -0.264
Absolute structure parameter		-0.018(10)

Table A.23: Crystal data and structure refinement for **19a** and **19b**

	19a	**19b**
Identification code	b1943	b1922
Empirical formula	$C_{15}H_{22}Cl_2N_4O_2Zn$	$C_{19}H_{28}N_4O_6Zn$
Formula weight / g mol^{-1}	426.64	473.82
Temperature / K	120(2)	120(2)
Wavelength / Å	0.71073	0.71073
Crystal system	Monoclinic	Orthorhombic
Space group	Cc	$P2_12_12_1$
Unit cell dimensions:		
a / Å	12.9551(19)	9.8816(14)
b / Å	11.8601(17)	14.027(2)
c / Å	12.7535(19)	14.950(2)
β /°	105.318(3)	
Volume / Å^3	1889.9(5)	2072.3(5)
Z	4	4
D_{calc} / Mg cm^{-3}	1.499	1.519
μ / mm^{-1}	1.597	1.229
F(000)	880	992
Crystal size / mm	0.38 x 0.37 x 0.29	0.35 x 0.25 x 0.20
Θ_{max} / °	26.37	27.87
Index ranges	-15≤h≤16, -14≤k≤14, -15≤l≤15	-13≤h≤12, -18≤k≤18, -19≤l≤18
Reflections collected	6837	17215
Independent reflections	3431 [R(int) = 0.0285]	4941 [R(int) = 0.0273]
Absorption correction	Semi-empirical from equivalents	Semi-empirical from equivalents
Transmission (max. and min.)	0.6545 and 0.5821	0.7911 and 0.6729
Refinement method	Full-matrix least-squares on F^2	Full-matrix least-squares on F^2
Data / restraints / parameters	3431 / 2 / 217	4941 / 0 / 273
Goodness-of-fit on F^2	1.031	1.050
R1 [I > 2σ(I)]	0.0324	0.0276
wR2 (all data)	0.0758	0.0672
Largest diff. peak, hole / e Å^{-3}	0.749, -0.224	0.489, -0.280
Absolute structure parameter	0.015(12)	-0.016(7)

Table A.24: Crystal data and structure refinement for **20a** and **21a**

	20a	**21a**
Identification code	b1949	b1916
Empirical formula	$C_{13}H_{20}Cl_2N_4OZn$	$C_{22}H_{32}Cl_2N_8Zn$
Formula weight / g mol^{-1}	384.60	544.83
Temperature / K	120(2)	120(2)
Wavelength / Å	0.71073	0.71073
Crystal system	Monoclinic	Monoclinic
Space group	$P2_1/c$	$P2_1/n$
Unit cell dimensions:		
a / Å	13.189(3)	9.924(2)
b / Å	7.904(2)	20.210(5)
c / Å	16.369(4)	13.221(3)
β /°	101.360(7)	101.611(6)
Volume / Å^3	1672.9(7)	2597.4(11)
Z	4	4
D_{calc} / Mg cm^{-3}	1.527	1.393
μ / mm^{-1}	1.791	1.177
F(000)	792	1136
Crystal size / mm	0.19 x 0.05 x 0.02	0.31 x 0.26 x 0.23
Θ_{max} / °	27.88	27.88
Index ranges	-17≤h≤16, -10≤k≤9, -21≤l≤21	-11≤h≤13, -26≤k≤26, -17≤l≤17
Reflections collected	13397	22905
Independent reflections	3990 [R(int) = 0.3676]	6194 [R(int) = 0.1621]
Absorption correction	Semi-empirical from equivalents	Semi-empirical from equivalents
Transmission (max. and min.)	0.9651 and 0.7272	0.7734 and 0.7116
Refinement method	Full-matrix least-squares on F^2	Full-matrix least-squares on F^2
Data / restraints / parameters	3990 / 0 / 192	6194 / 0 / 304
Goodness-of-fit on F^2	0.924	0.849
R1 [I > 2σ(I)]	0.1075	0.0567
wR2 (all data)	0.2270	0.1297
Largest diff. peak, hole / e Å^{-3}	0.749, -0.681	0.862, -0.697

Table A.25: Crystal data and structure refinement for **22a** and **22b**·THF

	22a	**22b**·THF
Identification code	b1749	b1883
Empirical formula	$C_{22}H_{36}Cl_2N_8Zn$	$C_{38}H_{62}N_8O_{13}Zn_3$
Formula weight / g mol^{-1}	548.86	1035.07
Temperature / K	120(2)	120(2)
Wavelength / Å	0.71073	0.71073
Crystal system	Monoclinic	Monoclinic
Space group	$P2_1/c$	C2/c
Unit cell dimensions:		
a / Å	17.266(2)	12.020(3)
b / Å	20.032(3)	14.228(3)
c / Å	17.113(2)	27.944(7)
β /°	114.990(2)	96.850(5)
Volume / Å^3	5364.9(12)	4744.7(19)
Z	8	4
D_{calc} / Mg cm^{-3}	1.359	1.449
μ / mm^{-1}	1.140	1.571
F(000)	2304	2160
Crystal size / mm	0.42 x 0.40 x 0.07	0.37 x 0.35 x 0.26
Θ_{max} / °	27.88	27.88
Index ranges	-22≤h≤22, -26≤k≤24, -22≤l≤22	-15≤h≤15, -18≤k≤18, -36≤l≤36
Reflections collected	46972	20336
Independent reflections	12788 [R(int) = 0.0366]	5666 [R(int) = 0.0679]
Absorption correction	Semi-empirical from equivalents	Semi-empirical from equivalents
Transmission (max. and min.)	0.9244 and 0.6459	0.6855 and 0.5941
Refinement method	Full-matrix least-squares on F^2	Full-matrix least-squares on F^2
Data / restraints / parameters	12788 / 0 / 615	5666 / 0 / 267
Goodness-of-fit on F^2	1.021	0.986
R1 [I > 2σ(I)]	0.0347	0.0519
wR2 (all data)	0.0861	0.1307
Largest diff. peak, hole / e Å^{-3}	0.427, -0.273	0.906, -0.433

Table A.26: Crystal data and structure refinement for **28a**·Me_3CN·2.5 Et_2O and **29a**

	28a·Me_3CN·2.5 Et_2O	**29a**
Identification code	b1726	b1959
Empirical formula	$C_{47}H_{98.50}Cl_4N_{14.50}O_{2.50}Zn_2$	$C_{21}H_{42}Cl_2N_{10}Zn$
Formula weight / g mol^{-1}	1179.44	570.92
Temperature / K	293(2)	120(2)
Wavelength / Å	0.71073	0.71073
Crystal system	Triclinic	Monoclinic
Space group	P1	$P2_1/n$
Unit cell dimensions:		
a / Å	14.634(5)	12.7319(5)
b / Å	19.394(6)	12.2079(5)
c / Å	19.710(6)	21.2143(7)
α /°	85.469(7)	
β /°	88.673(6)	126.773(2)
γ /°	71.414(6)	
Volume / $Å^3$	5286(3)	2641.21(17)
Z	4	4
D_{calc} / Mg cm^{-3}	1.482	1.436
μ / mm^{-1}	1.165	1.163
F(000)	2520	1208
Crystal size / mm	0.42 x 0.41 x 0.10	0.35 x 0.29 x 0.19
Θ_{max} / °	27.88	27.88
Index ranges	-19≤h≤19, -25≤k≤25, -25≤l≤25	-16≤h≤16, -16≤k≤16, -27≤l≤27
Reflections collected	46209	24158
Independent reflections	25018 [R(int) = 0.1927]	6295 [R(int) = 0.0334]
Absorption correction	Semi-empirical from equivalents	Semi-empirical from equivalents
Transmission (max. and min.)	0.8924 and 0.6403	0.8093 and 0.6863
Refinement method	Full-matrix least-squares on F^2	Full-matrix least-squares on F^2
Data / restraints / parameters	25018 / 0 / 1069	6295 / 0 / 313
Goodness-of-fit on F^2	0.764	1.029
R1 [I > 2σ(I)]	0.0883	0.0311
wR2 (all data)	0.2658	0.0792
Largest diff. peak, hole / e $Å^{-3}$	1.087, -0.695	0.537, -0.271

Table A.27: Crystal data and structure refinement for **30a*** and **32c**

	30a*	**32c**
Identification code	b1842	b1565
Empirical formula	$C_{22}H_{48}ClF_3N_{10}O_3SZn$	$C_{24}H_{22}F_6N_6O_6S_2Zn$
Formula weight / g mol^{-1}	690.58	733.97
Temperature / K	120(2)	293(2)
Wavelength / Å	0.71073	0.71073
Crystal system	Monoclinic	Triclinic
Space group	$P2_1/n$	$P\bar{1}$
Unit cell dimensions:		
a / Å	8.8569(10)	7.9796(11)
b / Å	16.9582(19)	8.4929(11)
c / Å	21.296(2)	11.4112(15)
α /°		101.670(3)
β /°	98.555(3)	105.193(3)
γ /°		100.996(3)
Volume / Å^3	3163.1(6)	706.15(16)
Z	4	1
D_{calc} / Mg cm^{-3}	1.450	1.726
μ / mm^{-1}	0.987	1.110
F(000)	1456	372
Crystal size / mm	0.47 x 0.09 x 0.08	0.41 x 0.37 x 0.22
Θ_{max} / °	27.88	27.88
Index ranges	-11≤h≤11, -20≤k≤22, -28≤l≤28	-10≤h≤10, -11≤k≤11, -15≤l≤14
Reflections collected	27710	6206
Independent reflections	7533 [R(int) = 0.1098]	3330 [R(int) = 0.0185]
Absorption correction	Semi-empirical from equivalents	Semi-empirical from equivalents
Transmission (max. and min.)	0.9252 and 0.6542	0.7924 and 0.6590
Refinement method	Full-matrix least-squares on F^2	Full-matrix least-squares on F^2
Data / restraints / parameters	7533 / 0 / 383	3330 / 0 / 206
Goodness-of-fit on F^2	0.967	1.051
R1 [I > 2σ(I)]	0.0582	0.0363
wR2 (all data)	0.1184	0.0972
Largest diff. peak, hole / e Å^{-3}	0.870, -0.396	0.524, -0.315

Table A.28: Crystal data and structure refinement for **33b** and **33c**

	33b	**33c**
Identification code	b1867 (CCDC-752689)	b1861 (CCDC-752691)
Empirical formula	$C_{32}H_{34}N_4O_{12}Zn_3$	$C_{22}H_{16}F_6N_4O_6S_2Zn$
Formula weight / g mol^{-1}	862.74	675.88
Temperature / K	120(2)	120(2)
Wavelength / Å	0.71073	0.71073
Crystal system	Triclinic	Monoclinic
Space group	P$\bar{1}$	C2/c
Unit cell dimensions:		
a / Å	8.0702(19)	9.9580(14)
b / Å	9.651(2)	14.126(2)
c / Å	12.668(3)	18.672(3)
α /°	105.050(4)	
β /°	98.355(4)	101.468(3)
γ /°	108.854(4)	
Volume / Å^3	872.9(3)	2574.1(6)
Z	1	4
D_{calc} / Mg cm^{-3}	1.641	1.744
μ / mm^{-1}	2.112	1.207
F(000)	440	1360
Crystal size / mm	0.43 x 0.42 x 0.20	0.50 x 0.47 x 0.21
Θ_{max} / °	27.87	27.88
Index ranges	-9≤h≤10, -12≤k≤12, -16≤l≤15	-13≤h≤10, -18≤k≤18, -24≤l≤24
Reflections collected	7570	11017
Independent reflections	4113 [R(int) = 0.0208]	3076 [R(int) = 0.0184]
Absorption correction	Semi-empirical from equivalents	Semi-empirical from equivalents
Transmission (max. and min.)	0.6774 and 0.4636	0.7856 and 0.5835
Refinement method	Full-matrix least-squares on F^2	Full-matrix least-squares on F^2
Data / restraints / parameters	4113 / 0 / 236	3076 / 0 / 186
Goodness-of-fit on F^2	1.108	1.067
R1 [I > 2σ(I)]	0.0276	0.0260
wR2 (all data)	0.0834	0.0714
Largest diff. peak, hole / e Å^{-3}	0.433, -0.464	0.455, -0.257
Extinction coefficient	0.0039(10)	

Table A.29: Crystal data and structure refinement for **34b** and **34c**

	34b	**34c**
Identification code	b1696 (CCDC-752690)	b1725 (CCDC-752692)
Empirical formula	$C_{32}H_{28}N_4O_8Zn_2$	$C_{26}H_{16}F_6N_4O_6S_2Zn$
Formula weight / g mol^{-1}	727.32	723.92
Temperature / K	120(2)	120(2)
Wavelength / Å	0.71073	0.71073
Crystal system	Monoclinic	Monoclinic
Space group	$P2_1/n$	C2/c
Unit cell dimensions:		
a / Å	11.296(5)	9.7694(14)
b / Å	19.857(8)	14.309(2)
c / Å	13.535(6)	19.609(3)
β /°	106.945(8)	95.235(3)
Volume / Å^3	2904(2)	2729.7(7)
Z	4	4
D_{calc} / Mg cm^{-3}	1.663	1.762
μ / mm^{-1}	1.714	1.145
F(000)	1488	1456
Crystal size / mm	0.42 x 0.40 x 0.37	0.48 x 0.39 x 0.36
Θ_{max} / °	27.88	27.87
Index ranges	-13≤h≤14, -25≤k≤26, -17≤l≤17	-12≤h≤12, -18≤k≤18, -25≤l≤23
Reflections collected	25283	11816
Independent reflections	6913 [R(int) = 0.0944]	3265 [R(int) = 0.0204]
Absorption correction	Semi-empirical from equivalents	Semi-empirical from equivalents
Transmission (max. and min.)	0.5696 and 0.5330	0.6833 and 0.6094
Refinement method	Full-matrix least-squares on F^2	Full-matrix least-squares on F^2
Data / restraints / parameters	6913 / 0 / 419	3265 / 0 / 204
Goodness-of-fit on F^2	0.957	1.062
R1 [I > 2σ(I)]	0.0420	0.0260
wR2 (all data)	0.1033	0.0723
Largest diff. peak, hole / e Å^{-3}	0.901, -0.951	0.436, -0.332

Table A.30: Crystal data and structure refinement for **39a** and **39b**

	39a	**39b**
Identification code	b1794 (CCDC-729874)	b1827 (CCDC-729875)
Empirical formula	$C_{11}H_{20}Cl_2N_2OZn$	$C_{15}H_{26}N_2O_5Zn$
Formula weight / g mol^{-1}	332.56	379.75
Temperature / K	120(2)	120(2)
Wavelength / Å	0.71073	0.71073
Crystal system	Orthorhombic	Orthorhombic
Space group	$P2_12_12_1$	$P2_12_12_1$
Unit cell dimensions:		
a / Å	7.2823(12)	7.9937(18)
b / Å	12.842(2)	12.400(3)
c / Å	14.557(2)	19.064(4)
Volume / Å^3	1361.3(4)	1889.7(7)
Z	4	4
D_{calc} / Mg cm^{-3}	1.623	1.335
μ / mm^{-1}	2.182	1.323
F(000)	688	800
Crystal size / mm	0.48 x 0.16 x 0.15	0.50 x 0.20 x 0.14
Θ_{max} / °	27.85	27.88
Index ranges	-9≤h≤9, -15≤k≤16, -19≤l≤19	-10≤h≤10, -15≤k≤16, -25≤l≤25
Reflections collected	11964	16697
Independent reflections	3247 [R(int) = 0.0285]	4515 [R(int) = 0.0761]
Absorption correction	Semi-empirical from equivalents	Semi-empirical from equivalents
Transmission (max. and min.)	0.7355 and 0.4206	0.8364 and 0.5575
Refinement method	Full-matrix least-squares on F^2	Full-matrix least-squares on F^2
Data / restraints / parameters	3247 / 0 / 155	4515 / 0 / 211
Goodness-of-fit on F^2	1.020	1.021
R1 [I > 2σ(I)]	0.0212	0.0510
wR2 (all data)	0.0481	0.0955
Largest diff. peak, hole / e Å^{-3}	0.307, -0.228	0.562, -0.336
Absolute structure parameter	0.018(9)	0.019(17)